

**THE UNIVERSITY OF HULL**

***Modified Cowpea Mosaic Virus as a  
Carrier of Antimalarial Drugs***

Being a thesis submitted for the Degree of Doctor of  
Philosophy

The University of Hull

**By**

***Rana Al-Refai'a***

***June 2018***

# *Contents*

Abbreviation.....	I
Acknowledgments.....	VIII
Abstract.....	IX
List of Figures .....	XI
List of tables .....	XXI
List of Schemes.....	XXIII
1 Introduction .....	1
1.1 Nanoparticles .....	1
1.1.1 Medicine and nanoparticles .....	4
1.1.2 Virus like particles (VLPs) .....	5
1.1.3 Virus nanoparticles (VNPs).....	6
1.2 The lifestyles of plant viruses .....	9
1.3 Cowpea mosaic virus .....	11
1.3.1 The advantages CPMV as a nanoparticle.....	14
1.3.2 Chemical modification on wild -type CPMV particles (wt CPMV) .....	14
1.4 Drug delivery based on plant viruses .....	19
1.5 Malaria.....	22
1.5.1 Malaria diagnosis .....	25
1.6 Antimalarial drugs .....	25
1.6.1 Chloroquine.....	28
1.6.2 The mechanism of action of chloroquine as antimalarial drug .....	31
1.6.3 The ferrocenyl antimalarial agents .....	33
1.6.4 Sugar transporters for anti-malarial drug targets.....	34
1.6.5 Approaches to Discovery of New Antimalarial Agents .....	37
1.7 Summary.....	39
1.8 Aim of this thesis .....	40
2 Experimental.....	42
2.1 Reagents.....	42
2.1.1 Sodium phosphate buffer .....	42

2.1.2	Sodium acetate buffer .....	42
2.2	Equipment .....	43
2.2.1	Inductively coupled plasma optical emission spectroscopy (ICP-OES analysis) 43	
2.2.2	Scanning electron microscopy (SEM).....	43
2.2.3	Powder X - ray diffraction .....	43
2.3	Particle purification .....	44
2.3.1	Ultrafiltration .....	44
2.3.2	Dialysis.....	44
2.4	Determination of virus concentration.....	45
2.4.1	UV–Vis determines concentration .....	45
2.4.2	Agarose–gel electrophoresis.....	46
2.4.3	SDS–PAGE.....	47
2.4.4	Transmission electron microscopy (TEM).....	47
2.5	Chemical synthesis .....	47
2.5.1	3-((7-Chloroquinolin-4-yl) amino) propan-1-ol (1) .....	47
2.5.2	Chloroquinoline derivatives:.....	49
2.5.3	Preparation of $\beta$ -D-glucosyl urea (3).....	52
2.5.4	Preparation of 3, 4, 5-(trihydroxy-6-(hydroxymethyl) tetrahydro-2-pyran-2-yl) carbamoyl azide (4) .....	53
2.5.5	Preparation of 3, 4, 5-(trihydroxy-6-(hydroxymethyl) tetrahydro-2-pyran-2-yl) carbamoyl -1, 2, 3-triazol-5-yl) acetic acid (5).....	54
2.6	Chemical modification of virus.....	55
2.6.1	Attachment of chloroquinoline derivatives to CPMV .....	55
2.6.2	Labelling of CPMV-CQ -derivatives with Alexa fluorescent dye .....	56
2.6.3	Attachment of glucuronic acid to CPMV.....	56
2.6.4	Attachment of glucuronic acid to CPMV-CQ- derivatives.....	57
2.6.5	Attachment of propiolic acid and butyric acid to CPMV .....	57
2.6.6	The coupling of N <sub>3</sub> -bodipy dye to CPMV- P.A and CPMV- B.A.....	58
2.6.7	Coupling of CPMV-B.A with 3, 4, 5(-trihydroxy-6-(hydroxymethyl) tetrahydro-2-pyran-2-yl) carbamoyl azide. ....	58

2.6.8	Attachment of 3, 4, 5-((-trihydroxy-6-(hydroxymethyl) tetrahydro-2-pyran-2-yl) carbamoyl) -1, 2, 3-triazol-5-yl) acetic acid to CPMV .....	58
2.6.9	Attachment of 3, 4, 5-((-trihydroxy-6-(hydroxymethyl) tetrahydro-2-pyran-2-yl) carbamoyl) -1,2,3-triazol-5-yl) acetic acid to CPMV-CQ- derivatives .....	59
2.6.10	Labelling of CPMV-CQ- Glu (compound 5) with Alexa fluorescent dye....	59
2.6.11	Attachment of ferrocene to CPMV-CQ- derivatives .....	60
2.6.12	Attachment of ferrocene to CPMV-CQ-derivatives- G.A (triple modification).....	60
2.7	The modification of CPMV-ferrocene .....	61
2.7.1	The modification of CPMV-ferrocene with CQ- derivatives .....	61
2.8	Colorimetric method to measure beta- haematin crystal growth in vitro .....	62
2.9	Purification method to measure beta- haematin crystal growth in vitro.....	63
2.10	Beta- haematin production for IR and SEM measurements .....	63
2.11	The reaction of iron oxide with beta-haematin in vitro:.....	64
3	Chemical characterisation .....	65
3.1	Preparation of 3-(7-chloroquinolin-4-ylamino) propan-1-ol (1) .....	65
3.2	Preparation of chloroquinoline propionic acid (CQp)(2) .....	67
3.3	Preparation of (7-chloroquinolin-4-yl) alanine (2a) .....	68
3.4	Preparation of (7-chloroquinolin-4-yl) valine (2b) .....	68
3.5	Preparation of $\beta$ -D-glucosyl urea (3).....	71
3.6	Preparation of 3, 4, 5-(trihydroxy-6-(hydroxymethyl) tetrahydro-2-pyran-2-yl) carbamoyl azide (4) .....	71
3.7	Preparation of 3, 4, 5-((-trihydroxy-6-(hydroxymethyl) tetrahydro-2-pyran-2-yl) carbamoyl) -1, 2, 3-triazol-5-yl) acetic acid (5).....	72
3.8	Determination of virus concentration.....	73
3.8.1	UV-Vis spectroscopy.....	73
3.8.2	Gel electrophoresis .....	74
3.9	Summary.....	76
4	Chemical modification of CPMV particles .....	77
4.1	Addressability of amines on external surface of CPMV (single modification) .	78
4.1.1	Chemical modification of CPMV with EDC/NHS and chloroquinoline propionic acid (2) .....	78

4.1.2	The synthesis of chloroquinoline propionic acid (CQp) and coupling to CPMV	82
4.1.3	Chemical modification of CPMV with (7-chloroquinoline-4-yl) alanine and (7-chloroquinoline-4-yl)valine (2a and 2b): single modification.	84
4.1.4	The modification of CPMV with glucuronic acid (G.A)	88
4.1.5	Quantification of chloroquinoline propionic acid (CQp) binding on external surface of CPMV:	91
4.1.6	Quantification of CPMV-CQ-ala and CPMV-CQ-val	106
4.1.7	The attachment of propionic acid (P.A), butyric acid (B.A) to CPMV	109
4.1.8	The modification of CPMV by 3, 4, 5-(trihydroxy-6-(hydroxymethyl) tetrahydro-2-pyran-2-yl) carbamoyl -1, 2, 3-triazol-5-yl) acetic acid (Glu) (5)	111
4.2	Double addressability of amines on external surface of CPMV	116
4.2.1	Modification of CPMV-CQp with glucuronic acid (G.A)	116
4.2.2	Modification of CPMV-CQ-ala and CPMV-CQ-val with glucuronic acid	125
4.2.3	Modification of CPMV-CQp with 3, 4, 5-(trihydroxy-6-(hydroxymethyl) tetrahydro-2-pyran-2-yl) carbamoyl -1, 2, 3-triazol-5-yl) acetic acid (Glu)	127
4.2.4	Quantification of CPMV-CQp-Glu	131
4.2.5	Modification of CPMV-CQ-ala and CPMV-CQ-val with 3, 4, 5-(trihydroxy-6-(hydroxymethyl) tetrahydro-2-pyran-2-yl) carbamoyl -1, 2, 3-triazol-5-yl) acetic acid (Glu)	134
4.2.6	Attachment of modified CPMV to Alexa Fluor 488 dye	136
4.3	Summary	137
5	Redox-active ferrocene-modified CPMV nanoparticles	139
5.1	The modification of CPMV with aminoferrocene(Fc)	140
5.1.1	Addressability of carboxylates on external surface of CPMV (single modification)	140
5.2	Methods	141
5.2.1	Attachment of ferrocene to CPMV-CQ- derivatives (double modification)	142
5.2.2	Attachment of ferrocene to CPMV-CQ- derivatives- G.A (triple modification)	142
5.2.3	Addressability of amines on external surface of CPMV (double modification)	142
5.2.4	Electrochemical measurements:	142

5.3	Results and discussion	144
5.3.1	Addressability of carboxylates on external surface of CPMV (double labelling)	148
5.3.2	Addressability of carboxylates on external surface of CPMV (triple modification)	151
5.3.3	Addressability of amines on external surface of CPMV (double modification)	155
5.4	Conclusions	166
6	Malaria and chloroquinoline derivatives (CQ-derivatives) as inhibitor of haemozoin or beta-haematin formation in vitro	167
6.1	Malaria	168
6.2	Haemozoin or beta-haematin formation	169
6.3	Antimalarial drugs as beta-haematin or haemozoin inhibitors	171
6.4	The relationship between malaria and iron oxide treatment	174
6.5	Methods	175
6.5.1	Determination of beta-haematin crystal growth using colorimetric method	175
6.5.2	Purification method to measure beta-haematin crystal growth	175
6.5.3	Beta-haematin production for FT-IR and SEM measurements synthetic	175
6.5.4	The reaction of iron oxide with beta-haematin (BH) in vitro	175
6.6	Results and discussion	176
6.6.1	The effect of iron oxide on BH formation	191
6.7	Conclusions:	197
7	Chloroquinoline as haemozoin or beta-haematin inhibitor	198
7.1	Chloroquine-Resistant Malaria	198
7.2	Materials and methods	199
7.2.1	Drugs	199
7.2.2	Growth inhibition assays	199
7.3	Results and discussion	200
7.3.1	The fluorometric SYBR Green I assay	200
7.3.2	The colorimetric lactate dehydrogenase (LDH) assay	208

7.4	Conclusions.....	217
8	Conclusions and future work.....	218
9	References .....	220
	Publications.....	240
	Appendix 1 .....	241
	Appendix 2 .....	244



## *Abbreviation*

AQ	Amodiaquine
ApQ	Amopyroquine
Å	Angström
Asp	Aspartic acid
A	Absorbance
Au NPs	Gold nanoparticles
BH	Beta-haematin
B.A	Butyric acid
CPMV	Cowpea mosaic virus
CNS	Central nervous system
CCMV	Cowpea chlorotic mottle virus
CMV	Cytomegalovirus
CQ	Chloroquine
Control CQ	N <sup>4</sup> - (7-chloroquinolin-4-yl)-N <sup>1</sup> ,N <sup>1</sup> - dimethylpentane-1,4-diamine phosphate
CQR	Chloroquine resistance

CS–TPP	Chitosan–tripolyphosphate
CSA	Chondroitin sulfate A
CrO <sub>3</sub>	Chromium oxide
cm	Centimetre
CQp	Chloroquinoline propionic acid
CQ-ala	(7-chloroquinoline-4-yl)alanine
CQ-val	(7-chloroquinoline-4-yl)valine
3D	Three dimensional
DNA	Deoxyribonucleic acid
Da	Dalton
Dox. or dox.	Doxorubicin
DOTA	1,4,7,10-tetraazacyclododecane-1,4,7,10-tetraacetic acid
DMSO	Dimethyl sulfoxide
DCM	Dichloromethane
DV	Digestive vacuole
ds	Double stranded

ELD	Electroless Deposition
EMP	Ethylmercury phosphate
EDC	1-ethyl-3-[(3-dimethylaminopropyl)]carbodiimide hydrochloride
FV	Food vacuole
FQ	Ferroquine
Fe(III) PPIX	Iron(III) protoporphyrin IX
Fc	Ferrocene or Aminoferrocene
Gd(DOTA)	Gadoteric acid
Gd <sup>3+</sup>	Gadolinium cations
GLUTI	Glucose transporter
G.A	Glucuronic acid
Glu	Glutamic acid
Glu	3,4,5-(trihydroxy-6-(hydroxymethyl)tetrahydro-2-(pyran-2-yl)carbamoyl)-1,2,3-(triazol-5-yl)acetic acid
HRP	Horseradish peroxidase

kb	Kilo bases
Lys	Lysine
L subunit	Large subunit
MQ	MilliQ water
MeOH	Methanol
mRNA	Messenger RNA
MRI	Magnetic resonance imaging
μl	Microliter
mg	Milligram
ml	Milliliter
mM	Millimolar
Min.	Minute
m.p.	Malting point
mV	Millivolt
nm	Nanometer
NPs	Nano particles
NH <sub>4</sub> Cl	Ammonium chloride

ND	Nano drop
N	Normality
NHS	N-hydroxysuccinimide
PVX	Potato virus X
<i>P.vivax</i>	<i>Plasmodium vivax</i>
<i>P. ovale curtisi,</i>	<i>Plasmodium ovale curtisi</i>
<i>P.ovale wallikeri</i>	<i>Plasmodium ovale wallikeri</i>
<i>P. malariae</i>	<i>Plasmodium malariae</i>
<i>P. knowlesi</i>	<i>Plasmodium knowlesi</i>
<i>P. falciparum</i>	<i>Plasmodium falciparum</i>
PV	Parasitophorous vacuole membrane
PBS	Sodium phosphate buffer
pfCRT	P. falciparum Chloroquine Resistance Transporter
PFHT	Principal hexose transporter
P.A	Propiolic acid
pH	Negative logarithm to the base ten of the concentration of [H] <sup>+</sup> ions
RNA	Ribonucleic acid
ROS	Reactive oxygen species

rpm	Revolution per minute
RDTs	Rapid diagnostic tests
SEM	Scanning Electron Microscopy
S subunit	Small subunit
SCE	Saturated calomel electrode
ss	Single stranded
SDS	Sodium dodecylsulfate
TEM	Transmission Electron Microscopy
TLC	Thin layer chromatography
TMV	Tobacco mosaic virus
TYMV	Turnip yellow mosaic virus
TBE	Mixture of Tris base, boric acid and EDTA
THPTA	Tris(3-hydroxypropyltriazolylmethyl)amine
<sup>t</sup> BuOH	Tert-butanol
<sup>t</sup> BuNO	Tert- butyl nitrite
UV	Ultra violet
VLPs	Virus-like particle
VNP(s)	Virus nanoparticle(s)

v/v	Volume per Volume
Vis	Visible
w/v	Weight per volume
wt CPMV	Wild-type Cowpea mosaic virus

## *Acknowledgments*

I would like to express my heartfelt thanks to the Iraqi Ministry of Higher Education and Scientific Research (HESR), the Iraqi cultural attaché in London and Ireland, and the University of Babylon for their financial support and encouragement to conduct my study.

I take this opportunity to express my profound gratitude and deep regards to my supervisor (Professor David Evans) for his exemplary guidance, monitoring and constant encouragement throughout the course of this work.

Moreover, I would also like to thank with much appreciation Dr. Sachin Shah for his help with TEM imaging, and especial thanks to Dr. Don van Schalkwyk for antimalarial test.

Furthermore, I would also like to thank with much appreciation the University of Hull, Chemistry Department and Mr. Tony Sinclair for his help with SEM analysis. As well as, special thanks to all my friends for their support.

I would also like to express my big thanks to my parents, my brother and my sisters for their unceasing encouragement and prayers, and great special thanks to my husband and my children for all their patience, love, help, care and generous support in every aspect of my life.

*Rama*

## ***Abstract***

Plant viruses provide exceptional advantages in the field of nanotechnology as multifunctional nanoparticles. Cowpea mosaic virus (CPMV) is being developed as a carrier vehicle for chemotherapeutic drugs. The ability to modify the amine groups on the external capsid surface with three different new chloroquinoline derivatives, and together with sugar, has been demonstrated. Additionally, addressable carboxylates on the external capsid surface have been modified with ferrocene to produce a multifunctional drug carrier.

The redox-active ferrocene on the outer surface of the unmodified and modified CPMV with each chloroquinoline derivative are electrochemically independent. The ability of binding ferrocene to modified and unmodified CPMV as a first or second conjugated compound has been confirmed.

The effectivity of chloroquinoline-derivatives, with and without conjugation to CPMV, has been investigated by beta-haematin inhibition *in vitro* and *in vivo* using *P. falciparum* strain.

(7-chloroquinolin-4-yl) alanine has shown a significant effect as an antimalarial compound after conjugation with CPMV compared to the other chloroquinoline derivatives. This conjugate led to a 90% inhibition of beta-haematin or haemozoin formation, which is necessary for the parasite to survive.

The significance of modified CPMV as a carrier is discussed in relation to developing novel strategies to solve the problem of chloroquine resistant.

The activities of ferrocene *in vitro* after conjugation to the external surface of CPMV particle was evaluated against *P. falciparum strain* resulting in a, surprisingly, high kill effect. The IC<sub>50</sub> values for conjugated (7-chloroquinolin-4-yl) alanine and conjugated

ferrocene were 0.275 nM and 0.309 nM respectively compared to a range from 7.8-10 nM for control chloroquine.

Overall CPMV plays an important role in increasing the effectiveness of (7-chloroquinolin-4-yl) alanine and ferrocene as an antimalarial drugs compared to unconjugated compounds.

## *List of Figures*

Figure 1.1 Gold nanoparticles in biomedical applications. (a) Gold nanorods, (b) silica–gold core–shell nanoparticles, and (c) gold nanocages.....	3
Figure 1.2 Scheme of the three different virus surface that are available for chemical and genetic modification. Interior, exterior and the interface have been utilised for the formation of multifunctional viral–cage–based materials.....	6
Figure 1.3 Icosahedral plant VNPs/VLPs-based nanomaterials and their applications in nanotechnology and nanomedicine.....	9
Figure 1.4 A: CPMV capsid that include the S and L subunits that form three $\beta$ sandwich domains in asymmetric icosahedral unit. Two domains of L subunit occupy B5 (red), and C (green) positions, S subunit occupies A (blue) positions around the fivefold axis. Sixty copies of the S and L subunits insert in the viral capsid. B: A ribbon diagram of three $\beta$ barrel domains which comprise an asymmetric icosahedral unit. C: A space-filling drawing of CPMV capsid. The particle diameter is 30 nm. D: Two RNA molecules of virus genome are encapsidated separately, both types of the particles are required for infection. The empty particles are formed. E: the two RNA molecules, comprise the CPMV genome, with RNA-2 encoding L and S capsid proteins.....	13
Figure 1.5 Illustration of the surface exposed amines and carboxylates of the CPMV capsid.....	16
Figure 1.6 Different types of plant viruses used in drug delivery.....	20
Figure 1.7 The stages in the life cycle of plasmodium. ....	24
Figure 1.8 Structures of the currently antimalarial drugs in clinical use. ....	27
Figure 1.9 summary of findings regarding the roles of various substituents on 4-aminoquinolines with respect to antiplasmodial activity and activity against CQ resistant strains .....	29
Figure 1.10 structures of some 4-aminoquinoline antimalarials.....	30
Figure 1.11 Accumulation of CQ in the parasitic food vacuole .....	32
Figure 1.12 metabolic diversion of glucose in a blood vessel containing infected red blood cells shown how high level of glucose consumption may divert glucose away from host tissue .....	36

Figure 2.1 A typical UV/Vis spectrum of purified CPMV particles in phosphate buffer pH 7.....	45
Figure 2.2 Agarose gel imaging for wt CPMV at different concentrations staining with ethidium bromide lane 1, CPMV (24 a.a missing) 10 µg/ ml, lane 2 CPMV 40 µg/ml lane 3, CPMV (24 aa missing) 40 µg/ ml. ....	46
Figure 3.1 Asymmetric unit of compound (1) with atoms drawn as 50% probability ellipsoids. (Selected hydrogen atoms are labelled). The crystal structure confirms the expected composition.....	66
Figure 3.2 The UV chart shows the maximum absorbance of 0.093 mg/ml of wild type CPMV in sodium phosphate buffer. ....	74
Figure 4.1 Agarose gel imaging of CPMV before and after modification: Lane1, 2, 4 wt CPMV in different concentrations, lane3 CPMV-CQp, lane5 CPMV-CQp and lane6 CPMV–NHS-ester. ....	78
Figure 4.2 Modified and unmodified wt CPMV with CQp on a 1.2 % (w/v) agarose gel without staining: lane 1 wt CPMV, lane 2 CPMV-NHS-ester, lane 3 CQp in 100% DMSO and lane 4 CPMV-CQp. ....	79
Figure 4.3 Zeta potential measurement of modified and unmodified CPMV (A) wt CPMV (B) CPMV-NHS-ester and (C) CPMV-CQp particles. ....	81
Figure 4.4 A A typical UV/Vis spectrum for modified and unmodified CPMV with CQp; Blue line is wt CPMV, purple line is CQp and red line is CPMV-CQp. The CQp absorption maxima still observed after conjugation with CPMV as shown in purple arrows.....	83
Figure 4.5 UV/ Vis spectrum of wt CPMV: A- before and after modification with CQ-ala and B- before and after modification with CQ-val, both CQ derivatives have kept their absorption maxima after conjugation with CPMV as shown in blue arrows.....	86
Figure 4.6 Agarose gel electrophoresis 1.2 % w/v agarose, 60 V: Lane 1- wt CPMV, 2- CPMV- CQp, 3- empty , 4- CPMV- CQ- ala, 5- CQ-ala, 6- CPMV-CQ-val, 7- CQp and 8- CQ-val.....	87
Figure 4.7 Coomassie stained 12% SDS-PAGE of 1. wt CPMV; 2. CPMV-CQ-val ; 3. CPMV-CQ- ala. CQ-ala has extra band easily noticeable on the gel confirm the	

conjugation. CPMV-CQ-val showed a slight cleavage on the small subunit (lane 2) compared to unmodified CPMV. ....	88
Figure 4.8 Digital image of agarose gel electrophoresis 1.2 % w/v agarose, 60 V, lane 1 wt CPMV 0.05 mg/ml, 2 CPMV-G.A, 3 CPMV- G.A., 4 G.A in MQ water and 5 G.A in PBS buffer. ....	90
Figure 4.9 The UV/Vis spectrum of wt CPMV and CPMV-G.A. ....	90
Figure 4.10 A, Modified and unmodified CPMV particles on a 1.2 % (w/v) agarose gel with ethidium bromide (EtBr) staining: lane 1 wt CPMV; 2 CQp ; 3 CPMV- dye after 2washes ; 4 CPMV-CQp-dye after 2washes ; 5 CPMV- dye after 1 wash; 6, CPMV-CQp- dye after 1 wash ; 7, CPMV- dye after 3washes and 8, CPMV-CQp- dye after 3 washes. B, Unstained agarose gel imaging of CPMV particle before and after labelling with Alexa Fluor 488 dye: lane1 wt CPMV, 2 CPMV-CQ-p, 3 CPMV- dye. ....	92
Figure 4.11 modified and unmodified CPMV particles on a 1.2 % (w/v) agarose gel with ethidium bromide (EtBr) staining: lane 1 wt CPMV; 2 CPMV-CQp; 3 CPMV- dye after 1 wash ; 4 CPMV- dye after 2 washes; 5 CPMV- CQp; 6 CPMV- CQp- dye after 2 washes; 7, 8 CPMV- dye elute. ....	93
Figure 4.12 UV–Vis spectrum of CPMV-dye after washing with sodium phosphate buffer pH 7. The maximum absorbance for CPMV and Alexa Fluor dye still noticeable after conjugation (red arrows). ....	95
Figure 4.13 agarose gel imaging of CPMV stained with ethidium bromide: lane1 wt CPMV lane 2 CPMV- dye, lane 3 CPMV-CQp- dye after 1 wash, lane 4 CPMV- dye elute after1wash, lane 5 CPMV- dye after 1 wash, lane 6 CPMV-dye elute after 2 washes, lane7 CPMV dye-elute after 3 washes. Clear cleavage of both S units in lanes 3 and 5 emphasised by red arrows corresponds to the CQp and dye conjugation. ....	95
Figure 4.14 agarose gel imaging of CPMV staining with ethidium bromide : lane 1 wt CPMV, lane 2 CPMV- dye before purification , lane 3 CPMV -dye after 1 wash, lane 4 CPMV- dye elute after1 wash, lane 5 CPMV- dye after 2 washes, lane 6 CPMV- dye elute after 2washes. ....	97
Figure 4.15 Cowpea mosaic virus (CPMV) particles on a 1.2 % (w/v) agarose gel stained with EtBr: lane 1 wt CPMV, 2 CPMV- dye 10h dialysis, 4 CPMV- dye 8h dialysis, 6 CPMV- dye 19h dialysis and 8, CPMV- dye 6h dialysis. ....	98

Figure 4.16 Cowpea mosaic virus (CPMV) particles on a 1.2 % (w/v) agarose gel stained with EtBr: lane 1 wt CPMV, 2 CPMV- dye 16h dialysis, 3 CPMV- dye 22h dialysis, 4 CPMV- dye 19h dialysis, 6 CPMV- dye elute.....	99
Figure 4.17 UV/Vis spectrum of CPMV- dye after dialysis against PBS buffer pH 7.	100
Figure 4.18 V/Vis spectrum of CPMV-dye and CPMV-CQp-dye with and without using EDC/NSH as conjugation reagents to active the carboxyl group of CQp before modifying with CPMV after 22h dialysis against PBS buffer pH 7.....	101
Figure 4.19 Cowpea mosaic virus (CPMV) particles on a 1.2 % (w/v) agarose gel with and without staining: A and B , lane 1 CPMV 0.05mg/ml, 2 CPMV- dye before dialysis, 3 CPMV-CQp,4 CPMV-dye 22h dialysis, 5 CPMV-CQp-dye before dialysis, 6 CPMV-CQp-dye 22h dialysis, C, lane 3 CPMV- dye 10h dialysis, 4 CPMV- dye 22h dialysis, 5 CPMV- CQp, 6 CPMV- CQp- dye before dialysis, 7 CPMV–CQp- dye 10h dialysis, 8 CPMV- CQp- dye 22h dialysis. ....	102
Figure 4.20 Cowpea mosaic virus (CPMV) particles on a 1.2 % (w/v) agarose gel with EtBr staining:, lane 1 wt CPMV, 2 CPMV-dye before dialysis, 3 CPMV-dye 6h dialysis, 4 CPMV- dye 8h dialysis, 5 CPMV-dye 22h dialysis, 6 CPMV-CQp- dye 6h dialysis, 7 CPMV-CQp-dye 8h dialysis, 8 CPMV-CQp-dye 22h dialysis . Extra bands have been observed in lane 2, 3 and 4 (shown in red arrows) corresponding to CPMV dye conjugation.....	103
Figure 4.21 V/Vis spectrum of CPMV- dye and CPMV- CQp- dye after 22h dialysis against PBS buffer pH 7. The absorbance of CPMV at 260 nm and the absorbance of dye at 494 nm shown the successful conjugation between modified and unmodified CPMV with Alexa Fluor dye.....	103
Figure 4.22 UV/Vis spectrum of CPMV-dye and CPMV-CQp-dye after 16h dialysis against PBS buffer pH 7.....	105
Figure 4.23 Modified and unmodified CPMV particles on a 1.2 % (w/v) agarose gel with EtBr staining; lane 1,3 and 6 wt CPMV, 2 CPMV- dye before dialysis, 4 CPMV- dye 16h dialysis, 5 CPMV- CQp- dye before dialysis, 7 CPMV- CQp- dye 16h dialysis. .	105
Figure 4.24 UV/Vis spectrum of CPMV-CQ-ala-dye and CPMV-CQ-val- dye after 4h dialysis. The absorbance of both CQ-ala and CQ-val still noticeable after medication with Alexa Fluor dye (red and purple arrows). ....	107

Figure 4.25 Agarose gel electrophoresis 1.2 % w/v agarose, 60 V with EtBr staining: lane 1-wt CPMV, 2- CPMV- dye, 3- CPMV-CQ- ala-dye, 4- CPMV-CQ-ala-G.A -dye, 5- CPMV-CQ- ala-Glu- dye, 6- CPMV- CQ-ala-Glu –dye .....	108
Figure 4.26 Agarose gel electrophoresis 1.2 % w/v agarose, 60 V with EtBr staining. lane 1- CPMV- dye, 2- CPMV -CQ-val-dye, 3- CPMV-CQ-val-G. A-dye, 5- CPMV-CQ- val-Glu- dye and 6- CPMV-dye. ....	108
Figure 4.27 The image of agarose gel electrophoresis 1.2 % w/v agarose, 60 V, stained with ethidium bromide: Lane1 wt CPMV, lane 2 CPMV- P.A, lane3 CPMV-B.A. ....	110
Figure 4.28 The image of SDS gel electrophoresis, 180 V, stained with Coomassie: Lane1 wt CPMV, lane 2 CPMV- P.A, lane3 CPMV- B.A.....	110
Figure 4.29 Stained TEM images of externally modification of CPMV- P.A shown the denaturation of CPMV (between blue arrows). ....	111
Figure 4.30 A. Digital image of agarose gel electrophoresis 1.2 % w/v agarose, 60 V, stained with Coomassie: Lane1, CPMV-B.A -dye and lane 2, wt CPMV, B. UV/Vis spectrum of CPMV- B.A -dye modification.....	113
Figure 4.31 UV/Vis spectrum of the conjugation of B.A with N <sub>3</sub> -bodipy dye.....	114
Figure 4.32 The UV/Vis spectrum shows the maximum absorbance of wt CPMV, CPMV-CQp and CPMV-CQp-G.A .....	116
Figure 4.33 Digital image of agarose gel electrophoresis 1.2 % w/v agarose, Lane 1- marker,2- wt CPMV, 3-CPMV- ester, 4-CPMV- CQp, 5- CPMV-CQp- G.A.....	117
Figure 4.34 The UV spectrum of wt CPMV, CPMV-G. A and CPMV-G. A-CQp. ...	119
Figure 4.35 Digital image of agarose gel electrophoresis 1.2 % w/v agarose, 60 V, lane 1 wt CPMV, 2 CPMV-CQp, 3 CPMV-CQp-G. A, 4 CPMV-G.A and 5 CPMV-G.A-CQp. ....	119
Figure 4.36 The image of agarose gel electrophoresis 1.2 % w/v agarose, 60 V, stained with ethidium bromide. Lane1 wt CPMV, lane 2 CPMV- dye, lane3 CPMV-CQp-dye, lane 4 CPMV-CQp-G.A-dye. ....	122
Figure 4.37 UV /Vis spectrum of CPMV- dye, CPMV-G.A- dye and CPMV-G.A-CQp- dye. ....	123

Figure 4.38 UV/Vis spectrum of CPMV- dye (green line), CPMV-G.A –dye (red line) and CPMV-G.A-CQp –dye (blue line) after 4h dialysis.....	123
Figure 4.39 Stained TEM image of wt CPMV and B- CPMV-CQp-G.A.....	124
Figure 4.40 UV/ Vis spectrum of singly and doubly functionalised CPMV particle. .	125
Figure 4.41 UV / Vis spectrum of singly and doubly functionalised CPMV particle. .	125
Figure 4.42 Agarose gel (1.2%) of CPMV particles visualised by ethidium bromide staining (A) and Coomassie blue staining (B). Lane 1, wt CPMV 2, CPMV-CQ-ala 3, CPMV-CQ -ala-G.A 4, CPMV- CQ- ala- Glu 5, wt CPMV 6, CPMV- CQ- val 7, CPMV -CQ -val- G.A and 8, CPMV-CQ- val- Glu. ....	126
Figure 4.43 TEM images of (A) uranyl acetate stained CPMV-CQ-ala-G.A, (B) uranyl acetate stained CPMV-CQ-val-G.A.....	127
Figure 4.44 Digital image of agarose gel electrophoresis 1.2 % w/v agarose, 60 V, stained with A: ethidium bromide, B: Coomassie, Lane 1: wt CPMV, lane 2: CPMV-CQp and lane 3 CPMV-CQp-Glu.....	129
Figure 4.45 UV /Vis spectrum of CPMV before and after modification with CQp and Glu. ....	129
Figure 4.46 SDS-PAGE of CPMV particles, 180 V, stained with Coomassie: Lane 1- CPMV- CQ- ala, 2- CPMV- CQ- ala- Glu, 3- CPMV -CQ- ala- G. A, 4- wt CPMV, 5- CPMV-CQ-val, 6- CPMV-CQ-val-G.A and 7-CPMV-CQ-val-Glu.....	130
Figure 4.47 A The UV spectrum of CPMV wild type, CPMV-CQp and CPMV-CQp-Glu- dye after 8h dialysis. ....	132
Figure 4.48 Digital image of agarose gel electrophoresis 1.2 % w/v agarose, 60 V, stained with both ethidium bromide and Coomassie staining Lane 1: wt CPMV, lane 2: CPMV- dye 8h dialysis, lane3: CPMV-CQp -dye 8h dialysis, lane4:CPMV-CQp-Glu-dye 8h dialysis, lane5:CPMV-dye 10h dialysis, lane6:CPMV-CQp- dye 10h dialysis and lane7:CPMV-CQp-Glu-dye 10h dialysis. ....	133
Figure 4.49 Digital image of agarose gel electrophoresis 1.2 % w/v agarose, 60 V, stained with A: ethidium bromide staining, B: Coomassie staining: Lane 1. wt CPMV, lane 2. CPMV-ester, lane3. CPMV-CQ-ala-Glu, lane4. CPMV-CQ-val-Glu. ....	134
Figure 4.50 UV/Vis spectrum of singly and doubly functionalised CPMV particles...	135

Figure 4.51 UV/Vis spectrum of singly and doubly functionalised CPMV particles...	135
Figure 5.1 Digital image of agarose gel electrophoresis 1.2 % w/v agarose, 60 V, stained with A: Coomassie staining B: EtBr staining, lane 1: wt CPMV, lane 2: CPMV-NHS-ester, lane3: CPMV-Fc. For C: Coomassie staining D: EtBr staining, Lane 1, CPMV- CQp –Fc, 2, CPMV-CQ-ala-Fc, 3, CPMV-CQ-val- Fc and 4,wt CPMV .....	145
Figure 5.2 Examples of zeta potential results for (A) wt CPMV, (B) CPMV-Fc.....	147
Figure 5.3 UV/Vis spectrum of doubly functionalised wt CPMV particles. Blue line unmodified CPMV, orange line CPMV-CQp-Fc, green line CPMV-CQ-ala-Fc and red line CPMV-CQ-val-Fc.....	148
Figure 5.4 UV/Vis spectrum of modified and unmodified CPMV, A. CPMV-CQ -ala-G.A to aminoferrocene and B.CPMV-CQ-val-G.A to aminoferrocene.....	152
Figure 5.5 Agarose gel electrophoresis 1.2 % w/v agarose, 60 V.1- wt CPMV, 2- CPMV-Fc, 3-CPMV-CQp-G.A-Fc, 4- CPMV-CQ-ala-G.A-Fc and 5-CPMV-CQ-val-G.A-Fc. ....	153
Figure 5.6 Transmission electron microscopy image of Cowpea mosaic virus (CPMV) particles displaying triple modification, A. CPMV-CQp-G.A-Fc, B.CPMV-CQ-ala-G.A-Fc and C. CPMV-CQ-val-G.A-Fc.....	154
Figure 5.7 A: Agarose gel electrophoresis 1.2 % w/v agarose, 60 V. B: SDS-PAGE .Lane1, wt CPMV 2, CPMV-Fc-CQp 3, CPMV-Fc-CQ-ala 4, CPMV-Fc-CQ-val and 5, CPMV-Fc. An extra band (shown in black arrow) may be confirmed the conjugation of Fc to the external surface of CPMV particle.....	155
Figure 5.8 Cyclic voltammogram of ferrocene modified CPMV particles at 15mV. (Fc1), CPMV- Fc. (Fc2), CPMV-CQ-ala-Fc. (Fc3), CPMV-CQp-Fc and (Fc4), CPMV-CQ-val-Fc.....	161
Figure 5.9 Cyclic voltammogram for some of ferrocene modified CPMV-CQ particles at 30mV. Red line is Fc2, grey line is Fc3 and yellow line is Fc4. Very weak reduction signal has been observed (shown by black arrow) may be due to irreversible oxidation of alanine or could be presented from the highest potential signal.....	162
Figure 5.10 Variation of peak current with the square root of the scan rate of; A. anodic current and B. cathode current. ....	163

Figure 6.1 Chemical structure of haem, BH, and haemozoin. The structure of haemozoin, showing hydrogen bonds between BH units as dotted lines, and coordinate bonds between iron atoms and carboxylate side chains as red lines.....	169
Figure 6.2 Process of haemoglobin degradation and haem detoxification by intraerythrocytic malaria parasite.....	171
Figure 6.3 Structures of CQ and related 4-aminoquinolines having antimalarial activity. ....	172
Figure 6.4 Time courses of BH crystal growth in acetate buffer in the presence of 10 $\mu$ M and 50 $\mu$ M CQp.....	177
Figure 6.5 Time courses of BH crystal growth in acetate buffer in the presence of 10 $\mu$ M and 50 $\mu$ M of CQ-ala. ....	177
Figure 6.6 Time courses of BH crystal growth in acetate buffer in the presence of 10 $\mu$ M and 50 $\mu$ M CQ-val. ....	178
Figure 6.7 Time courses of BH crystal growth in acetate buffer in presence of 10 $\mu$ M CQ-derivatives and commercial CQ.....	180
Figure 6.8 Inhibition of BH growth after treatment with 10 - 50 $\mu$ M CQp. The fraction of haem converted to BH was calculated from the absorbance at two different wavelengths (400 and 650 nm) for treated and untreated BH. ....	182
Figure 6.9 Inhibition of BH growth after treatment with 10 - 50 $\mu$ M CQ-ala. The fraction of haem converted to BH was calculated from the absorbance at two different wavelengths (400 and 650 nm) for treated and untreated BH. ....	182
Figure 6.10 Inhibition of BH growth after treatment with 10 - 50 $\mu$ M CQ-val. The fraction of haem converted to BH was calculated from the absorbance at two different wavelengths (400 and 650 nm) for treated and untreated BH. ....	183
Figure 6.11 Inhibition of BH growth using 10 - 50 $\mu$ M of CQ-alanine and commercial CQ as BH inhibitors. ....	184
Figure 6.12 FT-IR spectrum of BH formation without treatment with CQ-derivatives. The two most main absorbance peaks of the BH shown by red arrows.....	185
Figure 6.13 Scanning electron micrographs (SEM) of (A) BH formation without treatment, (B) BH formation with 10 $\mu$ M CQp, (C) BH formation with 10 $\mu$ M CQ-ala,	

(D) BH formation with 10 $\mu\text{M}$ CQ-val (red arrows shown the differences of BH crystal structures).....	186
Figure 6.14 Comparative Analysis of Different Synthetic BH. Scanning electron micrographs of (A) BH formation without treatment, (E) BH formation with 50 $\mu\text{M}$ CQp, (F) BH formation with 50 $\mu\text{M}$ CQ-ala, and (G) BH formation with 50 $\mu\text{M}$ CQ-val (red arrows shown the differences of BH crystal structures). .....	188
Figure 6.15 X-ray powder diffraction patterns (Cu) of A. published BH-crystal, B. synthesised BH without treatment. The pattern of synthetic BH from this work is identical to that previously reported as shown in red arrows.....	189
Figure 6.16 X-ray powder diffraction patterns (Cu) of B. synthesised BH without treatment, C. BH-CQp treated, D. BH-CQ-val treated and E. BH-CQ-ala treated.....	190
Figure 6.17 BH formation with and without 10 mM of both iron oxide and ( $\text{Fe}^{2+}/\text{Fe}^{3+}$ ) mixture. ....	192
Figure 6.18 FT-IR spectra of BH after different treatments. A. BH formation without treatment. B. BH formation after $\text{Fe}^{2+}/\text{Fe}^{3+}$ treatment, C. BH formation after iron oxide treatment.....	195
Figure 6.19 FTIR spectra for iron oxide ( $\text{Fe}_3\text{O}_4$ ).....	195
Figure 6.20 Scanning electron micrographs of different synthetic BH. (A) BH formation without treatment, (B) iron oxide nanoparticles ( $\text{Fe}_3\text{O}_4$ ), (C) BH formation with $\text{Fe}^{2+}/\text{Fe}^{3+}$ , (D) BH formation with iron oxide. The change in the crystal shapes was highlighted by red arrows.....	196
Figure 7.1 Antimalarial activity of CQp and control CQ against <i>Plasmodium falciparum</i> (strain 3D7). ....	201
Figure 7.2 Antimalarial activity of CQ-ala against <i>Plasmodium falciparum</i> (strain 3D7). ....	202
Figure 7.3 Antimalarial activity of CQ-derivatives analogues against <i>P. falciparum</i> (strain 3D7). ....	204
Figure 7.4 A: Microscopic image shown the contamination due to pollution by bacteria in CPMV-CQ-ala and CPMV-CQ-val solutions, B: Example of a 96-well plate were screened for their ability to inhibit BH formation. The dark colour observed from CPMV	

samples in each plate identical the contamination (between black arrows) compared with the light colour of control CQ. ....	206
Figure 7.5 Antimalarial activity of CPMV-CQ-ala analogues against <i>P. falciparum</i> (strain 3D7). ....	207
Figure 7.6 Antimalarial activity of CPMV-CQ-derivatives analogues against <i>P. falciparum</i> (strain 3D7). Two different CQ-ala samples have been tested one was dissolved completely in DMSO and another one was dissolved in 50% volume ratio DMSO/ PBS buffer. ....	209
Figure 7.7 Antimalarial activity of CPMV-Fc analogues against <i>P. falciparum</i> (strain 3D7). ....	213
Figure 7.8 Antimalarial activity of CPMV-CQ-derivatives-Fc analogues against <i>P. falciparum</i> (strain 3D7). Sample 4 is CPMV-CQp-Fc and sample 5 is CPMV-CQ-ala-Fc. ....	215

## *List of tables*

Table 1.1 A range of virus particles that have been investigated and utilized for nanobiosciences /technology.....	7
Table 1.2 Factors determining the probability of selection of de novo antimalarial drug resistance. ....	26
Table 3.1 IR and <sup>1</sup> HNMR spectroscopic data for compound (1).....	66
Table 3.2 <sup>1</sup> HNMR and IR spectroscopic data for CQ-derivatives .....	70
Table 4.1 The reaction of CPMV, CPMV- CQp and CPMV-CQp-G. A with Alexa Fluor dye 488 after 8h dialysis against 500 ml PBS buffer. ....	120
Table 4.2 The reaction of CPMV, CPMV- G. A and CPMV-G.A- CQp with Alexa Fluor dye 488 after 8h dialysis against 500 ml PBS buffer. ....	121
Table 4.3 The reaction of CPMV, CPMV-CQp and CPMV-CQp-Glu with Alexa Fluor dye 488 after 8-10h dialysis against 500 ml PBS buffer pH7.....	131
Table 4.4 The reaction of CPMV, CPMV-CQ-ala, CPMV-CQ-ala-G.A and CPMV-CQ-ala-Glu with Alexa Fluor dye 488 after 8h dialysis against 500 ml PBS buffer. ....	136
Table 4.5 The reaction of CPMV, CPMV- CQ-val, and CPMV-CQ-val-G. A and CPMV-CQ-val-Glu with Alexa Fluor dye 488 after 8dialysis against 500 ml PBS buffer. ....	137
Table 5.1 The minimum and maximum number of attached ferrocene (Fc2) per particle .....	158
Table 5.2 The minimum and maximum number of attached ferrocene (Fc3) per particle. ....	159
Table 5.3 The minimum and maximum number of attached ferrocene (Fc4) per particle. ....	160
Table 5.4 The ratio of the peak currents to the square root of the scan rate. ....	164
Table 5.5 The average number of attached ferrocene per CPMV particle using ICP-OES and electrochemical measurements.....	165
Table 6.1 The effect of CQ-derivatives on BH formation after 800 sec.....	179
Table 6.2 The effect of CQ-derivatives on BH formation after 20 h reaction using purification method. ....	181

Table 7.1 Proliferation of <i>P. falciparum</i> for CPMV-CQ-ala inhibitor assessed using the (LDH) assay. ....	210
Table 7.2 Proliferation of <i>P. falciparum</i> for CPMV-CQ-val inhibitor assessed using the (LDH) assay. ....	211
Table 7.3 Proliferation of <i>P. falciparum</i> for CPMV-Fc inhibitor assessed using the (LDH) assay. ....	212
Table 7.4 IC <sub>50</sub> value against <i>P. falciparum</i> 3D7 for some of known antimalarial drugs. ....	216

## *List of Schemes*

Scheme 3.1 Synthesis of (7-Chloroquinolin-4-yl) alanine (2a) .....	68
Scheme 3.2 Synthesis of (7-Chloroquinolin-4-yl) valine (2b).....	69
Scheme 3.3 Synthesis of $\beta$ -D-glucosyl urea (3) .....	71
Scheme 3.4 Synthesis of 3,4,5-(trihydroxy-6-(hydroxymethyl) tetrahydro-2-pyran-2-yl) carbamoyl azide (4).....	72
Scheme 3.5 Synthesis of 3, 4, 5-(trihydroxy-6-(hydroxymethyl) tetrahydro-2-pyran-2-yl) carbamoyl -1, 2, 3-triazol-5-yl) acetic acid (5).....	73
Scheme 4.1 Synthesis and decoration of chloroquinoline propionic acid: a-3-amino-1-propanol, 140 °C 24 h b- $\text{KMnO}_4 + \text{NaOH}$ or c- $\text{CrO}_3 +$ periodic acid room temperature for 2h. d- EDC e- NHS f- CPMV.....	82
Scheme 4.2 The modification of CPMV with CQ-ala and CQ-val.....	85
Scheme 4.3 decoration of wt CPMV with glucuronic acid (G.A) .....	89
Scheme 4.4 The modification of CPMV with 3, 4, 5-trihydroxy-6-(hydroxymethyl) tetrahydro-2-pyran-2-yl) carbamoyl -1, 2, 3-triazol-5-yl) acetic acid (Glu).....	112
Scheme 4.5 The modification of CPMV-B.A with $\text{N}_3$ -bodipy dye. ....	115
Scheme 4.6 D ecoration of CQp(2) & G.A(1') on external surface of CPMV particle. .....	118
Scheme 0.7 The modification of CPMV-CQ- derivatives with 3, 4, 5-(trihydroxy-6-(hydroxymethyl) tetrahydro-2-pyran-2-yl) carbamoyl -1, 2, 3-triazol-5-yl) acetic acid.....	129
Scheme 5.1 Activation of carboxylic acids with EDC/NHS to generate an active intermediate that reacts with amine containing molecules to generate a peptide bond.	141
Scheme 5.2 Decoration of CQ- derivatives & Fc on external surface of CPMV particle. .....	150

# ***1 Introduction***

## ***1.1 Nanoparticles***

Nanoparticles are defined as small entities that behave as entire units in terms of their transportation and properties. Nanoparticles have been exploited for their potential applications in the biotechnological, pharmacological and pure technological sectors. They are an intermediate between bulk materials and atomic species. This is where a series of atoms will generate a cluster; a collection of clusters will form a nanoparticle. Large quantities of nanoparticles will aggregate to form a bulk particle, often on the micron scale or above. The majority of nanomaterials have physical properties independent of size, the size of most nanoparticles regularly dictates their physical and chemical properties.<sup>1</sup> The term nano is used to refer to both science and technology; where nanoscience appears within life sciences, physical sciences and materials science. However, nanotechnology has a wider scope as it expands into different disciplines such as; medicine, energy, textiles, transportation, and electronics.

Generally, when the size range of a nanoparticle lies between 1 and 100 nm, the properties are vastly different, depending on the application at hand. If a nanoparticle is very small, the surface area will far exceed their volume, causing larger surface-to-volume ratios than for larger nanoparticles or bulk materials in general.<sup>2</sup> The greater surface area for nanomaterials can mean a much higher reactivity, magnetic properties or conductivity.<sup>3</sup>

However, how nanoparticles are viewed depends on the specific application. There has been a lot of research over recent years to investigate methods of synthesising size specific nanoparticles. This has especially been the case for fields such as heterogeneous catalysis, surface science and very recently pyrolysis. Size specific nanoparticles can

benefit both the activity and selectivity of a number of chemical reactions, as well as gas adsorption for the automotive or CO<sub>2</sub> capture industries.<sup>4</sup>

Moreover, nanoparticles (NPs) are a wide class of materials that not only include synthesised entities. They include particulate substances as a result of side reactions, often in the form of carbonaceous deposits.<sup>5</sup> The importance of these materials was realized when researchers found that particle size can influence the physicochemical properties of a substance for example, their optical properties. Precious metals such as Au, Pt, Ag, and Pd nanoparticles have characteristic colours at ~20 nm, exhibiting red, grey, dark grey and black colours respectively. **Figure 1.1** illustrates this point as it shows the different colours observed by Au NPs synthesized with different sizes and shapes. Variations of size and shape can alter the nanoparticle's physicochemical properties, as mentioned above. These distinctions can be utilised for a variety of applications including bioimaging.<sup>6</sup> As **Figure 1.1** indicates, the colour of the solution changes because of a variation in the aspect ratio, nanoshell thickness and Au % concentration. The alteration of any of these factors influence the light absorption properties of the NPs and thus different reflected colours are observed.<sup>7</sup>

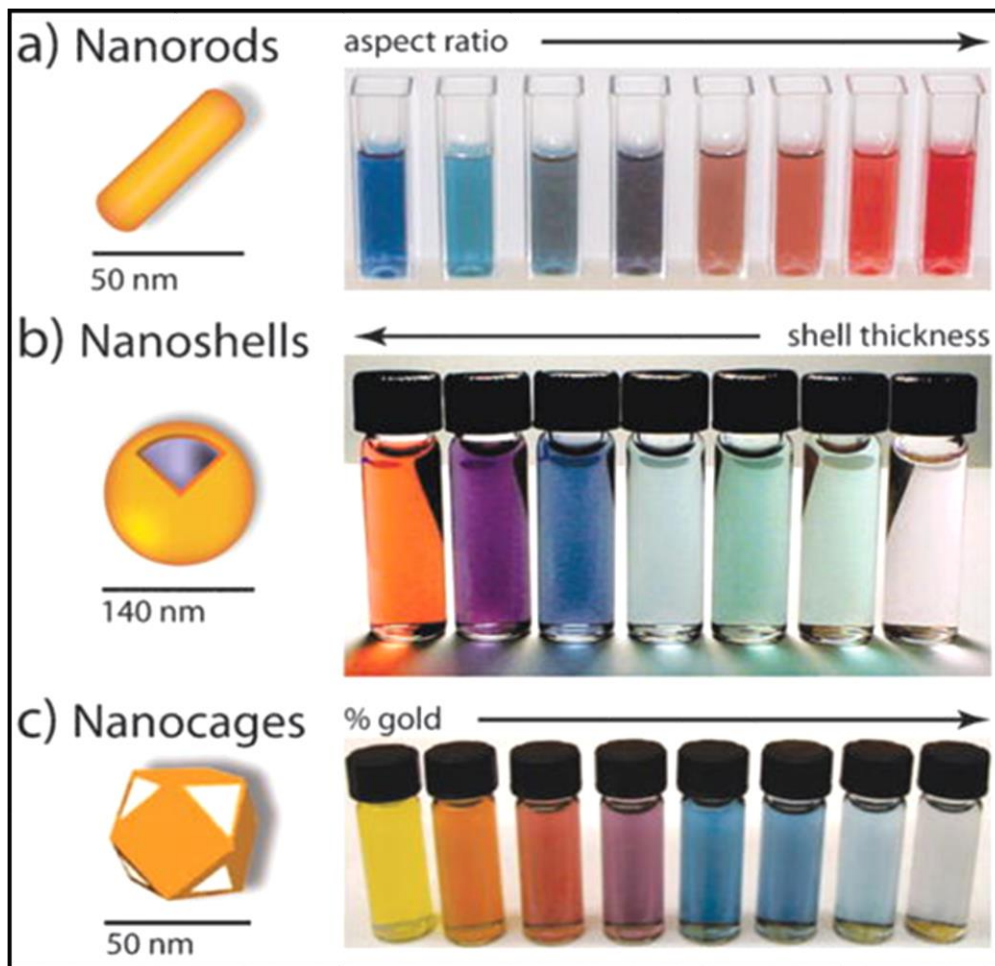


**Figure 1.1 Gold nanoparticles in biomedical applications. (a) Gold nanorods, (b) silica–gold core–shell nanoparticles, and (c) gold nanocages.<sup>6</sup>**

Though NPs are useful for many applications, there are still a number of health concerns due to their uncontrollable use (ingestion / inhalation) and discharge into the environment. Potential health and environmental risks should be considered to ensure NP usage is safe for the environment.<sup>8</sup>

### ***1.1.1 Medicine and nanoparticles***<sup>9</sup>

Nanoparticles have received significant attention in the last decade for their use in drug delivery systems. Some nanoparticle applications in biology and medicine include:

- Biological labels for significant biological markers and molecules in research and diagnosis of illnesses.
- Genetic therapy as gene delivery systems
- Eradication of tumours with medicines or heat
- Biological recognition of disease
- Protein identification
- Drug delivery systems
- Genetic and tissue engineering
- Pharmacokinetics
- For purification and separation of cells and biological molecules
- Investigating the structure of DNA
- MRI investigations

In recent years, these materials have emerged as important players in modern medicine, with clinical applications ranging from contrast agents in imaging to carriers for drug and gene delivery into tumours. The benefits of nanoparticles in modern medicine are diverse. Certainly, there are some instances where nanoparticles are an essential requirement to conduct analyses and carry out therapies that simply cannot be performed otherwise. However, nanoparticles also bring with them unique environmental and societal challenges, particularly in regard to toxicity, especially if metal nanoparticles are used.<sup>10</sup> The work presented in this thesis lies in the area of drug delivery systems. Recently, several substances have been explored for the drug delivery of antimalarial therapy and cancer treatment. Nanoparticles are used to significantly reduce toxicity and side effects

of pharmaceuticals, they are used as a vehicle to deliver small and large molecules by changing their pharmacodynamics and pharmacokinetic properties.<sup>11</sup>

Nanotechnology has grown significantly over recent years and has been applied to medical applications, focusing on the treatment and diagnosis of diseases. Both *in vitro* and *in vivo* drug delivery applications consist of diagnostics, nutraceuticals and developing biocompatible materials.<sup>12-15</sup>

Moreover, nanoparticles can be prepared to inhibit the release of the drug during its location and transportation, until they reach an area at which they are activated. As a result, targeting drugs may be developed.<sup>9</sup>

### ***1.1.2 Virus like particles (VLPs)***

Virus like particles (VLPs) are utilised as scaffolds, coat proteins and templates for the creation of novel nanostructured materials with both inorganic and organic moieties, by mineralization and bioconjugation. Numerous virus coat proteins can accumulate *in vitro* into non-infectious containers called VLPs, normally after genetic modification. Viruses can be found in a multiplicity of distinct shapes, most usually icosahedrons (sphere-like) and rod shaped.<sup>16, 17</sup>

Plant viruses present little biological risk and they are non-infectious toward animals. High expression yields can be achieved when produced in the natural host and heterologous expression systems can increase the yields of VLPs.<sup>18</sup> The majority of viruses have rare properties as they exhibit the ability to self-assemble. This increases the ease of functionalization and provides a high stability in a range of temperatures and pH. Furthermore, some viruses have shown a significant plasticity in their dynamics and capsid structure.<sup>19</sup>

Viruses have three distinct surfaces: the interior, exterior, and the interface between subunits which can be exploited, this is shown in **Figure 1.2**. In addition, the exterior surface has been used for genetic and chemical modification, this allows multivalent ligand display.<sup>20</sup>

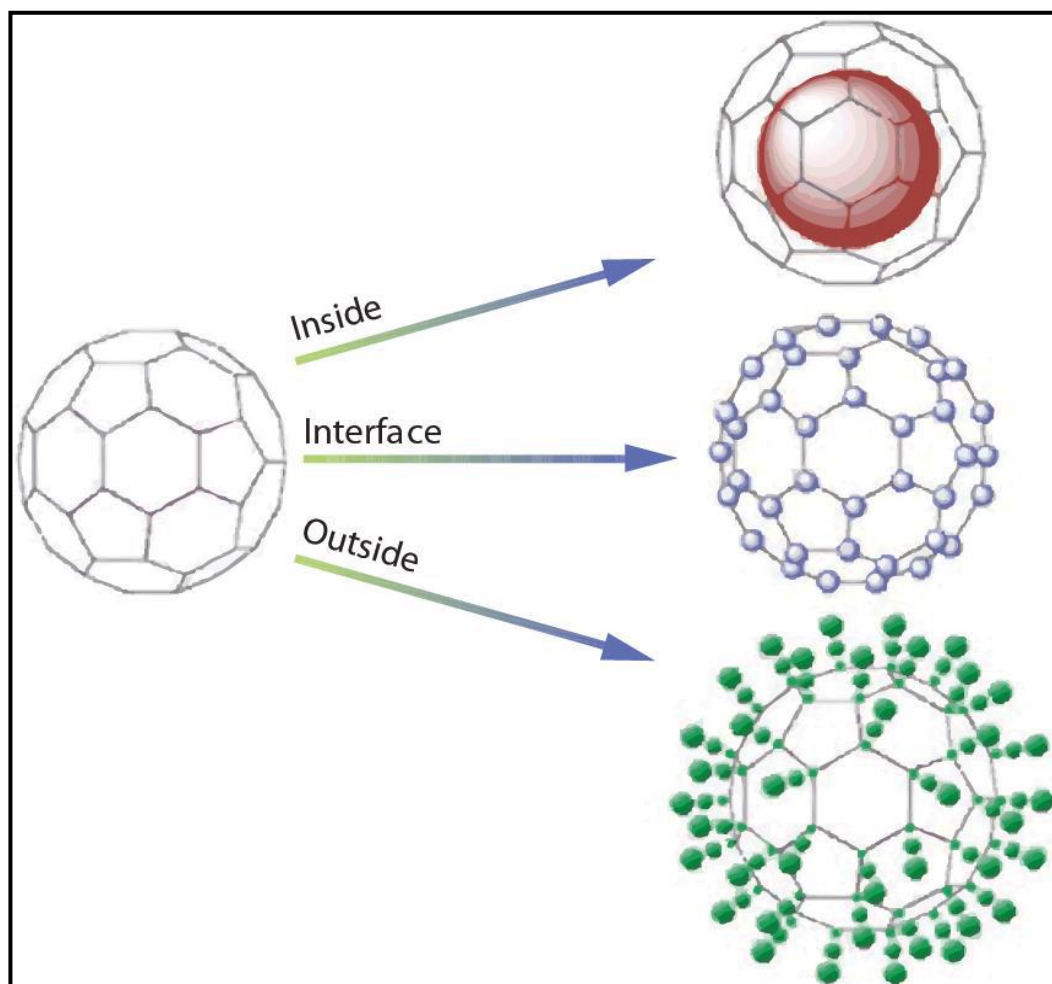


**Figure 1.2** Scheme of the three different virus surface that are available for chemical and genetic modification. Interior, exterior and the interface have been utilised for the formation of multifunctional viral-cage-based materials.<sup>21</sup>

### ***1.1.3 Virus nanoparticles (VNPs)***

Virus nanoparticle (VNP) derived materials in the medical field is becoming a fast moving, high impact area of research. There are several new types of VNPs in development with bacteriophages and plant viruses chosen. These are safer inside humans

than mammalian viruses.<sup>22</sup> Viruses can be considered as nature's delivery systems, VNPs are genetically encoded and self-assemble into discrete and monodisperse structures of a particular size and shape, similar to their inorganic counterparts. Their structures are recognised to atomic determination. However, this level of quality control cannot be achieved as easily with synthetic nanoparticles, until very recently.<sup>23</sup>

Virus particles contain nucleic acid, this can be in the form of ribonucleic acid (RNA) or deoxyribonucleic acid (DNA). This can exist as either double or single stranded (ds or ss), these strands dictate the genetic information and ultimately the function of the capsid.

**Table 1.1** provide a sample of the range of virus particles investigated and typically used for nano-bioscience technologies, most of these are plant viruses.<sup>24</sup>

**Table 1.1 A range of virus particles that have been investigated and utilized for nanobiosciences /technology.**

<b>Virus</b>	<b>Name</b>	<b>Shape</b>	<b>Dimensions (diameter/nm)</b>
Plant viruses	Cowpea mosaic virus	icosahedron	28
Plant viruses	Cowpea chlorotic mottle virus	icosahedron	28
Plant viruses	Tobacco mosaic virus	rigid rod	18 x 300
Plant viruses	Brome mosaic virus	icosahedron	28
Plant viruses	Red clover necrotic mosaic virus	icosahedron	36
Bacteriophages	M13	flexuous rod	6.5 x 900
Bacteriophages	MS2	icosahedron	27
Bacteriophages	T7	head-tail, head has icosahedral symmetry	56
Animal viruses	Chilo iridescent virus	sphere	140

VNPs such as cowpea mosaic virus (CPMV) display a natural affinity to cells and could be utilised for a plethora of biomedical applications. They present a strong scaffold that enables functionalization via chemical conjugation, these therefore can act as an effective drug carrier platform that can be used to target specific cells and tissues.<sup>25</sup>

Viral nanotechnology use VNPs and VLPs of plant viruses as highly useful building blocks for synthetic materials and molecular entrapment systems that can be specifically used for: targeting, therapeutic delivery and non-invasive *in vivo* imaging with high precision and selectivity. Using genetic and protein engineering of icosahedral viruses with a variety of sizes presenting the three surfaces mentioned previously, subunits can be manipulated to fabricate materials with a wide range of desirable properties allowing for biomineralization, encapsulation, infusion, controlled self-assembly and multivalent ligand display of nanoparticles or molecules for varied applications. VNPs and VLPs of icosahedral plant viruses are highly regarded as potential starting points for the development of nanobiomaterials for the fields of nanoelectronics, nanobiotechnology and nanomedicine.<sup>22, 26, 27</sup> an illustration of this is depicted in **Figure 1.3**.

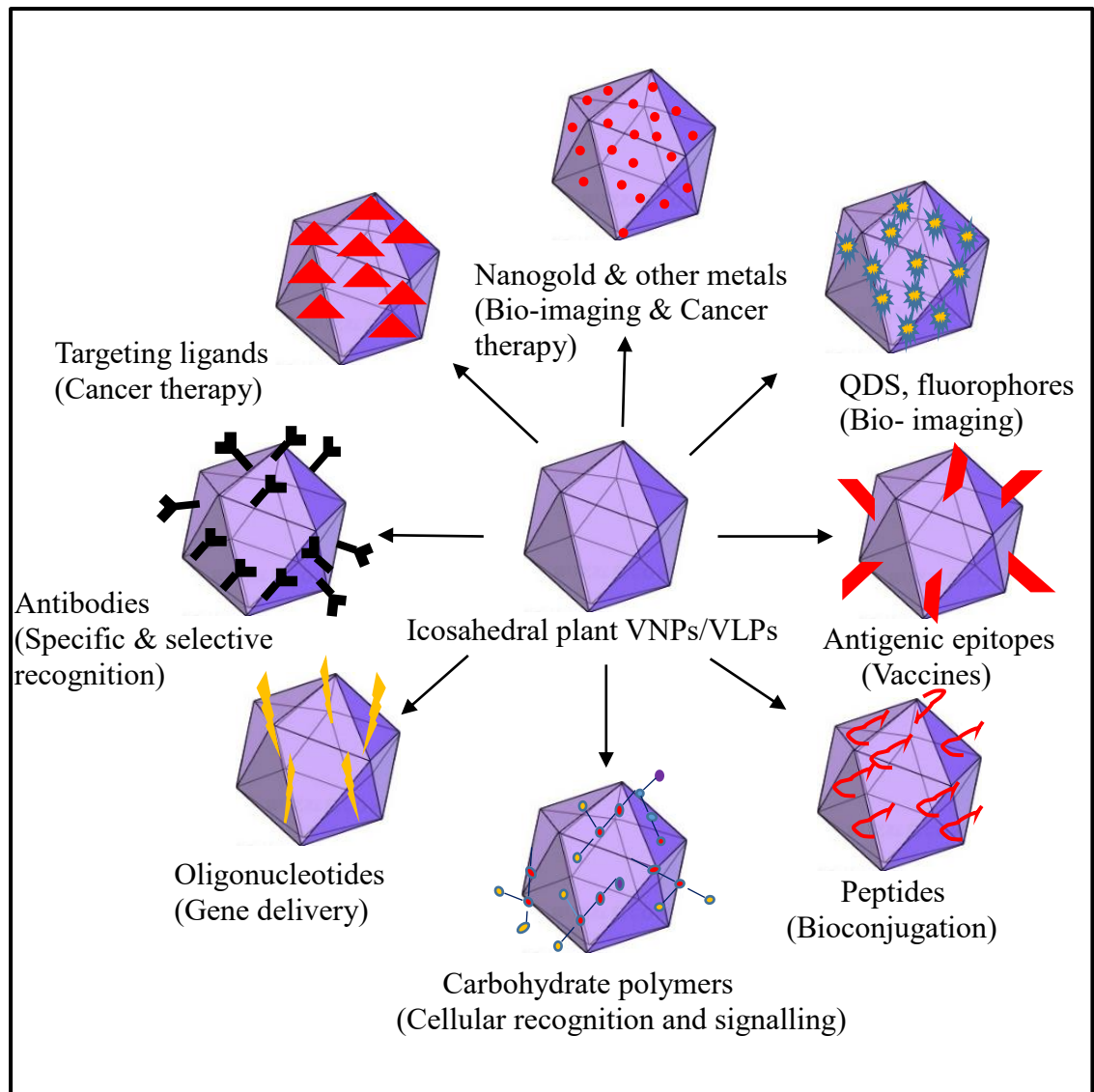


**Figure 1.3 Icosahedral plant VNPs/VLPs-based nanomaterials and their applications in nanotechnology and nanomedicine.<sup>28</sup>**

## ***1.2 The lifestyles of plant viruses***

There are four different lifestyles of plant viruses; these are, persistent, acute, chronic and endogenous. Some viruses may be able to change from one lifestyle to another, particularly between acute and chronic; further changes are possible but their occurrence is very uncommon. Persistent plant viruses have the following features: they are generally asymptomatic, although a lack of uninfected plants in most cases makes this difficult to fully assess; they are transmitted vertically via gametes but not horizontally, they cannot

transfer between cells in plants. Finally, they are also found in every cell including the meristem.<sup>29</sup> So far, all of the viruses in this classification possess double-strands (ds) of RNA genomes. All of the virus families containing persistent plant viruses also have members that infect fungi and particularly endophytic fungi. Ecogenomic studies of wild plants present findings that persistent viruses make up the majority of all plant viruses. Incidence rates are as high as 70% in some plant families, as presented in unpublished data acquired by M. J. Roossinck. This definition of a persistent plant virus is worlds apart from that of the persistent mode of vector transmission. Vector transmission refers to the dispersion of a pathogen via both airborne and land based arthropods. This is therefore not relatable with the lifestyle of the plant virus itself.<sup>30</sup>

Acute plant viruses in contrast to persistent viruses have an alternative life cycle. They are transmitted horizontally, some hosts allow the virus to be transmitted vertically, where vertical transmission can be through embryos or gametes. This is where special proteins are designed and encoded to allow cell-to-cell movement.<sup>29</sup> Acute viruses are flourishing in monoculture. This is comparable with acute animal viruses and it has been suggested that the lifestyle of an acute human virus is typically associated with large built up human areas, as well as domesticated animals.<sup>31</sup>

Acute animal viruses are host specific, strikingly different to the acute plant virus which is specialist. Examples of specialist viruses are the barley stripe virus, this will only infect closely related plants. The cucumber mosaic virus on the other hand has a host range exceeding 1000 species.<sup>32, 33</sup> Specialist viruses spread must faster between like for like plant species, they will therefore spread poorly where multiple species exist. The length of the infection period is often related to the type of virus, subtle differences describe the acute and chronic viruses. An acute virus has three very simple methods of resolution, the first is the death of the host itself. The second is that the host may recover completely

from the infection. Finally, the virus may convert to a chronic version of itself. Chronic plant viruses have a far longer lifespan than the acute virus counterpart, due to the long incubation period, symptoms may or may not be visible.<sup>33</sup>

Another group of plant viruses are called endogenous, this species integrates with the genome of the plant directly. A sizeable amount of these viruses are actually remnants of a benign ancient virus infection. These can be made active under specialised conditions.<sup>34</sup>

Discovering new plant viruses is imperative due to a matter of plant biosecurity. The motivation for identifying new plant viruses impact on the following; the causes of viral diseases in crops, specific virus screening and the ability to sequence viruses regardless of initial symptoms in an ecosystem. The main motivation for this is that new sequencing technologies have paved the way to discover new viruses and a range of other microorganisms.<sup>35, 36</sup>

Plant virus classification is dependent on aspects such as size, shape, type and organisation of genome, chemical structure of proteins and replication. Nucleotide sequences of viral genomes have been determined. However, virus classification will remain important for the future as the majority of phenotypic characters used at the present time will still be relevant.<sup>37</sup>

### ***1.3 Cowpea mosaic virus***

The organic nanobiological platform, cowpea mosaic virus (CPMV) is naturally occurring. The virus capsid contains 60 copies of two subunits – Large subunit (two domains) and small subunit (one domain), the 60 asymmetric units are arranged in icosahedral symmetry, the diameter of the capsid is 28-30 nm.<sup>38</sup> CPMV has two forms of RNA, the first is called RNA-1 (Large) to govern virus replication whereas the smaller RNA-2 controls viral movement protein. Two capsid proteins are shown in **Figure 1.4**,

this highlights both large and small RNA, as well as the domains involved. Both RNA molecules are encapsidated in isometric particles separately, these are fundamental for infection.<sup>39</sup> The nominal yield of CPMV is roughly 0.001 kg per kg of infected leaves, at this scale there are suitable protocols for virus purification.<sup>40</sup>

CPMV is a non-enveloped virus with a diameter of roughly 30 nm. It presents no biological hazard and is not infectious towards mammals. The structure of CPMV is a Picorna-like  $T = 1$  ( $P = 3$ ) protein shell with an asymmetric unit containing three jelly-roll  $\beta$  barrel sandwich folds formed by two polypeptides.<sup>38, 39, 41</sup> Sixty copies of the two protein asymmetric units, comprised of small subunit (A domain) and a second larger subunit, as represented in **Figure 1.4** by both B5 + C domains. The domains are assembled in an icosahedral lattice located around the single-stranded viral genomic RNA, forming the virus particle. There are three components isolated from the typical virus preparation. These are described by their varying densities in sucrose gradients. There are small quantities of the initial component and this contains no RNA, in this respect it is an empty vessel. The molecular mass of the empty capsids is  $\sim 3.94 \times 10^6$  g mol<sup>-1</sup>, this is also represented with the unit of Daltons (Da). The two other components contain the two different RNA molecules required for infection. The two capsid structures give virions with different densities and molecular masses ( $5.16 \times 10^6$  and  $5.98 \times 10^6$  Da).<sup>42</sup> The structure on a whole provides sufficient stability and chemical reactivity to be considered as a molecule, due to its shape and surface structure it is very similar to a dendrimer. The overall design is a very symmetrical, spherical like object.<sup>43</sup>

CPMV is affected freely in a diversity of cell types containing endothelial cells, fibroblasts, macrophages, besides in the central nervous system (CNS), atherosclerotic plaque and inflammatory lesions.<sup>44</sup> CPMV interacts precisely with a surface-displayed form of the cytoskeletal protein vimentin which is responsible for maintaining cell shape,

cytoplasm integrity and stabilizing cytoskeletal interaction. However, internalization of CPMV into alternative cell types is limited by cell surface-expressed vimentin.<sup>45-47</sup>

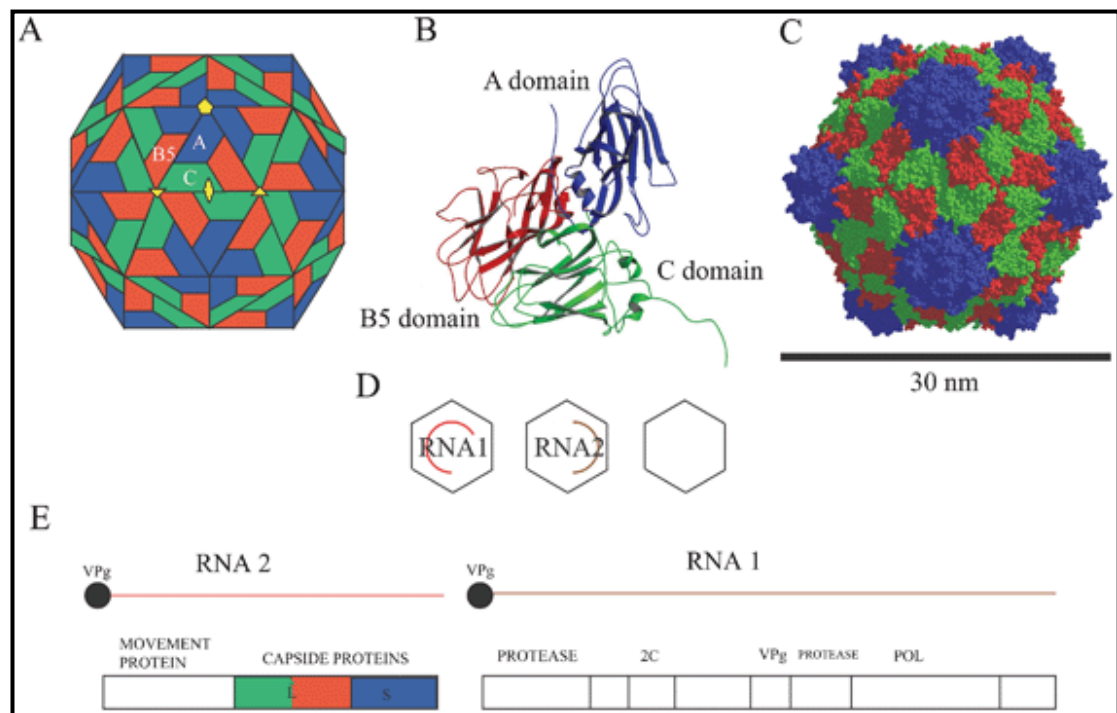


**Figure 1.4** A: CPMV capsid that include the S and L subunits that form three  $\beta$  sandwich domains in asymmetric icosahedral unit. Two domains of L subunit occupy B5 (red), and C (green) positions, S subunit occupies A (blue) positions around the fivefold axis. Sixty copies of the S and L subunits insert in the viral capsid. B: A ribbon diagram of three  $\beta$  barrel domains which comprise an asymmetric icosahedral unit. C: A space-filling drawing of CPMV capsid. The particle diameter is 30 nm. D: Two RNA molecules of virus genome are encapsidated separately, both types of the particles are required for infection. The empty particles are formed. E: the two RNA molecules, comprise the CPMV genome, with RNA-2 encoding L and S capsid proteins.<sup>39</sup>

Due to the robust nature of CPMV, it is easily delivered both intravenously or orally due to its bioavailability.<sup>48,49</sup> CPMV has also been studied for materials applications such as multilayer assembly and chemical scaffolds.<sup>26</sup>

Recent publications and studies have shown that CPMV can be chemically altered.<sup>50</sup> With modification, the CPMV can be used for a number of applications such as tumour specific treatment.<sup>51</sup> By using fluorescently-labelled CPMV particles, a very powerful imagery instrument called an Intravital Microscope, can be used to provide high-resolution images of normal and tumour vasculature *in vivo*. These imaging studies showed that CPMV particles were used before in mouse and chick endothelial cells following intravenous administration in living embryos. This provided very high resolution images in real-time using epifluorescence microscopy.<sup>52</sup>

### ***1.3.1 The advantages CPMV as a nanoparticle***<sup>53</sup>

- The virus can be modified genetically and chemically
- Multi-layer arrays can be constructed
- It can be conjugated with inorganic, organic & biological molecules
- Electro-active nanoparticles can be prepared
- It can work as a template for metallization and mineralization

### ***1.3.2 Chemical modification on wild -type CPMV particles (wt CPMV)***

Protein capsids derived from viruses may be developed and purified on a large scale with relative ease. Recently, chemical derivatization has been possible and this used to broaden the properties and functions to ensure monodisperse particles at the nanoscale. Typical modification is via conjugation to lysine, cysteine, and tyrosine side chains on the surface of the nanoparticle, as well as incorporating unnatural amino acids. Cowpea chlorotic mottle virus (CCMV) and Cowpea mosaic virus (CPMV) are two of the more common protein capsids that have been exploited.<sup>54</sup>

In this work, the wild-type CPMV was modified chemically to prepare a carrier for antimalarial compounds as it provides numerous advantages. Some of which are that the virus synthesis and purification are simple, even on a multigram scale. The virus dendrimer structure is a capsule with both interior and exterior surfaces that can be differentially addressed. The interior surface can in theory be used as the encapsulation site for the active molecule of choice. Finally, the reactivity of the virus is adjustable by genetic and chemical modification.<sup>55,56</sup>

The surface of CPMV particles have exposed accessible functionalities including, carboxylates and phenolic groups which previously have been utilised to selectively attach entities such as metallic and semi-conducting nanoparticles. Organic components such as DNA, fluorescent dyes, carbohydrates, proteins and antibodies have also been exploited.<sup>57</sup> Structural data from the CPMV capsid shows that five outer lysines are solvent-exposed, as observed in **Figure 1.5**.

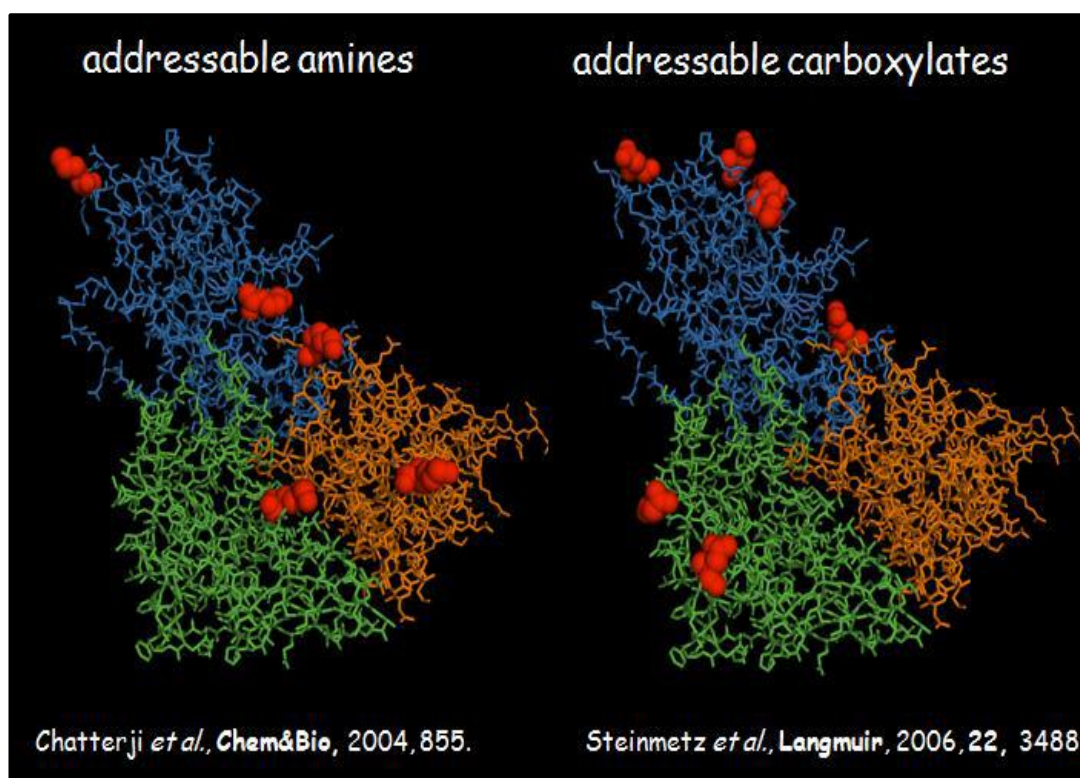


**Figure 1.5** Illustration of the surface exposed amines and carboxylates of the CPMV capsid.<sup>58, 59</sup>

Probing CPMV and mutant free lysine with lysine-selective fluorescent dyes and metals confirmed that all exposed lysine groups are addressable to a different degree.<sup>58, 60</sup> It was found that a maximum quantity of dyes per particle is ~300 when labelling CPMV. However, only 240 can be easily achieved. The most reactive lysines were found to be Lys 38 on S subunit and Lys 99 on C domain of L subunit.<sup>41</sup>

These functional groups have also been found to facilitate the electroless deposition (ELD) of metals such as platinum, nickel, cobalt and iron. It has also been used on various alloyed materials such as nickel–iron and cobalt–platinum on to the surface of CPMV.<sup>61</sup> ELD is a process utilizing chemicals for the reduction of metals onto organic surfaces. This is the alternative for electric current deposition which is not a viable method for these applications.<sup>62</sup>

CPMV has also been previously decorated with Gd ions as well as clinical approval being acknowledged for Gd(DOTA) (DOTA also known as tetraxetan has the chemical composition of  $(\text{CH}_2\text{CH}_2\text{NCH}_2\text{CO}_2\text{H})_4$ ) paramagnetic complexes. Gd ions can coordinatively bind to CPMV, or alternatively Gd(DOTA) complexes can be attached by Cu-mediated azide–alkyne cycloaddition to linkers which have been NHS/EDC conjugated to the CPMV surface exposed amine groups.<sup>63</sup>

Gadolinium attached to CPMV has been found to exhibit a three-fold enhancement in relaxivity compared to free Gd(DOTA). This indicates that modified CPMV has the potential to be a superior contrast agent. The authors also indicated that the utility could be further refined by targeting the CPMV-Gd complexes to particular tissue types of interest by attachment to recognition motifs, which would serve to enhance the local concentration of Gd.<sup>64</sup>

Ferrocene has also been used to decorate CPMV. Previously, the Evans group showed that CPMV can be decorated covalently with 240 redox-active ferrocene moieties.<sup>38, 39</sup>

Evans and co-workers have also shown the versatility of decorated CPMV particles by utilising carboxylate groups attached to the exterior surface. This resulted in an increase in the number and type of addressable surface groups available. This addressability of carboxylates was demonstrated using a carboxylate-selective fluorescent dye, N-cyclohexyl-N'-(4-(dimethylamino)-naphthyl) carbodiimide. A CPMV particle can be decorated with approximately 180 redox active, methyl (aminopropyl) viologen moieties by coupling to the surface carboxylate groups. The display of multiple redox sites on the virus particle surface may lead to the development of novel electron-transfer mediators in redox homogeneous catalysis, to biosensors as well as nanoelectronic devices.<sup>58</sup>

Moreover, CPMV has been recognised as a chemotherapeutic drug for doxorubicin (DOX) delivery. CPMV conjugates 80 DOX molecules bound to outer surface carboxylates of the virus nanoparticle.<sup>65</sup> DOX has been utilised for different cancer treatments, however, it has limited clinical efficiency because of severe adverse side effects such as congestive heart failure and the disadvantage of low solubility. A carrier system is necessary to reduce the hazardous effects and increase the overall efficiency.<sup>66</sup> Viruses provide a means for the improvement of targeted drug delivery vehicles, for example they carry the desired encapsulated material to host cells with high efficiency.<sup>67</sup>

A CPMV capsid includes sixty copies each of the two types of coated proteins, these are organised in the asymmetric unit. The multiple copies of the asymmetric unit provide regularly spaced units, facilitating the coupling and presentation of a widespread of different moieties on the external surface.<sup>26, 68-70</sup> CPMV can also be used to design enzyme-functionalised virus particles.<sup>71</sup> The advantages of enzymes coupled onto VNPs involves multiple conjugation sites, defined geometry and the potential for the construction of multilayer arrays.<sup>72, 73</sup>

Besides the reactive exterior, addressable groups have also been found on the interior of the capsid. CPMV has at least two reactive interior cysteine residues, it is however not found on the exposed exterior surface.<sup>74, 75</sup> It has been shown that small thiol-selective chemical moieties such as ethylmercury phosphate (EMP), 5-maleimidofluorescein and thiol-selective stilbene derivatives readily react with internal cysteines.<sup>41, 75</sup> The L subunit was found to couple with EMP via an internal cysteine residue at the amino acid position 295.<sup>76</sup> On the other hand, 5-maleimidofluorescein was found to attach to cysteine on both the small and large subunits, however, the exact binding site is currently unknown. Small molecules have been found to diffuse into the capsid, this can occur through the small hole that appears in the crystal structure at each five-fold axis.<sup>75</sup> At its narrowest point

the opening of the hole is 0.75 nm, this explains why internal labelling with nanogold, with a diameter of 1.4 nm, could not be achieved.<sup>74, 77</sup>

#### ***1.4 Drug delivery based on plant viruses***

Viral nanoparticles have many potential applications in the medical sector, including their ability to carry larger payloads of drug treatments or contrast agents for imaging. This makes them more viable than current drug delivery systems, Their advanced targeting abilities allow for precision when delivering to specific sites.<sup>78</sup>

There are many advantages for using plant virus as carriers for drug delivery, some of these include: degradability, safety for humans, the possibility of attaching ligands with precise control, availability for additional genetic and chemical manipulations and very flexible methods to prepare and purify them. A variety of plant viruses have been modified by chemical and genetic modification of their inner cavities and their exterior surfaces. These modifications provide suitable sites for the attachment of markers and drug molecules for vascular imaging and tumour targeting without significantly affecting normal tissue .<sup>79</sup>

The development and use of plant a virus is a currently a hot topic in the biochemistry field, this is due to the potential high impact because of their regular geometries and uniformity of size, variety of distinct forms (most commonly icosahedrons, spheres, tubes, and helices) as well as a variety of physical properties such as high stability toward variations of pH, temperature, salt and solvent suitability. Many novel types of viral nanoparticles such as plant viruses are being explored due to their non-infectious nature and safety when delivered to humans as compared with mammalian viruses that may

present a biological risk. **Figure 1.6** shows some of the plant viruses used in drug delivery.<sup>26</sup>

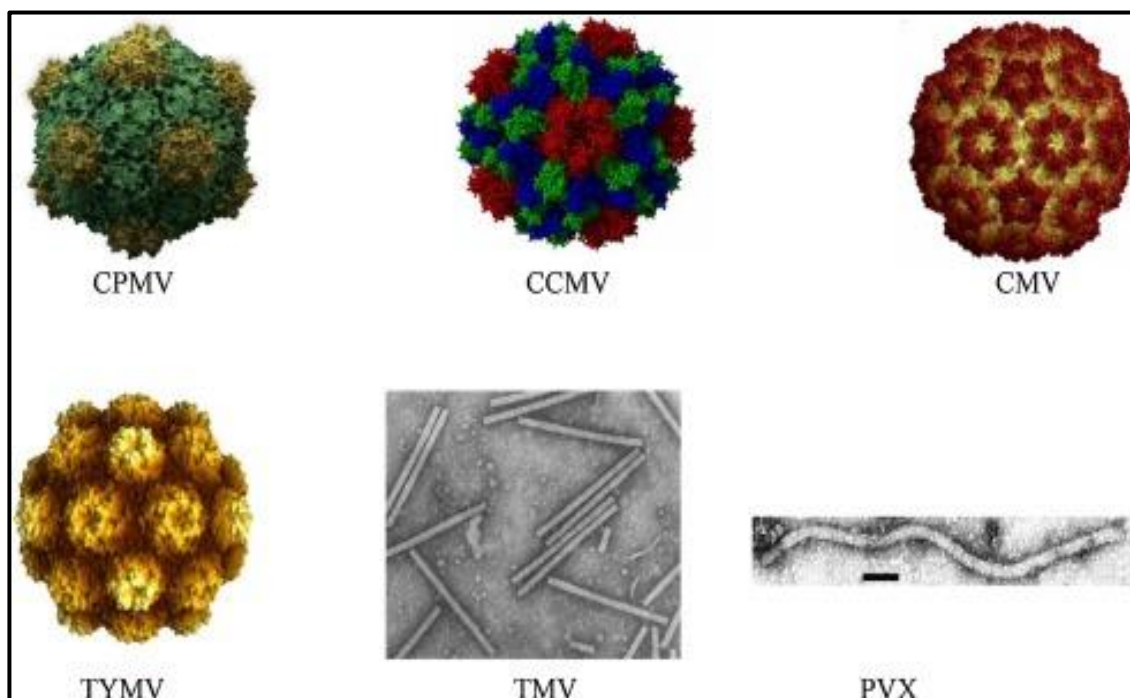


**Figure 1.6** Different types of plant viruses used in drug delivery.<sup>79</sup>

Virus nanocarriers are highly promising scaffolds for the design of delivery systems that are triggered to release their cargo in response to variations in pH, redox status or temperature.<sup>80</sup> Plant based viruses and bacteriophages are typically considered safer delivery vehicles than mammalian viruses because they cannot proliferate in humans and hence are less likely to trigger negative downstream effects.<sup>81-83</sup>

Although drug molecules can be loaded into plant viruses by disassembly or reassembly of the viral capsid, covalent attachment to reactive functional groups on the capsid proteins is also possible. For the attachment of drug molecules to viruses, different chemical reactions have been designed and implemented. First, coat proteins of viruses can be chemically modified. The most common sites of virus capsid used for modification include the side chains of lysine, cysteine and aspartic or glutamic acid residues.

Functionalization is achieved by conjugating antibodies, oligonucleotides, peptides, proteins, carbohydrates, fluorescent reagents and drugs to the capsid through different pathways by using N-hydroxysuccinimidyl ester (NHS), maleimide, isothiocyanate and carbodiimide to bind different amino group containing biomolecules.<sup>67</sup>

The first use of this concept was by Wang et al. They used NHS esters of fluorescein or biotin to modify the surface of the CPMV particle.<sup>41</sup>

A more recent approach is the use of bioconjugation in the form of 'Click Chemistry'. A major advance in chemoselective ligation on virus surfaces utilises copper (I)-catalysed azide-alkyne [3 + 2] cycloaddition, where both VNPs and the desired substrate can be specifically coupled in an orthogonal manner without the use of protecting groups.<sup>84, 85</sup> Copper click chemistry reactions are preferred for bioconjugation because it is bioorthogonal, quicker and more readily proceeds than corresponding NHS or maleimide reactions.<sup>84</sup>

The majority of studies in this field of work involve providing an oral dose of the virus based nanoparticles or by the administration of an injection. There has also been reports showing that the virus can be delivered by inhalation and through the eye.<sup>48</sup> However, until recently, the fate of the (virus) nanoparticles was unknown. As CPMV particles are highly stable and have a slightly negative surface charge at acidic pH, Manchester and co-workers investigated the suitability of CPMV for uptake in the intestinal epithelium as a potential oral delivery agent for vaccine or therapeutic applications. This study confirmed the ability of CPMV to traffic into the systemic circulation from the gastrointestinal tract.<sup>48, 86</sup>

Many different carrier systems are currently under investigation and development for drug delivery and tissue specific imaging. Each system has its own advantages and

disadvantages with regard to physiochemical properties, biodistribution, pharmacokinetics and toxicity.<sup>87</sup> All in all there is, without a shadow of a doubt that a plant virus protein like CPMV with specific properties and surface modifications makes for an attractive drug delivery carrier.

## ***1.5 Malaria***

Malaria remains a disease of global health importance with 3.3 billion people in 97 countries at risk, leading to an estimated 200 million cases and around 600,000 deaths per year.<sup>88</sup>

In many southern African countries, malaria has been greatly reduced through the use of indoor residual spraying as well as effective management.<sup>89</sup> In the south eastern region, recent success can be attributed to the Lubombo Spatial Development Initiative (LSDI), a collaborative approach to malaria control between Mozambique, Swaziland and South Africa.<sup>90</sup> The Southern African Development Community (SADC) is one of the few regions in Africa with the potential to fully eradicate malaria.<sup>91</sup>

There are various plasmodial species of malaria, each in turn pose a significant health threat for humans. In total there are six species of malaria, these consist of; *Plasmodium falciparum*, this is usually considered the most aggressive form of the disease due to the large number of deaths associated with it, *P. vivax* is a major cause of illness across large parts of the world, and it is discussed that fatalities, due to this parasite, have been understated.<sup>92</sup> *P. ovale curtisi*, *P. ovale wallikeri*, and *P. malariae* are much less common causes of significant disease. Recently the simian parasite *P. knowlesi* has emerged as a local but important cause of disease in Malaysia and other areas of Southeast Asia. Here it is predominantly a zoonosis, with no definite evidence of primary human-to-human transmission.<sup>93</sup>

Humans have struggled to adapt to *P. falciparum* as it remains a very dangerous parasite, more so than any other pathogen. Despite *P. falciparum*'s presence throughout the tropics, the health impact is far from even, with the large majority of the world's parasitized individuals in Asia and south Asia (reflecting the significant human population) and large scores of deaths occurring in Africa, mostly in children.<sup>88</sup>

Plasmodium spp. are global pathogens with a complex life cycle alternating between female anopheles mosquitoes and vertebrate hosts that require the formation of unique zoite forms to invade different cell types at specific stages, this is depicted very well in **Figure 1.7**. As the foreign bodies enter the host, they infect hepatocytes, this is followed by the asexual cycle in the blood. Sexual forms that develop during the blood stage are ingested by a feeding mosquito, this completes the cycle.<sup>94</sup>

Inside the food vacuole parasite haemoglobin is degraded and released free haem that would be toxic to the malaria parasites therefore, the parasite must provide a way for detoxification, which it achieves by converting the haem monomer into insoluble and chemically inert  $\beta$ -haematin crystals (called haemozoin) and also infect red blood cells.<sup>95</sup>

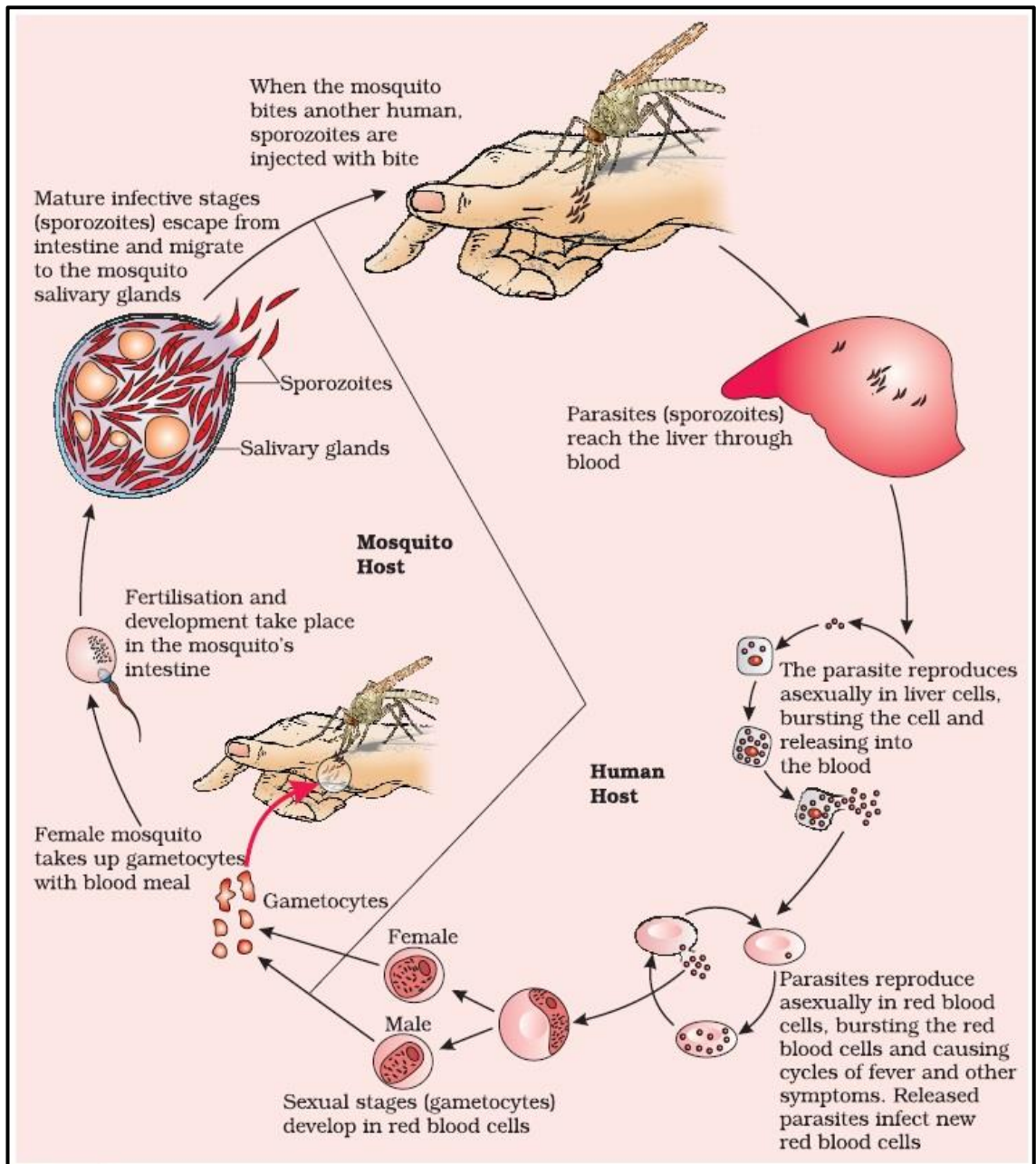


Figure 1.7 The stages in the life cycle of plasmodium.<sup>96</sup>

### ***1.5.1 Malaria diagnosis***

Malaria diagnosis involves the identification of malaria antigens and products in the blood stream. In theory this has an aura of simplicity; the reality is thwart with difficulty. There are different polymorphs of the six species of malaria; the different stages of erythrocytic schizogony, the endemicity of different species, the interrelation between levels of transmission, population movement (large scale transmission), immunity, drug resistance, the problems of recurrent malaria, persisting viable or non-viable parasitemia and sequestration of the parasites in the deeper tissues. Also, the use of chemoprophylaxis or even presumptive treatment on the basis of clinical diagnosis will all influence the identification and interpretation of malaria parasitemia in a diagnostic test. Malaria is a clear medical emergency and should be treated with utmost haste. Slow response to diagnosing and treatment are the driving force for many deaths across the world.<sup>97, 98</sup>

Giemsa microscopy and rapid diagnostic tests (RDTs) describe the two diagnostics most likely to have the largest effect on malaria control today. These two methods, each with specific strengths and limitations, together represent the best hope for correct diagnosis as a key component of successful malaria control.<sup>99</sup>

### ***1.6 Antimalarial drugs***

Malaria is a major cause of death every year, millions of people succumb to it across 90 countries where; 1 in 10 of the world's population are infected. There are four major types of malaria carried by mosquitoes, these included *P. vivax*, *P. ovale*, *P. malariae*, and *P. falciparum*.<sup>100-102</sup>

Malaria due to being transmitted predominantly by anopheline mosquitoes, can be controlled by relying on numerous preventative measures. These include the control of

the anopheline mosquito population through removal of breeding sites, the use of insecticides and the prevention of contact with humans who are infected. In the long run, the ultimate aim would be the successful implementation of an effective malaria vaccine. However, this is presently not the case and may not be expected for another decade.<sup>103</sup>

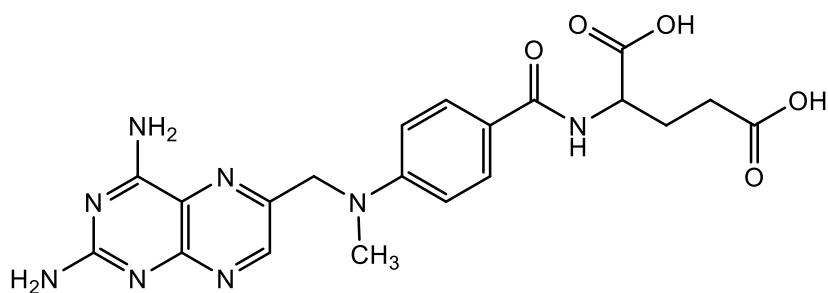
The plasmodia that cause malaria is the main reason for developing resistance to antimalarial drugs not a resistance to the mosquitoes that transmit the disease. Drug resistance can be defined such as the ability of a parasite species to survive and multiply despite the administration of a drug in doses equal to or higher than those typically recommended but within the limit of acceptance. Many deaths related to malaria are due to the increase in resistance to some drugs.<sup>104</sup>

There are a number of factors determining malaria's growing resistance to drugs, these are shown in (Table 1.2). Resistance, particularly in *P. falciparum*, has been a major contributor to the global resurgence of malaria in the last three decade.<sup>105</sup>

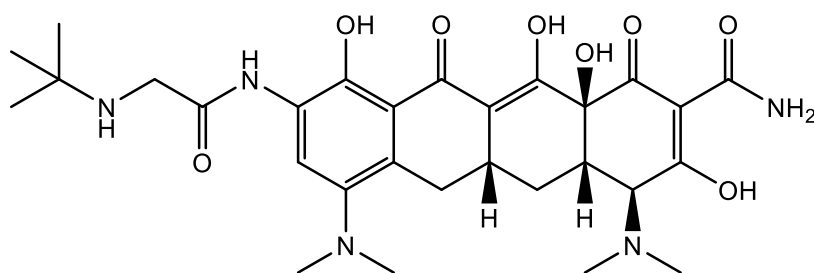
**Table 1.2 Factors determining the probability of selection of de novo antimalarial drug resistance.**

1- The frequency with which the resistance mechanism arises.
2- The fitness cost to parasite associated with the resistance mechanism.
3- The number of parasites in the human host that are exposed to the drug.
4- The simultaneous presence of other antimalarial drugs in the blood that still kill the parasite if it develops resistance to one drug.
5- The level of the host defence (nonspecific and specific immunity).
6- The pharmacodynamics properties of antimalarial drugs.
7- The degree of resistance that results from the changes.
8- The concentration of drug to which these parasites are exposed

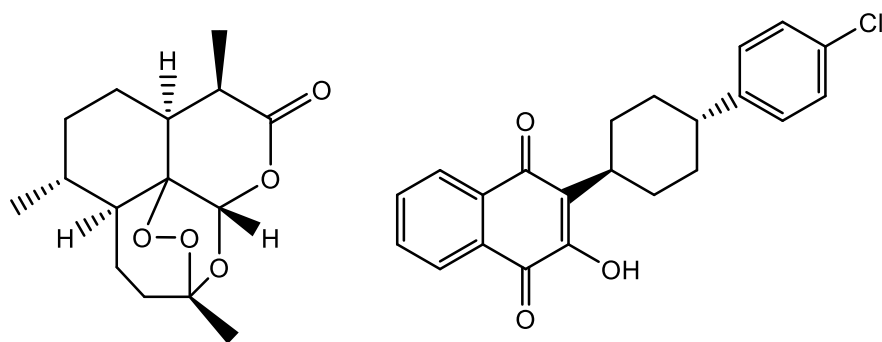
Several antimalarial drugs have been introduced for both treatment and preventative measures, constantly the quest for novel treatments of malaria is a very active research area. The drugs are classified according to their molecular structure and their mode of action. The most important antimalarials currently in clinical use include quinolines, antifolates, antibiotics, endoperoxides related to artemisinin and the hydroxynaphthoquinone atovaquone but most of these drugs have problems such as short plasma half-life, toxicity and widespread resistance.<sup>106</sup> **Figure 1.8**



**Antifolate (Methotrexate)**



**Antibiotic (Tigecycline)**



**Artemisinin**

**Atovaquone**

**Figure 1.8 Structures of the currently antimalarial drugs in clinical use.**

### ***1.6.1 Chloroquine***

Recently, chloroquine (CQ) is the major drug that had been used as a treatment for diseases. It was safe, widely available, effective, and cheap, it can also be used by children and pregnant women. However, the most aggressive parasite *P. falciparum*, is rapidly becoming resistant to all traditional treatments such as CQ. It appears that drug resistance mechanisms recognize the amino alkyl side chain of CQ.<sup>107</sup> This is indicated by the fact that CQ analogues with side chains much shorter (2-3 carbon atoms long) or much longer (10-12 carbon atoms long) maintain full activity against resistant strains, this is shown in **Figure 1.9**. CQ analogues with chain lengths closer to that of the standard CQ have intermediate activities between that of CQ and the fully active compounds. Activity has been related to the distance between the aminoquinoline amine group and the tertiary amino group of the side chain.<sup>108</sup>

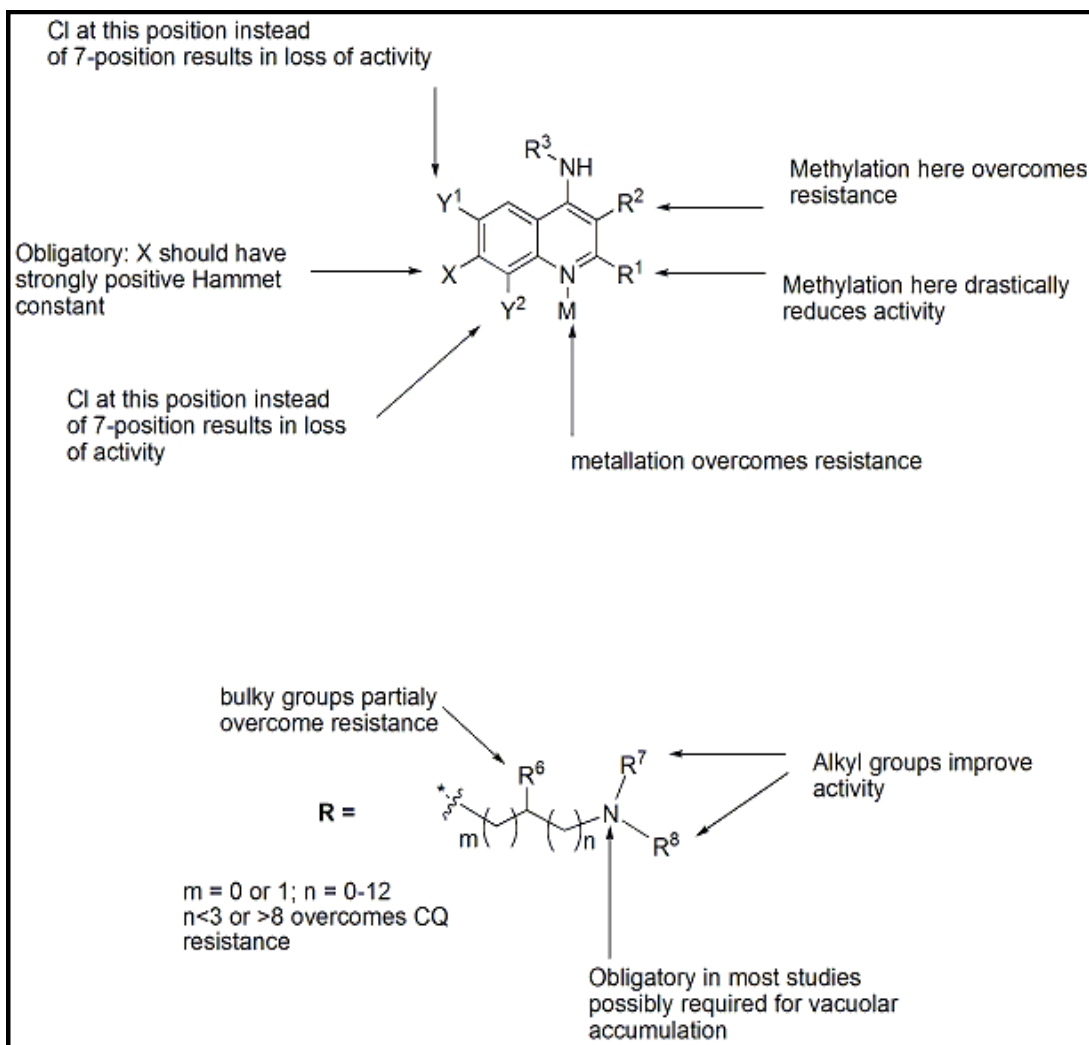


**Figure 1.9 summary of findings regarding the roles of various substituents on 4-aminoquinolines with respect to antiparasmodial activity and activity against CQ resistant strains.**<sup>107</sup>

The wide-spread emergence of parasites that are resistant to antimalarials that are currently used, notably CQ **Figure 1.10**, has caused a re-evaluation of alternative drugs to circumvent the growing concern. Haemoglobin degradation within the parasite food vacuole and the subsequent interaction with the host-dependent haem molecule remains a promising route for potential future antimalarials.<sup>109</sup> 4-aminoquinoline drugs such as chloroquine (CQ), amodiaquine (AQ), and ampyroquine (ApQ) **Figure 1.10** are heavily concentrated in the parasite food vacuole and are thought to act by preventing or

disrupting the effective formation of haemozoin. This results in haem-mediated toxicity to the parasite.<sup>109</sup> 4-aminoquinoline resistance spreads relatively slowly and has been associated mainly with mutations in genes of transporter proteins, such as the *P. falciparum* Chloroquine Resistance Transporter (pfCRT). This affects drug access or extrusion in the parasite food vacuole.<sup>110, 111</sup> It can be expected that relatively small structural changes could enhance drug accumulation in resistant parasites. AQ, developed in the early 1950s, has proved to be effective against many CQ resistant malaria strains.<sup>112</sup> However, the use of this drug was limited in the mid-1980s due to isolated cases of agranulocytosis and hepatotoxicity in prophylaxis.<sup>113</sup>

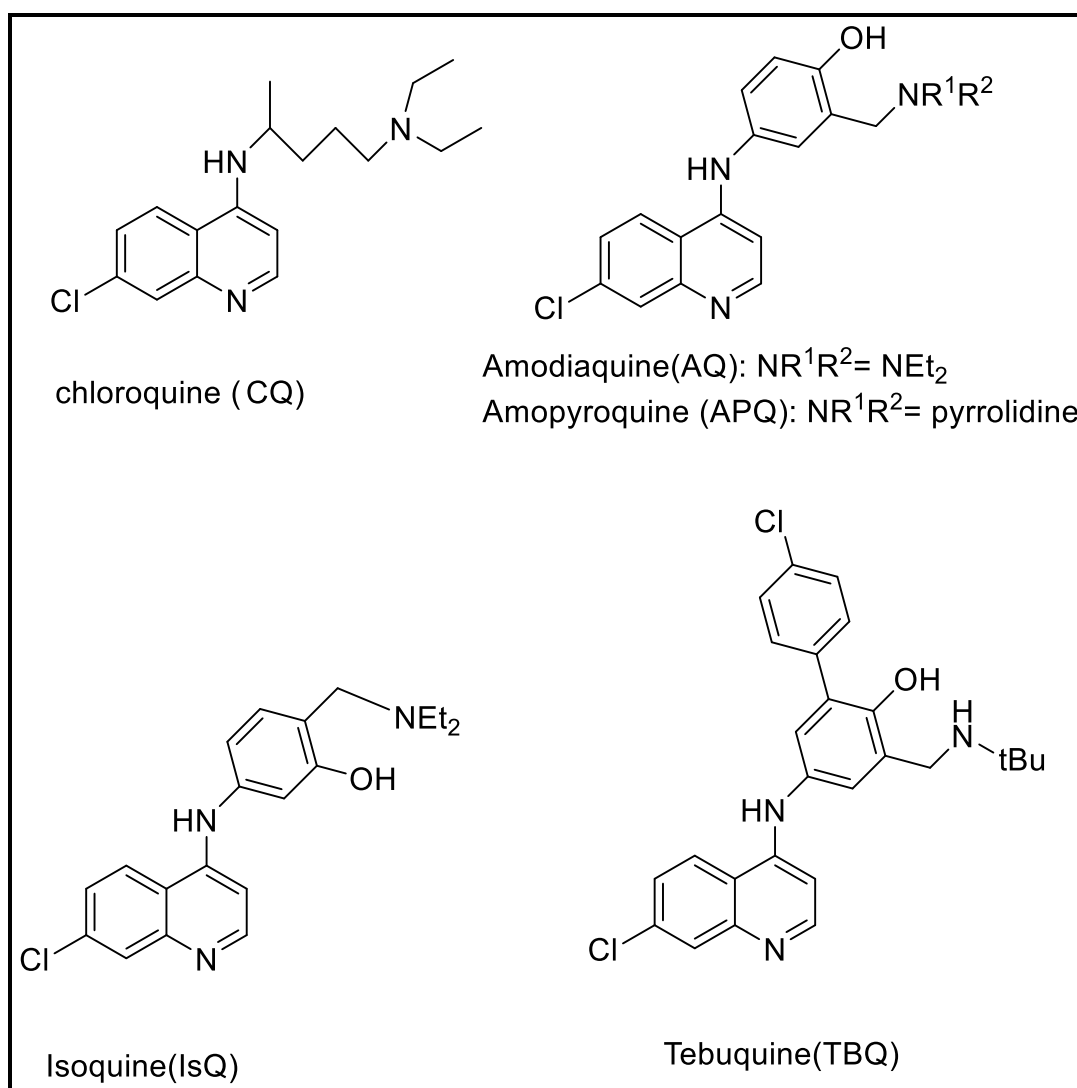


**Figure 1.10 structures of some 4-aminoquinoline antimalarials.<sup>114</sup>**

Compared with alternative antimalarial drugs, the resistance to CQ developed and spread relatively slowly. This is because resistance means that mutations have built up in the genes that encode transport proteins. AQ maintains its efficiency in many endemic zones and is still recommended by the WHO, but numerous studies have highlighted its potential toxicity in prophylactic use. Nevertheless, relatively small structural modifications to AQ can lead to a significant increase in antimalarial activity against CQ resistant strains and can impart greater metabolic stability to these compounds. 4-aminoquinoline accumulates in the acidic region of the cell, specifically the food vacuole of the intraerythrocytic malaria parasite. This prevents the detoxification of haematin released during haemoglobin digestion. Haematin is the haem released by the digestion of haemoglobin in infected red blood cells by the parasite. Normally it is aggregated (detoxified) into an insoluble material called haemozoin or 'malaria pigment'. The mechanism of interaction between CQ drugs and beta-haematin (BH) has been widely investigated, and provides useful guidance for the discovery of new non-resistance antimalarial drugs.<sup>115, 116</sup>

The effectiveness of CQ and AQ differ due to lipophilicity and side chain rigidity. The structural differences of AQ include an additional aromatic ring, this allows for  $\pi$ - $\pi$  stacking inside the food vacuole. Thus, AQ is more effective than CQ as it can easily build up. The role of the amino side chain in both CQ and AQ compounds were of primary importance for the inhibition of BH formation.<sup>117</sup>

### ***1.6.2 The mechanism of action of chloroquine as antimalarial drug***

Previously CQ was used with a side chain containing up to 4 carbon atoms and an amine group, this leads to complete protonation after reducing the pH from 7.4 to 5.5 inside the parasite food vacuole. The most dangerous parasite *P. falciparum* has developed

resistance against this compound.<sup>118</sup> A new study of a novel CQ derivative has been created with a short side chain that has shown the ability to reverse the parasite resistance.

**Figure 1.11** shows the suggested mechanism for a new CQ internal to the parasitic food vacuole.

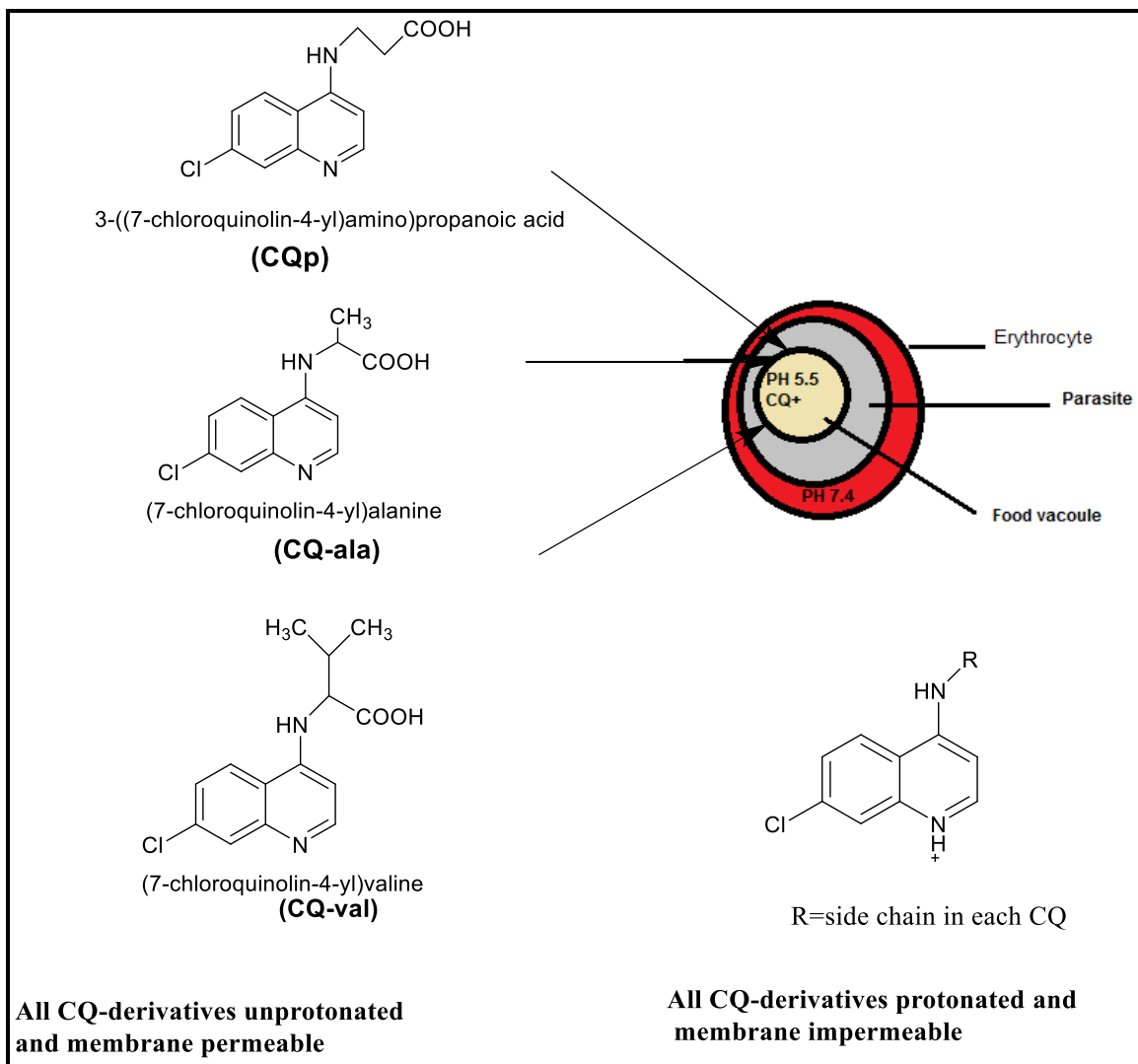


**Figure 1.11** Accumulation of CQ in the parasitic food vacuole<sup>119</sup>

The food vacuole (FV) is acidified by a vacuolar proton pump to create a suitable environment for haemoglobin digestion. The acidic nature of the FV leads to near complete protonation of CQ. This diffuses across the FV membrane as an uncharged form

and then accumulates as a charged form  $CQ^+$  that interferes with the polymerization of toxic haem to non-toxic haemozoin. As a result the parasite is rapidly eliminated.<sup>59</sup>

### ***1.6.3 The ferrocenyl antimalarial agents***

Ferrocene is an organometallic compound with the formula  $Fe(C_5H_5)_2$ , ferrocene and its derivatives have an extremely promising activity in medicinal applications for both *in vivo* and *in vitro* use against various diseases.<sup>120</sup> It has received special attention because of its high chemical stability, neutrality and safety to humans.<sup>121</sup> It can be functionalized or oxidized to ferricenium salts. Several ferrocenyl compounds show cytotoxic<sup>122-124</sup>, anti-tumour<sup>125</sup>, anti-malarial<sup>126</sup>, anti-fungal<sup>127</sup> and DNA-cleaving activity showing their potential in the field of medicinal chemistry.<sup>128</sup>

Dyson and co-workers are one of several researchers who focused on the chemistry of ferrocene and the various properties of organometallic compounds. The results of these compounds are then carried forward to be used in appropriate pharmaceutical applications.<sup>129</sup> In the last ten years, research has been developed around the inclusion of a metallocene moiety into identified antimalarial compounds. Ferroquine is the most successful of these compounds. Ferroquine (FQ) and other ferrocenyl chloroquine analogues have been shown to be effective *in vitro* in both chloroquine-sensitive and chloroquine-resistant *P. falciparum* across a variety of strains.<sup>130-132</sup>

It was found that the active mechanism of CQ and FQ are similar and most likely includes haematin as the drug target and inhibition for the haemozoin formation. Nevertheless, basicity and lipophilicity of FQ are markedly changed from those of CQ. The lipophilicity of FQ and CQ are similar when protonated at pH 5.2 in the putative food vacuole but vary significantly at pH 7.4.<sup>133</sup> Moreover, the  $pK_a$  values of CQ are higher than FQ. This leads to the conclusion that there is a slight decrease in accumulation in the food vacuole of FQ as compared with CQ. FQ single crystal structure determination as acquired through X-

ray diffraction reveals the presence of a robust hydrogen bonding network between terminal N atom and the 4-amino group. This, as well as the electron donating properties of ferrocene may provide a decrease in the overall p*K*<sub>a</sub>. The decreased accumulation arising from the less basic behaviour of this compound is partly compensated by its stronger  $\beta$ -haematin inhibition. Rising lipophilicity, differences in geometric and electronic structure, as well as changes in the N–N distances in FQ compared with CQ can clearly explain its activity against CQ-resistant parasites.

In addition, there is no evidence for toxicity of ferroquine and its derivatives therefore ferrocenyl complexes have been used and developed as active antimalarial drugs for example, ferrocenyl-mefloquine and ferroquine.<sup>120</sup>

#### ***1.6.4 Sugar transporters for anti-malarial drug targets***

One of the main sources of energy in most human cells is glucose. The prevention of cellular glucose absorption has become a popular area of research. This could be a potential therapeutic strategy to heal many unrelated diseases including cancers and malaria.<sup>134</sup> Blood glucose is delivered by sugar transporters into the intraerythrocytic malarial parasite and are found in the host parasite's plasma membranes. Glucose transporter 1 (GLUT1) is a primary transporter from blood plasma to erythrocyte cytosol. This is due to it being extremely abundant in the erythrocyte plasma membrane. GLUT1 is an inactive carrier that reduces solute concentration gradients.<sup>135</sup> Malarial parasites are surrounded by an additional membrane inside the erythrocyte, the glucose molecules pass this membrane before reaching the parasite surface. The parasite vacuole membrane is highly permeable to glucose and solutes. The molecular weights of this membrane are up to 1400 g mol<sup>-1</sup>. These molecules permeate easily between the erythrocyte cytoplasm and the vacuole space via low selectivity channels and utilise a high capacity of amino acids

and monosaccharides.<sup>136, 137</sup> Glucose absorption into the parasite is inhibited by a facilitative transport process.<sup>138</sup>

In the case of *P. falciparum*, PfHT is the principal hexose transporter expressed in the parasite plasma membrane. Hexose transporters of pathogenic malarial parasites, *P. falciparum*, have been confirmed as new drug targets. Moreover, an important role of plasmodial hexose transporters is in parasite blood stages, these transporters can also have a vital role for liver and insect stages of malarial parasite life cycles. The prevention of hexose transport can be seen as a smart approach for the development of other novel anti-parasitic drugs in order to discover new anti-malarial agents.<sup>139</sup> PfHT is an important target for chemotherapeutic design because it is involved in the initial step (rate-limiting transport) of glucose metabolism upon which the parasite wholly depends. As expected for an essential protein, inhibition of PfHT kills parasites. Hypoglycemia is a serious and common complication of severe malaria. Increased glucose consumption by infected red cells may divert glucose away from host tissue, this is illustrated clearly in **Figure 1.12**. It has been suggested that the rapid inhibition of glucose uptake by parasites may not only kill them, it may reduce the metabolic diversion in host tissues that have a high density of infected red blood cells.<sup>140</sup>

Studies using intact red blood cells, infected with *P. falciparum*, suggested the presence of a glucose carrier protein within the parasite plasma membrane. However, this work was not conclusive because intact infected red blood cells are very complex systems.<sup>138, 141</sup> An alternative approach is the use of the *Xenopus laevis* oocyte heterologous expression system and total messenger RNA (mRNA) from parasites. This confirmed without a doubt the presence of a glucose transporter.<sup>142</sup>

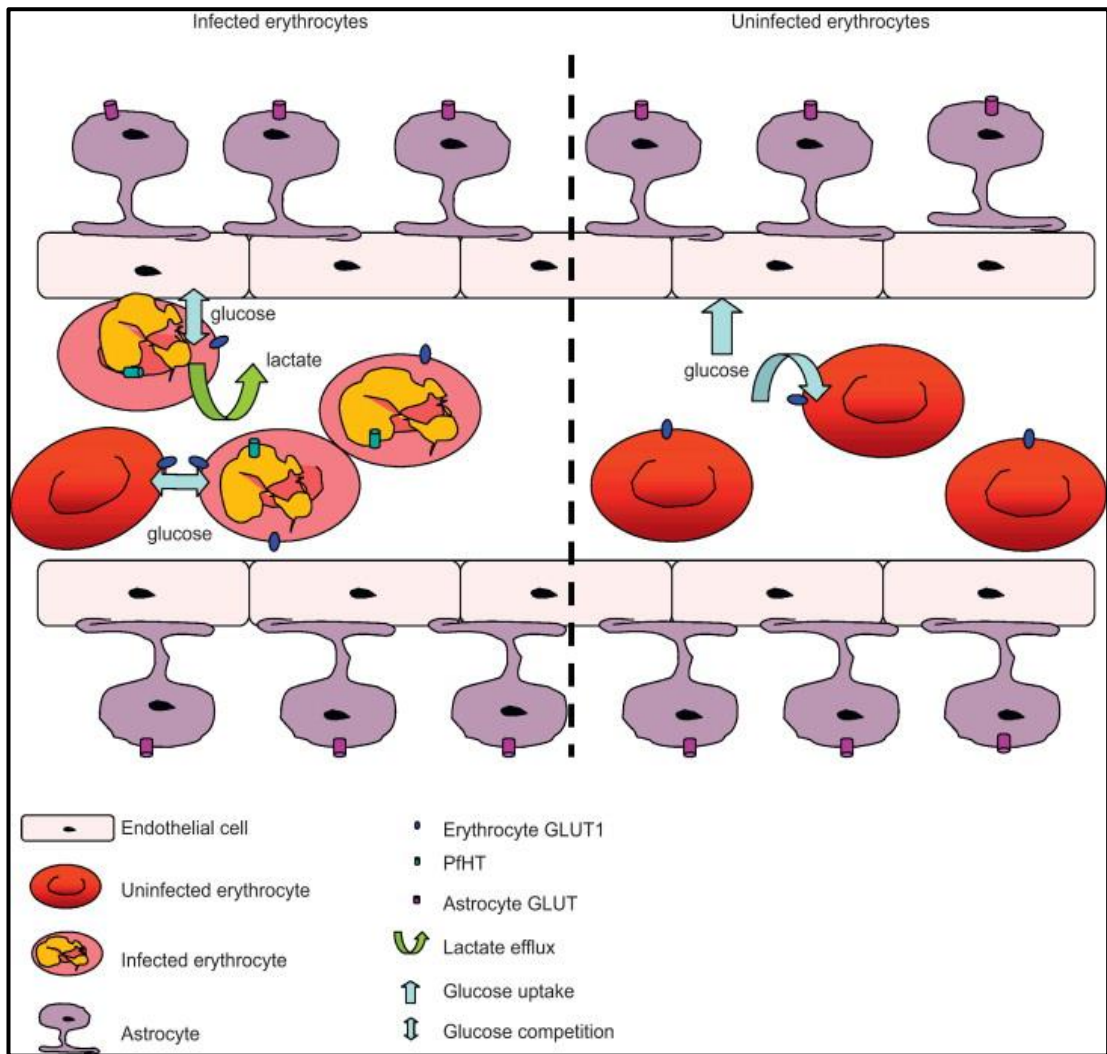


**Figure 1.12 metabolic diversion of glucose in a blood vessel containing infected red blood cells shown how high level of glucose consumption may divert glucose away from host tissue .<sup>140</sup>**

A new clinically recognised anti-malarial agent is artemisinin, as well as its various derivatives. Artemisinin is an unusual sesquiterpene lactone possessing a unique chemical structure, coupled with its low human toxicity and proven antimalarial efficacy have attracted vast attention since its discovery in the early 1970s.<sup>143, 144</sup> The practical use of artemisinin as an antimalarial agent is however over shadowed by its low solubility in

both water and oil, its poor efficacy by oral administration and high rate of recrudescence in treated patients.<sup>145, 146</sup> It has been previously shown that artemisinin derivatives are not cross-resistant with any of the existing antimalarial agents such as chloroquine, pyrimethamine, sulfadoxine, and quinine. As a result, the search for newer antimalarial drugs is becoming even more urgent.<sup>146</sup>

### ***1.6.5 Approaches to Discovery of New Antimalarial Agents***

The development of novel antimalarial agents is imperative in the fight against drug resistance. Six approaches to the discovery of new antimalarial agents have been acknowledged, namely: combination therapy, structural modifications of old drugs, and the use of natural products and their derivatives. Also, the use of compounds that are active against other diseases. Finally, the use of resistance reversers is receiving consideration, these can modify existing treatments enough to be active again. A number of antimalarial agents have been developed using these strategies and most have made it to the clinical trial phase.<sup>147, 148</sup> Furthermore, CQ-resistance reversers (CQ<sup>R</sup>) have been identified to have the key elements of a CQ resistance reverser, pharmacophore, this includes a hydrogen bond acceptor and two hydrophobic aromatic rings.<sup>149</sup> The continuing spread of CQ<sup>R</sup> and resistance to other drugs has increased significantly, this therefore has a consequence on the incidence of malaria globally.<sup>104</sup>

There is a hope that the *P. falciparum* genome can be mapped and therefore identification of new targets will be expedited. An example of such targets is the *Plasmodia* proteases which are appealing targets for chemotherapy as they are essential for the survival of the parasite.<sup>150</sup> The 4-aminoquinolines have been proven as effective compounds for malaria therapy and prophylaxis due their relative ease of synthesis, acceptable toxicity profiles, their tolerance and effectiveness against a number of chloroquine-resistant strains and their cost effectiveness.<sup>151</sup>

Clinical malaria cases, as described by the antimalarial drug policy should be treated with CQ in full therapeutic doses. CQ, although has been found in some cases to not be as effective as it once was, is still a successful drug for five species of the malaria parasite. This also includes some strains of *Plasmodium falciparum*, therefore, CQ remains the primary drug for the treatment of all malarias species, until CQ-resistance is detected.<sup>152</sup>

Novel biodegradable nanoparticles have been successfully utilised as drug delivery vehicles. These entities allow for better encapsulation, higher bioavailability, less toxicity and can operate under a regulated release procedure. Researchers groups have developed numerous nano-sized drug delivery systems based on a natural polysaccharide for delivering the CQ antimalarial drug. It was discovered that the free chloroquine was not as effective at eliminating malaria parasites in mice as when CQ is conjugated to the polysaccharide.<sup>153</sup> In addition to the above mentioned delivery system, chitosan–tripolyphosphate (CS–TPP) nanoparticles have also been developed. Here CQ can be conjugated once again and has be used for the attenuation of *P. berghei* infection in mice.

This is another potential therapeutic antimalarial agent, a free radical scavenger and antioxidative product against malaria infection by decreasing free radical generation, lipid and protein damage, and also by increasing the antioxidant status.<sup>154, 155</sup>

Furthermore, in order to explore the possibilities of designing chemically, physically, and biologically stable drug delivery systems. It was reported that chondroitin sulfate A (CSA) coated PEGylated poly-L-lysine-based dendrimers have been used for the controlled delivery of chloroquine phosphate.<sup>156</sup> The CSA coated or uncoated systems both can be appropriately regarded as suitable and safe drug delivery carriers for the selected antimalarial CQ due to their ability to control and sustain release of drug molecules from each carrier.<sup>156</sup>

In this thesis, chloroquinoline-derivatives (CQ-derivatives) with short side chains have been synthesised. Chain modification was assumed to increase the activity of each CQ-derivative against a CQ-resistance malaria strain. A CQ-derivative was conjugated to the external surface of CPMV. The CPMV's highly symmetrical structure allows for the multivalent presentation of surface molecules for enhanced molecular targeting and simultaneously enables exceptionally high payload capacities for drug delivery. By increasing the CQ concentration that can be delivered, the time retained inside the parasite food vacuole will be longer. This results in the inhibition of haemozoin formation, necessary for parasite survival.

## ***1.7 Summary***

In this chapter, many different examples of protein based nanomaterials have been described. The role of organic nanoparticles such as plant viruses and their applications in medicinal research has been described. As well as the ability to modify the interior and exterior surface with both organic and inorganic components. This results in both a monodisperse, size specific structure and a chemically diverse surface with various potential functional groups. The positive properties of viral nanoparticles for applications in medicine, including their ability to carry payloads of drugs far larger than traditional drug delivery systems has been discussed.

## ***1.8 Aim of this thesis***

There are six parasite species which cause malaria in humans, all of which are transmitted by mosquitoes. The most dangerous parasite is *P. falciparum* and this has become resistant to standard treatments including the 4-aminoquinoline chloroquine (CQ). Indeed, in some areas of the world none of the classic drugs are effective in the fight against malaria. It has been found that incorporation of an organometallic metallocene moiety into the structure of CQ can provide effective therapeutics and reversal of resistance.<sup>157-159</sup> Incorporation of the metatallocene, ferrocene, into the structure of CQ gives the effective anti-malarial ferroquine (FQ).<sup>158</sup> CQ is thought to act by interfering with haem metabolism, by binding to haematin preventing its aggregation into haemozoin, a similar mechanism of action has been proposed for FQ. In comparison to CQ the presence of the ferrocene modifies the properties of the drug due to its different shape, volume, basicity, lipophilicity and electronic properties. These changes appear to reduce affinity for the CQ transporter thought to be linked to CQ resistance.<sup>159</sup> However, reversal of resistance does not necessarily require incorporation of metallocene into the structure. By attaching, for example, one ferrocene and two CQ molecules to an organic template, a molecule effective against CQ-resistant *P. falciparum* was obtained.<sup>160</sup> Further, non-CQ based ferrocenyl-carbohydrate conjugates are also effective; the carbohydrate acts as a targeting molecule as at all stages of the parasite's life cycle glucose uptake and metabolism is raised in infected erythrocytes.<sup>127, 161, 162</sup>

The aim of this thesis is to take a novel and unique approach to optimize the delivery and efficacy of organometallic based therapeutics by utilizing the natural, biological nanoparticle CPMV. The objective is to greatly enhance the delivery, efficacy and reversal of resistance by organometallic anti-malarials by being coupled, together with targeting agents, to the external surface of a natural bionanoparticle vector. The idea is

unconventional and creative as it exploits a naturally occurring bionanoparticle, CPMV, as a device for the targeted delivery of specific therapeutics or combinations thereof.

CPMV particles are biocompatible, non-infectious and non-toxic to humans, and their physical properties are well understood.<sup>163</sup> Importantly, they display on their external surface amino acid side-chains that are readily addressable by chemical coupling strategies.<sup>26</sup> As a range of chemical coupling strategies have been defined, and mixed decoration of the virus surface with various chemicals has been demonstrated, it is expected that the synthesis of new virus-templated therapeutic agents will be readily achieved. By exploiting the multidenticity of the virus surface, the loading of drug relative to resistance reversing molecules or targeting agents should be greatly enhanced, with consequent improvement in dose response: e.g. in comparison to the organic template that carries one ferrocene and only two CQ molecules.<sup>160</sup> The virus template could potentially carry one ferrocene and more than 200 CQ molecules.

The first phase will develop the techniques required to generate a library of chemically modified virus-like particles carrying a range of single or mixed therapeutic agents and/or targeting molecules. Synthetic strategies will be designed and developed for the preparation of new CQ-derivatives with amino acids linked by short aliphatic chains, for coupling CQ-derivatives to the virus surface, and to control relative coverage. The ideal will be to have, for example, low ferrocene and high CQ coverage. The second phase will exploit the library of chemically modified VNPs. The contents of the library will be screened for antimalarial activity by *in vitro* and *in vivo* methods.

## ***2 Experimental***

### ***2.1 Reagents***

*N*-Ethyl-*N'*-(3-dimethylaminopropyl) carbodiimide hydrochloride, Alexa Fluor 488 carboxylic acid succinimidyl ester, *N*-hydroxysuccinimide, dimethyl sulfoxide, periodic acid, DNA loading dye 6X, chromium(VI) oxide, agarose low melting molecular biology grade, nitroso-2-naphthol, filter membranes, nitrocellulose, tert-butyl nitrite were purchased from Sigma-Aldrich, Alfa Aesar or Thermo Fisher Scientific. CPMV samples were supplied by Prof. George Lomonosoff (John Innes Centre, Norwich, UK). MilliQ Water was from Elga pure lab Ultra 18.2 mΩcm. RunBlue LDS Sample Buffer, 12% SDS, RunBlue Precast Gel - 8x10 cm and RunBlue SDS Run Buffer TEO-Tricine were purchased from Expedeon. N<sub>3</sub>-bodipy dye was supplied by Prof. Ross Boyel group (Hull University, Chemistry Department, Hull, UK).

#### ***2.1.1 Sodium phosphate buffer***

Solutions of Na<sub>2</sub>HPO<sub>4</sub> (13.5 g, 0.095 mol) in Milli-Q water (500 ml) and of NaH<sub>2</sub>PO<sub>4</sub> (14.2 g, 0.118 mol) in Milli-Q water (500 ml) were prepared, and autoclaved before mixing. To prepare 0.1 M buffer solution; Na<sub>2</sub>HPO<sub>4</sub> solution (305 ml) and NaH<sub>2</sub>PO<sub>4</sub> solution (195 ml) were added to Milli-Q water (500 ml) to give pH 7.<sup>164</sup>

#### ***2.1.2 Sodium acetate buffer***

A solution of sodium acetate (15 g, 0.183 mol) was dissolved in Milli-Q water (25 ml). Exactly 1.5 ml of glacial acetic acid was then added very slowly into the sodium acetate aqueous solution. Finally, Milli-Q water was added into the solution to fill the volume to 100 ml and give pH 5.<sup>165</sup>

## ***2.2 Equipment***

UV-Vis spectra were recorded using a Perkin Elmer Lambda25 UV-Vis Spectrophotometer and UVWINLab software and a NanoDrop Spectrometer ND 1000, Chemi Doc XRS+ system; NMR on a Jeol JNM ECP 400 Spectrophotometer; mass spectra using a DecaXPplus ion trap and TEM studies were performed using a JEOL JEM-1200 EX EM.

### ***2.2.1 Inductively coupled plasma optical emission spectroscopy (ICP-OES analysis)***

CPMV- Fc, CPMV-CQp- Fc, CPMV-CQ -ala- Fc and CPMV-CQ- val- Fc (50 mg, 500µl) were each homogenised with 2% w/v nitric acid for dissolution of samples. Minimum quantity (1-5 ml) of the acid was used.

### ***2.2.2 Scanning electron microscopy (SEM)***

Ten millimetre diameter cover glasses were attached to 12mm diameter aluminium SEM sample holders. The surface of the cover glasses was then cleaned with isopropanol.

Approximately 50µl of sample was pipetted on to a cover glass and allowed to air-dry. All samples were then sputter coated with 2nm of gold and examined using Zeiss, EVO 60. Scanning electron microscopy was performed with Polaron, SC7640 scanning electron microscope.

### ***2.2.3 Powder X-ray diffraction***

PXRD patterns were collected for samples. PANalytical (Empyrean series 2) X-Ray diffractometer instrument was used. As it was an automatic slit, a nickel filter was used , the angle range was 20-80°, step size 0.0262606°, time per step 1521.075 s, net time per step 1518.015 s, scan speed 0.004402°/s, and number of steps 2285.

As a result of the constructive interference between the waves, diffraction occurs when an object blocks the path of constructive waves. Beams are scattered in various directions at specific angles when X-rays interact with them. The equation below explains the relationship between the angles of incidence, wavelength of the incident X-rays, and spacing between the crystal lattice planes of atoms and is known as Bragg's Law, expressed as:

$$n \lambda = 2d \sin \theta \text{ ----- Eq1}$$

Where  $\lambda$  is the wavelength of the incident X-rays,  $n$  (an integer) is the order of reflection,  $\theta$  is the angle of incidence and  $d$  is the interplanar spacing of the crystal.

## ***2.3 Particle purification***

### ***2.3.1 Ultrafiltration***

Ultrafiltration was used as a method for purification and concentration of virus particles. Samples were purified using (100  $\mu$ l – 0.5 ml) of 100 kDa molecular-weight cut-off columns (Microcon, Amicon Millipore) and centrifuged. The particles are placed on the filter, while the buffer and small impurities pass through the membrane.

### ***2.3.2 Dialysis***

This method is very effective in particle purification. The semi-permeable membrane keep the particles within, while small molecules pass through. On the other hand if the protein concentration is too dilute for further processing or analysis, the sample can be concentrated quickly using centrifugal concentrators. Float-A-Lyze tubing 100KD has been used throughout the research.

## 2.4 Determination of virus concentration

### 2.4.1 UV-Vis determines concentration

(CPMV) concentration was determined by photometrical measurement at room temperature using a 1 cm quartz cuvette as shown in **Figure 2.1**.

CPMV particles have an absorption maximum at a wavelength of  $\lambda = 260$  nm (derived from the encapsidated RNA molecules) with molar extinction coefficient of  $\epsilon = 8.1$  ml  $\text{mg}^{-1}$   $\text{cm}^{-1}$ . The law of Beer Lambert can be used to calculate the concentration by the following Eq. (2)

$$[A = c d \epsilon] \text{-----Eq2}$$

Where A is the absorbance, c is the concentration of the particles in  $\text{mg ml}^{-1}$ , d is the length of the light path in cm and  $\epsilon$  the molar extinction coefficient in  $\text{ml mg}^{-1}$   $\text{cm}^{-1}$ .<sup>164</sup>

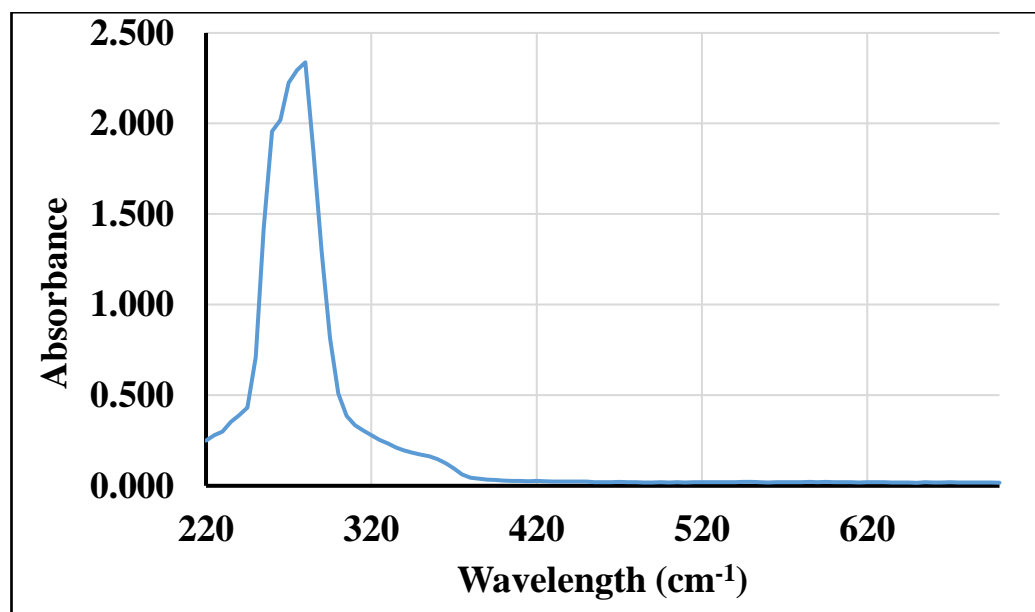


**Figure 2.1** A typical UV/Vis spectrum of purified CPMV particles in phosphate buffer pH 7.

### 2.4.2 Agarose–gel electrophoresis

CPMV particles (30 µg) were suspended in 10 mM sodium phosphate buffer pH 7 with loading dye (3 µl Coomassie staining solution or MBI Fermentas dye) and analysed on 1.2% agarose gel in 50 ml TBE buffer using an electric field of 1–5 V cm<sup>-2</sup> for 1–2 hours. For ethidium bromide staining (nucleic acid staining) 0.1 µg/ ml ethidium bromide (4-5 µl) in 1x TBE buffer was added to the gel. Particles were visualised on a UV transilluminator at 302 nm using Gene Genius Bio Imaging System with Gene Snap software (Syngene) as shown in **Figure 2.2**. For coat protein visualisation gels were stained with Coomassie staining solution overnight. Gel images were recorded using a camera or scanner.<sup>164</sup>



**Figure 2.2 Agarose gel imaging for wt CPMV at different concentrations staining with ethidium bromide lane 1, CPMV (24 a.a missing) 10 µg/ ml, lane 2 CPMV 40 µg/ ml lane 3, CPMV (24 aa missing) 40 µg/ ml.**

### 2.4.3 SDS-PAGE

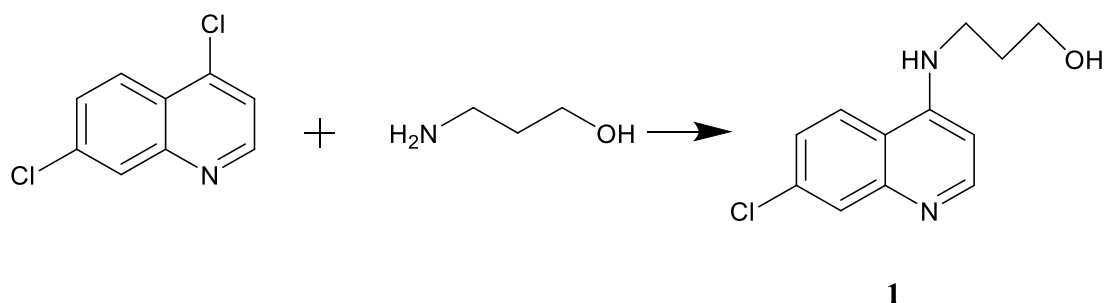
Sodium dodecylsulfate polyacrylamide gel electrophoresis (SDS-PAGE) was performed on 30 µg of virus in 10 mM sodium phosphate buffer pH 7 mixed with 4x RunBlue LDS Sample Buffer (3µl). Samples were heated for 10 minutes at 100 °C in order to denature the protein. The samples were analysed on 12 % TEO-CI SDS RunBlue precast gels at 180 V for 30 minutes using 600–700 ml of 20:1 dilution of 20x RunBlue SDS Running Buffer. After that the gel was stained with Blue Instant (Expedeon) the bands were visible after a few minutes. Gels were washed with Milli-Q water prior to imaging.<sup>24</sup>

### 2.4.4 Transmission electron microscopy (TEM)

For visualisation the particles were negatively stained with uranyl acetate. 7.5 µl of 0.1mg/ml of virions and 7.5 µl 2% (w/v) uranyl acetate were incubated on carbon film coated nickel or copper grids (400 mesh; obtained from Agar Scientific) for 3-5 min.. The solution was removed with filter paper and the grid was dried in air.<sup>24</sup>

## 2.5 Chemical synthesis

### 2.5.1 3-((7-Chloroquinolin-4-yl) amino) propan-1-ol (1)

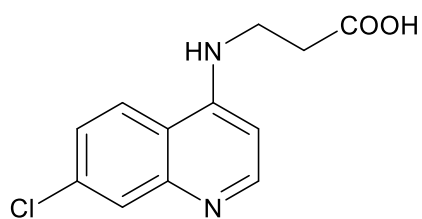


A mixture of 4,7-dichloroquinoline (2.73 g, 0.0138 mol) and 3-aminopropanol (12 ml, 0.159 mol) were heated with stirring at 140 °C for 24 h. After cooling, the reaction was

poured into water (50ml) and filtered, the solid residue was dried then boiled in ethyl acetate (25 ml) to give an off-white solid (2.53 g, 90%).<sup>166</sup> Elemental analysis expected C: 60.45%, H: 5.80%, N: 11.84%: found C: 61.10%, H: 5.79 %, N: 11.80%.

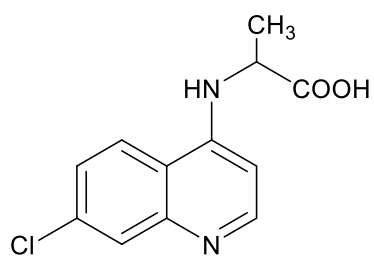
<sup>1</sup>H NMR (400 MHz, CDCl<sub>3</sub>):  $\delta_{\text{H}}$  /ppm 1.64 (bs, 1H, OH), 2.14 – 1.56 (m, 2H, CH<sub>2</sub>), 2.36 (t,  $J = 7.4$  Hz, 2H, CH<sub>2</sub>), 3.76 – 3.60 (m, 2H, CH<sub>2</sub>), 6.94 (bs, 1H, NH), 7.11 (d,  $J = 8.4$  Hz, 1H, ClQ-C3-H), 7.57 (dd,  $J = 8.1$  Hz, 1H, ClQ-C6-H), 8.10 (d,  $J = 8.2$  Hz, 1H, ClQ-C5-H), 8.83 (s, 1H, ClQ-C8-H). For C<sub>12</sub>H<sub>13</sub>ClN<sub>2</sub>O 236.5, mass spectrum 237.0 m/z (M +H)<sup>+</sup>

### 2.5.2 Chloroquinoline derivatives:



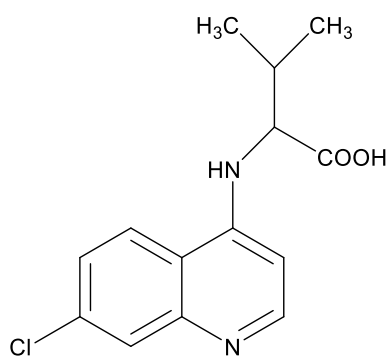
3-((7-chloroquinolin-4-yl)amino)propanoic acid

**2**



(7-chloroquinolin-4-yl)alanine

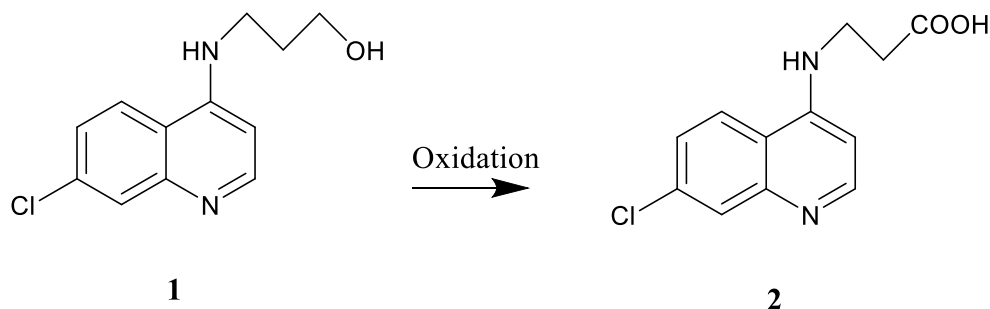
**2a**



(7-chloroquinolin-4-yl)valine

**2b**

### 2.5.2.1 3-((7-chloroquinolin-4-yl) amino) propionic acid preparation



#### 2.5.2.1 A. Oxidation using potassium permanganate

Potassium permanganate (3.16 g, 0.02 mol) was reacted with compound **1** (3.18g, 0.013mol) in aqueous NaOH (1N, 0.4 ml) for 3h stirring at room temperature. The mixture was acidified with HCl (12N) and filtered, the precipitate was washed with chloroform and the crude was purified by TLC (DCM/MeOH, 4/1) to give the chloroquinoline amino acid compound as a dark yellow solid (2.55g, 80% yield), m.p 290-300°C. Elemental analysis expected C: 57.48%, H: 4.39%, N: 11.17%, found: C: 56.87%, H: 4.90%, N: 11.03%. IR: OH broad band at 3000  $\text{cm}^{-1}$ , NH stretch at 3300  $\text{cm}^{-1}$  and C=O stretch at 1721  $\text{cm}^{-1}$ .  $^1\text{H}$  NMR(400 MHz, DMSO- $d_6$ ):  $\delta_{\text{H}}$  /ppm 1.88 – 1.79 (m, 2H- $\text{CH}_2$ ), 3.53 (t, 2H,  $\text{CH}_2$ ), 6.92 (s, 1H, NH), 7.30 (d,  $J = 2.1$  Hz, ClQ-C3-H), 8.02 (d,  $J = 5.1$  Hz, ClQ-C2-H), 8.47 (dd,  $J = 7.8$  Hz, ClQ-C6-H), 8.72 (d,  $J = 2.1$  Hz, 1H, ClQ-C5-H), 9.13 (s, 1H, ClQ-C8-H), 11.60 (s, 1H, COOH). For  $\text{C}_{12}\text{H}_{11}\text{ClN}_2\text{O}_2$  250.5, mass spectrum 251.4 (M +H) $^+$ , ESI 249.

#### 2.5.2.1 B. Oxidation using periodic acid<sup>167</sup>

Compound **1** (0.5 g, 0.0021 mol) and acetonitrile (30 ml) was added to a solution of periodic acid (1.07 g, 0.0047 mol) in molar ratio (1:2) and a very small amount of  $\text{CrO}_3$  in acetonitrile (20 ml) as catalyst. After stirring at room temperature for 2h, the mixture

was filtered and washed with acetonitrile and the crude residue was purified by TLC (DCM/MeOH 4/1) to give the chloroquinoline amino acid compound as a dark yellow solid (0.45g, 90% yield), m.p 290-300 °C. Elemental analysis expected C: 57.48%, H: 4.39%, N: 11.17%, found C: 57.15%, H: 4.52%, N: 11.23%. IR: OH broad band at 3000  $\text{cm}^{-1}$ , NH stretch at 3300  $\text{cm}^{-1}$  and C=O stretch at 1720  $\text{cm}^{-1}$ .

$^1\text{H}$  NMR(400 MHz, DMSO- $\text{d}_6$ ):  $\delta_{\text{H}}$  /ppm 3.53 (t, 2H,  $\text{CH}_2$ ), 4.1 (t, 2H,  $\text{CH}_2$ ), 6.56 (d,  $J = 6.1$  Hz, 1H, ClQ-C3-H), 7.58 (dd,  $J = 7.2$  Hz, 1H, ClQ-C6-H), 7.60 (d,  $J = 7.8$  Hz, 1H, ClQ-C5-H), 7.92 (d,  $J = 6.8$  Hz, 1H, ClQ-C8-H), 8.49 (d,  $J = 7.2$  Hz, 1H, ClQ-C2-H), 9.58 (s, 1H, NH), 11.66 (s, 1H, COOH). For  $\text{C}_{12}\text{H}_{11}\text{ClN}_2\text{O}_2$  250.5, mass spectrum 251.1 ( $\text{M} + \text{H}$ ) $^+$ , ESI 249.9.

#### 2.5.2.2 Preparation of (7-chloroquinolin-4-yl) alanine (2a)

A mixture of 4,7-dichloroquinoline (12.675 g, 0.0928 mol) and alanine (82.85 g, 0.93mol) were heated with stirring at 140 °C for 20 h then ethanol (50 ml) was added to the mixture and stirring continued for an extra 6 h. After cooling, the reaction was poured into water (50ml) and filtered, the solid residue was dried then boiled in ethyl acetate (50 ml) to give brown solid (8.175 g, 70%), m.p 260-270 °C. Elemental analysis expected for  $\text{C}_{12}\text{H}_{11}\text{ClN}_2\text{O}_2$ , C: 57.48%, H: 4.39%, N: 11.17%, found C: 56.78%, H: 4.3%, N: 8.27%. IR: OH broad band at 3100  $\text{cm}^{-1}$ , NH stretch at 3250  $\text{cm}^{-1}$ , C-N stretch at 1200  $\text{cm}^{-1}$  and C=O stretch at 1745  $\text{cm}^{-1}$ .  $^1\text{H}$  NMR (400 MHz, DMSO- $\text{d}_6$ ):  $\delta_{\text{H}}$  /ppm 1.31 – 1.19 (m, 3H,  $\text{CH}_3$ ), 3.53 (d,  $J=2.3\text{Hz}$ , 1H- CH), 6.04 (d,  $J = 15.7$  Hz, ClQ-C3-H), 7.33 (d,  $J = 10.7$  Hz, ClQ-C5-H), 7.57 (d,  $J=5.2$  Hz, 1H- ClQ-C6-H), 7.93 (d,  $J = 4.0$  Hz, 1H, ClQ-C7-H), 8.08 (d,  $J = 8.6$  Hz, ClQ-C2-H), 8.32 (s, 1H- ClQ-C8-H), 9.32 (s, 1H, NH), 11.81 (s, 1H- COOH).  $^{13}\text{C}$  NMR (101 MHz)  $\delta$  175.84, 156.88, 156.12, 144.57, 130.85, 106.22, 62.19,

61.59, 59.24, 54.47 – 53.91, 46.98, 44.43. For  $C_{12}H_{11}Cl N_2O_2$  250.5, mass spectrum 251.91 and 252.20 (M +H)<sup>+</sup>.

### 2.5.2.3 Preparation of (7-chloroquinolin-4-yl) valine (2b)

A mixture of 4,7-dichloroquinoline (2.534 g, 0.0107 mol) and valine (18.64 g, 0.159 mol) were heated with stirring at 140 °C for 20 h then 20ml ethanol was added to the mixture and stirring continued for extra 6h . After cooling, the reaction was poured into water (50ml) and filtered, the solid residue was dried then boiled in ethyl acetate (50 ml) to give off white solid (2.1g, 83%), m.p more than 300°C. Elemental analysis expected C: 60.33%, H: 5.42%, N: 10.15%, found C: 59.87%, H: 5.90%, N: 10.93%. IR: OH broad band at 3000  $cm^{-1}$ , NH stretch at 3200  $cm^{-1}$ , C-N stretch at 1220  $cm^{-1}$  and C=O stretch at 1740  $cm^{-1}$ . <sup>1</sup>H NMR (400 MHz, DMSO- $d_6$ ):  $\delta_H$  /ppm 1.25 (d,  $J = 9.6$  Hz, 1H- CH), 1.77 (d,  $J = 9.8$  Hz, 1H-CH), 2.34 (s, 3H- CH<sub>3</sub>), 3.35 (s, 3H- CH<sub>3</sub>), 6.89 (d,  $J = 7.6$  Hz, 1H-C5-H), 7.82 – 7.79 (m, 2H, ClQ-C7), 7.83 (dd,  $J=8.0, 8.1$  HZ, 1H- ClQ-C6-H), 7.88 (d,  $J = 5.4$  Hz, ClQ-C3-H), 7.95 (s, 1H- ClQ-C8-H), 8.27 (s, 1H, NH), 8.56 (d,  $J = 7.4$  HZ, ClQ-C2-H), 10.45 (s, 1H-COOH). <sup>13</sup>C NMR (101 MHz,)  $\delta$  /ppm 178.42, 60.47, 57.43, 57.09, 54.33, 39.36 – 39.11, 38.79, 38.58, 38.37, 38.16, 37.94, 29.26, 17.62, 17.05. For  $C_{14}H_{15}Cl N_2O_2$  278.74, mass spectrum 279.087 (M +H)<sup>+</sup>.

### 2.5.3 Preparation of $\beta$ -D-glucosyl urea (3)

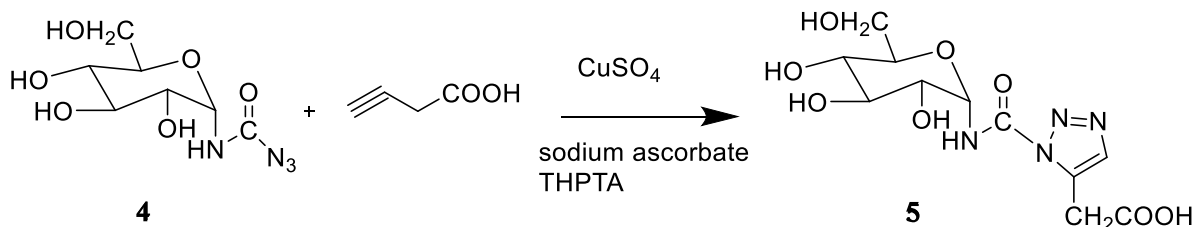
D-Glucose (0.6 g, 0.0033 mol), urea (1.4 g, 0.0233 mol) and NH<sub>4</sub>Cl (0.2 g, 0.0037 mol) were melted in a 25 ml reaction flask at 80 °C until a clear melt was formed. Amberlyst (0.2 g) was added as a catalyst and the reaction stirred for 2 h at 80 °C. Water was added to the warm melt and the catalyst was filtered off. After the removal of water, the brownish solid was twice recrystallised from MeOH to give pure  $\beta$  -D-glucosyl urea as white crystals (0.47 g, 78%).<sup>168</sup> Elemental analysis expected C: 37.52%, H: 6.41%, N:

12.66% found C: 37.09%; H: 6.02%; N: 12.43%.  $^1\text{H}$  NMR(400 MHz, DMSO- $d_6$ ):  $\delta_{\text{H}}$  /ppm 2.97–3.03 (m, 1H), 3.24–3.34 (m, 2H), 3.36–3.43 (m, 1H), 3.50–3.52 (m, 1H), 3.59–3.65 (m, 1 H), 4.41 (t, OH), 4.67 (s,1 OH), 4.76 (s,1 OH), 4.80 (m, 1 H), 4.83 (s,1OH), 5.84 (s,  $\text{NH}_2$ ), 6.47 (s, NH). Molecular weight for  $\text{C}_7\text{H}_{14}\text{N}_2\text{O}_6$  222.2, mass spectrum 222.8 (M +H) $^+$ .

#### ***2.5.4 Preparation of 3, 4, 5-(trihydroxy-6-(hydroxymethyl) tetrahydro-2-pyran-2-yl) carbamoyl azide (4)***

B-D-glucosyl urea (0.03g, 0.00014 mol), *t*-BuNO (0.029g, 0.000281 mol), sodium azide (0.009 g, 0.000138 mol) and 9/2 ratio *t* BuOH in water were mixed and gently stirred for 7h at room temperature. The mixture was concentrated by vacuum. The solid was recrystallised from MeOH to give pure 3,4,5-(trihydroxy-6-(hydroxymethyl) tetrahydro-2-pyran-2-yl) carbamoyl azide as reddish brown crystals (0.025 g, 84%). <sup>169</sup> Elemental analysis expected: C: 33.81%; H: 4.97%; N: 22.72%; found C: 34.01%; H: 5.08%; N: 22.51%.  $^1\text{H}$  NMR (400 MHz, DMSO- $d_6$ ):  $\delta_{\text{H}}$  /ppm 2.41(s, OH), 2.61 (d,  $J = 5.4\text{Hz}$ , 1 H-C6), 2.97 (d,  $J = 3.21\text{ Hz}$ , 1H- C<sub>1</sub>), 3.24–3.34 (m, 2H-C2), 3.50–3.52 (t, 2H-C4), 6.66 (s, 1H-NH), 6.94 (s, OH), 7.05 (s, OH), 7.93 (s, OH), 8.28–8.25 (m, 2H-C3), 8.34–8.30 (m, 3H, C5).  $^{13}\text{C}$  NMR (101 MHz)  $\delta$  /ppm 40.59, 40.40, 40.20, 39.96, 39.75, 39.55, 39.34. For  $\text{C}_7\text{H}_{12}\text{N}_4\text{O}_6$  248.20, mass spectrum 250.8 m/z (M +H) $^+$ .

**2.5.5 Preparation of 3, 4, 5-(trihydroxy-6-(hydroxymethyl) tetrahydro-2-pyran-2-yl) carbamoyl -1, 2, 3-triazol-5-yl) acetic acid (5)**



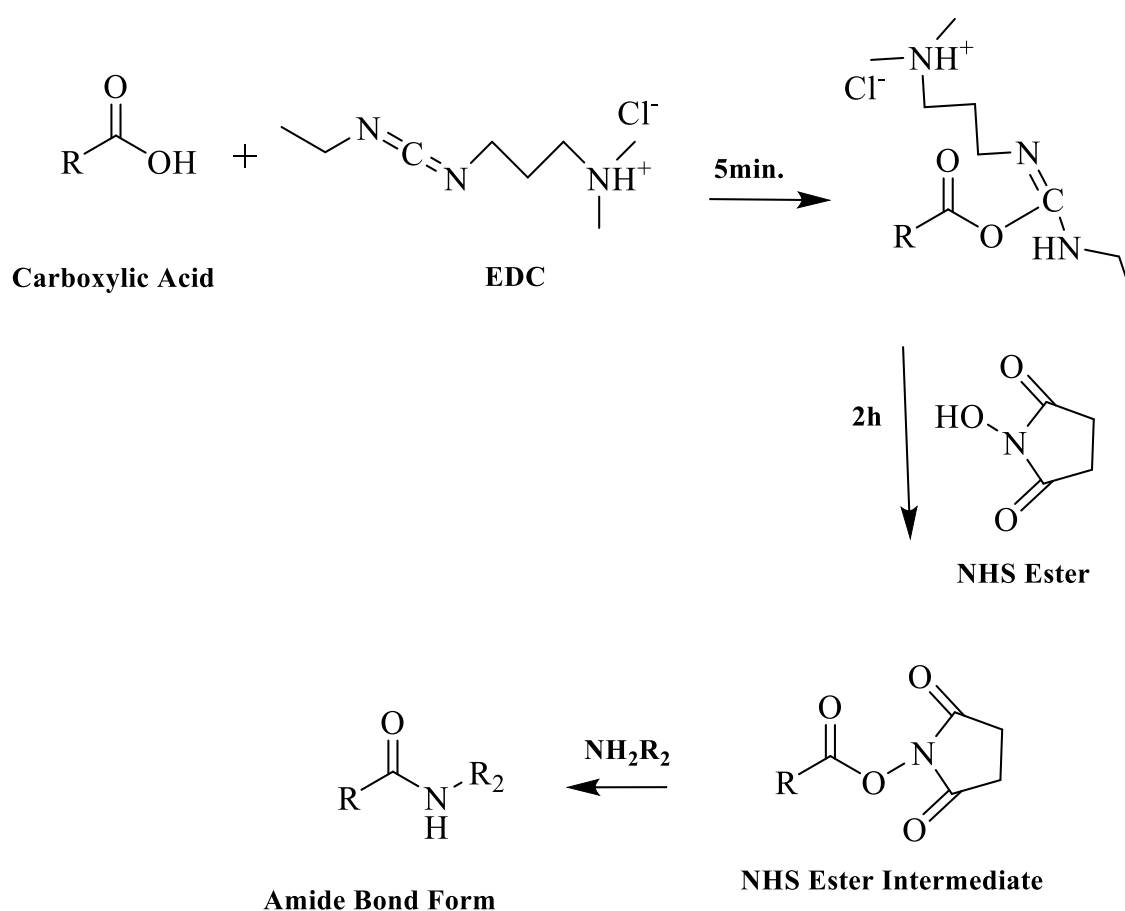
3,4,5-Trihydroxy-6-(hydroxymethyl)tetrahydro-2H-pyran-2-yl) carbamoyl azide (**4**) (0.012 g, 0.0483 mmol) was reacted with butyric acid ( 0.005 g, 0.058 mmol), CuSO<sub>4</sub> (0.002 g, 0.0075mmol) in 2.5ml water, sodium ascorbate (0.0025 g, 0.0126 mmol) and tris(3-hydroxypropyltriazolylmethyl)amine (0.0056 g, 0.028 mmol) were added together as a catalyst . The mixture was reacted at 40 °C by using a CEM Benchmate microwave reactor for 1.5 h. After that the crude brownish solid was recrystallised from MeOH to give compound (**5**) as pure solid (0.008 g, 67%). Elemental analysis expected: C: 33.79%, H: 4.52%, N: 22.32%, found C: 33.60%, H: 4.74%, N: 22.50%. <sup>1</sup>H NMR (400 MHz, DMSO-d<sub>6</sub>): δ<sub>H</sub> /ppm 1.92 (s, OH), 1.96 (s, H-triazol), 2.15 – 1.98 (m, 2H,CH<sub>2</sub>), 2.93 (t, *J* = 8.9 Hz, 2H-C2), 3.44 – 3.32 (m, 3H-C5), 3.59 (t, *J* = 12.6 Hz, 2H-C3), 4.80 (m, 1 H-C6), 4.51 (d, *J* = 7.4 Hz, 1H-C1), 4.73 (d, *J* = 5.3 Hz, 2H-C4), 6.71 (s, NH), 7.36 (s, OH), 7.48 (s, OH), 8.64 (s, OH) and 10.63 (s, 1H, COOH).

<sup>13</sup>C NMR (101 MHz, DMSO-d<sub>6</sub>): δ /ppm 172.38, 52.50–52.20, 52.02, 49.06, 43.01, 42.65, 39.27, 35.22, 31.76, 31.48. 62.50–62.70. For C<sub>11</sub>H<sub>16</sub>N<sub>4</sub>O<sub>8</sub> 332.07, mass spectrum 332.2 m/z (M +H)<sup>+</sup>.

## 2.6 Chemical modification of virus

### 2.6.1 Attachment of chloroquinoline derivatives to CPMV

0.675  $\mu\text{l}$  of chloroquinoline amino acid compound **2** and **2a** (0.002 gm, 0.0079 mmol) in 5 ml DMSO in 6000 molar excess and compound **2b** (0.3  $\mu\text{l}$  of 0.1 gm, 0.358 mmol) in 10% DMSO (10 ml) were added separately to 100  $\mu\text{l}$  CPMV (0.1 mg/ml) and the reaction left to proceed for 1.5 h with gentle stirring. *N*-ethyl-*N'*-(3-dimethylaminopropyl) carbodiimide hydrochloride (EDC) (0.002 g, 0.01 mmol) in 5 ml PBS buffer at pH 7.1 was added in a 1000 molar excess, and NHS (0.003g, 0.026 mmol) in 5 ml PBS buffer was added in a 4000 molar excess. The final DMSO concentration of the reaction mixture was adjusted to 20 % by volume.<sup>170</sup> The mechanism action of EDC/NHS as a conjugation reagents is shown below:<sup>164</sup>



After stirring for 24 h at room temperature the precipitate that formed was removed by centrifugation (14000 rpm, 10 min., room temperature); 100 kDa cut-off columns were used for purification of the derivatised virus particles; the columns were washed three times with PBS buffer (100  $\mu$ l). The modified virions were resuspended in 10 mM sodium phosphate buffer pH 7.1 (100  $\mu$ l). Recovery of virus was 70%, 76% and 76% respectively.

### ***2.6.2 Labelling of CPMV-CQ -derivatives with Alexa fluorescent dye***

Alexa Fluor 488 (succinimidyl ester) dye (0.028 g, 0.0435 mmol) a molar excess of 2000, was dissolved in dry DMSO (2 ml) and added to CPMV-CQp, CPMV-CQ- alanine and CPMV-CQ -valine particles (100  $\mu$ l) in 0.1 M sodium phosphate buffer (pH 7.1). The final DMSO concentration was adjusted to 20% (v/v). The reaction was incubated for 2h at room temperature then left to proceed at 4 °C for 23h while gently stirring. The final products were washed three times with 100  $\mu$ L sodium phosphate buffer pH 7.1 and centrifuged each time at 14000 rpm for 10 minutes.<sup>24</sup>

### ***2.6.3 Attachment of glucuronic acid to CPMV***

Glucuronic acid (0.5  $\mu$ l of 0.046 g in 5 ml MQ water) was added to (EDC) (0.01 g, 0.052 mmol), a 1000 molar excess in PBS buffer at pH 7 (10 ml), and NHS (0.01 g, 0.086 mmol) in PBS buffer (10 ml) was added in a 4000 molar excess and the reaction left to proceed for 1.5 h with gentle stirring, CPMV (100  $\mu$ l, 0.1 mg/ml) was added to the mixture. The final DMSO concentration of the reaction mixture was adjusted to 20 % by volume.<sup>170</sup>

After stirring for 24 h at room temperature the mixture was centrifuged (14000 rpm, 10 min., at room temperature). 100 kDa cut-off columns were used for purification of the derivatised virus particles; the columns were washed three times with PBS buffer (100  $\mu$ l). The modified virions were resuspended in (100  $\mu$ l) of 10 mM sodium phosphate buffer pH 7. Virus recovery was 60%.

#### ***2.6.4 Attachment of glucuronic acid to CPMV-CQ- derivatives***

EDC (0.01 g, 0.052 mmol) in PBS buffer(10 ml) was added in a 1000 molar excess to glucuronic acid (0.5  $\mu$ l of 0.046 g in 5 ml MQ water), after 5 min stirring, NHS (0.01 g, 0.086 mmol) in 10 ml PBS buffer was added in a 4000 molar excess. The reaction was left to proceed for 2 h with gentle stirring, CPMV-CQp, CPMV-CQ-alanine and CPMV-CQ-valine (100  $\mu$ l of 0.2 mg/ml) in PBS buffer were added from each to the mixture separately. The final DMSO concentration of the reaction mixture was adjusted to 20 % by volume.<sup>24</sup>

100 kDa cut-off columns (Millipore) were used for virus particle purification; the columns were washed three times with PBS buffer (80  $\mu$ l). The modified viruses were resuspended in 80  $\mu$ l of 10 mM sodium phosphate buffer pH 7. Recovery of virus was 67%, 70% and 55% respectively.

#### ***2.6.5 Attachment of propiolic acid and butyric acid to CPMV***

Propiolic acid (**P.A**) or butyric acid (**B.A**) (10  $\mu$ l) was added (in 3000 molar excess to CPMV) to EDC (0.009g, 0.0469 mmol) in a 1000 molar excess, and NHS (0.042 g, 0.365 mmol) in a 4000 molar excess, both reagents were dissolved in PBS buffer pH7(10 ml). The reaction was left to proceed for 2 h with gentle stirring, CPMV (100  $\mu$ l) was added to the mixture, and the final DMSO concentration of the reaction mixture was adjusted to less than 20 % by volume. The reaction was left to proceed overnight at room temp with stirring.

100 kDa cut-off column (Millipore) was used for purification; the column was washed three times with PBS buffer (80  $\mu$ l). The modified virus was resuspended in 10 mM sodium phosphate buffer pH 7 (80  $\mu$ l).<sup>170</sup> Recovery of virus was 75% and 45% respectively.

### **2.6.6 The coupling of $N_3$ -bodipy dye to CPMV- P.A and CPMV- B.A**

CPMV- P.A (100  $\mu$ l) and CPMV- B.A (100  $\mu$ l) were modified with  $N_3$ - bodipy Dye in 3000 molar excess with 10% (v/v) DMSO for 4 h as a catalyst L-ascorbic acid (0.0025 g, 0.014 mmol) and  $CuSO_4$  (0.002g, 0.0075mmol) were added together with tris-(benzyltriazolylmethyl)-amine (THPTA) (0.0056g, 0.013 mmol). The mixture was purified by 100 KDa cut off column centrifugal device.<sup>171</sup>

### **2.6.7 Coupling of CPMV-B.A with 3, 4, 5(-trihydroxy-6-(hydroxymethyl) tetrahydro-2-pyran-2-yl) carbamoyl azide.**

CPMV-B.A (100  $\mu$ l) was modified with 3, 4, 5-trihydroxy-6-(hydroxymethyl) tetrahydro-2-pyran-2-yl) carbamoyl azide (0.012g, 0.0483 mmol) and 10% (v/v) DMSO for 4 h L-ascorbic acid (0.0025g, 0.014 mmol) and  $CuSO_4$  (0.002g, 0.0075 mmol) were added together with THPTA (0.0056g , 0.013 mmol). The final mixture was purified by 100 KDa cut off column centrifugal device.<sup>172</sup>

### **2.6.8 Attachment of 3, 4, 5((-trihydroxy-6-(hydroxymethyl) tetrahydro-2-pyran-2-yl) carbamoyl) -1, 2, 3-triazol-5-yl) acetic acid to CPMV**

3,4,5(-trihydroxy-6-(hydroxymethyl) tetrahydro-2-pyran-2-yl) carbamoyl) -1,2,3-triazol-5-yl) acetic acid compound **5** (0.8  $\mu$ l of 0.002 g in 5 ml MQ water) was added to EDC (0.01g, 0.052 mmol) in a 1000 molar excess, and NHS (0.01g, 0.0868 mmol) in a 4000 molar excess both reagents were dissolved in PBS buffer pH7 (10 ml). The reaction was left to proceed for 2 h with gentle stirring, CPMV (100  $\mu$ l, 0.2 mg/ml) was added to the mixture. The final DMSO concentration of the reaction mixture was adjusted to 20 % by

volume. The reaction was stirred overnight at room temp. The final mixture was purified by 100 KD cut off column centrifugal device.<sup>170</sup> Recovery of virus was 70%.

### ***2.6.9 Attachment of 3, 4, 5-((-trihydroxy-6-(hydroxymethyl) tetrahydro-2-pyran-2-yl) carbamoyl) -1,2,3-triazol-5-yl) acetic acid to CPMV-CQ- derivatives***

CPMV was first modified with 6000 molar excess of CQp, CQ- alanine and CQ- valine using an overnight reaction, then compound **5** (2000 molar excess 0.002g, 0.006 mmol in 5 ml MQ water) was added to EDC (0.009g, 0.0469 mmol) in a 1000 molar excess, and NHS (0.033g, 0.286 mmol) in a 4000 molar excess both were dissolved in PBS buffer pH7 (10 ml). The reaction was left to proceed for 2h with gentle stirring. CPMV-CQ derivatives each in 100  $\mu$ l was added to the mixture of compound **5**/ EDC/NHS and the final DMSO concentration of the reaction mixture was adjusted to less than 20% by volume. The reaction was stirred overnight at room temp. The final mixtures were purified by 100 KDa cut off column centrifugal device.<sup>58</sup> Recovery of virus was 60, 67, and 65% respectively.

### ***2.6.10 Labelling of CPMV-CQ- Glu (compound 5) with Alexa fluorescent dye***

Alexa Fluor 488 (succinimidyl ester) dye (0.028 g, 0.0435 mmol), a molar excess of 20000 dye molecules, was dissolved in dry DMSO (2 ml) and added to CPMV-CQ-Glu in 0.1 M sodium phosphate buffer (pH 7, 100  $\mu$ l). The final DMSO concentration was adjusted to 20% (vol/vol). The reaction was incubated for 1h at room temperature then left to proceed at 4 °C for 20 h while gently stirring. The final product was washed three

times with sodium phosphate buffer pH7 (80  $\mu$ l) by 100 KDa cut off column and centrifuged each time at 14000 rpm for 10 minutes.<sup>24</sup> Recovery of virus was 71%.

### ***2.6.11 Attachment of ferrocene to CPMV-CQ- derivatives***

CPMV (100  $\mu$ l) was first modified with 6000 molar excess of CQp, CQ-ala and CQ-val separately using an overnight reaction, then added to EDC (0.009g, 0.0469 mmol, 1000 molar excess ) in PBS buffer pH7 (10 ml), and NHS (0.033g, 0.286 mmol, 4000 molar excess ) in DMSO (5 ml). The reaction was left to proceed for 2h with gentle stirring. Amino ferrocene 3000 molar excess (0.12 g, 0.0005 mol) in DMSO (5ml) was added to each sample and the final DMSO concentration of the reaction mixtures were adjusted to less than 20 % by volume. The reaction was stirred overnight at 4 °C. The final mixtures were purified by dialysis using 100 kDa molecular weight cut-off membranes (Float-A-Lyzer G2) against 10 mM sodium phosphate buffer. The samples were concentrated on 100 kDa cut-off columns (Millipore).<sup>173</sup> Recovery of virus was 68%, 70% and 74% respectively.

### ***2.6.12 Attachment of ferrocene to CPMV-CQ- derivatives- G.A (triple modification)***

Each modified CPMV particle (CPMV-CQp-G.A, CPMV-CQ-ala-G.A and CPMV-CQ-val-G.A) (100  $\mu$ l) was reacted with freshly prepared EDC (0.005 g, 0.026 mmol, 1000 molar excess) in PBS buffer at pH 7 ( 5ml) and NHS (0.003g, 0.026 mmol, 4000 molar excess) in DMSO (5ml) . The reaction was left to proceed for 2h with gentle stirring then aminoferrocene 3000 molar excess (0.12 g, 0.0006 mole) in DMSO (5ml) was added. The final DMSO concentration of the reaction mixture was adjusted to 20 % by volume and the reaction was stirred overnight at 4 °C. The CPMV-ferrocene conjugate for each sample was purified by dialysis using 100 kDa molecular weight cut-off membranes

(Float-A-Lyzer G2) against 10mM sodium phosphate buffer pH7. The sample was concentrated on 100 kDa cut-off columns (Millipore).<sup>173</sup> Recovery of virus was 77-78%.

## ***2.7 The modification of CPMV-ferrocene***

CPMV particle (0.2 mg/ml), suspended in 10 mM sodium phosphate buffer pH7, was reacted with freshly prepared of EDC (0.005 g, 0.026 mmol, 1000 molar excess) in PBS buffer at pH 7 (5 ml), and NHS (0.003g, 0.026 mmol, 4000 molar excess) in DMSO (5 ml). The reaction was left to proceed for 2 h with gently stirring then aminoferrocene (0.12 g, 0.0005 mol, 3000 molar excess) in DMSO (5ml) was added. The reaction was stirred overnight at 4 °C with gentle stirring. The final DMSO concentration of the reaction mixture was adjusted to 20 % by volume. The CPMV-ferrocene conjugate was purified by dialysis using 100 kDa molecular weight cut-off membranes (Float-A-Lyzer G2) against 10 mM sodium phosphate buffer. The sample was concentrated on 100 kDa cut-off columns (Millipore).<sup>173</sup> Recovery of virus was 78%.

### ***2.7.1 The modification of CPMV-ferrocene with CQ- derivatives***

CPMV was first modified with a 3000 molar excess of aminoferrocene using an overnight reaction, then compound **2, 2a** (6000 molar excess 0.002 g in 5 ml DMSO) and **2b** (6000 molar excess: 0.1 g in 10ml 10% DMSO) were added to EDC (0.009g, 0.0469 mmol) in a 1000 molar excess, and NHS (0.033g, 0.286 mmol) in a 4000 molar excess both were dissolved in PBS buffer pH7 (10 ml). The reaction was left to proceed for 2h with gentle stirring. CPMV-Fc in PBS buffer (100 µl) was added to each sample and the final DMSO concentration of the reaction mixture was adjusted to less than 20 % by volume. The reaction was stirred overnight at room temp. The final mixtures were

purified by 100 KDa cut off column centrifugal device.<sup>58, 170</sup> Recovery of virus was 62, 65 and 68% respectively.

## ***2.8 Colorimetric method to measure beta- haematin crystal growth in vitro***

A stock solution of haemin chloride was prepared freshly by dissolving (0.0013g, 0.002mmol) haemin chloride in aqueous NaOH (0.1M, 10 ml) and then centrifuging for 10 min at 7000g to remove unreacted haem, the concentration of haemin chloride was calculated from the absorbance at 385 nm using  $\epsilon_{mM} = 58,400$  in 100 mM NaOH.

Beta-haematin (BH) formation was performed by heating (1ml ,0.2 mmol) from stock solution in sodium acetate buffer (1ml, 0.5M, pH 5) at 73 °C without chloroquinoline and at 70 °C with each CQ derivative (10  $\mu$ M). At selected times, solution was withdrawn and BH formation was evaluated. The control haemin chloride solution in the same buffer was kept at room temperature and withdrawn at the appropriate incubation time and their absorbance at 400 and 650 nm was measured spectrophotometrically.<sup>174</sup>

To subtract the turbidity of BH, haem fractions converted to BH were calculated by the following Eq. (3): This experiment was repeated three times.

$$(A_{400nm}-A_{650nm})_{control} - (A_{400nm} - A_{650nm})_{sample} / (A_{400nm} - A_{650nm})_{control} \text{ ----- Eq 3}$$

## ***2.9 Purification method to measure beta- haematin crystal growth in vitro***

Stock solution of haemin chloride was prepared freshly by dissolving (0.0013g, 2mmol) haemin chloride in aqueous NaOH (2ml, 20 mM) and then centrifuging for 10 min at 7000g to remove unreacted haemin. Haem concentration was calculated from the absorbance at 385 nm using  $\epsilon_{mM} = 58,400$  in 100 mM NaOH.

BH formation was performed by heating haem stock solution (0.1-0.5 mmol) with sodium acetate buffer (0.5 M, pH 5) overnight at 70 °C with and without each chloroquinoline derivative (10-50  $\mu$ M). After heating samples were centrifuged for 10 min at 7000g. BH was purified by suspending the pellet in sodium dodecylsulphate (SDS) buffer (1 ml of 2.5%) with 0.1 M sodium bicarbonate (pH 9.1) at room temperature for 1h with stirring to dissolve unreacted haem, the remaining insoluble material was recovered by centrifugation. This step was repeated once more, the haem concentration in the solution was calculated from the absorbance at 400 nm with an extinction coefficient of  $10^5$  nM as described previously with slight modification.<sup>175</sup> UV/Vis spectrophotometry and IR were used to characterise BH formation.

## ***2.10 Beta- haematin production for IR and SEM measurements***

Synthetic BH was obtained by the method described by Slater et al. (1991),<sup>175</sup> with some modifications. Haemin chloride (0.24 g, 0.368 mmol) was dissolved in aqueous NaOH (50 ml, 0.1N). Haemin chloride with and without of each CQ derivative (10 $\mu$ l) were precipitated by adding glacial acetic acid (17.5 ml) slowly. The mixtures were incubated overnight at 80°C. Non-crystalline haem was removed by centrifuging for 10 minutes at 7000g. The precipitate was washed three times with 100 mM sodium bicarbonate (pH 9.1, 50ml) during 3 hours then centrifuging for 15 minutes at 7000g. The pellet was further

washed three more times in ultrapure water (MilliQ Synthesis) and finally resuspended in 5 ml MQ water.

### ***2.11 The reaction of iron oxide with beta-haematin in vitro:***

A mixture of solutions of ferric and ferrous sulfate in a molar ratio of 2:1 (1.5 ml, 10mM: 5 mM) was prepared and divided into two parts.

1- 1 ml of this mixture was added to 15  $\mu$ l of 0.1N NaOH solution and left to react for 60 minutes with stirring, haem (0.5 ml of 7mM) in aqueous 0.1 N NaOH and glacial acetic acid (525  $\mu$ l) were added together then the mixture was left for 10h reaction at 80 °C.

2- Ferric and ferrous sulphate mixture (0.5 ml) was added to haem (7mM, 0.25 ml) in aqueous 0.1 N NaOH and glacial acetic acid (87.5  $\mu$ l) were added together, the reaction was left to proceed for 10 h at 80 °C.

Blank sample was prepared by mixing of haem stock solution (0.5 ml) with glacial acetic acid (175  $\mu$ l) and the reaction was left to proceed for 10 h at 80 °C. Non-crystalline haem was removed by centrifuging for 10 minutes at 7000g. The precipitate of all samples was washed three times with 100 mM sodium bicarbonate (pH 9.1, 50ml) during 3 hours then centrifuged for 15 minutes at 7000g. The pellet was further washed three more times in ultrapure water (MilliQ Synthesis) and finally resuspended in 5 ml MQ water.

The concentration of each sample was calculated spectrophotometrically at 400 nm with an extinction coefficient  $10^5$ mM. The fraction of haem formed beta-haematin samples were calculated from the comparison between the concentrations of haemin chloride solution before and after BH formation.<sup>175</sup>

### ***3 Chemical characterisation***

This chapter contains the most important characteristics of all compounds reported in chapter 2 (three different CQ-derivatives and three different glucose derivatives), including FTIR and <sup>1</sup>HNMR spectroscopy data for the main functional groups in each compound. Moreover, the reaction schemes for all compounds are illustrated.

The purity of each compound was monitored by using thin layer chromatography (TLC). The crystal structure for 3-((7-Chloroquinolin-4-yl) amino) propan-1-ol with full description of this crystal is also reported.

#### ***3.1 Preparation of 3-(7-chloroquinolin-4-ylamino) propan-1-ol (1)***

Compound **(1)** was prepared as an off white solid in 90% yield as described in (section 2.4.1),<sup>166</sup> in order to create chloroquinoline amino acid **(2)** which is required to target lysine groups on the CPMV surface. The purity of compound **(1)** was confirmed by two methods, first using TLC (DCM/ MeOH/ NH<sub>4</sub>OH, 4/1/1 volume ratio) which showed a single spot at R<sub>f</sub> 0.25. The second method is recrystallization from ethyl acetate as a solvent to give a novel crystal **Figure 3.1**. A full characterisation of compound **(1)** was described in chapter 2 (section 2.5.1). The <sup>1</sup>HNMR and IR characteristic frequency of absorption for the main functional groups of compound **(1)** are listed in **Table 3.1**.

**Table 3.1 IR and  $^1\text{H}$ NMR spectroscopic data for compound (1)**

IR data	3200 $\text{cm}^{-1}$	3300 $\text{cm}^{-1}$	1200 $\text{cm}^{-1}$
	OH	NH	C-N
$^1\text{H}$ NMR data	$\delta$ 1.8 ppm	$\delta$ 5.95 ppm	
	OH proton	NH proton	

The IR signals for O-H and N-H stretching occur around 3200  $\text{cm}^{-1}$  and 3300  $\text{cm}^{-1}$  respectively, yet, they look different. The OH stretching broad band vibrated at lower frequency than NH because the bonds between atoms of higher masses vibrate at lower frequencies.<sup>176</sup>

$^1\text{H}$ NMR data provided evidence for the characterisation of (1).

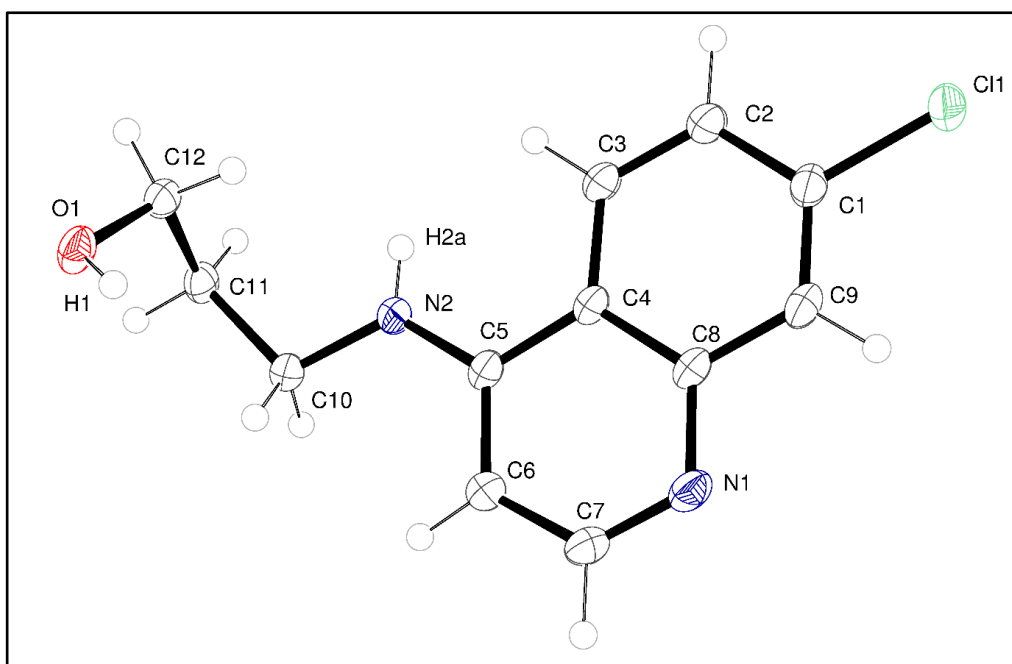


**Figure 3.1 Asymmetric unit of compound (1) with atoms drawn as 50% probability ellipsoids. (Selected hydrogen atoms are labelled). The crystal structure confirms the expected composition.**

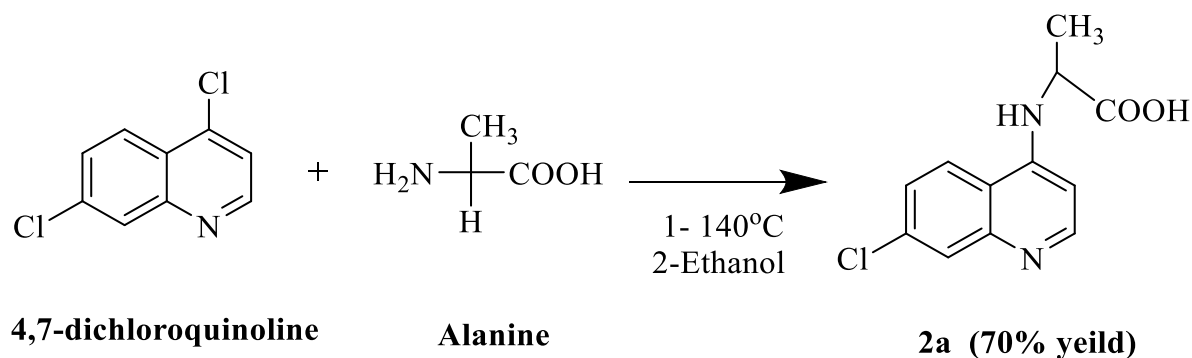
The asymmetric unit for compound (1) contains a single chloroquinoline molecule ( $C_{12}H_{13}Cl_1N_2O_1$ ) in a monoclinic crystal system with formula weight 236.69 g/mol. The crystal structure resolution was 0.71073 Å. There is no solvent and no disorder in the structure. The structure was solved using SHELXS-2013 and refined using full-matrix least squares refinement based on all unique  $F^2$  values. Hydrogen atoms were identified within Fourier difference maps. The  $CH_2$  groups were placed using a riding model but the C–H distances could refine subject to the restraint that all these C–H distances be equal within 0.03 Å. Similarly, the aromatic C–H hydrogen atoms were placed in a similar way subject to the restraint that these C–H distances be equal within 0.03 Å. The full crystallographic data are provided in Appendix II. The bond length and angles are slightly different compared with other chloroquinoline compounds.<sup>177</sup>

### ***3.2 Preparation of chloroquinoline propionic acid (CQp)(2)***

Compound (2) was prepared using the reaction of dichloroquinoline with amino acids in the presence of phenol in 40% yield without full characterisation.<sup>178, 179</sup> To increase the yield of compound (2), to make the reaction safer and to avoid the intermediate compound, CQp (2) was prepared from compound (1) by using two different oxidation methods as described in (sections 2.5.2.1A and 2.5.2.1B)<sup>180, 167</sup> in high yields (80% and 90%, respectively). The purity of this compound can be followed by TLC (DCM/MeOH 4/1 volume ratio), a single spot was observed at  $R_f$  0.31. Compound (2) was fully characterised in chapter 2 (sections 2.5.2.1A and 2.5.2.1B). The disappearance of characteristic  $^1H$ NMR of OH proton at 1.8 ppm and the appearance of a characteristic singlet at 11.66 ppm corresponding to (1H, COOH) provided good evidence for the production of compound (2).  $^1H$ NMR and IR characteristic frequency of absorption for main groups of compound (2) are listed in **Table 3.2**.

### 3.3 Preparation of (7-chloroquinolin-4-yl) alanine (2a)

Compound (2a) was prepared in the presence of phenol in 20% yield without full characterisation. To increase the yield of compound (2a) and make the reaction safer, the published method<sup>166, 179</sup> was significantly modified. The compound was prepared as brown solid in 70% yield as described briefly (section 2.5.2.2). Compound (2a) was fully characterised in the experimental chapter. <sup>1</sup>HNMR and IR characteristic frequency of absorption for main groups are listed in **Table 3.2**. The modified reaction is shown in **Scheme 3.1**.



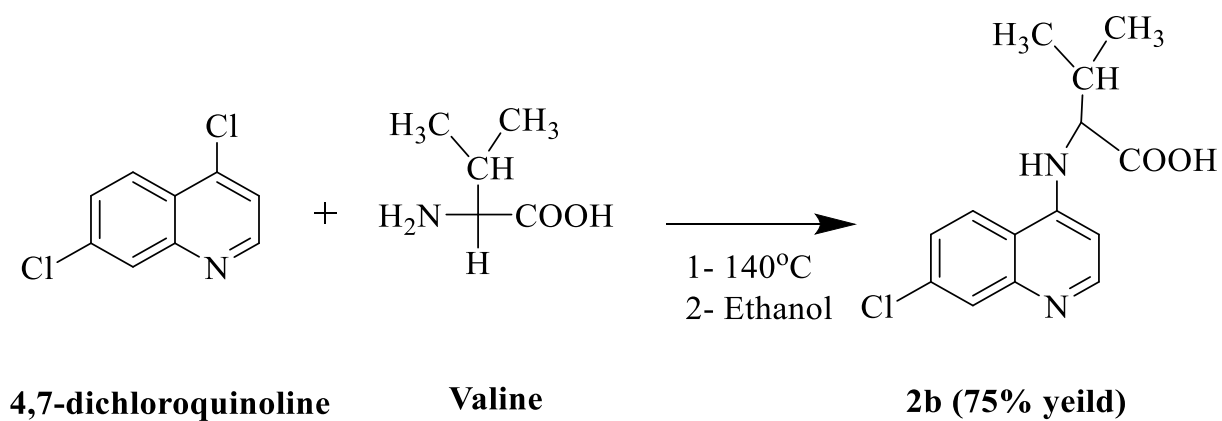
**Scheme 3.1** Synthesis of (7-Chloroquinolin-4-yl) alanine (2a)

Compound (2a) was purified by washing the final product with chloroform two times to remove unreacted compounds then the crude residue was run on TLC (DCM/ MeOH/ NH<sub>4</sub>OH, 4/1/1 volume ratio). A single spot at R<sub>f</sub> 0.28 was observed.

### 3.4 Preparation of (7-chloroquinolin-4-yl) valine (2b)

Compound (2b) was prepared by the procedure above as an off white solid in 75% yield (section 2.5.2.3).<sup>166, 179</sup>

The formation of the new compound (**2b**) with full characterization, has been described (section 2.5.2.3). <sup>1</sup>HNMR and IR characteristic frequency of absorption for main groups are listed in **Table 3.2**. The reaction is shown in **Scheme 3.2**



**Scheme 3.2 Synthesis of (7-Chloroquinolin-4-yl) valine (2b)**

**Table 3.2 <sup>1</sup>HNMR and IR spectroscopic data for CQ-derivatives**

CQ-derivatives	Yield	Function groups	IR data	<sup>1</sup> HNMR data
CQp compound ( <b>2</b> )	90%	OH	3000 cm <sup>-1</sup>	11.66 ppm
		NH	3300 cm <sup>-1</sup>	9.58 ppm
		C=O	1720-1721 cm <sup>-1</sup>	
CQ-ala compound ( <b>2a</b> )	70%	OH	3100 cm <sup>-1</sup>	11.81 ppm
		NH	3250 cm <sup>-1</sup>	9.32 ppm
		C-N	1200 cm <sup>-1</sup>	
		C=O	1745 cm <sup>-1</sup>	
CQ-val compound ( <b>2b</b> )	75%	OH	3000 cm <sup>-1</sup>	10.45 ppm
		NH	3200 cm <sup>-1</sup>	8.27 ppm
		C-N	1220 cm <sup>-1</sup>	
		C=O	1740 cm <sup>-1</sup>	

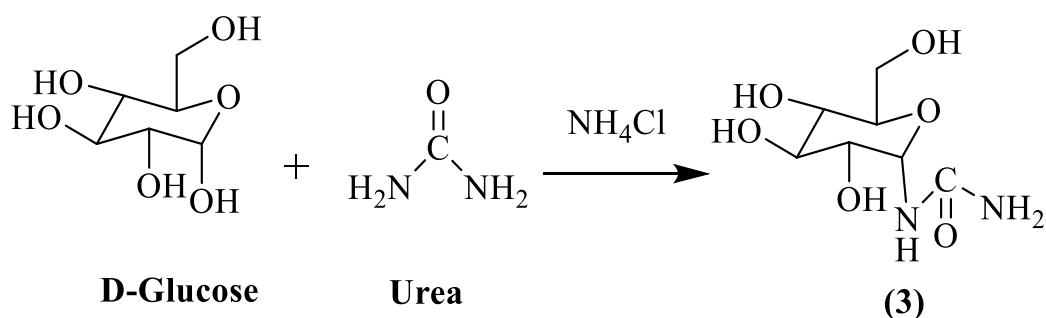
The CQ-derivatives have the same main functional groups but they are different in the length of the side chain. Therefore, all three CQ show similar FT-IR and <sup>1</sup>HNMR data

The chemical shift from OH and NH protons are seen at high ppm compared with other types of protons in each CQ derivatives due to the electronegativity difference between H and its surrounding atoms. Electronegative groups (O, N) move proton down field increasing the ppm values for OH and NH groups. The data in **Table 3.2** confirmed the

successful conjugation of amino acids with dichloroquinoline as described in each scheme. Moreover, each CQ derivative can be recognised from IR data depending on the frequency of each functional group.<sup>176</sup>

### 3.5 Preparation of $\beta$ -D-glucosyl urea (3)

$\beta$ -D-glucosyl urea (3) was prepared as described (section 2.4.3) as white crystals (0.47 g, 78%)<sup>168</sup> The compound (3) was purified by washing the final product with 20% (MeOH/water volume ratio) twice to remove unreacted compounds. TLC (MeOH/ DCM/ water, 30/5/65 volume ratio) was used to identify the purity, a single spot was observed at Rf 0.26. The compound has been fully characterised (section 2.5.3) and the reaction is shown in **Scheme 3.3**.

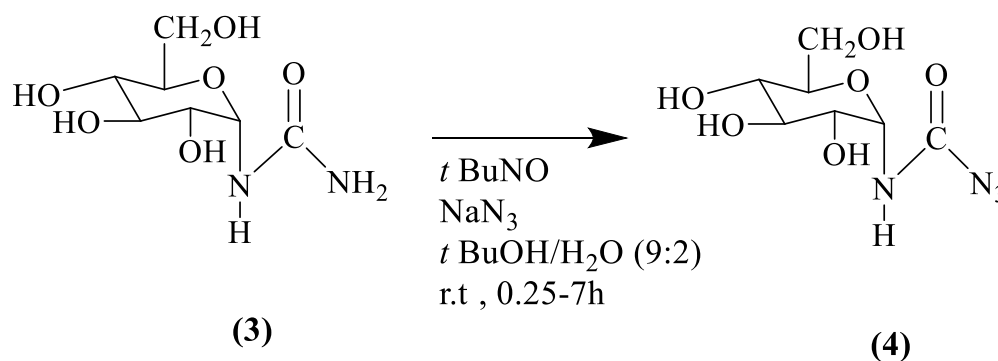


**Scheme 3.3** Synthesis of  $\beta$ -D-glucosyl urea (3)

### 3.6 Preparation of 3, 4, 5-(trihydroxy-6-(hydroxymethyl) tetrahydro-2-pyran-2-yl) carbamoyl azide (4)

Compound (4) was prepared by adaptation of a published procedure.<sup>169</sup> It was prepared from the reaction of  $\beta$ -D-glucosyl urea, <sup>t</sup>BuNO, sodium azide and 9/2 volume ratio <sup>t</sup>BuOH to water. Compound (4) was boiled in MeOH then left to recrystallise at room temperature for 3 days to give a pure and new reddish brown solid residue in 84% yield

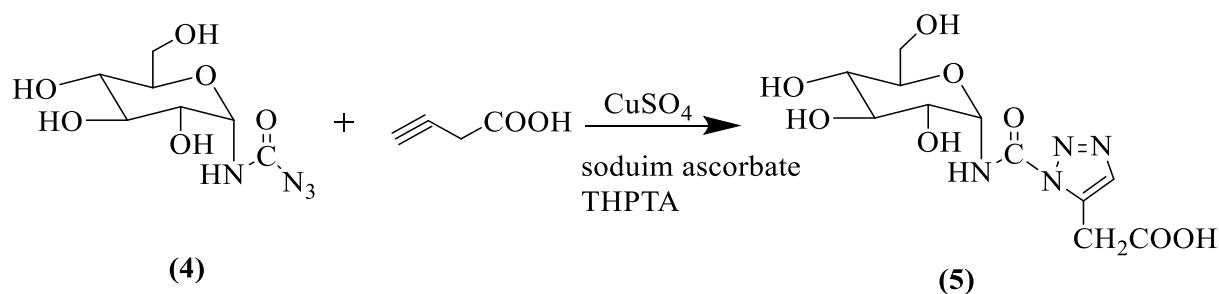
as described (section 2.5.4). The purity of compound (4) was followed by using TLC (MeOH/ DCM/ water, 30/5/65 volume ratio), a single spot was observed at R<sub>f</sub> 0.31. The full characterisation of compound (4) has been described (section 2.4.4). The reaction is shown in **Scheme 3.4**.



**Scheme 3.4** Synthesis of 3,4,5-(trihydroxy-6-(hydroxymethyl) tetrahydro-2-pyran-2-yl) carbamoyl azide (4)

### 3.7 Preparation of 3, 4, 5-((trihydroxy-6-(hydroxymethyl) tetrahydro-2-pyran-2-yl) carbamoyl) -1, 2, 3-triazol-5-yl) acetic acid (5)

Compound (5) was prepared by reacting one equivalent of compound (4) with one equivalent of butyric acid as described (section 2.5.5) by adaptation of a published method.<sup>171</sup> Some modification has been carried out as described briefly (section 2.5.5). The purity of compound (5) was followed by using TLC (ethanol/ DCM/ water, 40/15/45 volume ratio), a single spot was observed at R<sub>f</sub> 0.32. The modified reaction is shown in **Scheme 3.5**.



**Scheme 3.5** Synthesis of 3, 4, 5-(trihydroxy-6-(hydroxymethyl) tetrahydro-2-pyran-2-yl) carbamoyl -1, 2, 3-triazol-5-yl) acetic acid (5).

### 3.8 Determination of virus concentration

#### 3.8.1 UV-Vis spectroscopy

The preparation and purification of the wild type CPMV virus was performed by standard procedures.<sup>181</sup>

The integrity of viral particles was examined by UV/Vis spectroscopy as described (section 2.4.1). Intact CPMV particles have maximum absorption (A) at 260 nm, and the ratio of  $A_{260}:A_{280}$  is 1.52 as shown in **Figure 3.2**. This ratio provides additional information of the integrity of CPMV preparations, the peak at 260 nm is from the absorbance of encapsulated nucleic acids and the absorbance at 280 nm from the protein capsid.

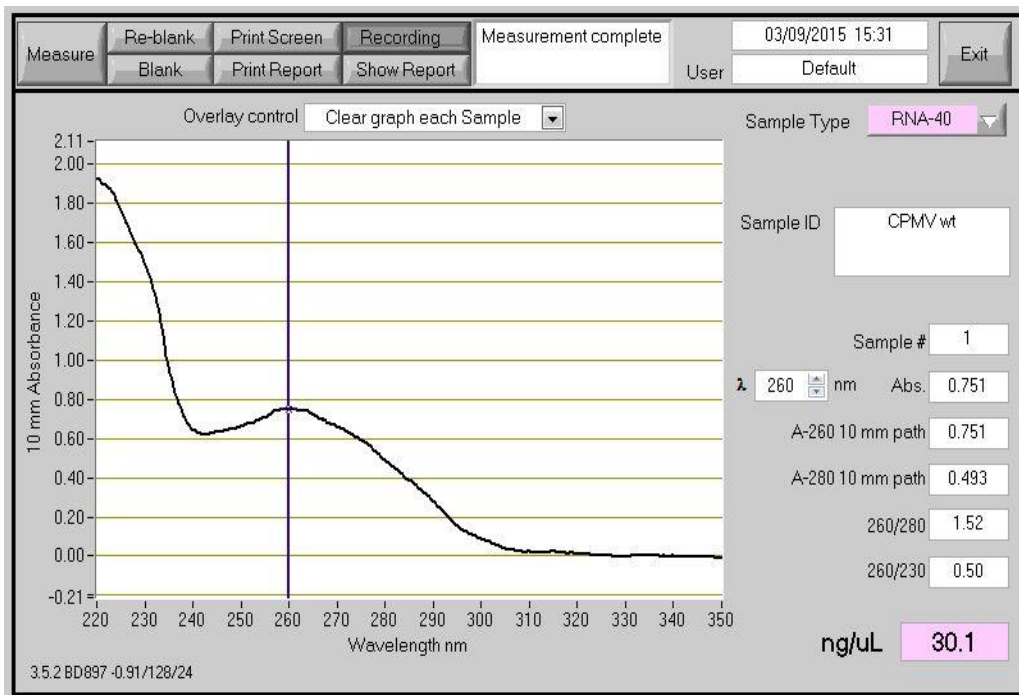


**Figure 3.2** The UV chart shows the maximum absorbance of 0.093 mg/ml of wild type CPMV in sodium phosphate buffer.

### 3.8.2 Gel electrophoresis

Electrophoresis is a process which allows the separation of molecules based on size. Using an electric field, molecules (such as RNA and DNA) can be made to move through a gel made of agarose or polyacrylamide. In addition, the electric field involves a negative charge at one end which pushes the molecules through the gel, and a positive charge at the other end that pulls the molecules through the gel. The molecules being sorted are distributed into a well in the gel material. The gel is placed in an electrophoresis chamber, which is then connected to a power supply. When the electric current is applied, the larger molecules move more slowly through the gel while the smaller molecules move faster. Buffer solutions were used in this method to reduce pH changes due to the electric field, which is essential because the charge of RNA depends on pH.<sup>182</sup>

Agarose gel electrophoresis is the most effective way for separating RNA fragments of varying sizes. It is used in biochemistry, molecular biology, and clinical chemistry to separate a mixed population of RNA or proteins in a matrix. Biomolecules are separated by applying an electric field to move the charged molecules through an agarose matrix, and the biomolecules are separated by size in the agarose gel matrix.<sup>183</sup> Agarose gels do not have unchanging pore size, but are best for electrophoresis of proteins that are larger than 200 kDa.<sup>184</sup>

Polyacrylamide gel electrophoresis (PAGE) is used for separating proteins ranging in size from 5 to 2,000 kDa due to the uniform pore size provided by the polyacrylamide gel.<sup>185</sup>

A number of factors can affect the migration of nucleic acids such as the dimension of the gel pores, gel concentration, size of RNA, the voltage, the ionic strength of the buffer, and the concentration of intercalating dye.<sup>151</sup> As a result, standard agarose gel electrophoresis should be used for good separation. For example, larger molecules are separated better using a low concentration gel whereas smaller molecules separate better at high concentration gel.<sup>186</sup>

### **3.9 Summary**

Three different CQ-derivatives and glucose derivatives have been synthesised successfully and characterised. Two different oxidation methods have been used to synthesis compound **(2)** in 80-90% yield.

Moreover, a significant modification of the published procedure was made to increase the yield of compound **(2a)** and to produce compound **(2b)** as a novel molecule. The crystal structure of the 3-(7-chloroquinolin-4-ylamino) propan-1-ol compound **(1)** has been resolved and identified. Finally, two different methods, UV/Vis spectroscopy and gel electrophoresis, have been used to identify the integrity of CPMV particles.

## ***4 Chemical modification of CPMV particles***

Chemical modification of proteins is a useful tool for investigating natural systems, creating new protein constructs, and producing therapeutic conjugates. These modifications can occur in natural deteriorations, generally, these modifications are with the most reactive side chains and are predominantly oxidations, reductions, nucleophilic and electrophilic substitutions.<sup>187</sup>

There are several goals of chemical modification such as the ability to identify which parts of the molecule are exposed to solvent and determination of important residues for a particular phenotype. Additionally, it was reported that chemical modification can provide a viable method for improving the functional properties of plant and yeast proteins and may make it possible to adapt proteins with specific functional properties.<sup>188</sup>

In this study, chemical modification of a plant virus is used in order to create novel drug candidates that may display powerful antimalarial activity. The chemical modification of addressable amines of CPMV particles was achieved by reaction with the carboxyl groups of each chloroquinoline derivative (CQ-derivative), which included chloroquinoline propionic acid, (7-chloroquinoline-4-yl)alanine and (7-chloroquinoline-4-yl)valine. Similarly, two different glucose derivatives have been separately attached to the external amines of CPMV to enable targeting to specific tissues. Moreover, the ability to single and double modify CPMV particles has been confirmed using UV/Vis spectroscopy, gel electrophoresis and TEM. Furthermore, the number of each CQ-derivative conjugated to the external surface of CPMV has been determined by a back-reaction using Alexa Fluor dye 488.

## ***4.1 Addressability of amines on external surface of CPMV (single modification)***

### ***4.1.1 Chemical modification of CPMV with EDC/NHS and chloroquinoline propionic acid (2)***

The addressable carboxylate on the external surface of CPMV was modified with EDC/NHS to form CPMV-NHS-ester, chloroquinoline propionic acid (**2**) was also conjugated to the external surface of CPMV to form CPMV-CQp. Alternatively, CPMV was reacted with chloroquinoline propionate ester to form also CPMV-CQp, the integrity, in each case, was confirmed by agarose gel electrophoresis **Figure 4.1**. Two bands were observed on ethidium bromide stained gels. These forms are derived from the different electrophoretic forms of the S subunit of CPMV, the slow (s) and fast (f) form, depending on their RNA content.<sup>164</sup>

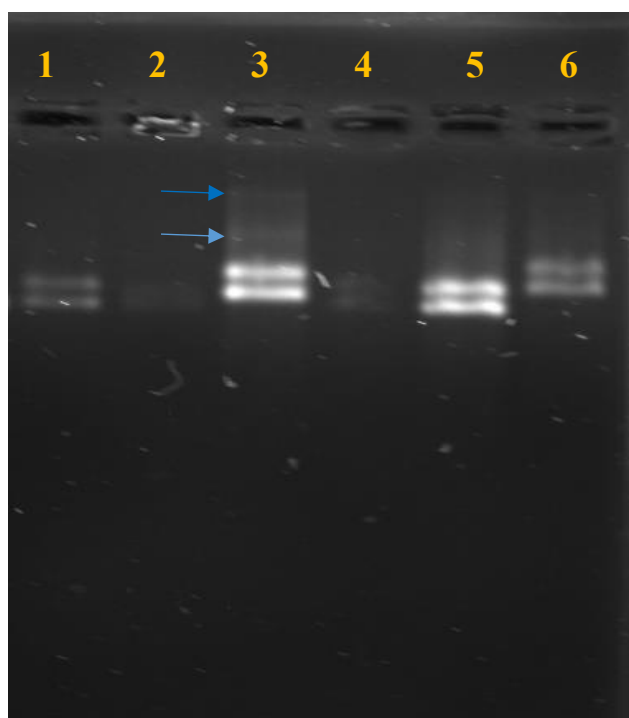


**Figure 4.1** Agarose gel imaging of CPMV before and after modification: Lane1, 2, 4 wt CPMV in different concentrations, lane3 CPMV-CQp, lane5 CPMV-CQp and lane6 CPMV–NHS-ester.

The O-succinimide esterified CPMV particles migrate more slowly toward the anode than wild-type and each of the modified CPMV. In addition, the difference in the band pattern shown in **Figure 4.1**, between lanes 3 and 5 (blue arrows) highlight that there are two extra bands. This is indicated the modification of carboxyl group in CQp, which is activated by EDC/NHS before modification with CPMV. This is noticeable on lane 3 and makes the characterisation of CQp on the external surface of CPMV far simpler. An increase in the band intensity is only observed when CQp is modified with CPMV without the presence of EDC/NHS, as compared with the unmodified particle (lane 1). In order to make sure whether or not CPMV was modified with CQp, the agarose gel electrophoresis was run without staining to confirm the CQp movement **Figure 4.2**.

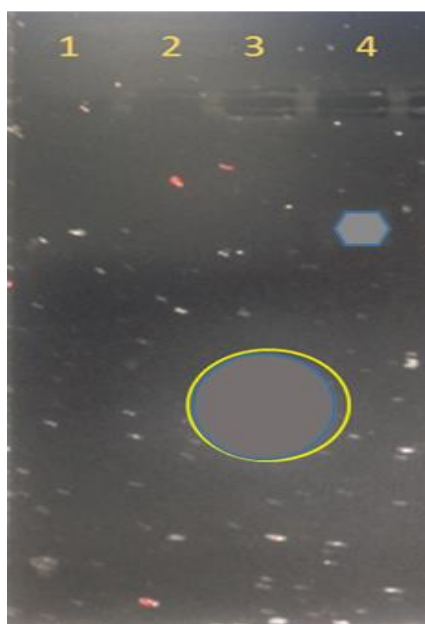


**Figure 4.2 Modified and unmodified wt CPMV with CQp on a 1.2 % (w/v) agarose gel without staining: lane 1 wt CPMV, lane 2 CPMV-NHS-ester, lane 3 CQp in 100% DMSO and lane 4 CPMV-CQp.**

Zeta potential (ZP) values have regularly been used as an indicator of the stability of colloidal particles. Particles are considered to exist as stable colloids if their zeta potentials are more positive than +30mV or more negative than -30mV.

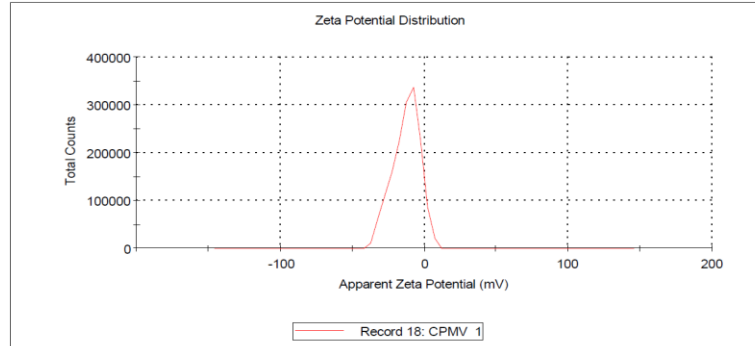
It was found that the zeta potential for CPMV- NHS-ester suspended in buffer was  $-8\text{mV}$ , it was significantly less negative than wt CPMV, while CPMV-CQp showed two peaks with zeta potential of  $-15\text{mV}$ , that may be due to the aggregation of the particle, and  $-35\text{mV}$  as shown in **Figure 4.3**.

**Results**

**A**

	Mean (mV)	Area (%)	St Dev (mV)
Zeta Potential (mV): -12.6	Peak 1: -12.6	100.0	9.34
Zeta Deviation (mV): 9.34	Peak 2: 0.00	0.0	0.00
Conductivity (mS/cm): 2.41	Peak 3: 0.00	0.0	0.00

Result quality **Good**

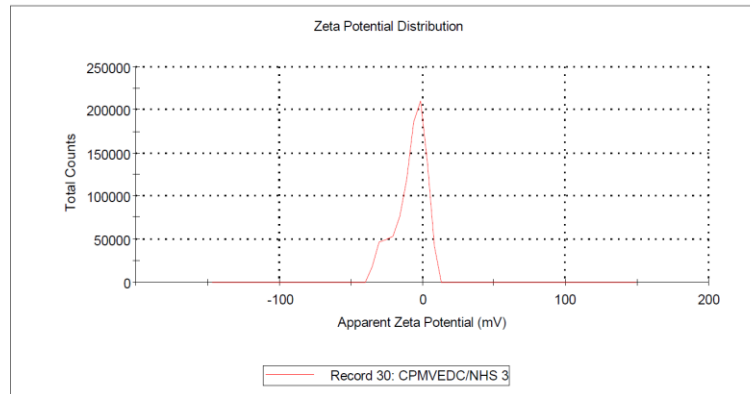


**Results**

**B**

	Mean (mV)	Area (%)	St Dev (mV)
Zeta Potential (mV): -8.06	Peak 1: -8.06	100.0	10.6
Zeta Deviation (mV): 10.6	Peak 2: 0.00	0.0	0.00
Conductivity (mS/cm): 1.32	Peak 3: 0.00	0.0	0.00

Result quality **Good**



**Results**

**C**

	Mean (mV)	Area (%)	St Dev (mV)
Zeta Potential (mV): -25.5	Peak 1: -15.6	56.3	6.17
Zeta Deviation (mV): 13.6	Peak 2: -38.4	43.7	7.79
Conductivity (mS/cm): 0.161	Peak 3: 0.00	0.0	0.00

Result quality **Good**

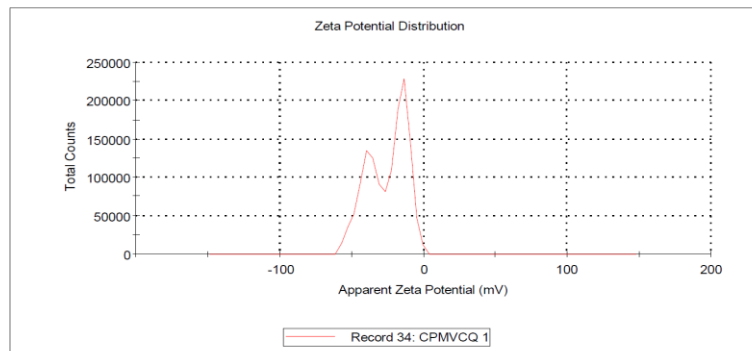
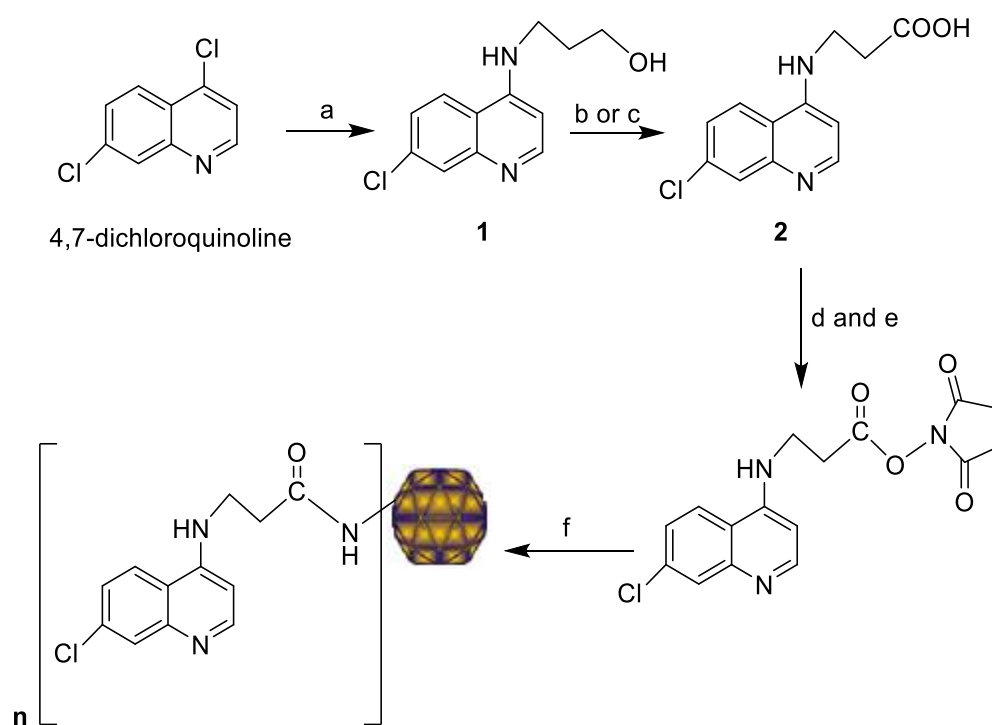


**Figure 4.3 Zeta potential measurement of modified and unmodified CPMV (A) wt CPMV (B) CPMV-NHS-ester and (C) CPMV-CQp particles.**

### 4.1.2 The synthesis of chloroquinoline propionic acid (CQp) and coupling to CPMV

The decoration of the external surface of CPMV with CQp has been described (section 2.6.1). In this study, solvent-exposed lysines on the external surface of the CPMV virus were utilised for the selective attachment of the CQp.<sup>170</sup> **Scheme 4.1.**



**Scheme 4.1** Synthesis and decoration of chloroquinoline propionic acid: a-3-amino-1-propanol, 140 °C 24 h b-  $\text{KMnO}_4 + \text{NaOH}$  or c-  $\text{CrO}_3 + \text{periodic acid}$  room temperature for 2h. d- EDC e- NHS f- CPMV.

Confirmation for CQp conjugation onto the external surface of CPMV was obtained by the UV–Vis spectrum of both modified and unmodified CPMV **Figure 4.4A**.

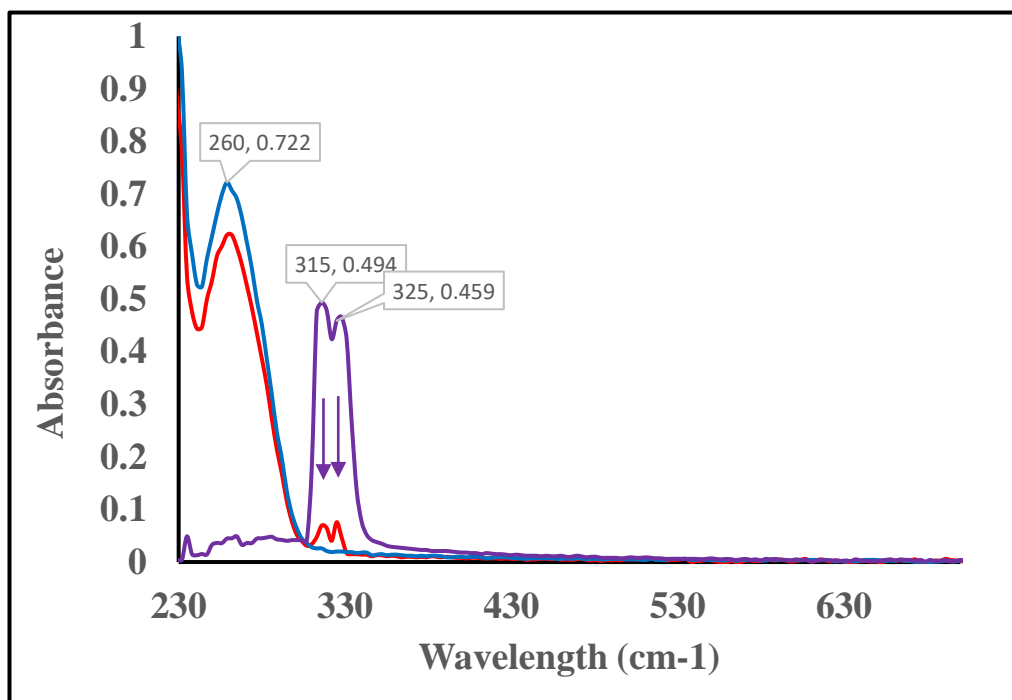


**Figure 4.4 A** A typical UV/Vis spectrum for modified and unmodified CPMV with CQp; Blue line is wt CPMV, purple line is CQp and red line is CPMV-CQp. The CQp absorption maxima still observed after conjugation with CPMV as shown in purple arrows.

CQp compound was characterized by UV/Vis spectroscopy in aqueous 20 % DMSO. It has two absorption maxima at 315 and 325 nm. Thus making easy identification of covalent binding of external surface of CPMV particle. The UV/Vis spectra of CQp, wt CPMV and CPMV-CQp, shown in **Figure 4.4 A** confirmed successful decoration of addressable amines.

Successful bioconjugation of CQp to the virus capsid was also demonstrated by comparison of the SDS-PAGE of denatured modified and unmodified CPMV particles **Figure 4.4 B**. There are two extra bands on lane 2 (shown in blue arrows) for CPMV-CQp compared to unmodified particle corresponding to conjugation of CQp to each of the S and L subunits.



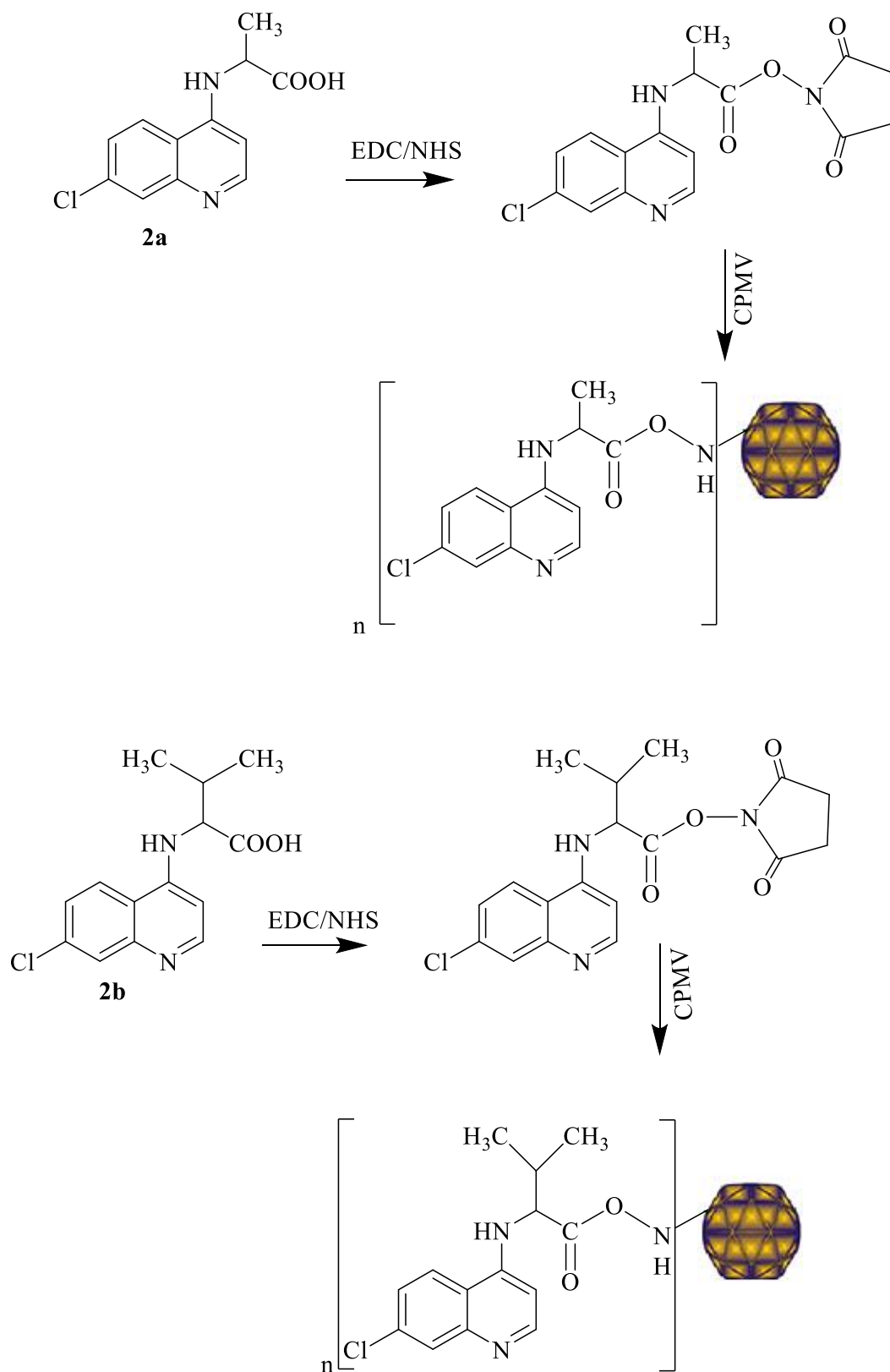
**Figure 4.4 B** Coomassie stained 12% SDS-PAGE of 1. wt CPMV; 2. CPMV-CQp; 3. wt CPMV. Two extra bands on lane 2 (shown in blue arrows) confirmed the modification of CPMV with CQp.

There is no clear band on lane 3 due to the low concentration of CPMV. The modification of addressable amines on external surface of CPMV with CQp is shown in **Scheme 4.1**

#### ***4.1.3 Chemical modification of CPMV with (7-chloroquinoline-4-yl)alanine and (7-chloroquinoline-4-yl)valine (2a and 2b): single modification.***

The reaction of (7-chloroquinoline-4-yl)alanine (CQ-ala) with addressable amines, derived from lysine groups exposed on the external surface of wt CPMV, produced CPMV-CQ-ala conjugates in 60-65% recovered yield based on the initial virus concentration. Similarly, the external surface of wt CPMV was modified with (7-chloroquinoline-4-yl)valine (CQ-val) to generate CPMV-CQ-val in 65-68% recovered yield based on the initial virus concentration. The decoration of the CPMV with each CQ

derivatives has been described (section 2.6. 1). The reaction scheme for each modification is shown in **Scheme 4.2**.



**Scheme 4.2** The modification of CPMV with CQ-ala and CQ-val

The integrity of the modified particles was confirmed by UV/Vis spectroscopy **Figure 4.5** and by agarose gel electrophoresis **Figure 4.6**.

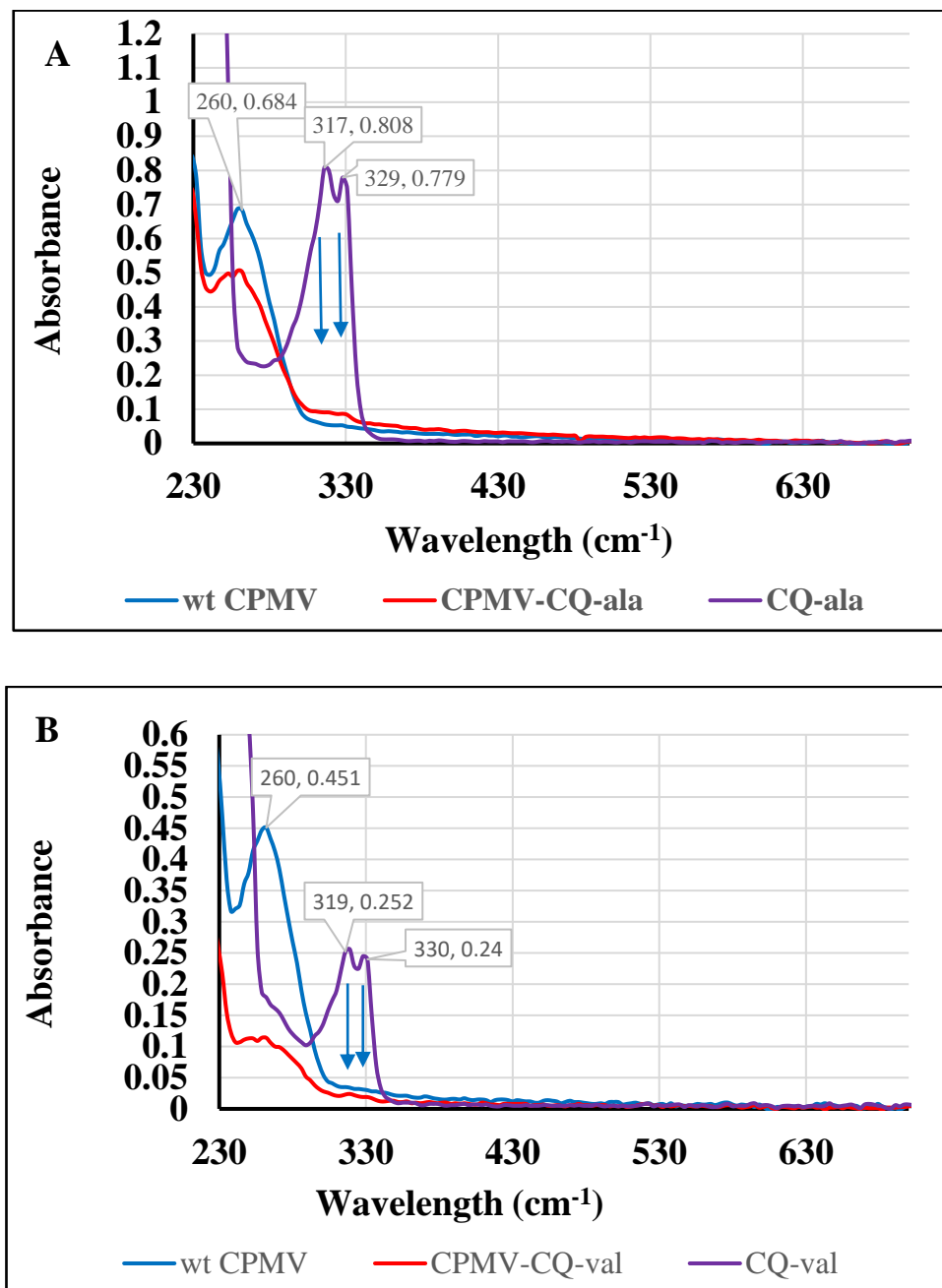
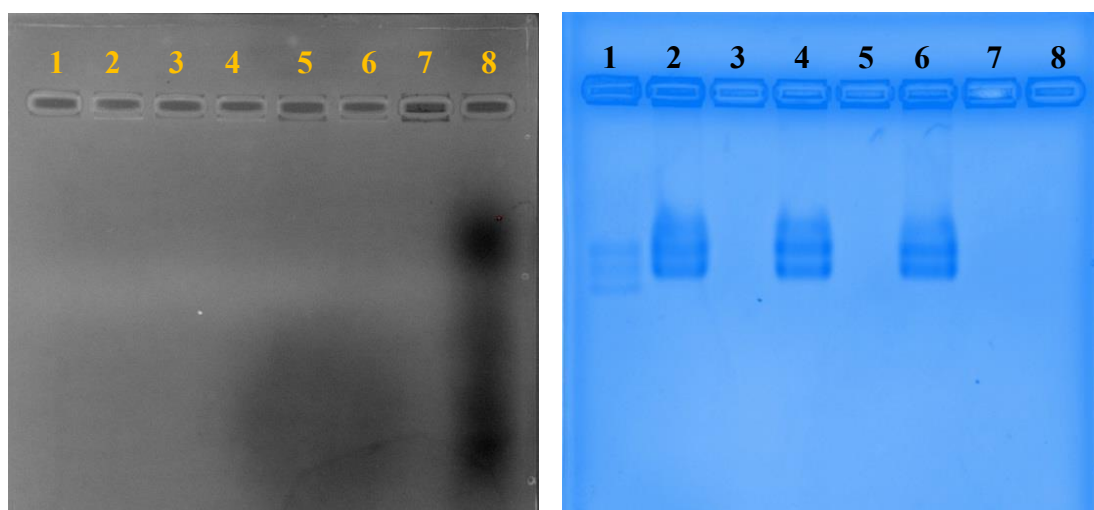


**Figure 4.5** UV/ Vis spectrum of wt CPMV: A- before and after modification with CQ-ala and B- before and after modification with CQ-val, both CQ derivatives have kept their absorption maxima after conjugation with CPMV as shown in blue arrows.

UV/Vis characterized both CQ-ala and CQ-val in aqueous 30% DMSO. Both CQ derivatives have two absorption maxima at 317, 329 and 319, 330 nm respectively, resulting in easy identification of covalent binding and successful conjugation of amines on the external surface of CPMV.

The conjugation of CQ derivatives with wt CPMV was confirmed by running stained agarose gel electrophoresis, whereas CQ-ala and CQ-val were run on unstained agarose gel; visible bands on unstained agarose gel confirmed the movement of each CQ **Figure 4.6A**.



**A: Unstained gel**

**B: Coomassie staining**

**Figure 4.6 Agarose gel electrophoresis 1.2 % w/v agarose, 60 V: Lane 1- wt CPMV, 2- CPMV- CQp, 3- empty , 4- CPMV- CQ- ala, 5- CQ-ala, 6- CPMV-CQ-val, 7- CQp and 8- CQ-val.**

The migration of RNA-containing unmodified CPMV particle is faster than that of modified CPMV resulting in a slow movement of CPMV-CQp, CPMV-CQ-ala and CPMV-CQ-val compared to wt CPMV **Figure 4.6B**. Further confirmation of CQ-ala and CQ-val binding to the exterior surface of CPMV is the SDS-PAGE which was used to separate proteins according to their molecular weight, based on their differential rates of migration through a gel under an electrical field.

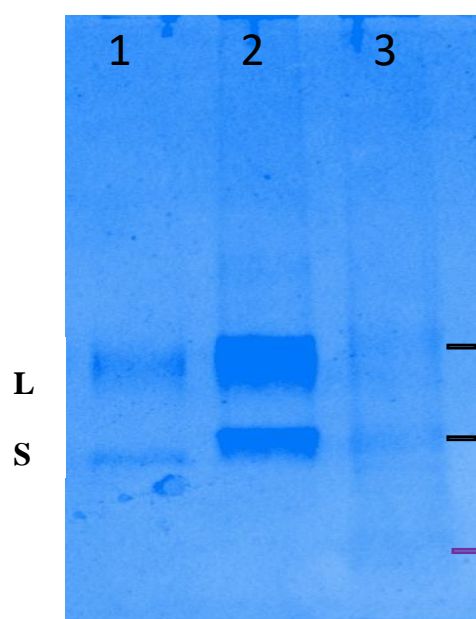


**Figure 4.7** Coomassie stained 12% SDS-PAGE of 1. wt CPMV; 2. CPMV-CQ-val ; 3. CPMV-CQ- ala. CQ-ala has extra band easily noticeable on the gel confirm the conjugation. CPMV-CQ-val showed a slight cleavage on the small subunit (lane 2) compared to unmodified CPMV.

The major difference between the samples was the degree of C-terminal processing of the S protein. In the case of the particle produced from the conjugation of CPMV with CQ-ala, three bands were easily noticeable on SDS gel corresponding to the denatured modified CPMV-CQ-ala on lane 3, while particles modified with CQ-val showed a slight cleavage on the small subunit (lane 2) compared to unmodified CPMV **Figure 4.7**.

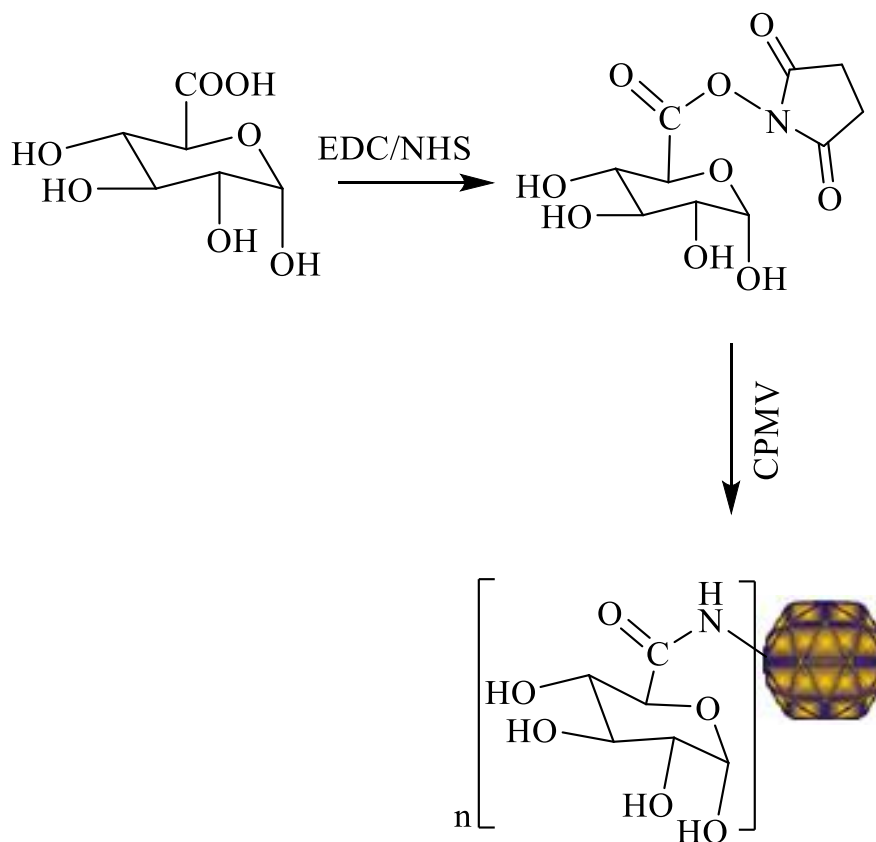
#### ***4.1.4 The modification of CPMV with glucuronic acid (G.A)***

CPMV was modified with glucuronic acid (G.A) as shown in **Scheme 4.3**, and the integrity was confirmed by agarose gel electrophoresis **Figure 4.8** and UV/Vis spectrophotometry **Figure 4.9**. It was found that G.A was attached to both the S subunit forms, the slow (s) and fast (f) form.<sup>164</sup>

A slight difference was noticed when G.A was activated with EDC/NHS then conjugated with CPMV (lane 3), while there was no change of the migration of modified CPMV with

G.A (lane 2). This means activation was required for formation of modified particles

**Figure 4.8.**



**Scheme 4.3 decoration of wt CPMV with glucuronic acid (G.A)**

There is a slight shift of a band when CPMV was modified with G.A. This could be derived from reacting G.A with EDC/NHS or when using EDC/NHS alone. In order to show whether or not the CPMV modified with G.A band moved, unstained agarose gel was run to confirm the G.A movement **Figure 4.8 C (blue brackets)**.

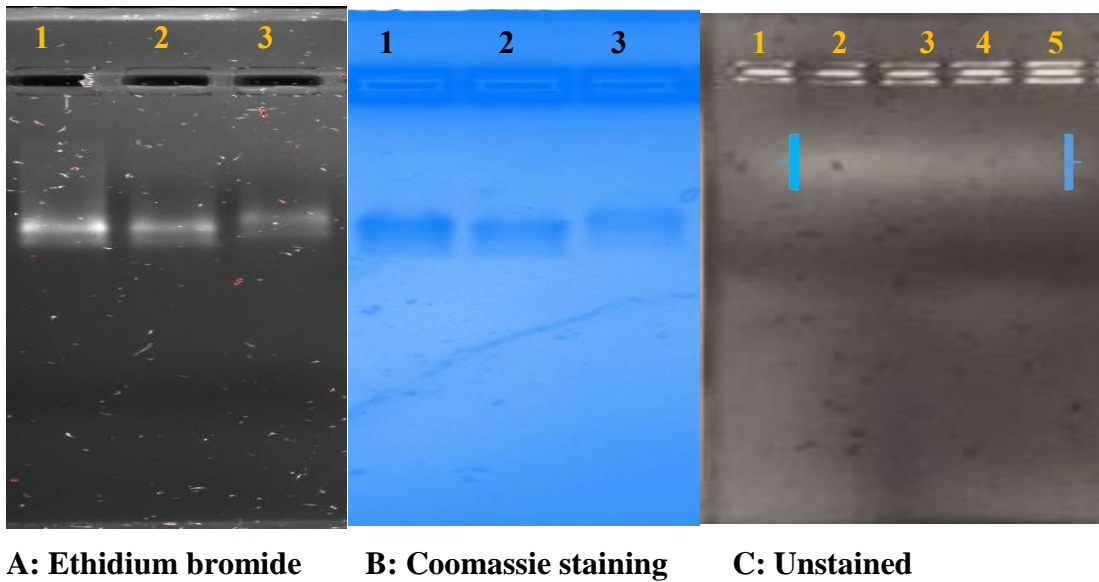


**Figure 4.8** Digital image of agarose gel electrophoresis 1.2 % w/v agarose, 60 V, lane 1 wt CPMV 0.05 mg/ml, 2 CPMV-G.A, 3 CPMV- G.A., 4 G.A in MQ water and 5 G.A in PBS buffer.

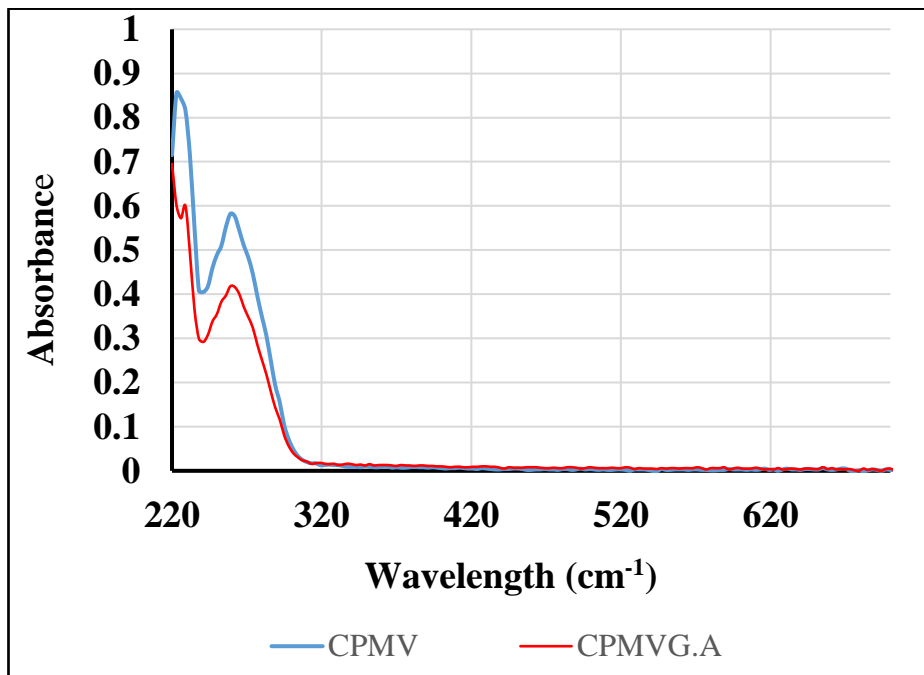


**Figure 4.9** The UV/Vis spectrum of wt CPMV and CPMV-G.A.

#### ***4.1.5 Quantification of chloroquinoline propionic acid (CQp) binding on external surface of CPMV:***

The number of CQ per particle was determined for CPMV with CQp as described in section (2.6.2). The functionalised particle was purified and concentrated on 100 kDa cut-off columns.

The number of unconjugated amines on the external surface of CPMV was determined from the absorbance of CPMV and the absorbance of Alexa Fluor dye, CPMV particles have an absorption maximum at a wavelength of  $\lambda = 260$  nm with molar extinction coefficient of  $\epsilon = 8.1 \text{ ml mg}^{-1} \text{ cm}^{-1}$ . Alexa Fluor dye has an absorption maximum at  $\lambda = 494$  nm with molar extinction coefficient of  $\epsilon = 73000 \text{ ml mg}^{-1} \text{ cm}^{-1}$ . Beer Lambert law was used to calculate the concentration of particle and dye, the number of CQp can be calculated as described in Eq 4 and Eq 5 below:

$$C_{\text{CPMV}} = A_{\text{CPMV}} / \epsilon_{\text{CPMV}} \cdot d, \quad C_{\text{dye}} = A_{\text{dye}} / \epsilon_{\text{dye}} \cdot d \quad \text{----- Eq 4}$$

$$\text{The number of free amines} = C_{\text{dye}} / C_{\text{CPMV}} \quad \text{----- Eq 5}$$

Where; A is the absorbance, C is the concentration of the particles and dye in  $\text{mg ml}^{-1}$ , d is the length of the light path in cm and  $\epsilon$  the molar extinction coefficient in  $\text{ml mg}^{-1} \text{ cm}^{-1}$ .<sup>189</sup> 240 is the maximum labelling of addressable amines on the external surface of CPMV.

The integrity of the CPMV particles before and after modification was confirmed by agarose gel electrophoresis **Figure 4.10**. EtBr stained gel imaging revealed an intense fluorescent band as a result of the fluorescent labelling of CPMV with Alexa dye that was slightly shifted compared to wt CPMV. The result was confirmed also by UV/Vis spectroscopy. The conjugation of CQp to the external surface of CPMV with and without

using EDC/NHS was confirmed before binding with Alexa dye and the difference of the number of CQp on CPMV surface was determined as described above.

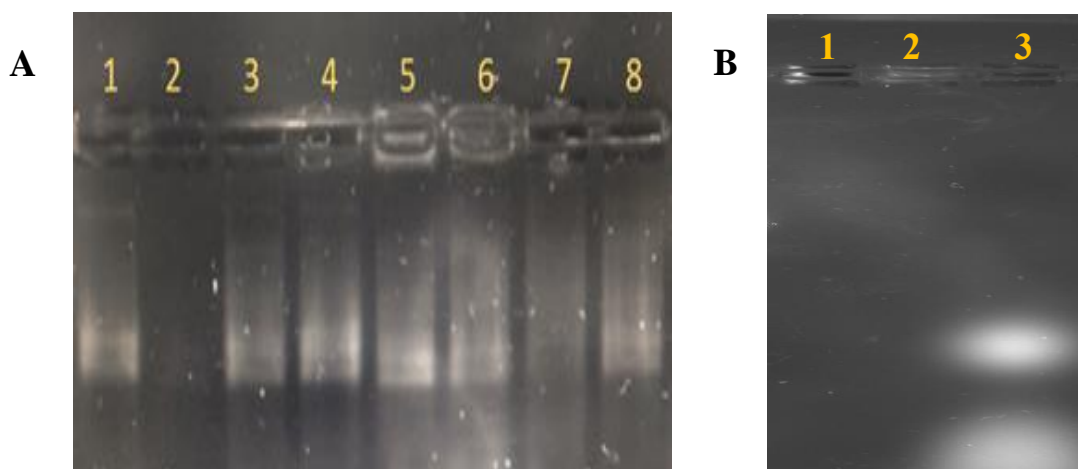


**Figure 4.10 A, Modified and unmodified CPMV particles on a 1.2 % (w/v) agarose gel with ethidium bromide (EtBr) staining: lane 1 wt CPMV; 2 CQp ; 3 CPMV- dye after 2washes ; 4 CPMV-CQp-dye after 2washes ; 5 CPMV- dye after 1wash; 6, CPMV-CQp- dye after 1 wash ; 7, CPMV- dye after 3washes and 8, CPMV-CQp- dye after 3 washes. B, Unstained agarose gel imaging of CPMV particle before and after labelling with Alexa Fluor 488 dye: lane1 wt CPMV, 2 CPMV-CQ-p, 3 CPMV- dye.**

The labelling of wt CPMV with Alexa dye was confirmed by running an unstained agarose gel, a fluorescent band was observed. **Figure 4.10 B.**

Comparison of agarose gel electrophoresis of wt CPMV, CPM-dye and CPMV-CQp showed that wt CPMV and CPMV-CQp were not visible without staining. In addition, it can be clearly seen in some wells that not all samples were completely mobile due to the lack of migration from the well. This is probably a consequence of the presence of electrostatic binding of CQp to the virus surface and not of particle aggregation. Moreover, it was found that it is difficult to efficiently remove the unconjugated dye from the dye-labelled protein with acceptable yields when the concentration of CPMV was less than 1 mg/ml **Figure 4.10A**. Therefore, all samples were washed several times to wash out excess dye. As a consequence, the low concentration of both CPMV and Alexa Fluor dye resulted in a slightly noisy UV/Vis spectrum (not shown) making it difficult to calculate the number of dye molecules. As a result, this experiment was repeated several times to find the best condition for this modification, the concentration of Alexa dye was reduced by half, and the conjunction with CPMV was confirmed by agarose gel electrophoresis **Figure 4.11**.

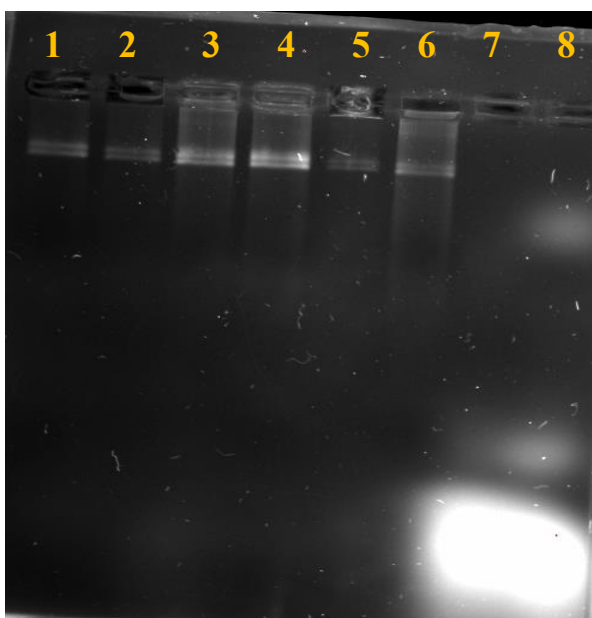


**Figure 4.11** modified and unmodified CPMV particles on a 1.2 % (w/v) agarose gel with ethidium bromide (EtBr) staining: lane 1 wt CPMV; 2 CPMV-CQp; 3 CPMV- dye after 1 wash ; 4 CPMV- dye after 2 washes; 5 CPMV- CQp; 6 CPMV-CQp- dye after 2 washes; 7, 8 CPMV- dye elute.

It was noticed that the excess dye in the CPMV samples was removed after one wash, while it was still observed in the eluent, it could be due to a low concentration of CPMV or due to the purification method. Another experiment was carried out where the CPMV concentration was increased twofold and fivefold in order to increase the efficiency of this reaction. The results were confirmed by UV/ Vis spectrophotometry **Figure 4.12**.

Gel electrophoresis of intact CPMV particles on nondenaturing agarose gel has previously proved to be an effective method for analysing the RNA content of CPMV particles.<sup>50</sup> It was used here to monitor the excess dye which was conjugated with both types of CPMV subunits **Figure 4.13**.

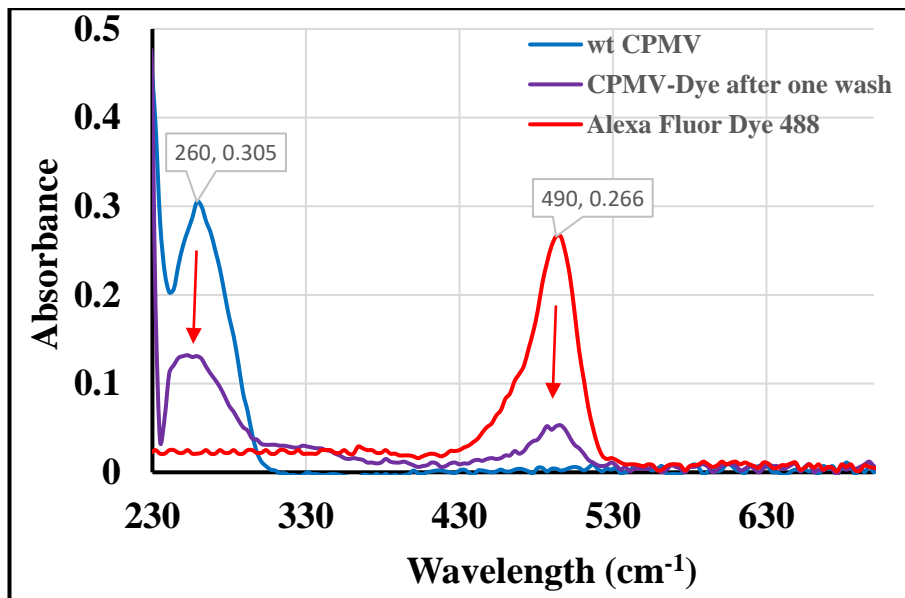


**Figure 4.12** UV-Vis spectrum of CPMV-dye after washing with sodium phosphate buffer pH 7. The maximum absorbance for CPMV and Alexa Fluor dye still noticeable after conjugation (red arrows).

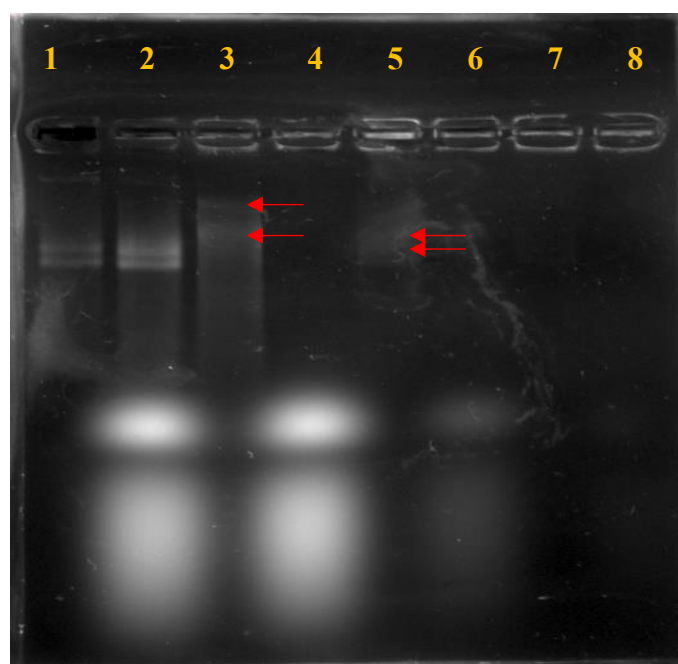


**Figure 4.13** agarose gel imaging of CPMV stained with ethidium bromide: lane1 wt CPMV lane 2 CPMV- dye, lane 3 CPMV-CQp- dye after 1 wash, lane 4 CPMV- dye elute after1wash, lane 5 CPMV- dye after 1 wash, lane 6 CPMV-dye elute after 2 washes, lane7 CPMV dye-elute after 3 washes. Clear cleavage of both S units in lanes 3 and 5 emphasised by red arrows corresponds to the CQp and dye conjugation.

After purification to remove unbound dye, all CPMV particles were analysed using agarose gel electrophoresis, the gel was imaged under UV light. All CPMV particles showed fluorescence and free dye was detected, indicating that excess dye was not removed completely.

The difference in the migration of CPMV-CQp-dye and CPMV- dye has been observed clearly in lanes 3 and 5 in the agarose gel. Lane 3 shows the modified CPMV has a slow movement after one wash and there was very clear cleavage of the S units as compared to the CPMV- dye in lane 5, this is emphasised by red arrows. This corresponds to the CQp and dye conjugation. In addition, there was a slight change on the migration of CPMV modified with Alexa dye in lane 2 compared with unmodified particle. In this experiment the CPMV- dye samples were washed with 90  $\mu$ l PBS buffer and centrifuged by using 100 KDa cut off column to wash out the excess dye.

The experiment was repeated by increasing the concentration of CPMV by ten times more than the previous experiment, to increase the brightness of CPMV in all samples and making the samples more easy to identify after two washes but excess dye was still observed in the eluate, meaning excess free dye was not removed completely from CPMV dye samples **Figure 4.14**.

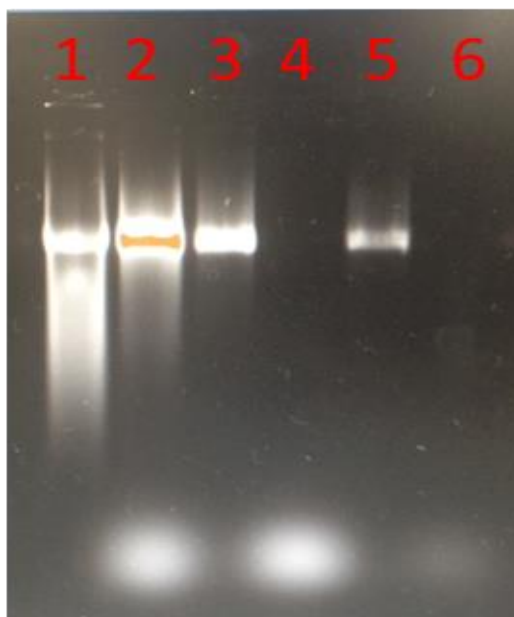


**Figure 4.14** agarose gel imaging of CPMV staining with ethidium bromide : lane 1 wt CPMV, lane 2 CPMV- dye before purification , lane 3 CPMV -dye after 1 wash, lane 4 CPMV- dye elute after1 wash, lane 5 CPMV- dye after 2 washes, lane 6 CPMV- dye elute after 2washes.

To confirm the conjugation of CPMV with Alexa Fluor 488 dye, it is clearly necessary to use another way for purification of CPMV-dye and CPMV-CQp-dye samples. It was found that the dialysis method is the best alternative way to purify CPMV-dye particles. The concentration of CPMV which was used in this experiment was 1mg/ml with 6000 molar excess Alexa Fluor dye. The CPMV-dye particle was purified using 100 kDa molecular-weight cut off membranes (Float-A-Lyzer G2, Spectrum Laboratories) against sodium phosphate buffer pH7. The concentration of CPMV was determined by using UV/Vis spectroscopy after 6, 8, 10 and 19h dialysis. The integrity of CPMV was confirmed by agarose gel electrophoresis, staining with EtBr as shown in **Figure 4.15**.

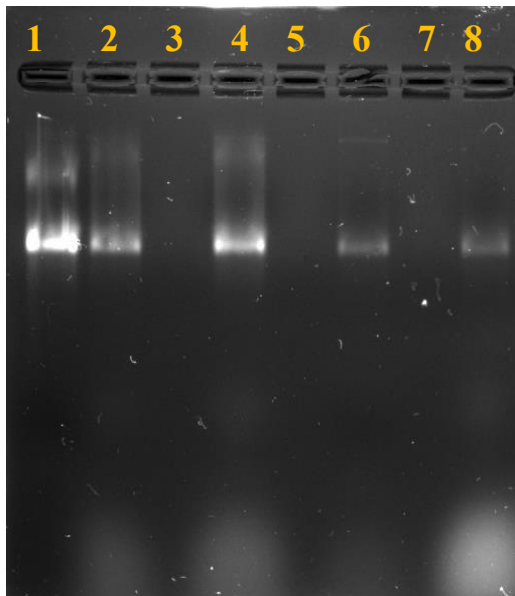


**Figure 4.15** Cowpea mosaic virus (CPMV) particles on a 1.2 % (w/v) agarose gel stained with EtBr: lane 1 wt CPMV, 2 CPMV- dye 10h dialysis, 4 CPMV- dye 8h dialysis, 6 CPMV- dye 19h dialysis and 8, CPMV- dye 6h dialysis.

There is no excess dye observed after 19h dialysis but the CPMV concentration was decreased after the same dialysis time to 0.18 mg/ml which affected the number of dyes conjugated to the CPMV surface. For more confirmation, wt CPMV was prepared using the same concentration of CPMV-dye after 19h dialysis and agarose gel electrophoresis was run **Figure 4.16**.

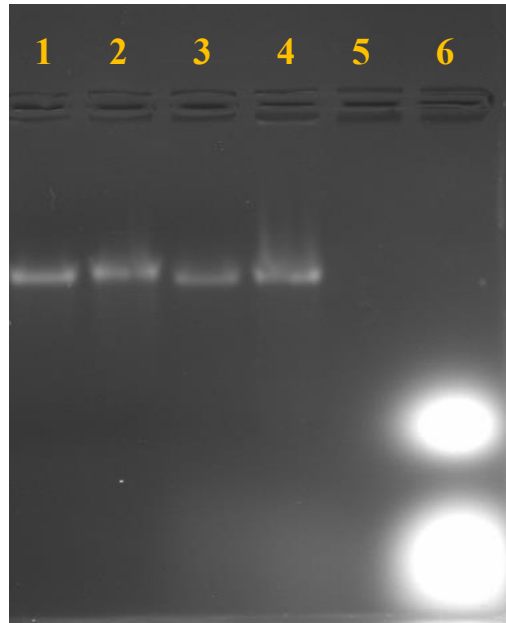


**Figure 4.16** Cowpea mosaic virus (CPMV) particles on a 1.2 % (w/v) agarose gel stained with EtBr: lane 1 wt CPMV, 2 CPMV- dye 16h dialysis, 3 CPMV- dye 22h dialysis, 4 CPMV- dye 19h dialysis, 6 CPMV- dye elute.

Some fluorescent intensity in lane 4 from a band of different mobility to wild-type was observed and there was no excess dye after 16-22h dialysis. Moreover, the migration pattern toward the anode differs for CPMV-dye. Alexa dye attached to surface lysines reduces the positive charge on the external surface of CPMV compared to wt CPMV, and thus CPMV- dye has increased mobility toward the anode. The result was also confirmed by UV/Vis spectrophotometry **Figure 4.17**.

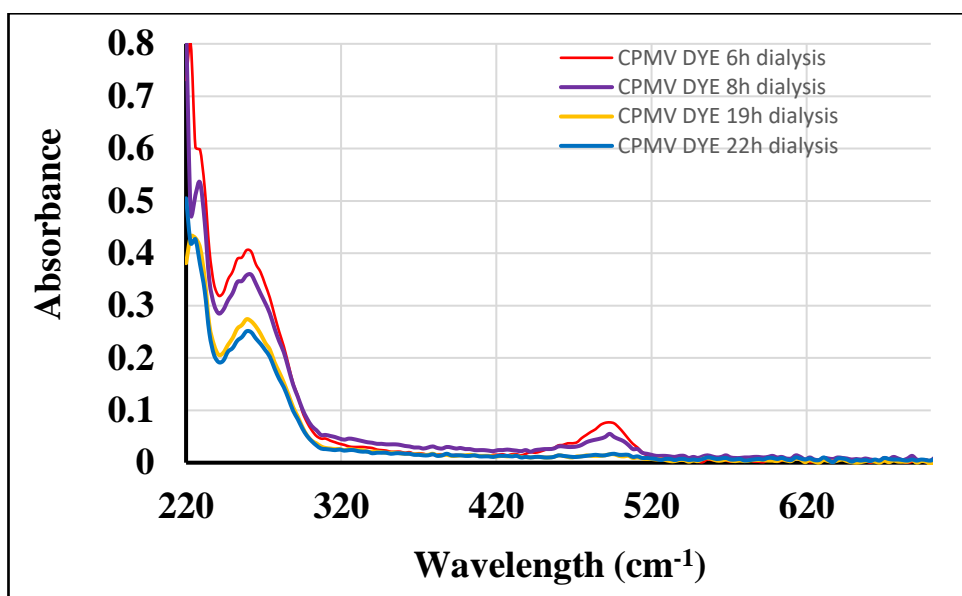


**Figure 4.17 UV/Vis spectrum of CPMV- dye after dialysis against PBS buffer pH 7**

The above experiment was repeated 3 times by using different conditions in order to achieve good labelling. In another experiment the CPMV and CPMV-CQp were modified with Alexa dye and the CPMV concentration was 0.7 mg/ml and dye concentration was 6000 molar excess. It was found that the number of CQp on the CPMV surface was 30 after 22h dialysis due to dilution. The result was confirmed by UV/Vis spectrophotometry and agarose gel electrophoresis **Figure 4.18** and **Figure 4.19** respectively.

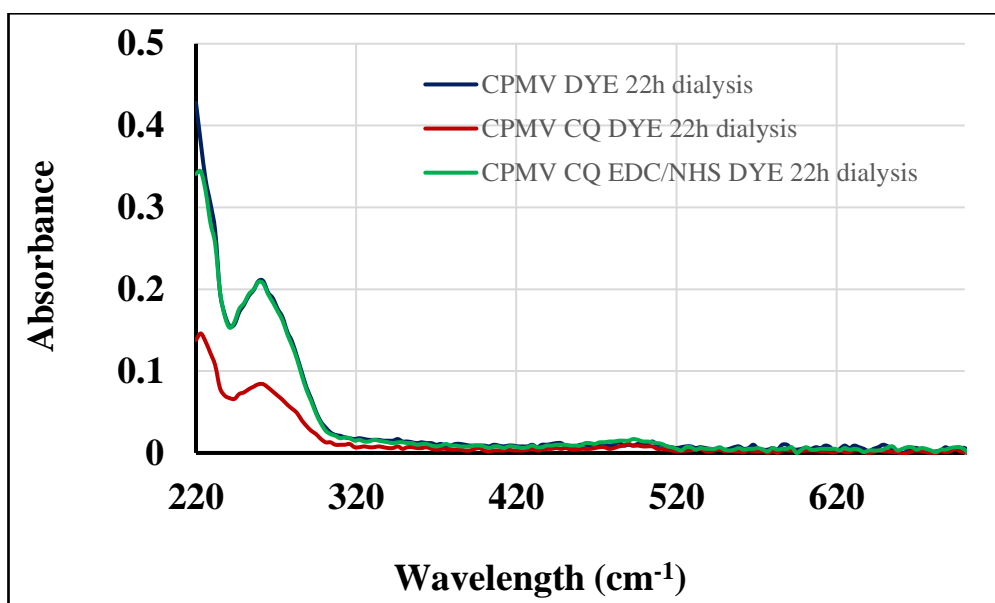


**Figure 4.18** V/Vis spectrum of CPMV-dye and CPMV-CQp-dye with and without using EDC/NSH as conjugation reagents to activate the carboxyl group of CQp before modifying with CPMV after 22h dialysis against PBS buffer pH 7.

The number of unconjugated amines on the external surface of CPMV was calculated from the absorbance of CPMV at 260 nm and the absorbance of dye at 494 nm, according to the UV/Vis spectrum the conjugated dye was not observed clearly compared with CPMV particle **Figure 4.18**.

The number of CQp increased about 20% when EDC/NHS was used to activate the carboxyl group of CQp before coupling to CPMV, means EDC/NHS are required for CPMV-CQp modification.

Unstained agarose gel electrophoresis showed fluorescence in lane 2 and 5 while, CPMV particles were not observed without staining, confirming the conjugation of Alexa dye to CPMV **Figure 4.19 B**.

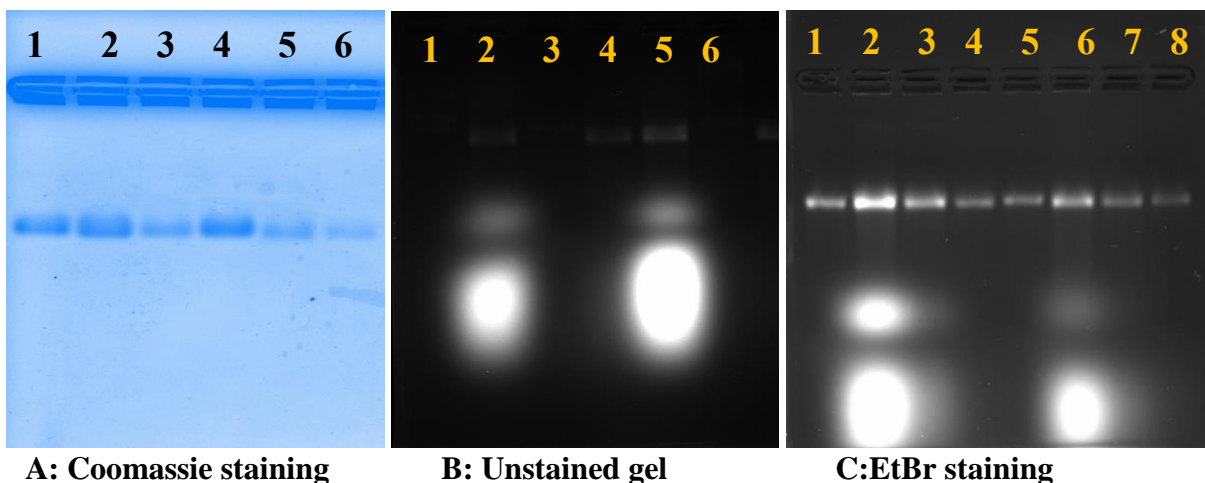


**Figure 4.19** Cowpea mosaic virus (CPMV) particles on a 1.2 % (w/v) agarose gel with and without staining: A and B , lane 1 CPMV 0.05mg/ml, 2 CPMV- dye before dialysis, 3 CPMV-CQp,4 CPMV-dye 22h dialysis, 5 CPMV-CQp-dye before dialysis, 6 CPMV-CQp-dye 22h dialysis, C, lane 3 CPMV- dye 10h dialysis, 4 CPMV- dye 22h dialysis, 5 CPMV- CQp, 6 CPMV- CQp- dye before dialysis, 7 CPMV–CQp- dye 10h dialysis, 8 CPMV- CQp- dye 22h dialysis.

The dye was binding on the external surface of CPMV and there was no excess dye after 22h dialysis but there was a problem with the dilution. The concentration of CPMV and dye were changed to 0.7 mg/ml and 3000 molar excess respectively, and the result analysed by both agarose gel electrophoresis and UV/Vis spectroscopy **Figurers 4.20 and 4.21.**

Although, the number of CQp was increased significantly to over 94 per particle, a poor UV/Vis spectrum was obtained after 22h dialysis, making it difficult to determine the maximum number of dye molecules on the CPMV surface. Although there was a clear difference between dyes modified and unmodified CPMV on agarose gel electrophoresis **Figure 4.20.**

The movement of each modified particle was faster than unmodified particle due to the difference of size and charges. Moreover, extra bands have were observed in lane 2, 3 and 4 (shown in red arrows) corresponding to CPMV dye conjugation **Figure 4.20.**

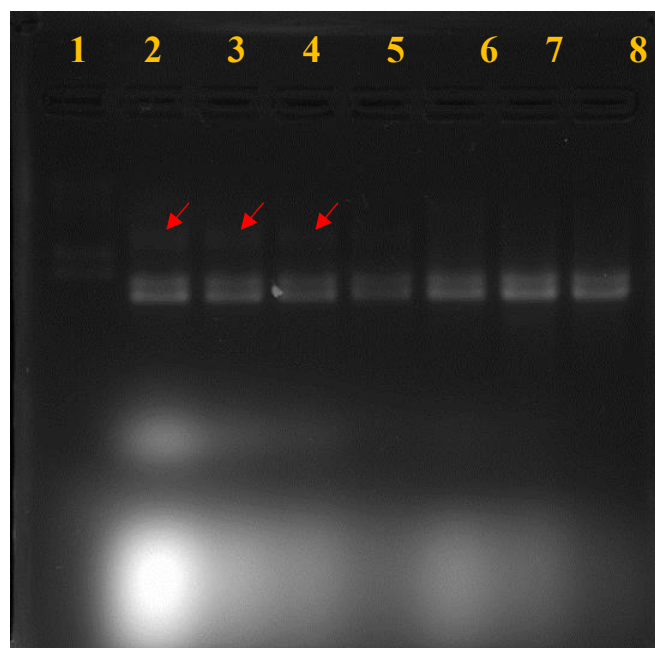


**Figure 4.20** Cowpea mosaic virus (CPMV) particles on a 1.2 % (w/v) agarose gel with EtBr staining: lane 1 wt CPMV, 2 CPMV-dye before dialysis, 3 CPMV-dye 6h dialysis, 4 CPMV- dye 8h dialysis, 5 CPMV-dye 22h dialysis, 6 CPMV-CQp- dye 6h dialysis, 7 CPMV-CQp-dye 8h dialysis, 8 CPMV-CQp-dye 22h dialysis . Extra bands have been observed in lane 2, 3 and 4 (shown in red arrows) corresponding to CPMV dye conjugation.

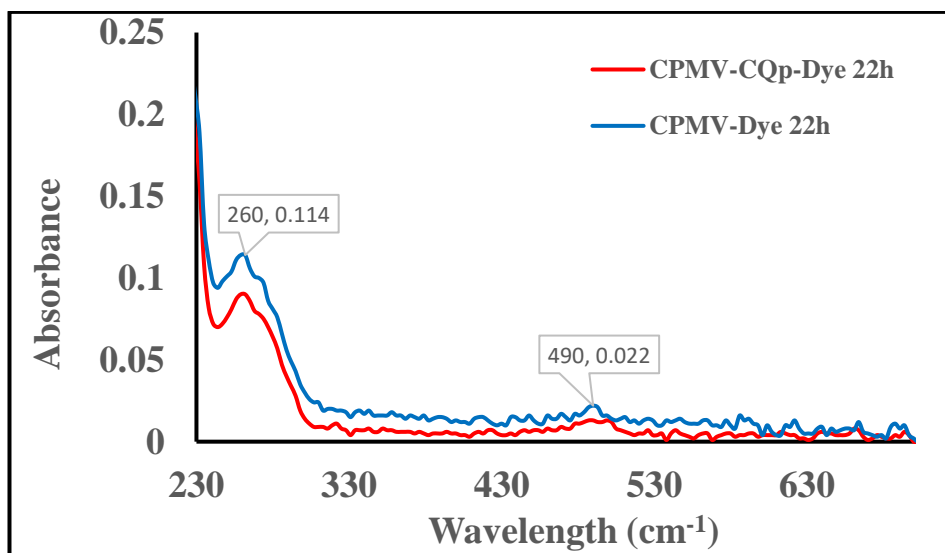


**Figure 4.21** V/Vis spectrum of CPMV- dye and CPMV- CQp- dye after 22h dialysis against PBS buffer pH 7. The absorbance of CPMV at 260 nm and the absorbance of dye at 494 nm shown the successful conjugation between modified and unmodified CPMV with Alexa Fluor dye.

In order to increase the number of CQp on the CPMV external surface, the experiment was repeated using 0.23 mg/ml CPMV, 3000 molar excess dye and reducing the dialysis time to 16h. This increased the number of bound CQp to 120 per virus. The result was confirmed by using UV/Vis spectroscopy and electrophoresis that both CPMV and CPMV-CQp were successfully modified with Alexa dye **Figures 4.22 and 4.23**, respectively.

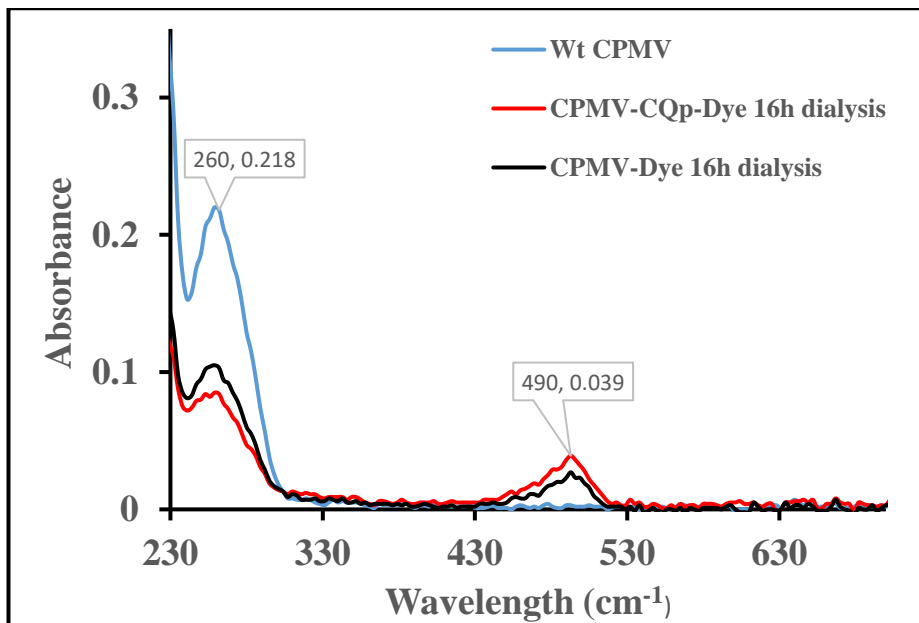


**Figure 4.22** UV/Vis spectrum of CPMV-dye and CPMV-CQp-dye after 16h dialysis against PBS buffer pH 7.

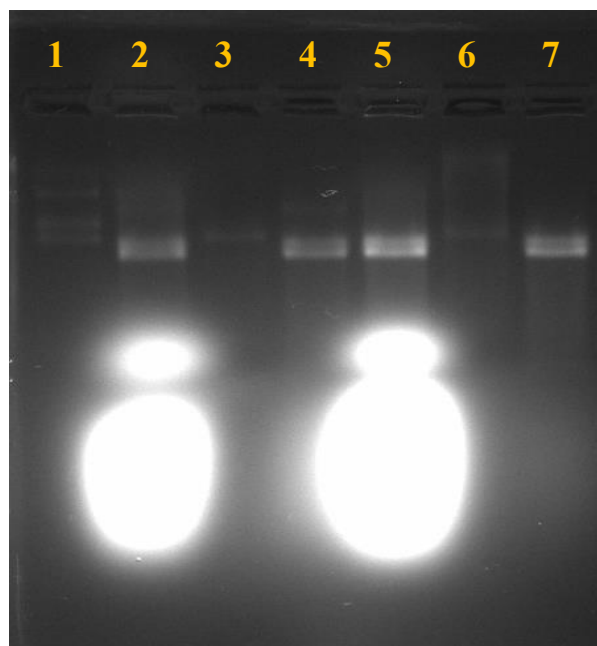


**Figure 4.23** Modified and unmodified CPMV particles on a 1.2 % (w/v) agarose gel with EtBr staining; lane 1,3 and 6 wt CPMV, 2 CPMV- dye before dialysis, 4 CPMV- dye 16h dialysis, 5 CPMV- CQp- dye before dialysis, 7 CPMV- CQp- dye 16h dialysis.

In agarose gel a slower migrating form of unmodified CPMV was observed in lanes 1, 3 and 6 compared with dye modified particles **Figure 4.23**, while excess dye was easily

recognised in lanes 2 and 5. Fluorescence was noticed in all lanes except lanes 1, 3 and 6 that did not include dye, confirming conjugation of dye to CPMV particles.

The experiment was repeated by using the same concentration of CPMV 0.2-0.25 mg/ml and a reduced dye concentration of 2000 molar excess. This time there was no excess dye observed after 8h dialysis and the number of CQp was increased to  $154\pm 4$  per particle. 86 free amines remain available for another modification on the external surface of the CPMV.

#### ***4.1.6 Quantification of CPMV-CQ-ala and CPMV-CQ-val***

The modification of CPMV-CQ-ala and CPMV-CQ-val with Alexa Fluor dye 488 have been described (section 2.6.2). The functionalised particles were purified by using the dialysis method against 500ml of (10mM) sodium phosphate buffer pH7 and the number of unconjugated amines on the external surface of CPMV was determined from the absorbance of dye at 494 nm and the absorbance of CPMV at 260 nm as described (section 4.1.5) and shown in **Figure 4.24**. The experiment was run for 8-10 h dialysis. The number of conjugated CQ-ala and CQ-val to the virus capsid was  $145\pm 5$  and  $150\pm 5$  per virus, respectively, as shown in **Tables 3, 4** which means approximately three of the four regularly addressable lysines are coupled to CQ-ala and CQ-val.

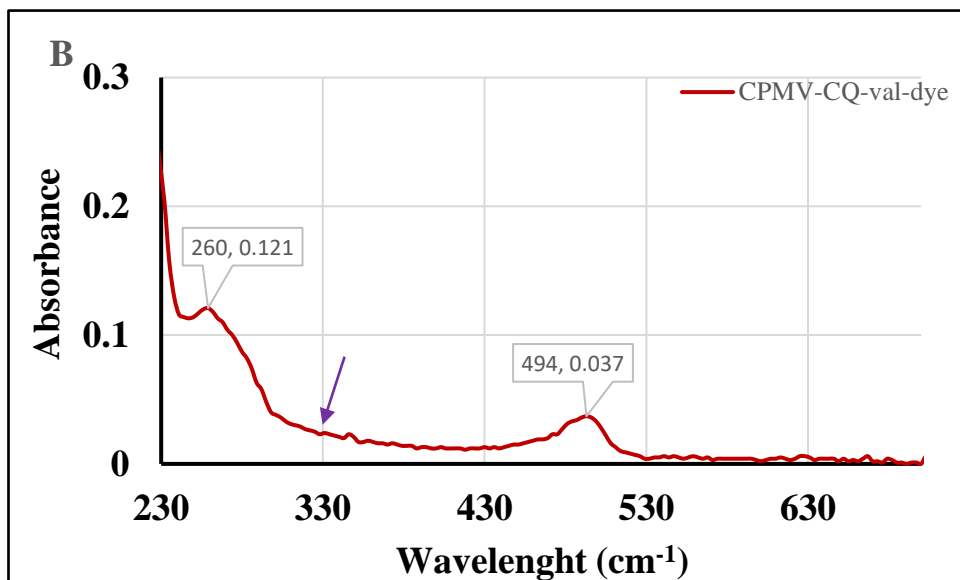
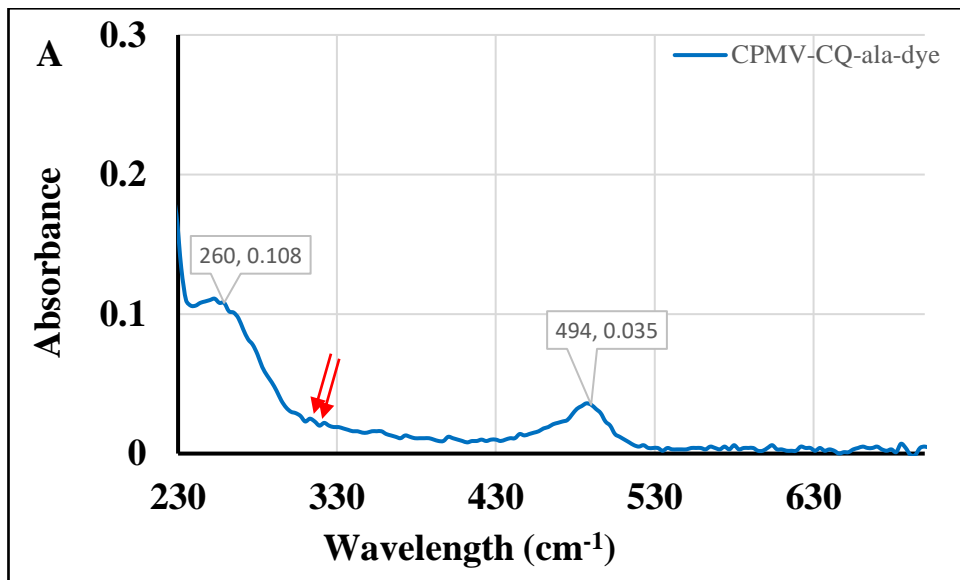
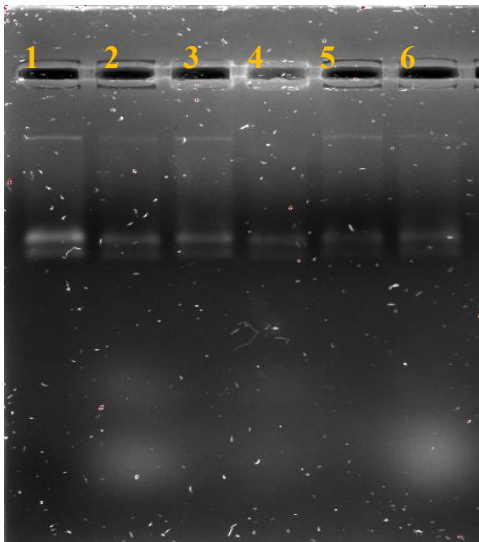
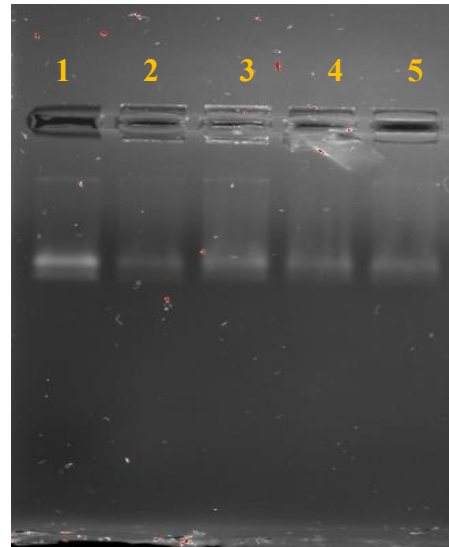


**Figure 4.24** UV/Vis spectrum of CPMV-CQ-ala-dye and CPMV-CQ-val- dye after 4h dialysis. The absorbance of both CQ-ala and CQ-val still noticeable after medication with Alexa Fluor dye (red and purple arrows).

Agarose gel electrophoresis was used to confirm that dye was coupled to the external surface of CPMV. Ethidium bromide stained native agarose gel electrophoresis revealed a visible fluorescent band after 4 to 6h dialysis, as a result of the fluorescent labelling of modified and unmodified CPMV, while it reveals that no free dyes were present after 8h **Figure 4.25 B** and **Figure 4.26 B**.

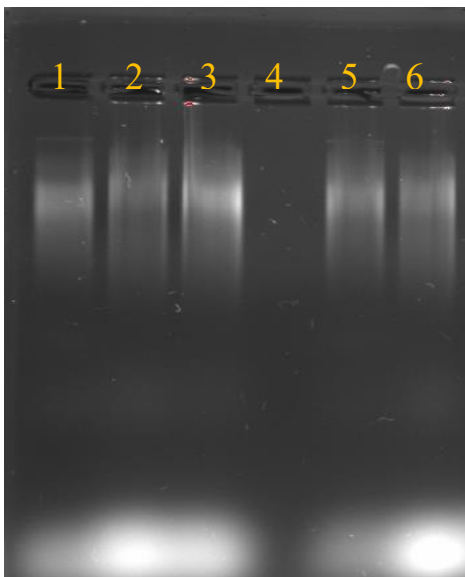


**A: 6h dialysis**

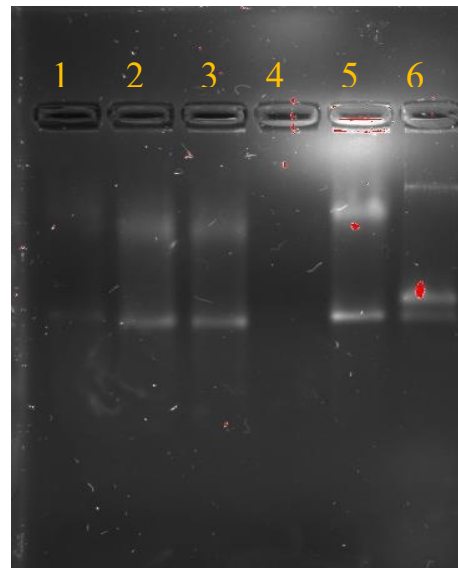


**B: 8h dialysis**

**Figure 4.25 Agarose gel electrophoresis 1.2 % w/v agarose, 60 V with EtBr staining: lane 1-wt CPMV, 2- CPMV- dye, 3- CPMV-CQ- ala-dye, 4- CPMV-CQ-ala-G.A -dye, 5- CPMV-CQ- ala-Glu- dye, 6- CPMV- CQ-ala-Glu -dye**



**A: 4h dialysis**



**B: 8h dialysis**

**Figure 4.26 Agarose gel electrophoresis 1.2 % w/v agarose, 60 V with EtBr staining. lane 1- CPMV- dye, 2- CPMV -CQ-val-dye, 3- CPMV-CQ-val-G. A-dye, 5- CPMV- CQ- val-Glu- dye and 6- CPMV-dye.**

Ethidium bromide stained agarose gel electrophoresis showed excess fluorescent intensity in all lanes after 4 and 6h dialysis, this means all modified particles still have

excess dye, therefore there is no possibility to calculate the correct number of bound CQ **Figure 4.25A and 4.26A**. The cleavage of dye modified CPMV and CPMV-CQ-val on agarose gel after 8h dialysis may be due to cleavage of the 24 amino acids terminus on the small subunits **Figure 4.26 B**.

#### ***4.1.7 The attachment of propiolic acid (P.A), butylic acid (B.A) to CPMV***

CPMV (100  $\mu$ l) was modified separately with propiolic acid (P.A) and with butylic acid (B.A) as described (Section 2.6.5). After reaction with P.A CPMV was not observed on an ethidium bromide stained native agarose gel, whilst SDS PAGE gel showed covalent attachment of both small and large CPMV subunits, this means that (P.A) caused denaturation of CPMV, and attachment to the surface of CPMV was unsuccessful. While clear band of CPMV modified B.A was observed on the same gel (**Figures 4.27 and 4.28**).

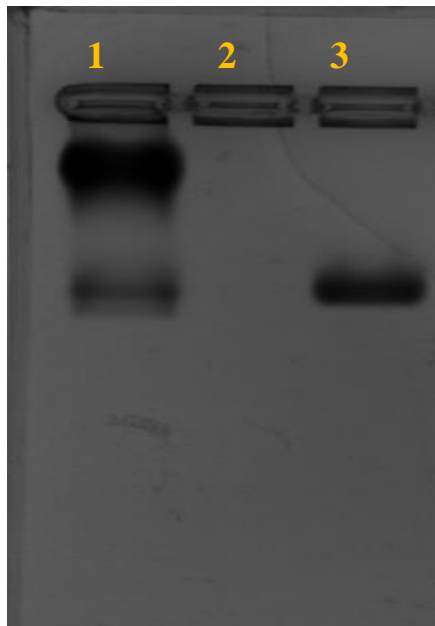


**Figure 4.27** The image of agarose gel electrophoresis 1.2 % w/v agarose, 60 V, stained with ethidium bromide: Lane1 wt CPMV, lane 2 CPMV- P.A, lane3 CPMV-B.A.

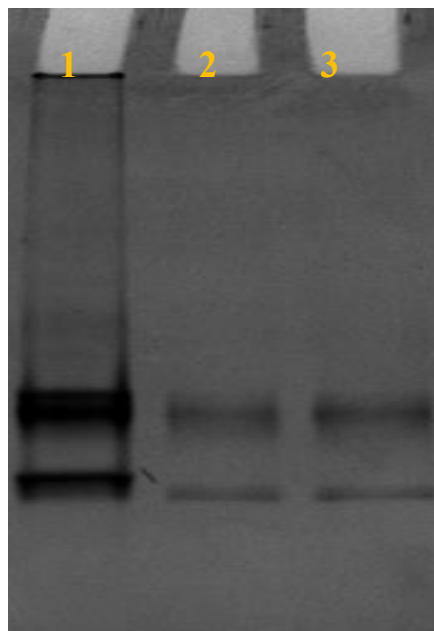


**Figure 4.28** The image of SDS gel electrophoresis, 180 V, stained with Coomassie: Lane1 wt CPMV, lane 2 CPMV- P.A, lane3 CPMV- B.A.

A negative stain of the modified particles with either 2% UA showed no CPMV particle on the grid because of the denaturation of CPMV **Figure 4.29**. For this reason B.A was used instead of P.A in 45 % recovered yield per virus.

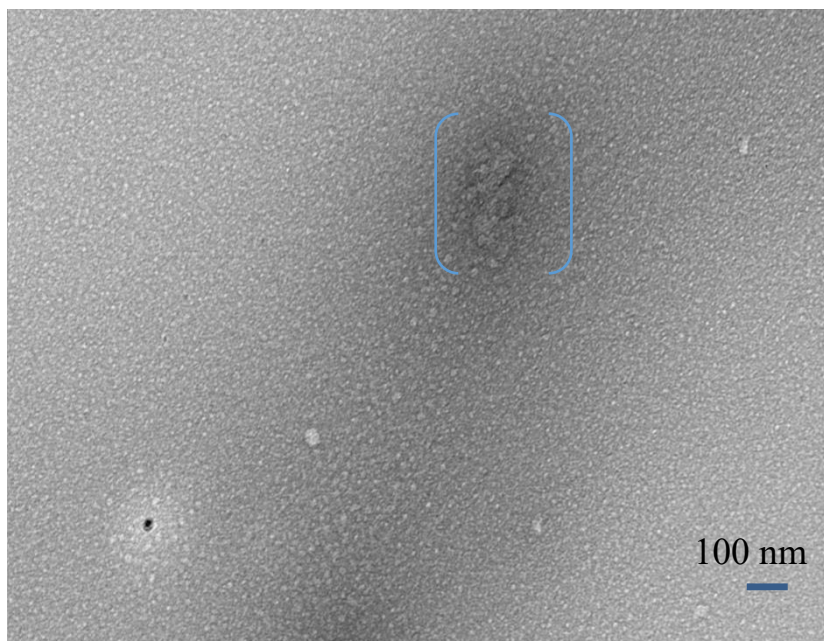
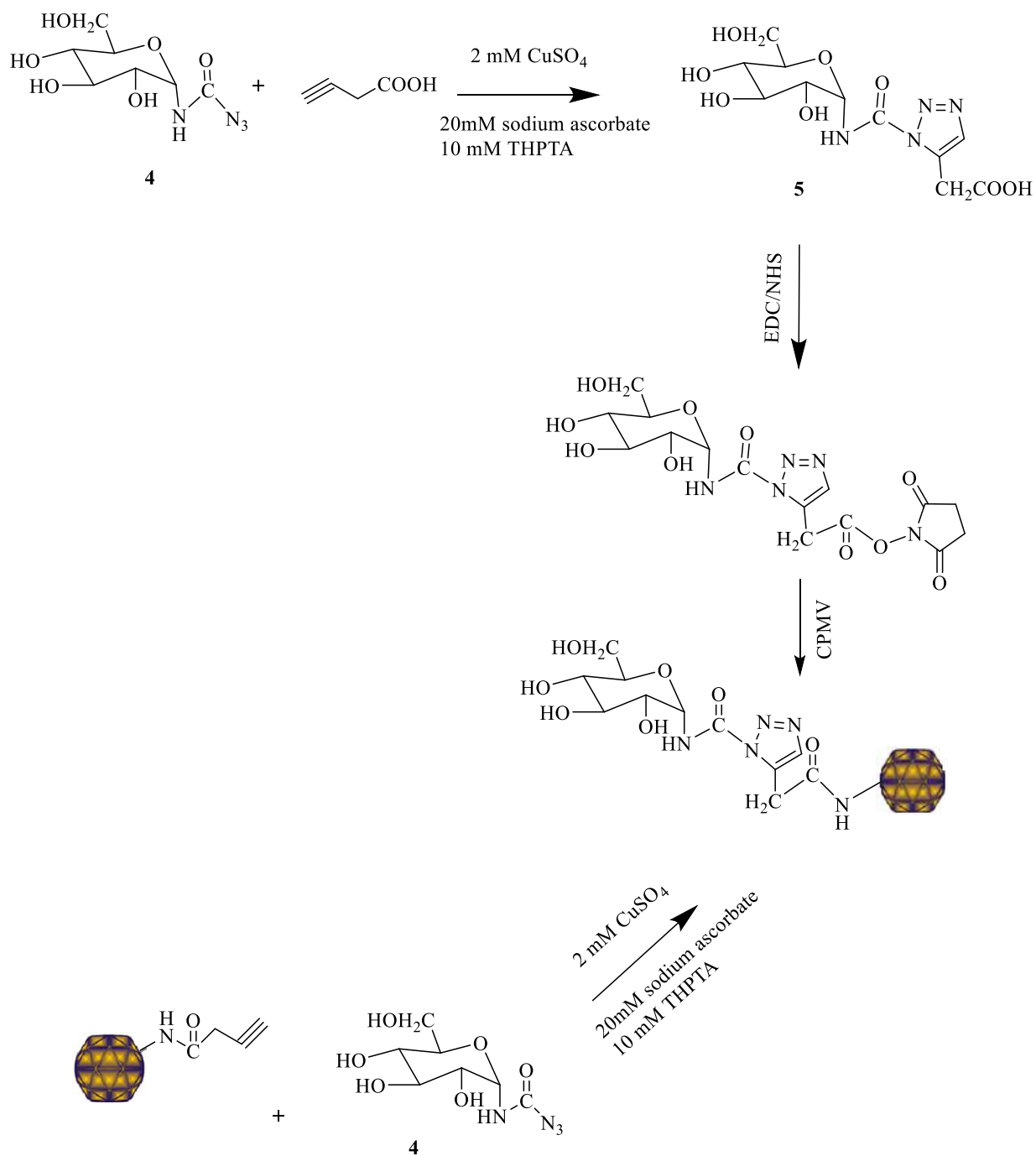


**Figure 4.29 Stained TEM images of externally modification of CPMV- P.A shown the denaturation of CPMV (between blue arrows).**

**4.1.8 The modification of CPMV by 3, 4, 5(-trihydroxy-6-(hydroxymethyl) tetrahydro-2-pyran-2-yl) carbamoyl)-1, 2, 3-triazol-5-yl) acetic acid (Glu) (5)**

The best method to attach glucose to the external surface of CPMV was investigated by conjugating compound (5) to CPMV by two methods:

1. CPMV-B.A was obtained in 43% yield and then reacted with compound (4) to give compound (5) in 23% yield based on the initial concentration of wt CPMV.
2. Compound (5) was synthesised first, then reacted with CPMV by following the same modification protocol used to prepare CPMV-CQp to give a 45% yield based on initial virus concentration (section 2.6.7 and 2.6.8) **Scheme 4.4**



**Scheme 4.4** The modification of CPMV with 3, 4, 5-trihydroxy-6-(hydroxymethyl) tetrahydro-2-pyran-2-yl) carbamoyl -1, 2, 3-triazol-5-yl) acetic acid (Glu).

The second method is the best way for glucose-CPMV conjugation for two reasons: Firstly, the number of B.A on the CPMV surface before reacting with an azide compound using N<sub>3</sub>-bodipy dye were not calculated. The reaction scheme is shown in **Scheme 4.5**. However, this dye caused the CPMV to precipitate out. This made it difficult to remove from the cut off column. As a result, CPMV was not observed on the agarose gel and in a UV/Vis spectrum **Figure 4.30**. Finally the yield of modified CPMV with compound (5) was increased by double as compared with the yield shown in the first method.

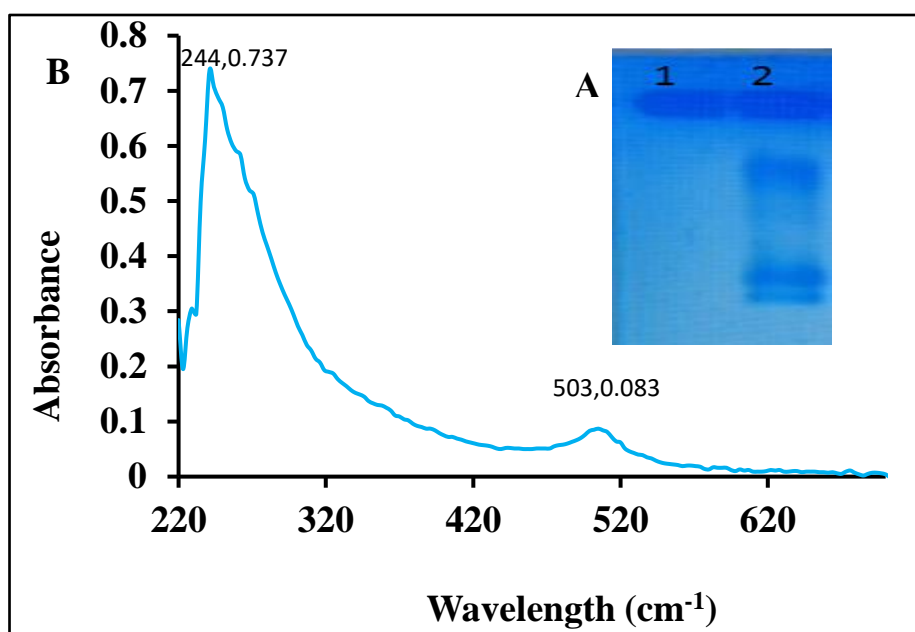


**Figure 4.30** A. Digital image of agarose gel electrophoresis 1.2 % w/v agarose, 60 V, stained with Coomassie: Lane1, CPMV-B.A -dye and lane 2, wt CPMV, B. UV/Vis spectrum of CPMV- B.A -dye modification.

To support whether or not B.A and N<sub>3</sub>-bodipy dye which was used to find out the number of B.A on the CPMV surface were reacted, the process was carried out without CPMV, this was confirmed by UV/Vis spectrophotometry. **Figure 4.31** shows two absorption maxima, one at 253 nm indicative B.A and 505 nm for N<sub>3</sub>-bodipy dye, this confirmed successful conjugation.

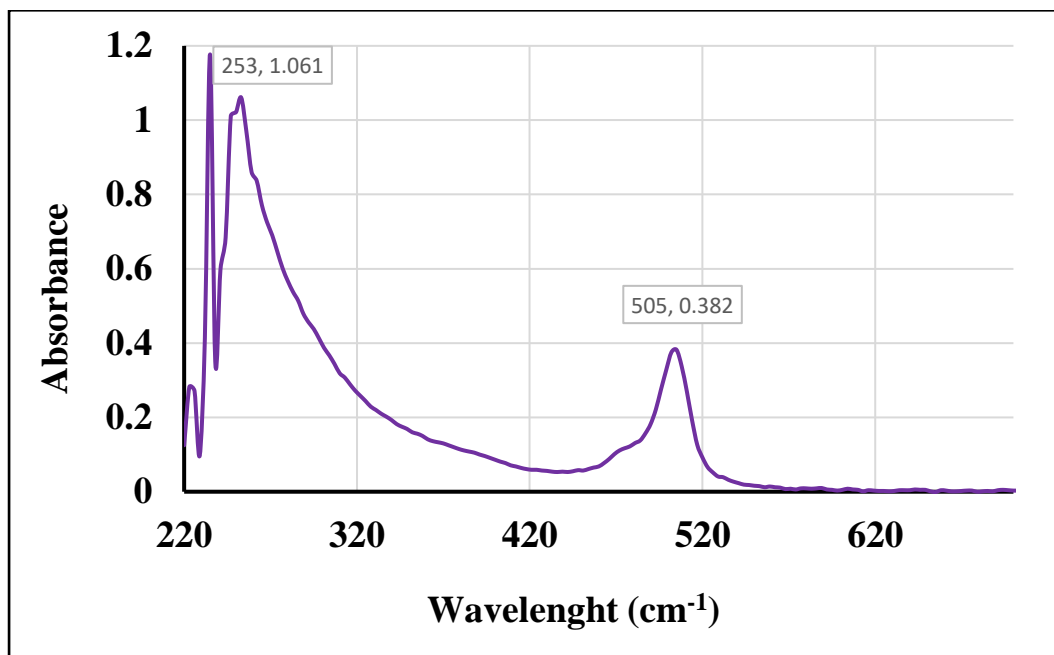
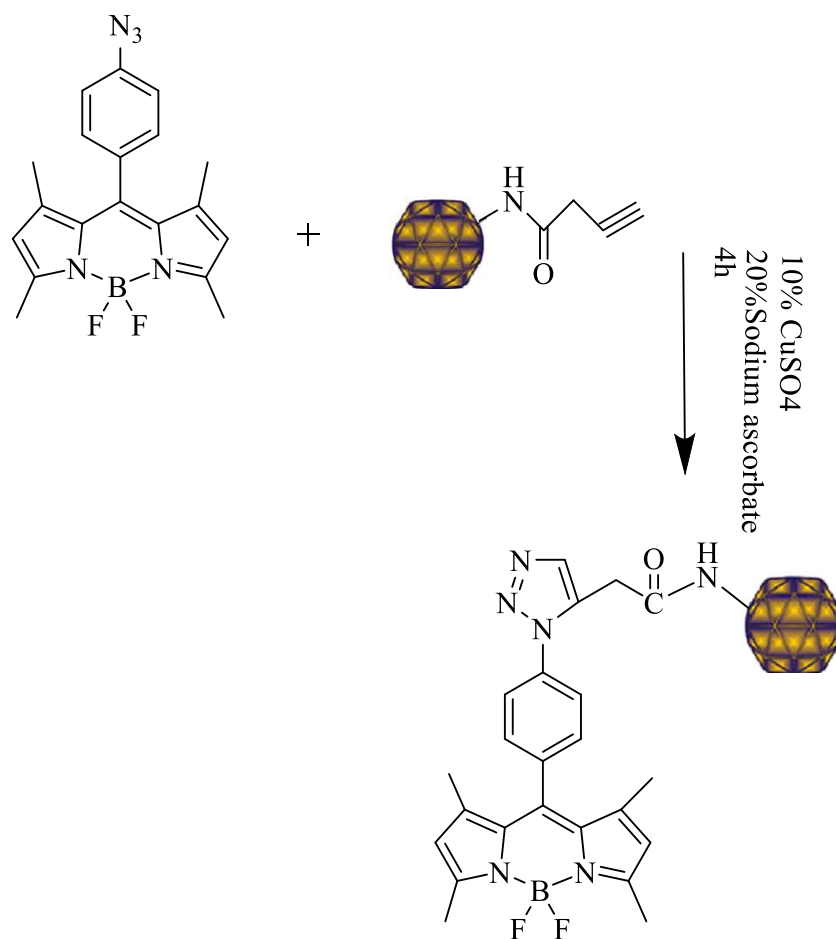


**Figure 4.31** UV/Vis spectrum of the conjugation of B.A with N<sub>3</sub>-bodipy dye.

The modification of CPMV-B.A with N<sub>3</sub>-bodipy dye was shown in **Scheme 4.5**.



**Scheme 4.5** The modification of CPMV-B.A with N<sub>3</sub>-bodipy dye.

## 4.2 Double addressability of amines on external surface of CPMV

### 4.2.1 Modification of CPMV-CQp with glucuronic acid (G.A)

CPMV-CQp was modified first and identified using UV/Vis spectrophotometry and agarose gel electrophoresis. To prepare CPMV-CQp-G.A, the carboxyl group of the G.A was first activated using EDC /NHS (section 2.6.4), the simplified reaction scheme is shown in **Scheme 4.6**. The reaction of G.A ester with virus surface amines, on CPMV-CQp, generated CPMV-CQp-G.A conjugates in 60 % recovered yield based on the initial CPMV-CQp concentration. The integrity of the product was confirmed by UV/Vis spectrophotometry and gel electrophoresis **Figure 4.32** and **Figure 4.33**.

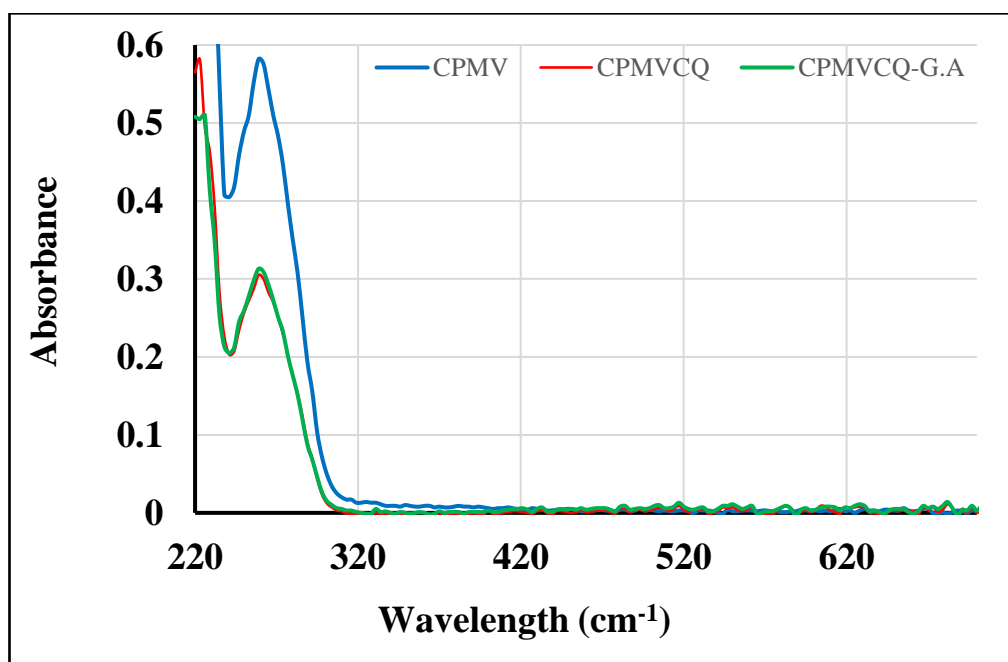
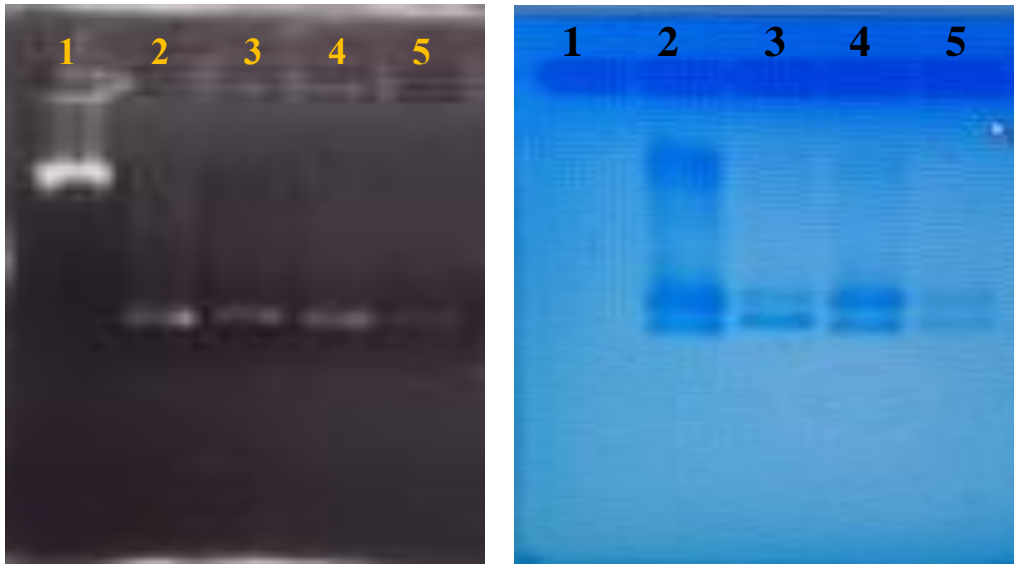


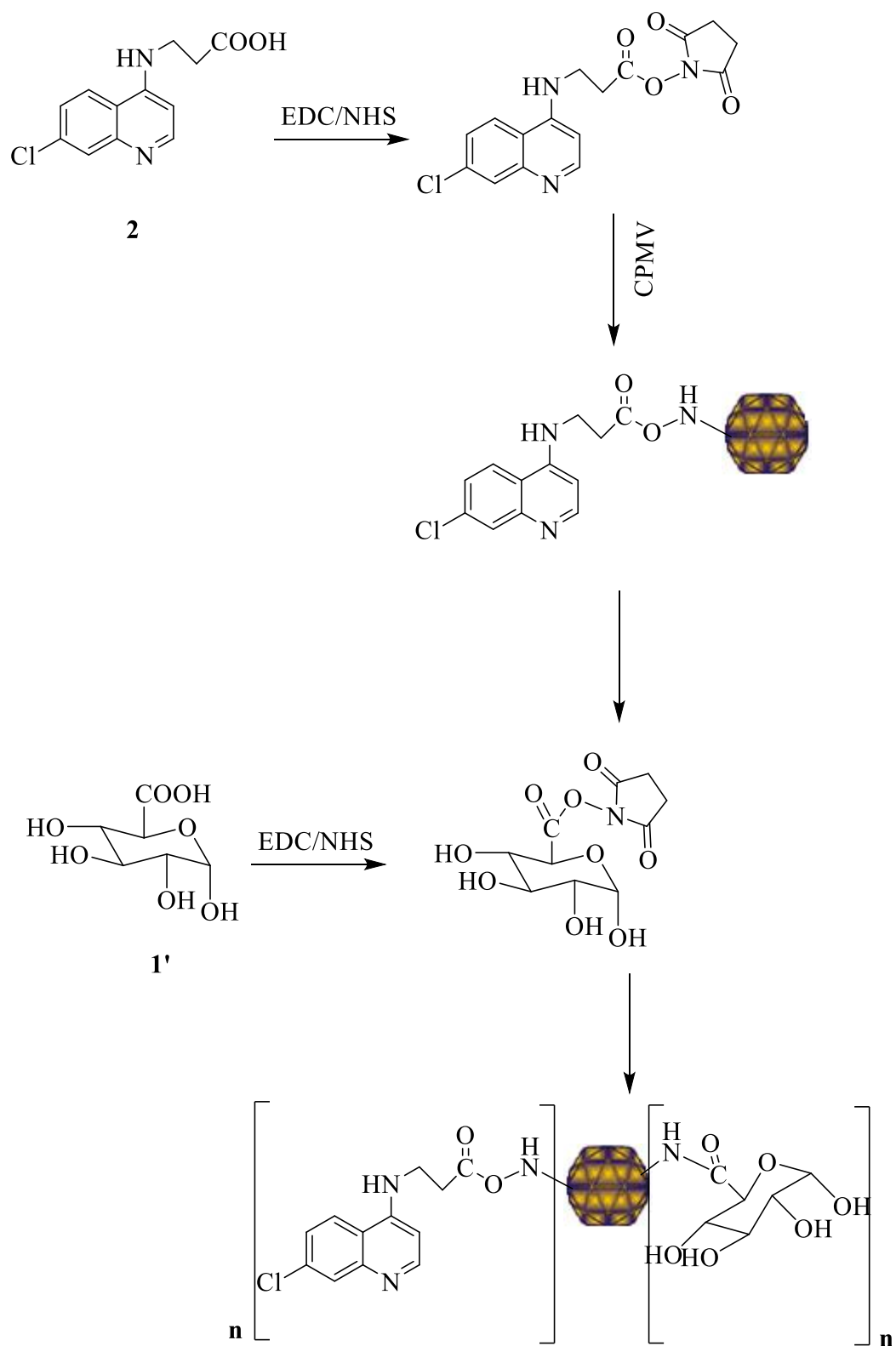
**Figure 4.32** The UV/Vis spectrum shows the maximum absorbance of wt CPMV, CPMV-CQp and CPMV-CQp-G.A



**A: EtBr staining**

**B: Comassie staining**

**Figure 4.33 Digital image of agarose gel electrophoresis 1.2 % w/v agarose, Lane 1- marker, 2- wt CPMV, 3-CPMV- ester, 4-CPMV- CQp, 5- CPMV-CQp- G.A**



**Scheme 4.6** Decoration of CQp(2) & G.A(1') on external surface of CPMV particle.

This experiment was repeated using another approach where CPMV was reacted with G.A first, then with CQp to determine if this favours a higher number of bound CQp. UV/Vis spectrophotometry and agarose gel electrophoresis of the product are shown in **Figure 4.34** and **Figure 4.35**.

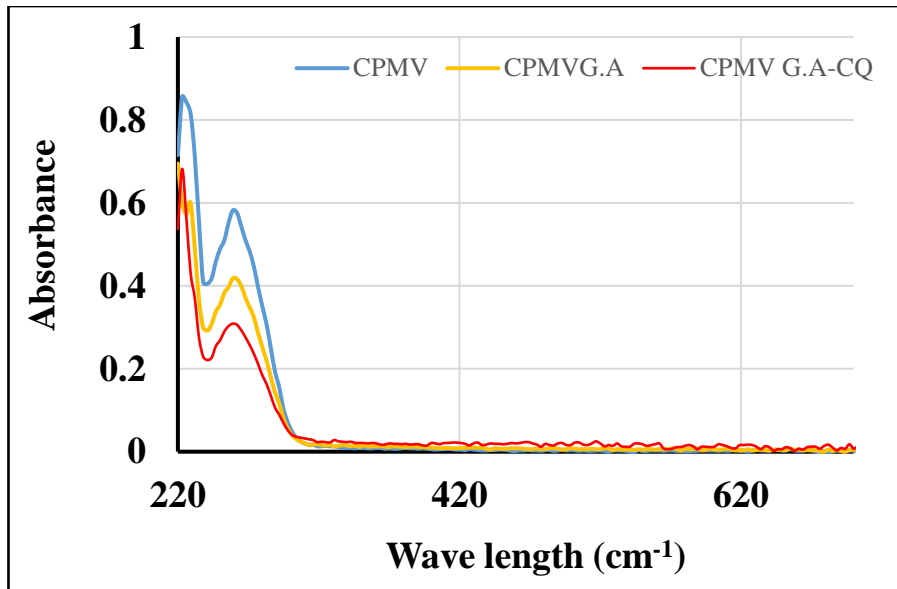
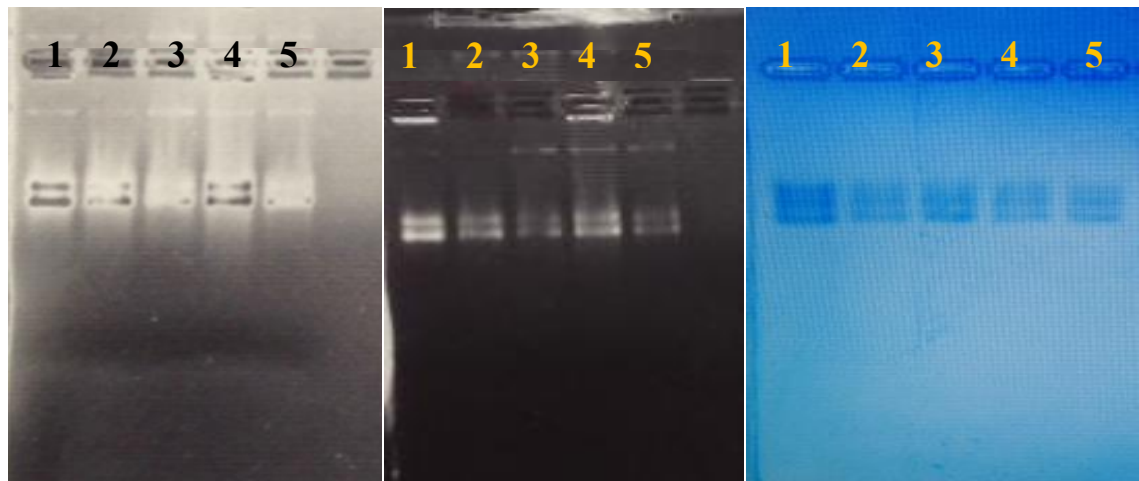


**Figure 4.34** The UV spectrum of wt CPMV, CPMV-G. A and CPMV-G. A-CQp.



**A: UV light**

**B: EtBr staining**

**C: Coomassie staining**

**Figure 4.35** Digital image of agarose gel electrophoresis 1.2 % w/v agarose, 60 V, lane 1 wt CPMV, 2 CPMV-CQp, 3 CPMV-CQp-G. A, 4 CPMV-G.A and 5 CPMV-G.A-CQp.

**Figure. 4.35** shows the large (L) and small (S) capsid proteins of wild-type before and after modification, binding of CQp and G.A caused only a slight shift in the positions of the S subunits, consistent with attachment of CQp and G.A to the external surface. It was found that modification of CPMV with CQp first then with G.A increased the number of CQp on the external surface of CPMV as estimated by reaction of undecorated lysine groups with Alexa Fluor 488 dye (section 2.6.2) **Tables 4.1 and 4.2.**

**Table 4.1 The reaction of CPMV, CPMV- CQp and CPMV-CQp-G. A with Alexa Fluor dye 488 after 8h dialysis against 500 ml PBS buffer.**

Reacted	Number of dye molecules/CPMV particle	CQ number	G. A number
CPMV dye	<b>240</b>	-----	-----
CPMV- CQp dye	86	154 ± 4	-----
CPMV -CQp-G. A dye	40	154 ± 4	46 ± 1

**Table 4.2** The reaction of CPMV, CPMV- G. A and CPMV-G.A- CQp with Alexa Fluor dye 488 after 8h dialysis against 500 ml PBS buffer.

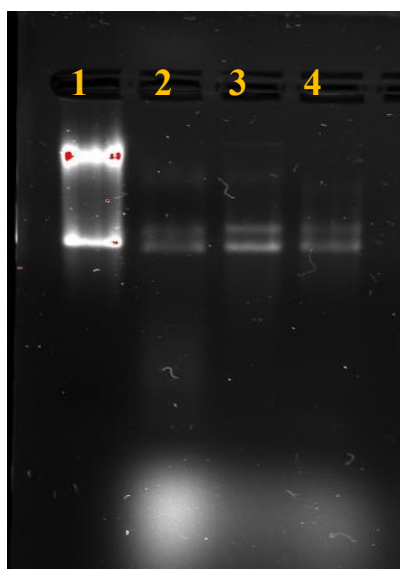
Reacted	Number of dye molecules/CPMV particle	CQ number	G. A number
CPMV dye	240	-----	-----
CPMV- G. A dye	185	-----	55 ± 2
CPMV- G. A-CQp dye	90	95 ± 2	55 ± 2

The number of bound CQp was reduced significantly when CPMV was modified first with G.A as shown in **Table 4.2**. The best conditions established for this reaction were:

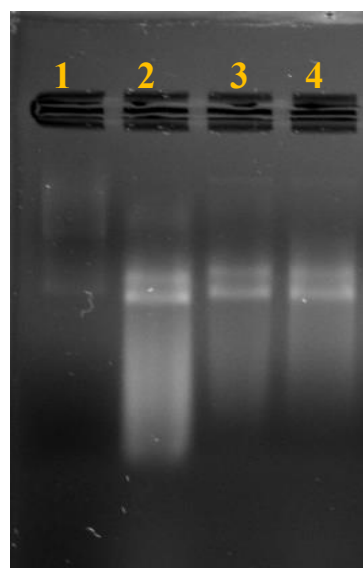
1- Initial concentration of CPMV 0.20-0.26 mg/ml

2- CPMV should be modified first with CQp then with G. A

Electrophoresis and UV/Vis spectrophotometry **Figure 4.36 and 4.37** were again consistent with formation of the desired product.



**A:6h dialysis**



**B: 10 h dialysis**

**Figure 4.36** The image of agarose gel electrophoresis 1.2 % w/v agarose, 60 V, stained with ethidium bromide. Lane1 wt CPMV, lane 2 CPMV- dye, lane3 CPMV-CQp-dye, lane 4 CPMV-CQp-G.A-dye.

Excess of non-reacted dye is visible after 6h dialysis, while it was no excess dye after 8-10 h dialysis. As a result, 8-10 h dialysis is perfect time to stop dialysis and calculate the correct number of G. A and CQp. The florescent intensity in all modified particles lanes compared to unmodified particle confirmed the conjugation of the dye on the external surface of CPMV **Figure 4, 36 B.**

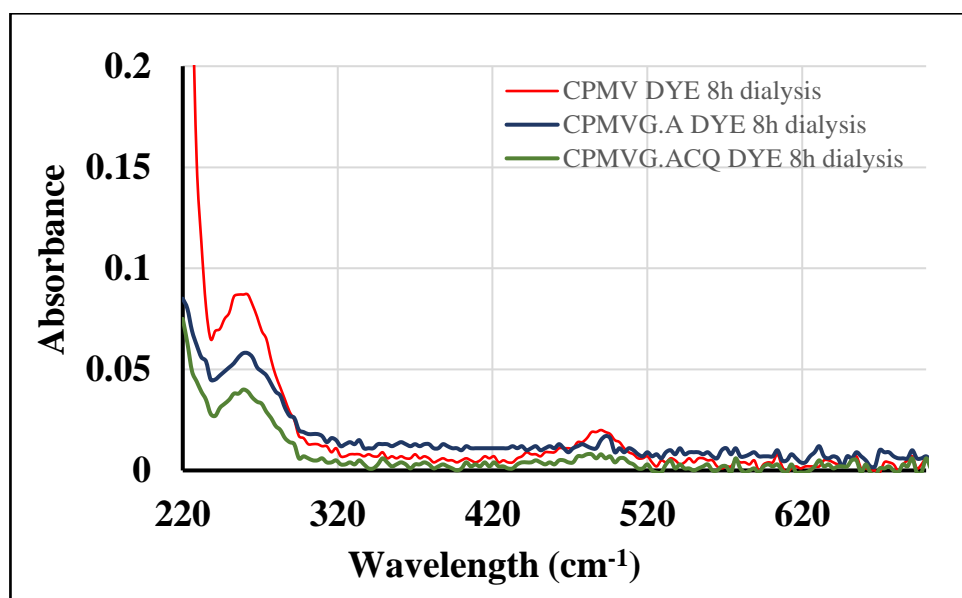


**Figure 4.37** UV /Vis spectrum of CPMV- dye, CPMV-G.A- dye and CPMV-G.A-CQp-dye.

To establish whether or not Alexa Fluor 488 dye remained conjugated to CPMV samples after purification, the UV/Visible spectrum was recorded, two maximum absorbance were observed, one at 260 nm for CPMV and another at 494 nm for dye **Figure 4.38**, confirming that the dye remained.

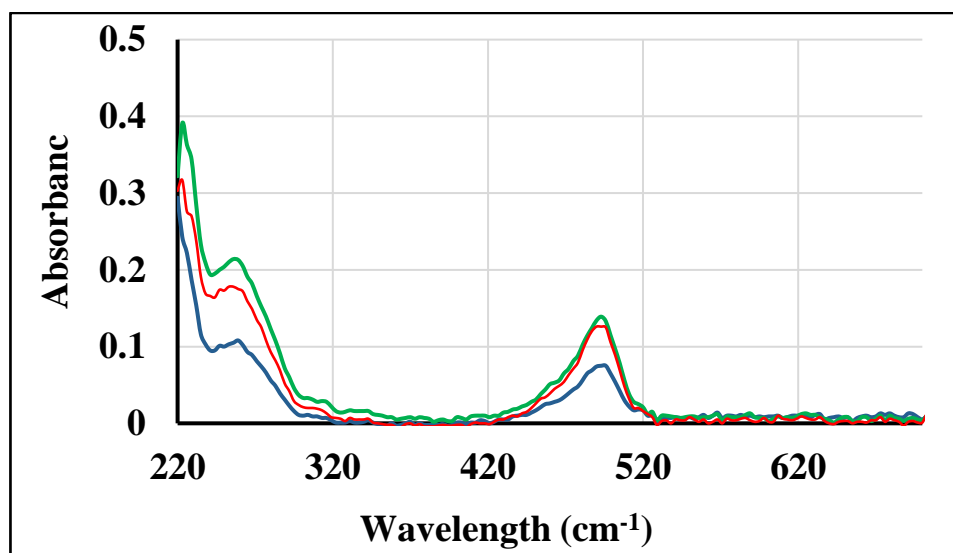


**Figure 4.38** UV/Vis spectrum of CPMV- dye (green line), CPMV-G.A -dye (red line) and CPMV-G.A-CQp -dye (blue line) after 4h dialysis.

Negatively stained transmission electron micrographs clearly show a slight increase in particle diameter, to 31.0 nm, compared with wild-type CPMV. This is consistent with formation of CPMV-CQp-G.A and it remaining intact after modification **Figure 4.39**.

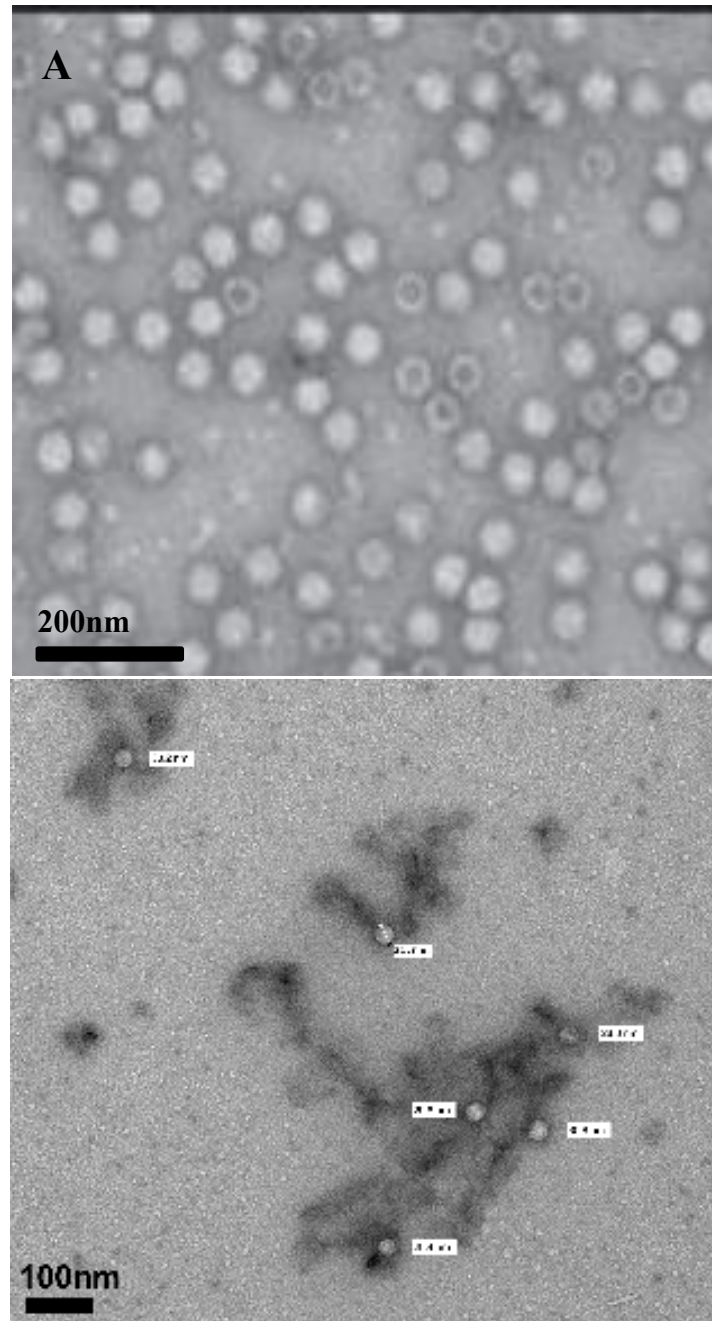


**Figure 4.39** Stained TEM image of wt CPMV<sup>128</sup> and B- CPMV-CQp-G.A.

#### 4.2.2 Modification of CPMV-CQ-ala and CPMV-CQ-val with glucuronic acid

Wt CPMV was modified with CQ derivatives, then after purification it was modified with G.A. Modification was confirmed by UV/Vis spectrophotometry and agarose gel electrophoresis. **Figures 4.40- 4.42.**

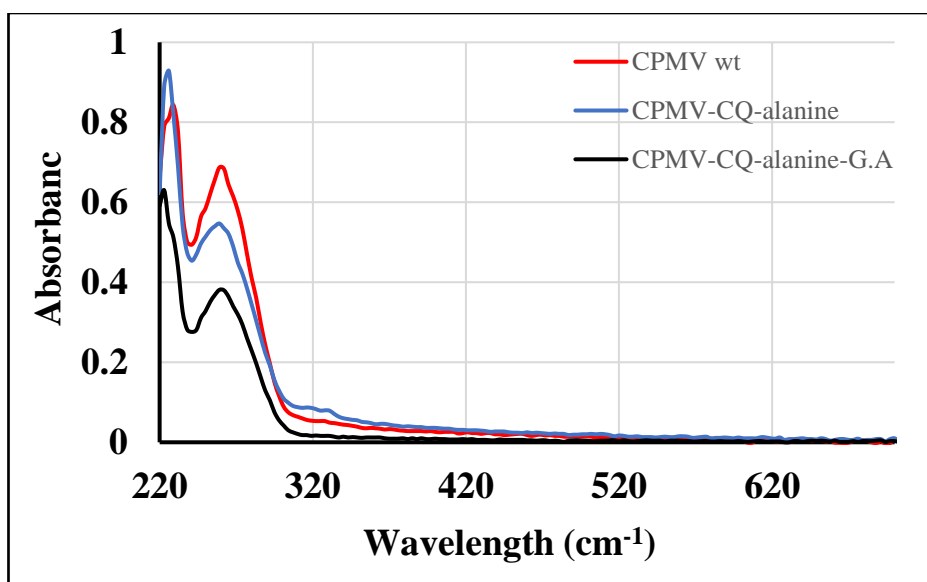


Figure 4.40 UV/ Vis spectrum of singly and doubly functionalised CPMV particle.

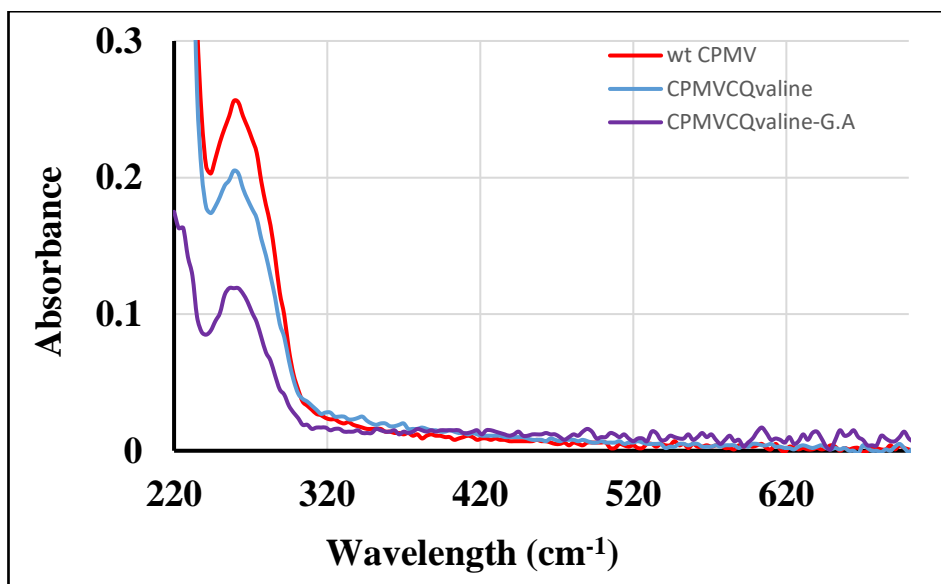
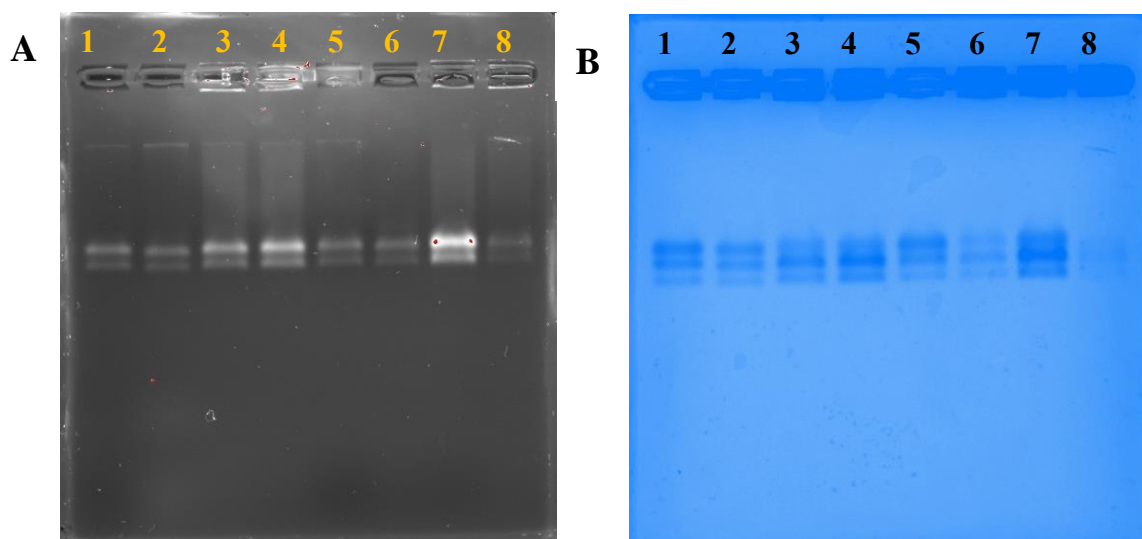


Figure 4.41 UV / Vis spectrum of singly and doubly functionalised CPMV particle.



**Figure 4.42** Agarose gel (1.2%) of CPMV particles visualised by ethidium bromide staining (A) and Coomassie blue staining (B). Lane 1, wt CPMV 2, CPMV-CQ-ala 3, CPMV-CQ-ala-G.A 4, CPMV-CQ-ala-Glu 5, wt CPMV 6, CPMV-CQ-val 7, CPMV-CQ-val-G.A and 8, CPMV-CQ-val-Glu.

Agarose gel electrophoresis followed by ethidium bromide staining and Coomassie blue staining showed a similar migration pattern on CPMV single modification and a slight change after double modification compared to unmodified CPMV **Figure 4.42**.

The integrity of CPMV-CQ-ala-G.A and CPMV-CQ-val-G.A were confirmed by negatively stained TEM **Figure 4.43**, the particles show similar morphology to wt CPMV. No aggregation was observed in any of the TEM samples.

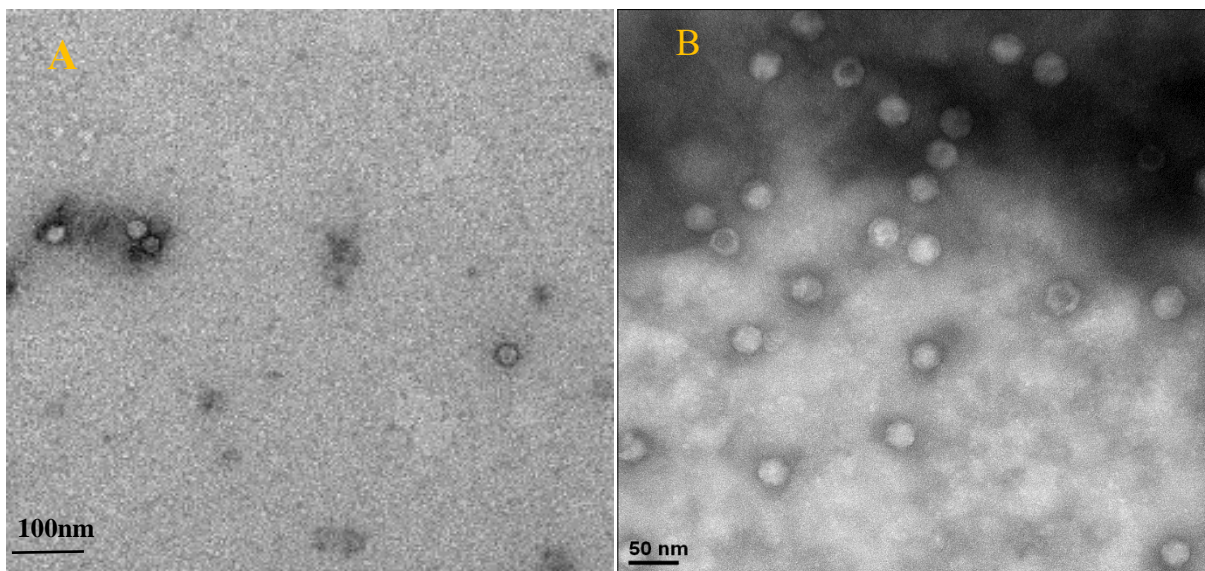
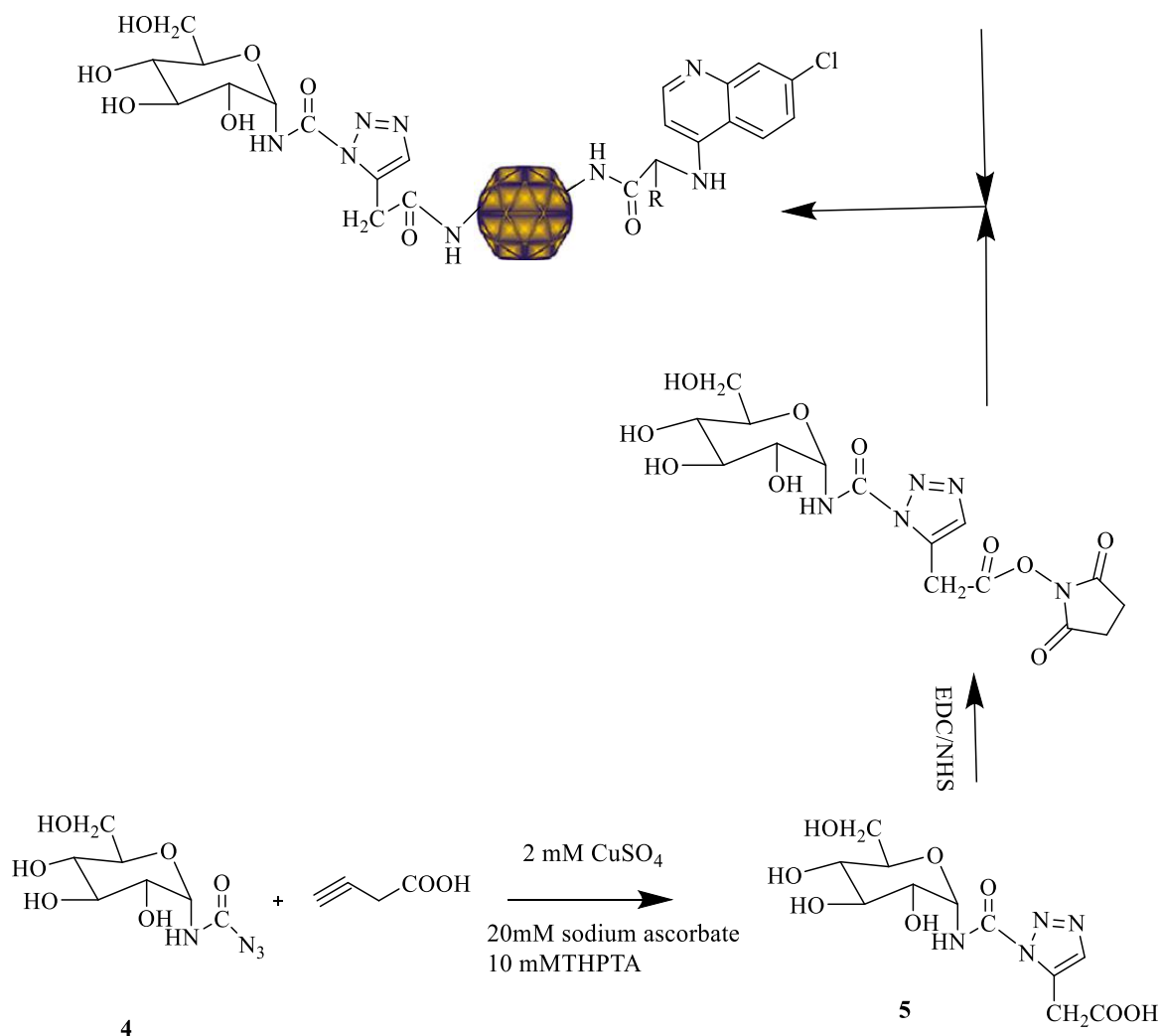
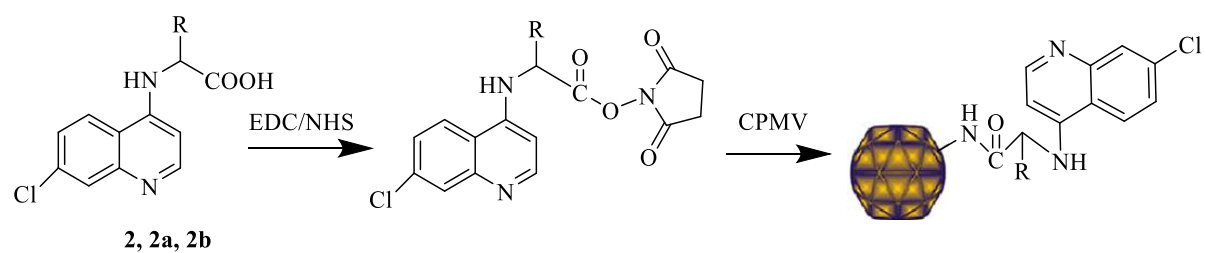


**Figure 4.43** TEM images of (A) uranyl acetate stained CPMV-CQ-ala-G.A, (B) uranyl acetate stained CPMV-CQ-val-G.A.

#### **4.2.3** *Modification of CPMV-CQp with 3, 4, 5(-trihydroxy-6-(hydroxymethyl) tetrahydro-2-pyran-2-yl) carbamoyl)-1, 2, 3-triazol-5-yl) acetic acid (Glu)*

CPMV-CQp was prepared first and the CPMV concentration was calculated. CPMV-CQp was divided into two parts, one part was kept and the second part was reacted with a 3000 molar excess of Glu to give 45% yield of modified CPMV, **Scheme 4.7**.



R	-CH <sub>2</sub>	<b>Compound 2</b>
R	-CH <sub>3</sub>	<b>Compound 2a</b>
R	-CH(CH <sub>3</sub> ) <sub>2</sub>	<b>Compound 2b</b>

**Scheme 4.7** The modification of CPMV-CQ- derivatives with 3, 4, 5-(trihydroxy-6-(hydroxymethyl) tetrahydro-2-pyran-2-yl) carbamoyl) -1, 2, 3-triazol-5-yl) acetic acid.

The result was confirmed by agarose gel electrophoresis **Figure 4.44** and UV/Vis spectrophotometry **Figure 4.45**. Staining of the gel with both ethidium bromide and Coomassie blue confirmed the integrity of the particles and a slight shift in band position was observed after modification.

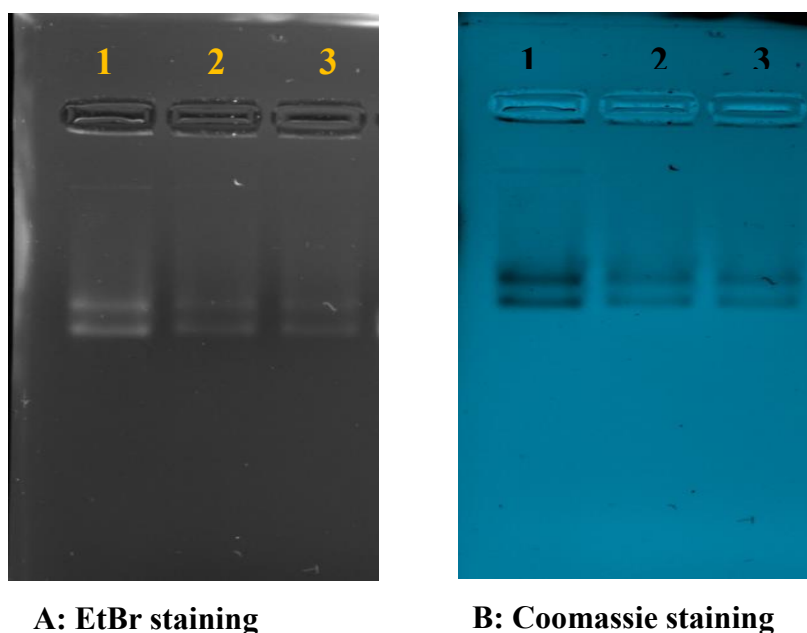


**Figure 4.44** Digital image of agarose gel electrophoresis 1.2 % w/v agarose, 60 V, stained with A: ethidium bromide, B: Coomassie, Lane 1: wt CPMV, lane 2: CPMV-CQp and lane 3 CPMV-CQp-Glu.

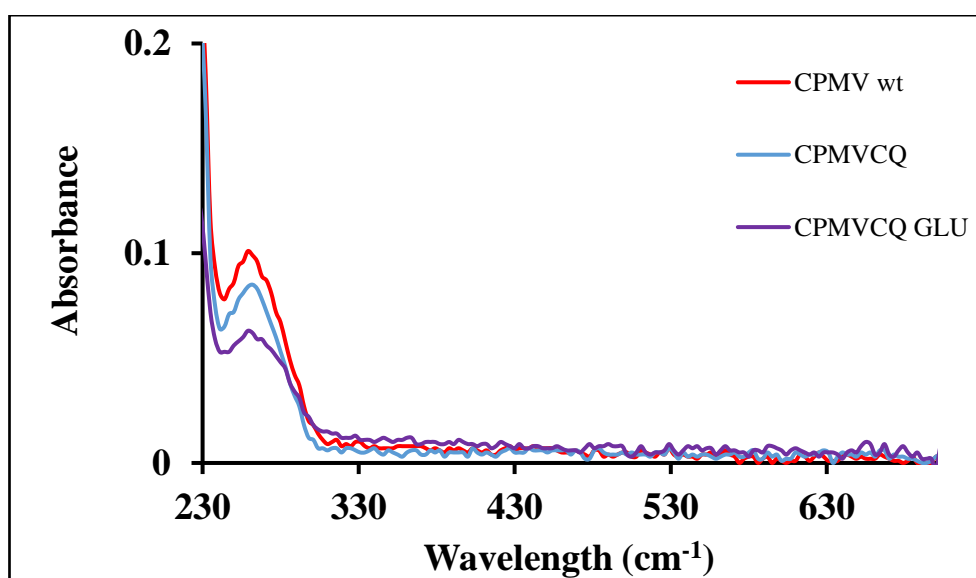


**Figure 4.45** UV /Vis spectrum of CPMV before and after modification with CQp and Glu.

Further support for modification on the external surface is provided by comparison of the SDS–PAGE of modified and unmodified CPMV particles **Figure 4.46**. Even under harsh denaturing conditions, such as with sodium dodecyl sulfate at 100 °C for 10 minutes, there was a minimal change to the coat proteins on the denatured CPMV particles, this is shown below in **Figure 4.46**. There is a faint band representing the large subunit coat protein on the SDS–PAGE gel in lane 3 and ss subunits in lane 6 and 7. This is what would be expected due to different mobility of particles after double modification.

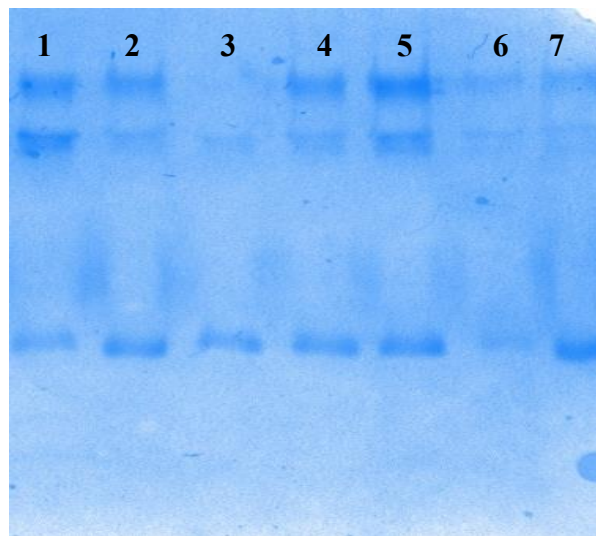


**Figure 4.46 SDS-PAGE of CPMV particles, 180 V, stained with Coomassie: Lane 1- CPMV- CQ- ala, 2- CPMV- CQ- ala- Glu, 3- CPMV -CQ- ala-G. A, 4- wt CPMV, 5- CPMV-CQ-val, 6- CPMV-CQ-val-G.A and 7-CPMV-CQ-val-Glu.**

As expected, analysis of the single modified and unmodified CPMV by SDS-PAGE proved that they are all located in the small and large subunits. This is where both the slow and fast forms of the small subunit can be seen. However, double modification of the virus indicated a slight cleavage due to the high molecular weight of the CPMV particles corresponding to their subunits.

#### 4.2.4 Quantification of CPMV-CQp-Glu

To estimate the number of Glu molecules per virus particle, CPMV-CQp-Glu was reacted with Alexa Fluor 488 dye as described (section 2.5.2). The functionalised particle was purified on 100 kDa cut-off columns and the number of free reactive lysines was calculated from the absorbance of CPMV and Alexa Fluor 488 dye.<sup>189</sup> **Table 4.3**. It was found that 54 Glu molecules were conjugated to the CPMV external surface and the number of CQp was 154 per virus. The result was confirmed by UV/Vis spectrophotometry and agarose gel electrophoresis **Figure 4.47** and **Figure 4.48** respectively.

**Table 4.3** The reaction of CPMV, CPMV-CQp and CPMV-CQp-Glu with Alexa Fluor dye 488 after 8-10h dialysis against 500 ml PBS buffer pH7.

Reacted	Number of dye molecules/CPMV particle	CQ number	Glu number
CPMV -dye	240	-----	-----
CPMV- CQp -dye	85	155 ± 2	-----
CPMV- CQp-Glu-dye	31	155 ± 2	54± 3

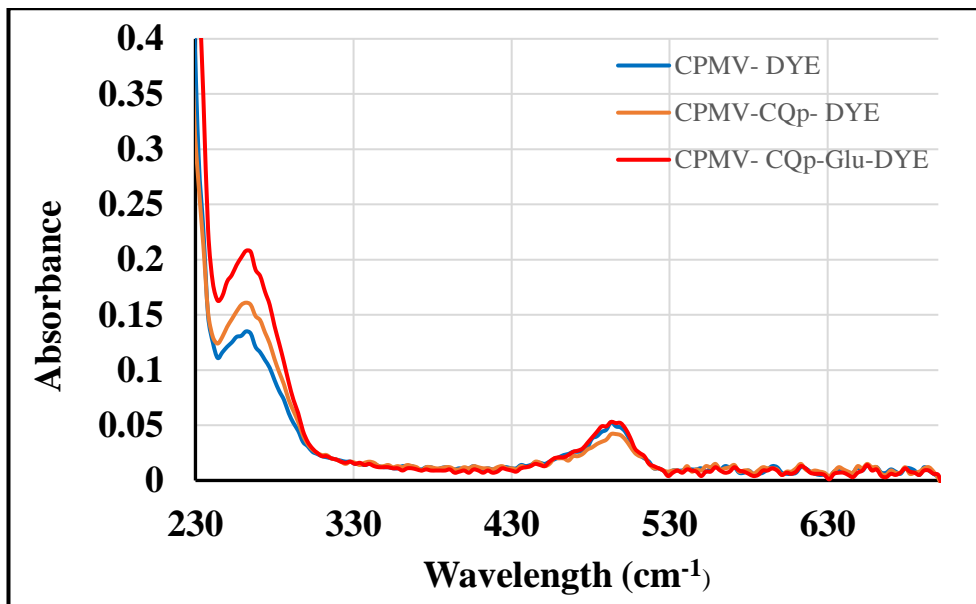


Figure 4.47 A The UV spectrum of CPMV wild type, CPMV-CQp and CPMV-CQp-Glu- dye after 8h dialysis.

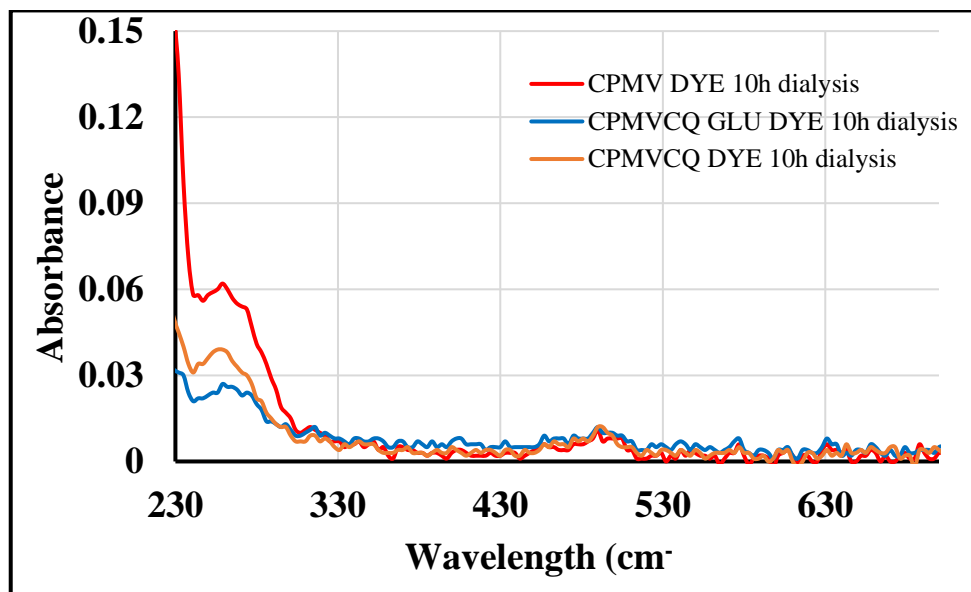


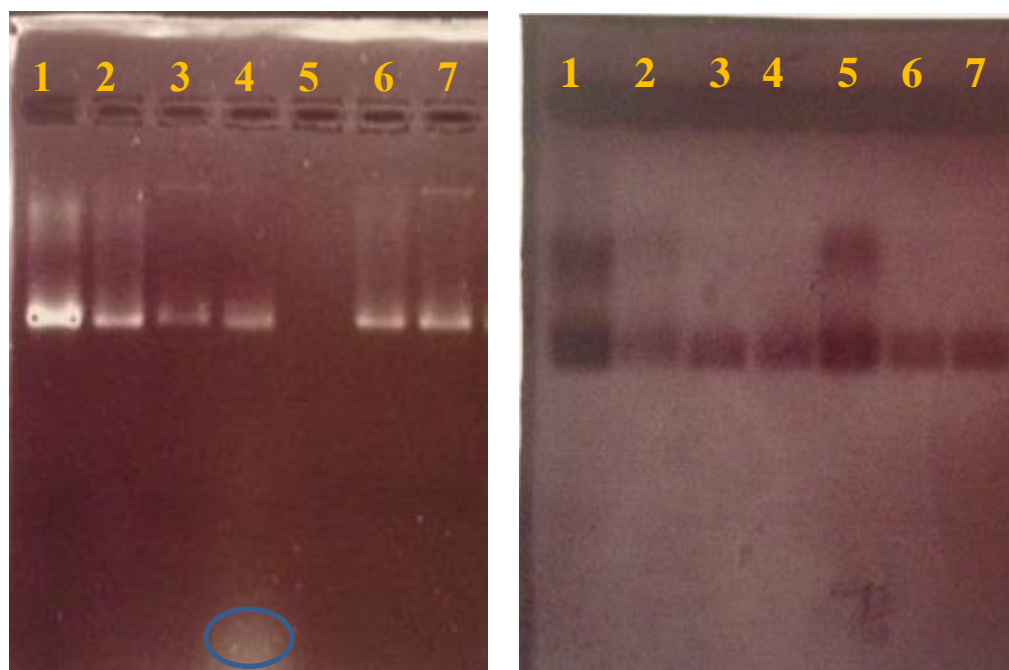
Figure 4.47 B the UV/Vis spectrum of CPMV- dye, CPMV-CQp-dye and CPMV-CQp -Glu -dye after 10h dialysis.

The best condition for this reaction was:

1- CPMV concentration 0.3 mg/ml

2-The concentration of Alexa dye 2000 molar excess

3- Dialysis time should be 8-10h to avoid dilution



**A: EtBr staining**

**B: Coomassie staining**

**Figure 4.48** Digital image of agarose gel electrophoresis 1.2 % w/v agarose, 60 V, stained with both ethidium bromide and Coomassie staining Lane 1: wt CPMV, lane 2: CPMV-dye 8h dialysis, lane3: CPMV-CQp -dye 8h dialysis, lane4:CPMV-CQp-Glu-dye 8h dialysis, lane5:CPMV-dye 10h dialysis, lane6:CPMV-CQp- dye 10h dialysis and lane7:CPMV-CQp-Glu-dye 10h dialysis.

The movement of single and double modified CPMV after reaction with Alexa Fluor 488 dye on agarose gel showed only one form of small subunit compared with CPMV-dye particle, this probably relates to cleavage of the carboxyl-terminus 24 amino acids of the small subunit. Additionally, only CPMV-CQp-Glu-dye showed excess of non-reacted dye in lane 4 after 8h dialysis but there was no excess dye observed after an extra 2h dialysis for the same sample. **Figure 4.48.**

#### 4.2.5 Modification of CPMV-CQ-ala and CPMV-CQ-val with 3, 4, 5-(trihydroxy-6-(hydroxymethyl) tetrahydro-2-pyran-2-yl) carbamoyl -1, 2, 3-triazol-5-yl) acetic acid (Glu)

CPMV-CQ-ala and CPMV-CQ-val were prepared first and the CPMV concentration was calculated. Each conjugated particle was modified with Glu **Schemes 4.7**, and the integrity of the intact particles was confirmed by agarose gel electrophoresis and UV/Vis spectrophotometry. The 260/280nm absorbance ratio of CPMV after double modification was (1.52), which confirmed that the particle was still intact. **Figures 4.49, 4.50 and 4.51.**

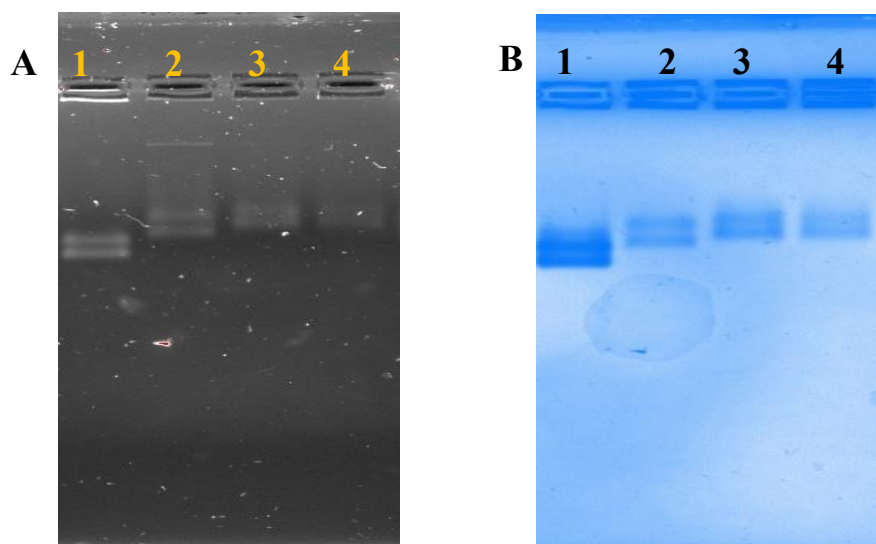


**Figure 4.49** Digital image of agarose gel electrophoresis 1.2 % w/v agarose, 60 V, stained with A: ethidium bromide staining, B: Coomassie staining: Lane 1. wt CPMV, lane 2. CPMV-ester, lane3. CPMV-CQ-ala-Glu, lane4. CPMV-CQ-val-Glu.

A slower migration of CPMV in the gel was observed when both CPMV-CQ-ala and CPMV-CQ-val were associated with the Glu molecules compared to unmodified particle because of a combination of size and charge effects, which affected mobility through the gel. The number of unconjugated amines on the external surface of CPMV

was determined by reaction with Alexa Fluor 488 dye.<sup>189</sup> The number of each compound attached to the external surface of CPMV particle is given in **Tables 4.4** and **4.5**.

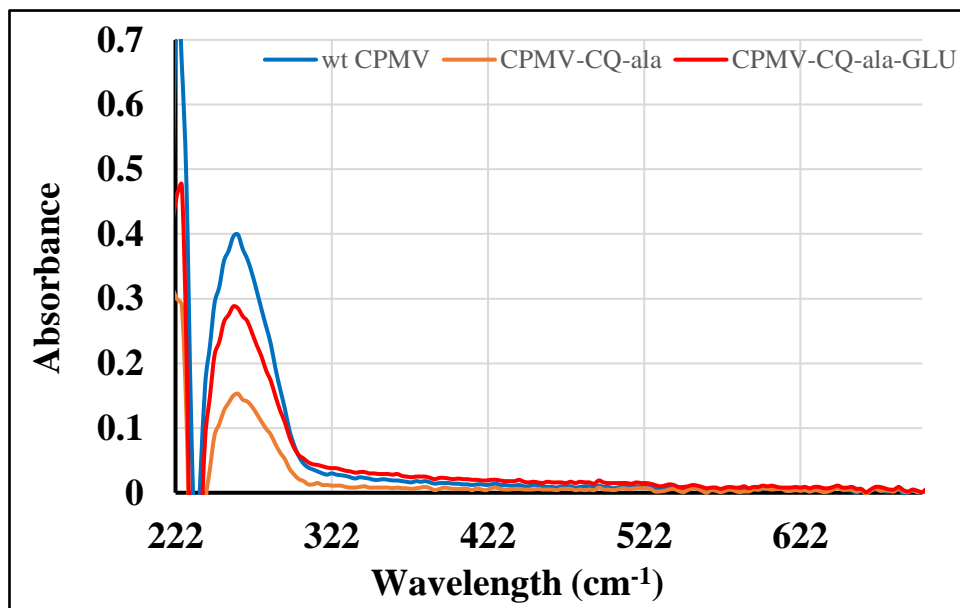


**Figure 4.50** UV/Vis spectrum of singly and doubly functionalised CPMV particles.

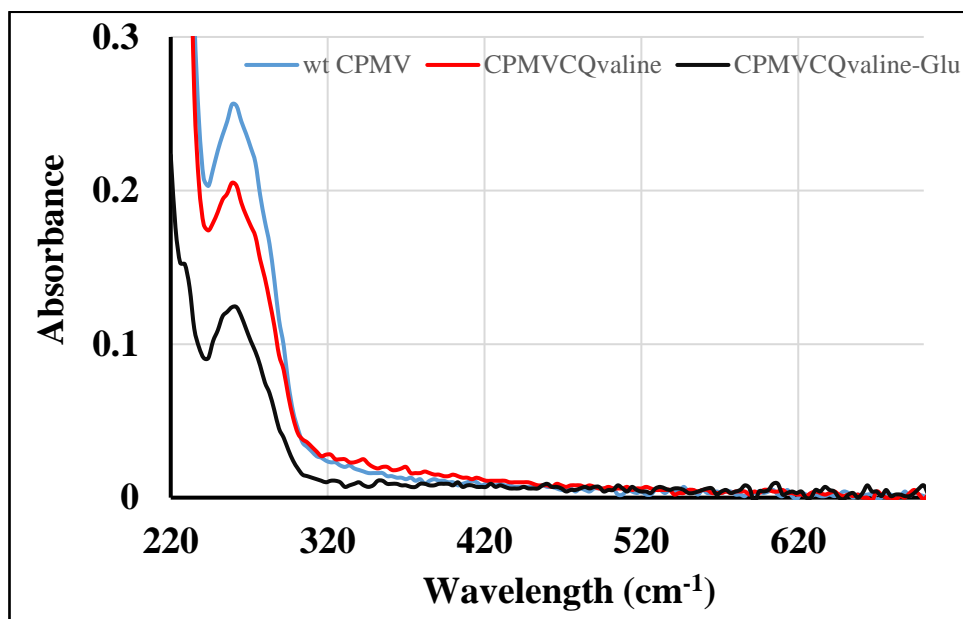


**Figure 4.51** UV/Vis spectrum of singly and doubly functionalised CPMV particles.

The best way to conjugate Glu to the external surface of CPMV-CQ-ala and CPMV-CQ-val is shown in **Schemes 4.7**.

#### 4.2.6 Attachment of modified CPMV to Alexa Fluor 488 dye

The number of unconjugated amines on the external surface of CPMV was determined from the absorbance of CPMV at 260nm and the absorbance of Alexa Fluor 488 dye at 494 nm.<sup>189</sup> The maximum number of addressable lysine with fluorescent dyes is 240 per virus as described in section (4.1.5).<sup>164</sup> The attached number of each compound to external surface of CPMV particle was shown in (Table 4.4) and (Table 4.5).

**Table 4.4** The reaction of CPMV, CPMV-CQ-ala, CPMV-CQ-ala-G.A and CPMV-CQ-ala-Glu with Alexa Fluor dye 488 after 8h dialysis against 500 ml PBS buffer.

Reacted	Number of dye molecules/CPMV particle	CQ number	G. A number
CPMV dye	240	-----	-----
CPMV- CQ-ala dye	95	145 ± 5	-----
CPMV- CQ- ala-G. A dye	30	145 ± 5	65 ± 1
CPMV- CQ- ala-Glu dye	40	145 ± 5	60 ± 1

**Table 4.5 The reaction of CPMV, CPMV- CQ-val, and CPMV-CQ-val-G. A and CPMV-CQ-val-Glu with Alexa Fluor dye 488 after 8dialysis against 500 ml PBS buffer.**

Reacted	Number of dye molecules/ CPMV particle	CQ number	G. A number
CPMV dye	240	-----	-----
CPMV CQ-val dye	90	150 ± 5	-----
CPMV CQ-val-G. A dye	30	150 ± 5	60 ± 2
CPMV CQ-val-Glu dye	32	150 ± 5	58 ± 1

### 4.3 Summary

During the past five decades chloroquine (CQ) and other related 4-aminoquinolines have played an important role to reduce the resistance of malaria parasite. CQ resistance (CQR) is related to a significant reduction in CQ accumulation by the parasite. In the presence of CQ, the rate of Digestive Vacuole (DV) alkalinisation followed by H<sup>+</sup> pump inhibition increased the effectivity of CQ<sup>R</sup>.<sup>190</sup>

Resistance to CQ is a major problem in the malaria reduction programme; looking for new, cheap, and structurally varied drugs has become a crucial need to remove this parasitic disease. It has been reported that chloroquine (CQ) is one of the most regularly used drugs for the clinical control of malaria. An attractive basis for improving drug action of CQ and its analogues relates to the accumulation of such compounds in the food vacuole of the parasite and its role in blocking or inhibition of haemozoin formation.<sup>191</sup>

As a result, research activity towards modifying CQ side chains has been promoted so as to get molecules active against CQ-resistant parasites. A number of modifications have been made in the side chain of chloroquinoline and studied in detail. It has been found that a significant increase in the antimalarial activity was achieved by shortening of the chain length or incorporation of intramolecular hydrogen bonding atoms in the side chain.<sup>192</sup>

In this chapter, CPMV has been developed as a potential carrier vehicle for CQ-derivatives. Three different chloroquinoline derivatives with short side chains were conjugated to addressable amines on the external surface of CPMV giving more than one molecule of CQ per virus particle. In addition, two different glucose derivatives were conjugated to the external surface of CPMV with the intention of targeting of the CPMV-drug conjugate to specific tissues and to reduce side effects.

## ***5 Redox-active ferrocene-modified CPMV nanoparticles***

Ferrocene is an example of a  $\pi$ -complex in which connections between the d-orbitals of the  $\text{Fe}^{2+}$  metal centre with the  $\pi$ -orbitals of the two planar cyclopentadienyl ligands ( $\text{C}_5\text{H}_5^-$ ) form the metal-ligand bonds. Therefore, all the carbon atoms in the cyclopentadienyl rings are bonded equally to the central  $\text{Fe}^{2+}$  ion. It is resistant to acidic and basic reagents, displays aromatic properties and it is thermally very stable.<sup>193</sup>

Ferrocenes, viologens, quinones, and transition metals have redox centres and are often used as active electrochemical components because they have two or three stable redox states and their electrochemical interconversion is completely reversible. Therefore, these redox centers are frequently used as active components in supramolecular assembly.<sup>194</sup>

Ferrocene has only one-electron oxidation at a low potential, around 500 mV against a saturated calomel electrode (SCE). This reversible oxidation has itself been used as standard in electrochemistry as  $\text{Fc}^+/\text{Fc} = 400$  mV against the standard hydrogen electrode.<sup>195</sup>

The oxidation state of ferrocene gives the stable blue-coloured iron (III) cation  $[\text{Fe}(\text{C}_5\text{H}_5)_2]^+$  called ferrocenium. Because ferrocene is relatively inert and readily separated from ionic products, sometimes ferrocenium salts are used as oxidizing agents.<sup>196</sup> Ferrocene is often used as an internal standard for calibrating redox potentials in non-aqueous electrochemistry.<sup>197</sup> Aniline as an electron-rich organic compound is also oxidized at low potentials, but irreversibly.

Ferrocene is an originator to iron nanoparticles and can be used as a catalyst for the production of carbon nanotubes.<sup>198</sup> The stability of the ferrocenyl group in aqueous aerobic media, and its suitable electrochemical properties have made ferrocene and its

derivatives very common molecules for biological applications and for biomolecule conjugation.<sup>199</sup>

It was reported that ferrocene moieties on the external surface of the CPMV are electrochemically independent and can be considered as multielectron reservoirs. The modified virus particles provide a selection of redox active nanocomponents, these can be assembled onto solid electrode surfaces where they may act as electron transfer mediators for the development of redox catalysts, biosensors and nanoelectronic devices.<sup>170</sup>

This chapter describes the modification of CPMV with ferrocene before and after single modification of CPMV with each chloroquinoline derivative (CQ-derivative) and shows the effect of each CQ-derivative on the number of conjugated ferrocene to the external surface of the CPMV particles.

## ***5.1 The modification of CPMV with aminoferrocene(Fc)***

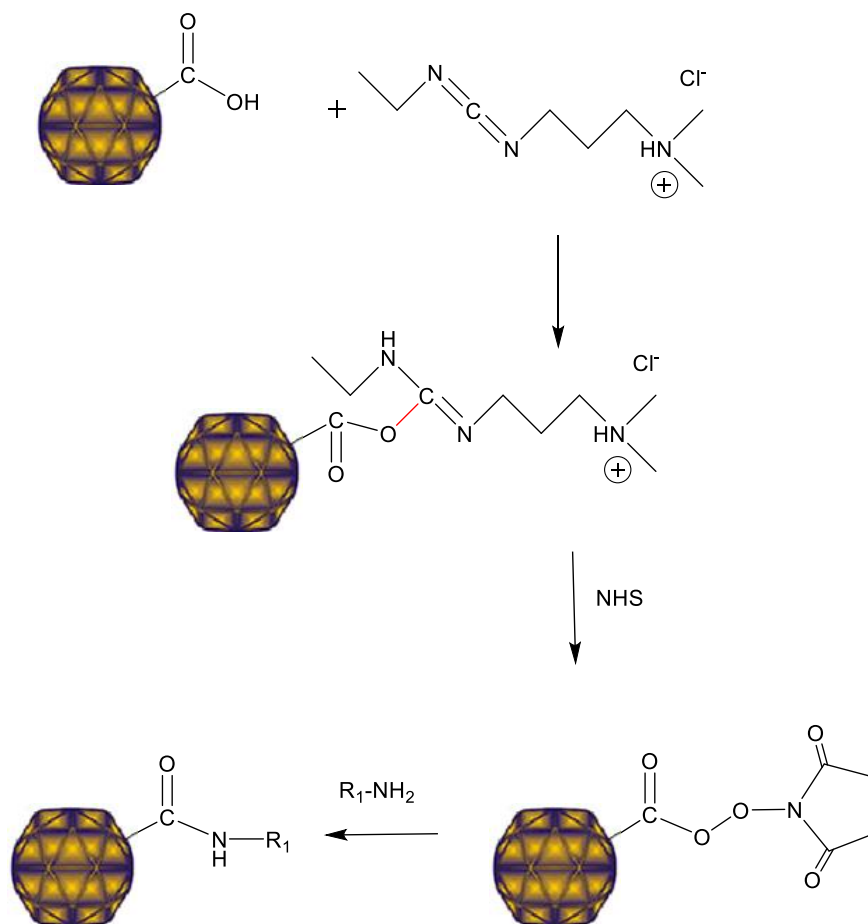
The modification of CPMV with Fc gives the valuable redox properties of ferrocene moieties together with the high symmetrical three dimensional (3D) architecture of the virus capsid. This allows accurate positioning of the ferrocene onto the virus capsid and makes CPMV an ideal scaffold for the synthesis of electro-active viral nanoparticles.<sup>164</sup>

### ***5.1.1 Addressability of carboxylates on external surface of CPMV (single modification)***

There are eight to nine solvent-exposed carboxylate groups on the CPMV particle surface derived from aspartic and glutamic acids: six to seven on the S subunit: Asp 26, Asp 44, Asp 45, Asp 85 and Glu 135, the carboxy-terminus of S itself, and an additional carboxylate derived from Glu 198. Glu 198 is only present in a small proportion of the

particles. This is due to cleavage of 24 amino acids of the S subunit in the plant.<sup>24</sup>

EDC/NHS is used to activate these carboxylates before modification **Scheme 5.1**.



**Scheme 5.1** Activation of carboxylic acids with EDC/NHS to generate an active intermediate that reacts with amine containing molecules to generate a peptide bond.

## 5.2 Methods

Aminoferrocene was conjugated to CPMV as described (section 2.7). The covalent coupling of the organometallic redox-active compound Fc to CPMV carboxylates was achieved by a standard protocol for the formation of peptide bonds: EDC and NHS.

**Scheme 5.1.**

### ***5.2.1 Attachment of ferrocene to CPMV-CQ- derivatives (double modification)***

CPMV was first reacted with 6000 molar excess of each CQ derivative (CQp, CQ-ala and CQ-val) separately using an overnight reaction as described (section 2.6.11).<sup>173</sup> Recovery of virus was 68%, 70% and 74%, respectively.

### ***5.2.2 Attachment of ferrocene to CPMV-CQ- derivatives- G.A (triple modification)***

Each CPMV-CQ- derivative- G.A was modified with 3000 molar excess of aminoferrocene as described (section 2.6.12).<sup>173</sup> Recovery of virus was 77-78%.

### ***5.2.3 Addressability of amines on external surface of CPMV (double modification)***

#### ***5.2.3.1 The modification of CPMV-Fc with CQ- derivatives***

CPMV-Fc was reacted with 6000 molar excess of each CQ-derivative using an overnight reaction as described in section (2.7.1).<sup>173</sup> Recovery of virus was 62, 65 and 68%, respectively.

### ***5.2.4 Electrochemical measurements:***

#### ***5.2.4.1 CPMV-Fc:***

Cyclic voltammetry was measured with an AUTOLAB PGSAT 30 potentiostat with the sample in 10 mM sodium phosphate buffer, pH7 in a traditional three-electrode cell at room temperature (ca. 25 °C). A pyrolytic graphite edge (PGE) disc was used as a working electrode with a diameter of 3 mm; Ag/AgCl (saturated KCl), the reference electrode,

platinum wire and the counter electrode (all experiments were conducted with the same electrodes except otherwise indicated). Analysis of the free ferrocene moieties was typically performed with a concentration of 5–10 mM (with 10% DMSO). Modified particles were usually studied at concentrations of 1mg/ml to 6 mg/ml. For each sample, cyclic voltammograms were recorded at scan rates from 10 to 100 mV s<sup>-1</sup> in duplicate sets with the working electrode polished by abrasion with an aqueous slurry of 0.3µM Al<sub>2</sub>O<sub>3</sub> immediately prior to measuring each set, these voltammograms were analysed to determine peak potentials (*E<sub>pa</sub>* and *E<sub>pc</sub>* for the anodic and cathodic scans respectively) and peak current magnitudes (*i<sub>pa</sub>* and *i<sub>pc</sub>* for the anodic and cathodic scans respectively) at each scan rate. Analysis of 20 mVs<sup>-1</sup> voltammetry performed at various times during the combination of each set of scan rates confirmed that the response was independent of time. Plots of peak current versus the square root of scan rate were found to be linear. The slopes were determined by linear regression and analysed by the Randles–Sevcik equation to determine the concentration of ferrocene in the sample and eventually the number of ferrocene moieties per virus particle.<sup>164</sup>

#### **5.2.4.2 PGE electrode modification**

Surface functionalisation of the graphite electrode was carried out at ice–cold temperature in a deaerated solution (with argon); 3ml of 0.1M HCl containing 2mM of 4–azidobenzene diazonium or 4–ethyl–benzene diazonium (BF<sub>4</sub> salts). The reductive electrodeposition of the aryl diazonium salts was achieved amperometrically. The working electrode potential was set between minus 1 and 0 V. After the functionalisation, the electrode surface was thoroughly washed with Milli–Q water followed by ethanol to remove any adsorbed species.<sup>164</sup>

### ***5.3 Results and discussion***

This chapter describes and evaluates different strategies for coupling of ferrocene onto CPMV capsid using different conjugation schemes. In each modification, ferrocene was used in a large excess to ensure maximum coupling. Virus particles were recovered in approximately 70 – 78% yield based on initial wild-type concentration.

Ferrocene was modified first with CPMV using EDC/NHS protocol and the particle was recovered in 78% yield. Intact modified CPMV was characterised by agarose gel electrophoresis **Figure 5.1**.

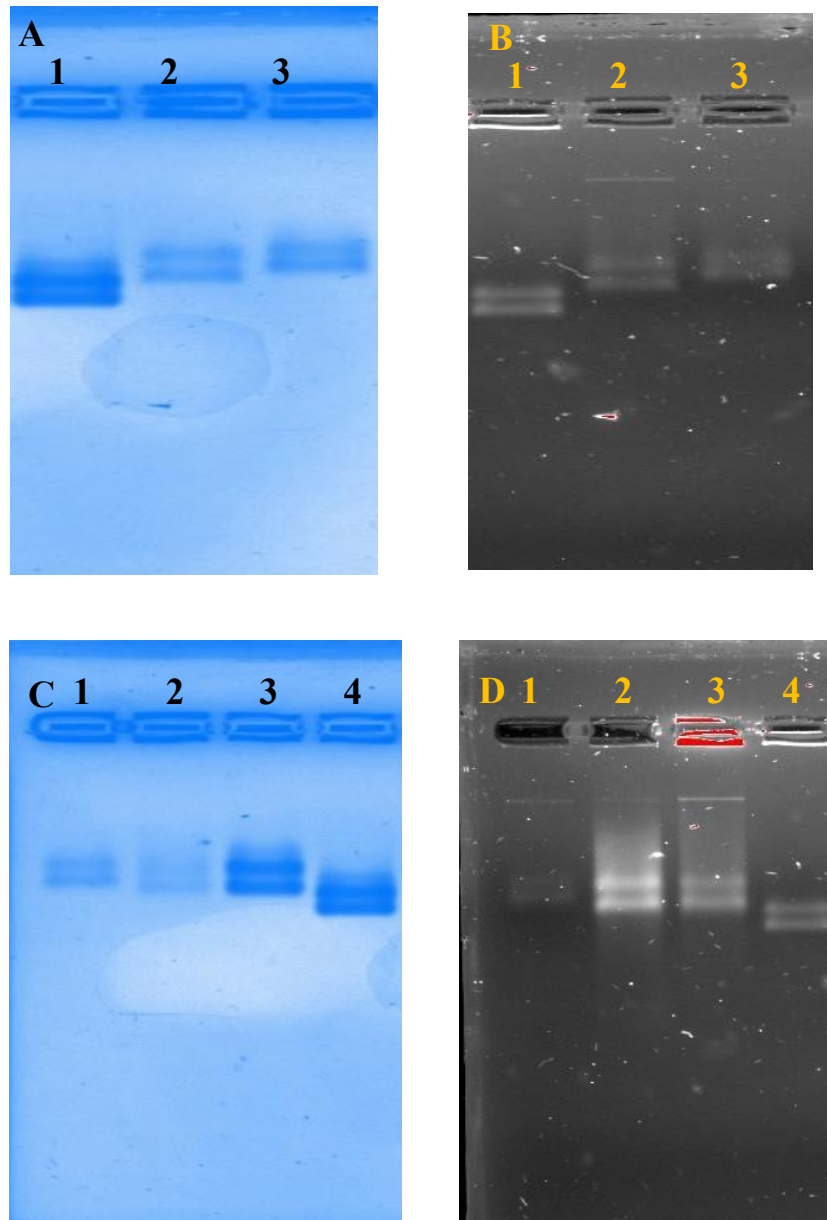


**Figure 5.1** Digital image of agarose gel electrophoresis 1.2 % w/v agarose, 60 V, stained with A: Coomassie staining B: EtBr staining, lane 1: wt CPMV, lane 2: CPMV-NHS-ester, lane3: CPMV-Fc. For C: Coomassie staining D: EtBr staining, Lane 1, CPMV- CQp -Fc, 2, CPMV-CQ-ala-Fc, 3, CPMV-CQ-val- Fc and 4,wt CPMV

Intact CPMV can be separated into two forms of higher and lower mobility form in the electric field, these forms are derived from the slow (s) and fast (f) form of the S subunit. The change from the s form to the f form is a consequence of a C-terminal cleavage of 24 amino acids of the S subunit causing different movement of modified CPMV compared to unmodified particle.<sup>200</sup>

Slow mobility of the ferrocene modified particle (lane 3) in agarose gel electrophoresis supports the decoration of the CPMV with ferrocene.

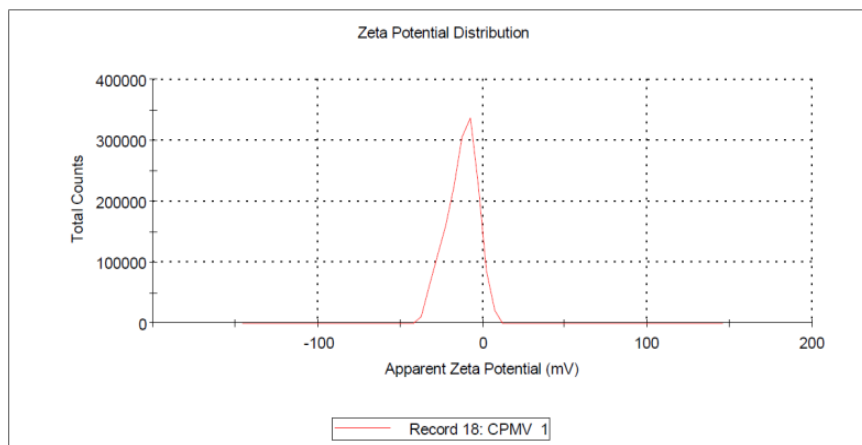
The zeta potentials, as shown in **Figure 5.2**, for suspensions of wt CPMV ( $-12.0 \pm 0.6$  mV) and CPMV-Fc ( $-22.0 \pm 1.2$  mV) indicate that the colloids have good stability and show no aggregation on particle modification.

**Results**

**A**

	Mean (mV)	Area (%)	St Dev (mV)
<b>Zeta Potential (mV):</b> -12.6	<b>Peak 1:</b> -12.6	100.0	9.34
<b>Zeta Deviation (mV):</b> 9.34	<b>Peak 2:</b> 0.00	0.0	0.00
<b>Conductivity (mS/cm):</b> 2.41	<b>Peak 3:</b> 0.00	0.0	0.00

**Result quality** Good



**Results**

**B**

	Mean (mV)	Area (%)	St Dev (mV)
<b>Zeta Potential (mV):</b> -22.3	<b>Peak 1:</b> -22.3	100.0	10.9
<b>Zeta Deviation (mV):</b> 10.9	<b>Peak 2:</b> 0.00	0.0	0.00
<b>Conductivity (mS/cm):</b> 0.250	<b>Peak 3:</b> 0.00	0.0	0.00

**Result quality** Good

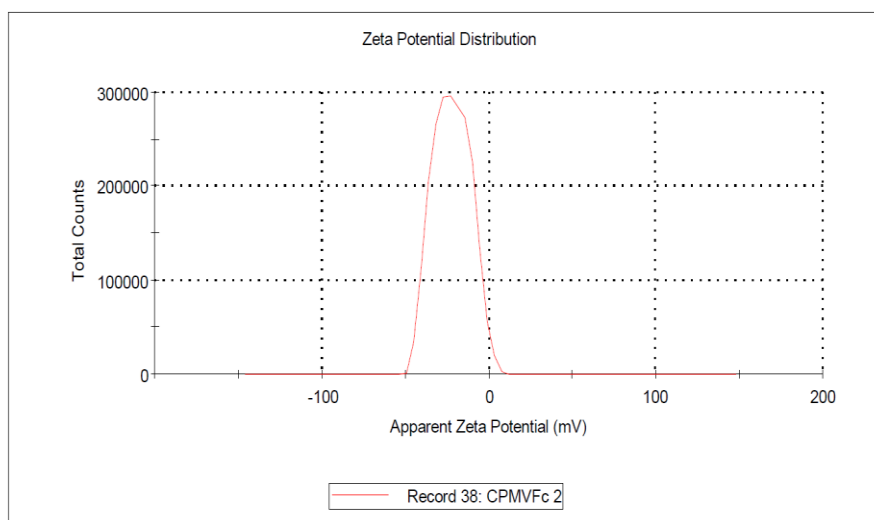


**Figure 5.2** Examples of zeta potential results for (A) wt CPMV, (B) CPMV-Fc.

### 5.3.1 Addressability of carboxylates on external surface of CPMV (double labelling)

#### 5.3.1.1 The conjugation of aminoferrocene to CPMV-CQ- derivatives

CPMV-CQp, CPMV-CQ-ala and CPMV-CQ-val were modified with Fc as described in (section 2.5.11).<sup>58</sup>

Characterization of CPMV modified particles using UV/Vis spectrophotometry and agarose gel electrophoresis are shown in **Figure 5.3** and **Figure 5.1**.

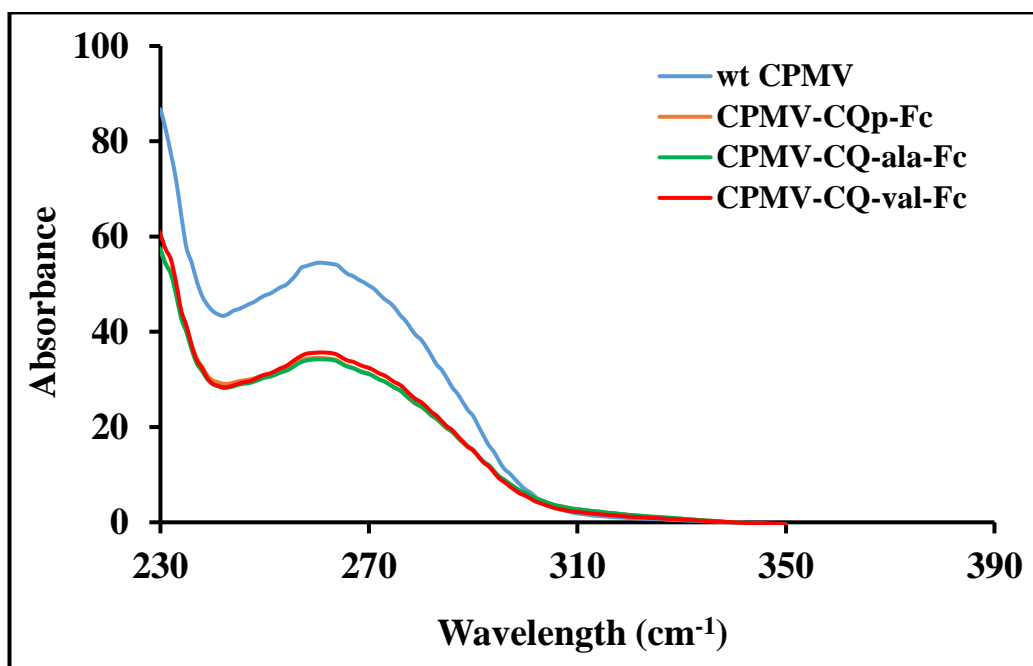
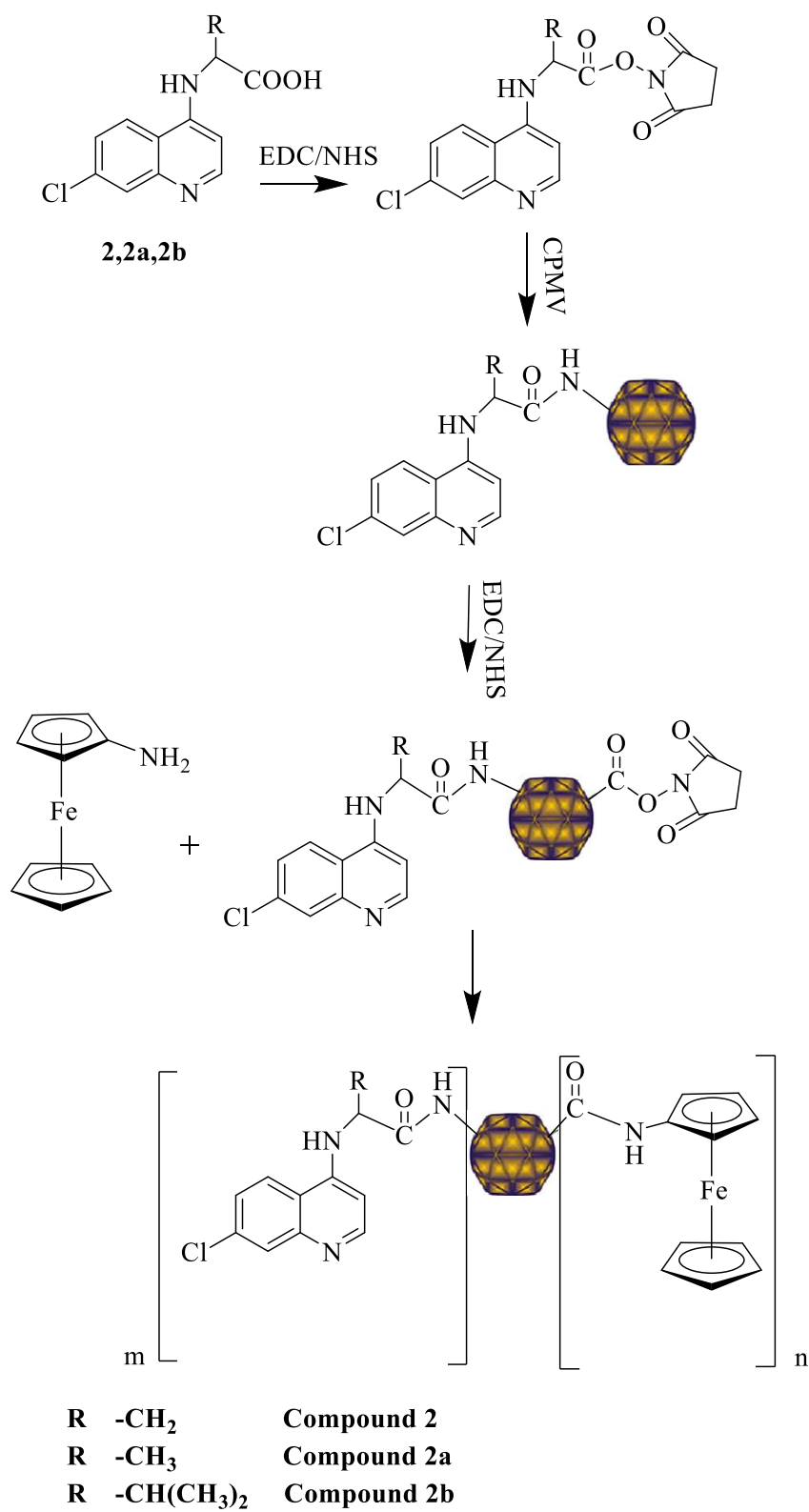


**Figure 5.3** UV/Vis spectrum of doubly functionalised wt CPMV particles. Blue line unmodified CPMV, orange line CPMV-CQp-Fc, green line CPMV-CQ-ala-Fc and red line CPMV-CQ-val-Fc.

The UV/Vis spectrum shows that CPMV particles still have the maximum absorbance ratio (1.4) at 260:280 nm which means the particle was still intact after double modification.

CPMV-CQp-Fc, CPMV-CQ-ala-Fc and CPMV-CQ-val-Fc show slow movement on a gel compared to unmodified CPMV. In addition, CPMV-CQ-ala-Fc and CPMV-CQ-val-Fc stained with ethidium bromide shown some fluorescent intensity from a band of different mobility to wt and to CPMV-CQ-Fc conjugate. This suggests that the CPMV-CQ-ala-Fc and CPMV-CQ-val-Fc surface have some limited permeability to allow intercalation of ethidium bromide with the encapsulated RNA.

The simple reaction scheme for each modification is shown in **Scheme 5.2**.



**Scheme 5.2** Decoration of CQ- derivatives & Fc on external surface of CPMV particle.

### ***5.3.2 Addressability of carboxylates on external surface of CPMV (triple modification)***

In this study, solvent-exposed carboxylates on the external surface of modified CPMV particles were used as groups for the selective attachment of the organometallic aminoferrocene.

#### ***5.3.2.1 The conjugation of aminoferrocene to CPMV-CQ-derivatives-G.A***

The integrity of multiple-functionalised particles was confirmed by UV/Vis spectrophotometry and agarose gel electrophoresis, staining with both ethidium bromide and Coomassie blue **Figures 5.4 and 5.5**, respectively.

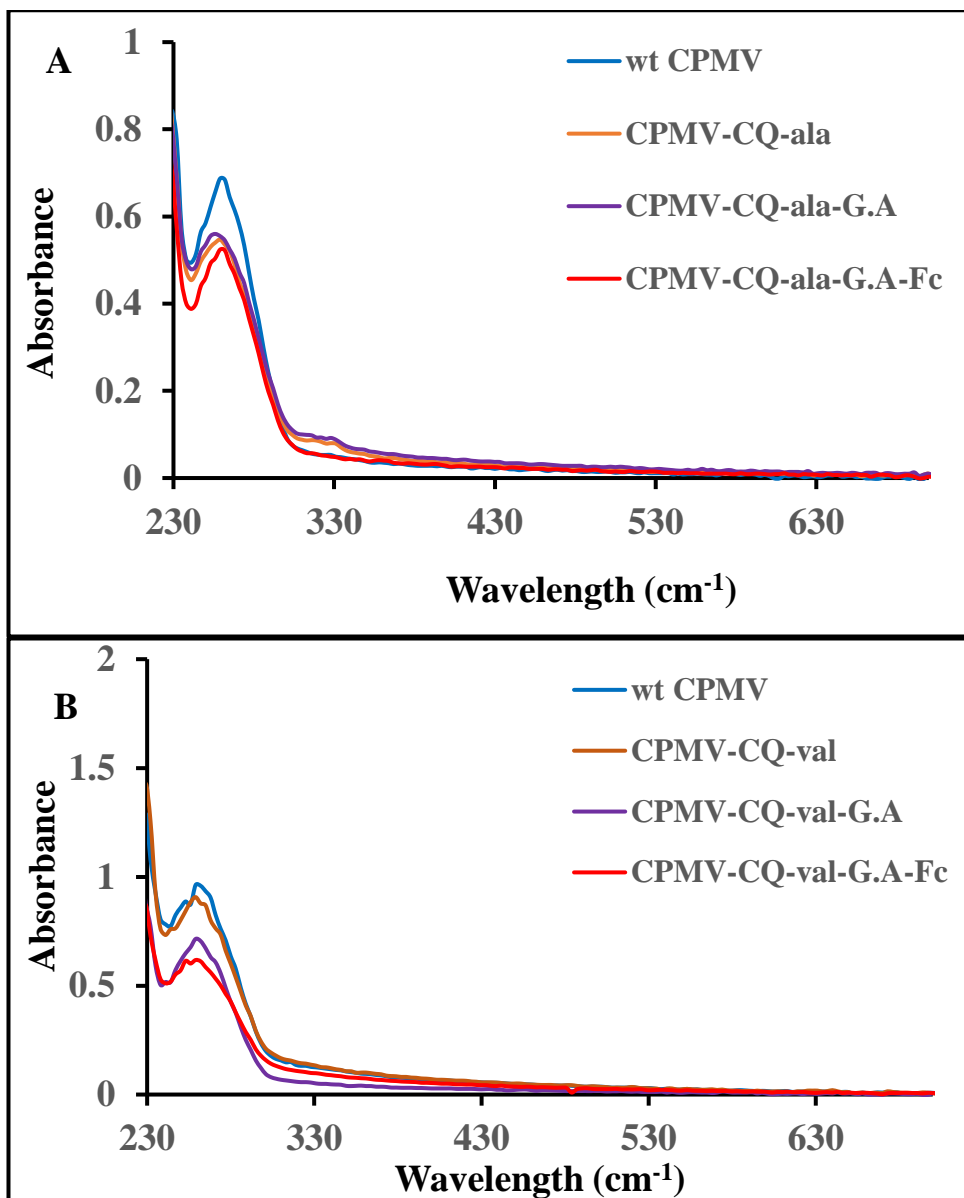


**Figure 5.4** UV/Vis spectrum of modified and unmodified CPMV, A. CPMV-CQ - ala-G.A to aminoferrrocene and B.CPMV-CQ-val-G.A to aminoferrrocene.

The CPMV particles after modification from UV/Vis spectrophotometry ratio (1.42) at 260:280 nm that confirmed the particle is still intact **Figure 5.4**.

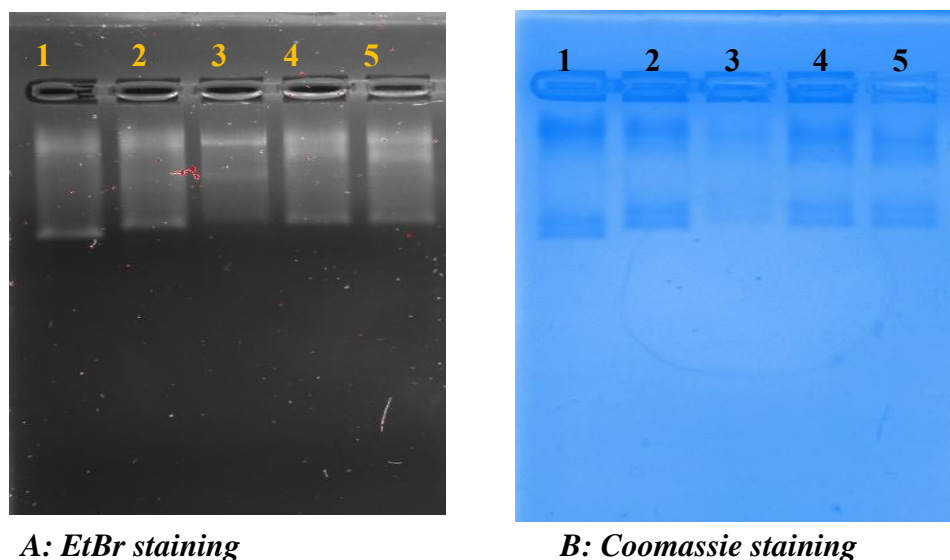


**Figure 5.5** Agarose gel electrophoresis 1.2 % w/v agarose, 60 V.1- wt CPMV, 2- CPMV-Fc, 3-CPMV-CQp-G.A-Fc, 4- CPMV-CQ-ala-G.A-Fc and 5-CPMV-CQ-val-G.A-Fc.

The migration pattern toward the anode differs for modified particles because of a combination of size and charge, modified CPMV particles moved slower on a gel than unmodified particle confirming covalent attachment of Fc to surface carboxylates of CPMV.

Transmission electron microscopy (TEM) confirmed that CPMV modified particles remain intact after triple modification **Figure 5.6** with the increase in averaged external diameter to 31 nm compared to wt CPMV particle (28-30 nm).

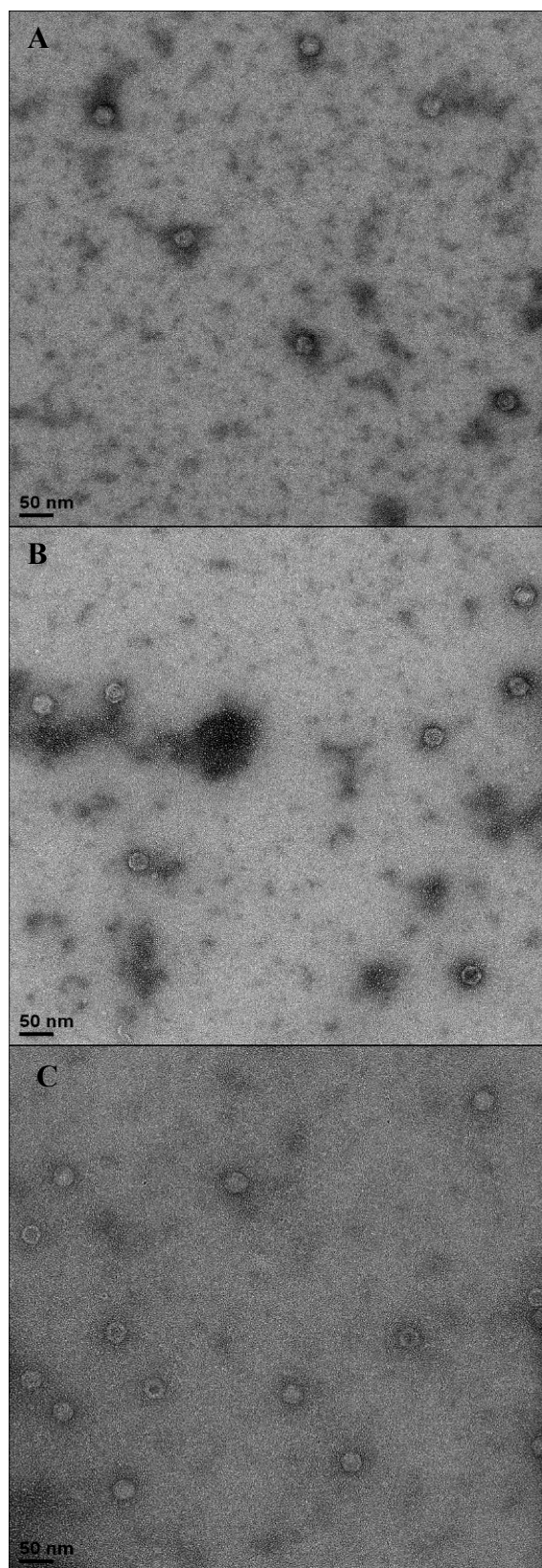


**Figure 5.6** Transmission electron microscopy image of Cowpea mosaic virus (CPMV) particles displaying triple modification, A. CPMV-CQp-G.A-Fc, B.CPMV-CQ-ala-G.A-Fc and C. CPMV-CQ-val-G.A-Fc.

### 5.3.3 Addressability of amines on external surface of CPMV (double modification)

#### 5.3.3.1 The modification of CPMV- Fc with CQ-derivatives

CPMV-Fc was modified with CQ-derivatives using the same protocol of CPMV-G.A modification.<sup>173</sup> Confirmation of modification of the external surface is provided by comparison of the agarose gel electrophoresis and SDS-PAGE of modified and unmodified CPMV particles **Figure 5.7**.

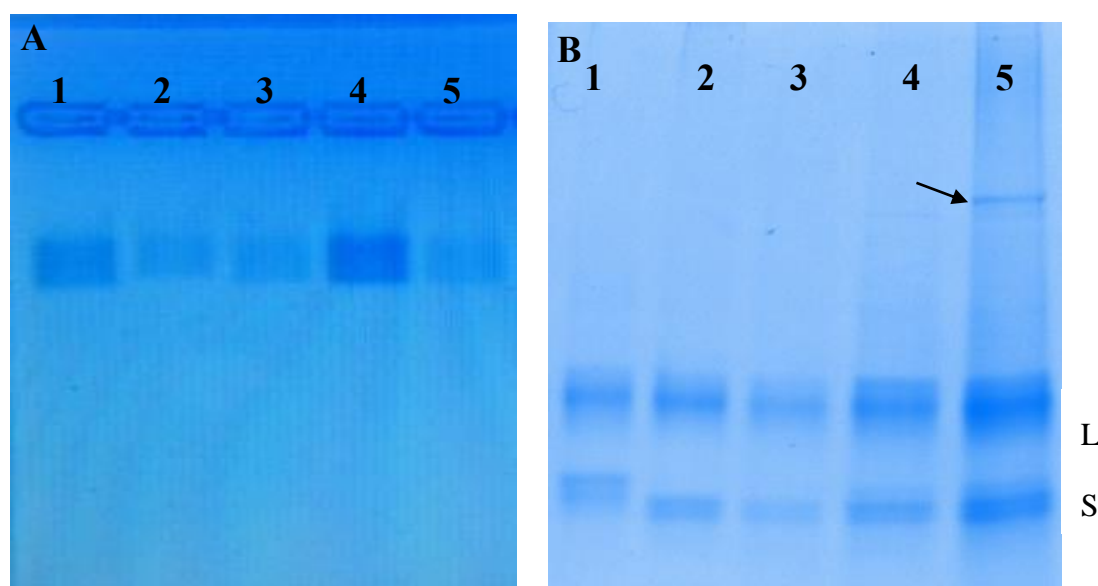


**Figure 5.7 A: Agarose gel electrophoresis 1.2 % w/v agarose, 60 V. B: SDS-PAGE .Lane1, wt CPMV 2, CPMV-Fc-CQp 3, CPMV-Fc-CQ-ala 4, CPMV-Fc-CQ-val and 5, CPMV-Fc. An extra band (shown in black arrow) may be confirmed the conjugation of Fc to the external surface of CPMV particle.**

Agarose gel electrophoresis using an agarose gel matrix of intact virus supported successful single and double modification. Particles were analysed on a 1.2 % agarose gel and stained with Coomassie blue **Figure 5.7A**. After Coomassie staining a comparison to wt CPMV particles showed that the double modification does not affect the mobility of CPMV significantly in the gel. It is clearly seen that the migration of modified particles is slow when compared to unmodified particle; this is due to CQ-

derivatives and Fc attachment to the external surface of CPMV particles. Both small subunits (f and s) were modified.

The single and double modification of CPMV were further studied by denaturing SDS-PAGE. This showed that CQ-derivatives and Fc were attached to both the S and the L subunits **Figure 5.7B**. Additionally, all modified particles showed slight cleavage of small subunits and only CPMV-Fc showed an extra band (shown in black arrow) which confirmed Fc attachment to the external surface of the particle **Figure 5.7B lane 5**.

Cyclic voltammetry recognised that the modified CPMV with each CQ-derivative-Fc has similar properties and displayed an electrochemically reversible ferrocene/ferrocenium couple. This means, the peak separation  $|E_p^a - E_p^c|$  from 55mV to 63mV is close to the theoretical value predicted for a one electron process (59 mV at 298 K as predicted from the Nernst equation) and the ratio of the peak currents,  $i_p^c/i_p^a$ , is close to unity **Figures 5.8 and 5.9** revealed that CPMV-CQp-Fc (Fc3), CPMV-CQ-val-Fc (Fc4) have one signal while CPMV-CQ-ala-Fc (Fc2) has two. Peak currents were measured and the linear plot of  $i_p$  against the square root of the scan rate ( $v^{1/2}$ ) showed that the oxidation was controlled as seen in **Figure 5.10 A and B**.

The number of ferrocene molecules attached per CPMV particles was calculated by using Randles-Sevcik Eq. <sup>201</sup>

$$i_p = k n^{3/2} A D^{1/2} v^{1/2} C_{Fc} \quad \text{----- Eq6}$$

Where  $i_p$  = current in A;  $k = 2.69 \times 10^5$  at 298 K (constant);  $n = 1$ , is the number of electrons transferred per molecule;  $A$  is the surface area of the working electrode,  $A = 0.07 \text{ cm}^2$ ;  $D$  is the diffusion coefficient of CPMV particles in aqueous buffer solution;  $D = 0.16 \times 10^{-6} \text{ cm}^2 \text{ sec}^{-1}$ .<sup>24</sup>

The scan rate  $v$  was measured over a range at scan rates from  $v = 10$  to  $100 \text{ mVsec}^{-1}$ ; and  $C_{\text{Fc}}$  is the concentration of Fc in each modified particle.

Fc showed maximum coverage on the CPMV surface, while with CPMV-CQ-derivatives, the coverage rate was inhibited. The decrease in the number of conjugated ferrocenes may be due to accumulation of NHS reagent on addressable carboxylates which was used to activate the carboxyl groups on each CQ-derivative before reacting with CPMV. It was found that CPMV-Fc particle has  $171 \pm 3$  Fc decorated on the external surface which was close to the reported number 174 per virus.<sup>173</sup> The minimum and maximum range for the number of attached ferrocene per particle were calculated on an error of  $\pm 5\%$  in the electrode area. This gives a more accurate evaluation of the number of redox groups attached.

Reduction and oxidation potential of CPMV-CQ-derivatives-Fc, vs. Ag/AgCl (saturated KCl) and the average number of ferrocenes per CPMV particle as calculated from the Randles–Sevcik equation are shown in **Table 5.1, 5.2 and 5.3**.

**Table 5.1 The minimum and maximum number of attached ferrocene (Fc2) per particle**

Scan Rate V	Square root for scan rate	Ipa (oxidation)	Ipa (reduction)
(V/Sec)	(V/Sec) <sup>1/2</sup>	(A)	(A)
0.01	0.1	4.5957E-08	6.5372E-08
0.015	0.122474487	6.66E-08	1.0452E-07
0.03	0.173205081	1.3176E-07	1.634E-07
0.05	0.223606798	2.386E-07	2.6596E-07
0.1	0.316227766	3.0609E-07	3.8814E-07
Ferrocene concentration = $I_p / [(k n^{3/2} A (DV)^{1/2})]$		1.00878E-07	1.29244E-07
Ferrocene moieties per virus		113.0	144.7
Ferrocene concentration with A - 5%		1.03E-07	1.31E-07
Ferrocene moieties per virus		115.2	146.95
Ferrocene concentration with A+ 5%		1.13E-07	1.41E-07
Ferrocene moieties per virus		126.4	158.2
CPMV concentration (5.0 mg/ml)		8.93E-10	8.93E-10
Average number of ferrocenes		118.2	150.0
Average ferrocenes from oxidation & reduction		<b>134</b>	

**Table 5.2 The minimum and maximum number of attached ferrocene (Fc3) per particle.**

Scan Rate V	Square root for scan rate	Ipa(oxidation)	Ipa (reduction)
(V/Sec)	(V/Sec) <sup>1/2</sup>	(A)	(A)
0.01	0.1	2.2999E-08	2.5955E-08
0.015	0.122474487	5.1153E-08	4.1875E-08
0.03	0.173205081	1.0355E-07	1.0061E-07
0.05	0.223606798	1.8237E-07	1.7501E-07
0.1	0.316227766	2.6523E-07	2.7412E-07
Ferrocene concentration = Ip/ [(k n <sup>3/2</sup> A ( DV) <sup>1/2</sup> ]		7.7E-08	7.5195E-08
Ferrocene moieties per virus		82.9	80.98
Ferrocene concentration with A - 5%		7.72E-08	7.54E-08
Ferrocene moieties per virus		83.0	81.1
Ferrocene concentration with A+ 5%		7.82E-08	7.64E-08
Ferrocene moieties per virus		84.1	82.15
CPMV concentration (5.2 mg/ml)		9.3E-10	9.3E-10
Average number of ferrocenes		83.34	81.4
Average ferrocenes from oxidation & reduction		<b>82</b>	

**Table 5.3 The minimum and maximum number of attached ferrocene (Fc4) per particle.**

Scan Rate V	Square root for scan rate	Ipa(oxidation)	Ipa (reduction)
(V/Sec)	(V/Sec) <sup>1/2</sup>	(A)	(A)
0.01	0.1	2.7738E-08	2.6051E-08
0.015	0.122474487	4.1696E-08	3.8645E-08
0.03	0.173205081	8.3324E-08	7.8377E-08
0.05	0.223606798	3.2383E-07	3.0879E-07
0.1	0.316227766	4.0856E-07	4.2055E-07
Ferrocene concentration = $I_p / [(k n^{3/2} A (DV)^{1/2})]$		1.02E-07	9.93E-08
Ferrocene moieties per virus		115.45	111.2
Ferrocene concentration with A - 5%		1.04E-07	9.95E-08
Ferrocene moieties per virus		116.5	111.42
Ferrocene concentration with A+ 5%		1.14E-07	1.05E-07
Ferrocene moieties per virus		127.7	117.6
CPMV concentration (5.0 mg/ml)		8.93E-10	8.93E-10
Average number of ferrocenes		119.9	113.4
Average ferrocenes from oxidation & reduction		<b>117</b>	

The cyclic voltammograms of single and double modified CPMV at scan rates  $15\text{mVs}^{-1}$  and  $30\text{mVs}^{-1}$  showed very clear changes in the cyclic voltammogram of Fc in each particle, provided that the electrode surface has been modified with PGE **Figure 5.8**. Moreover, there is an extra, modest oxidative current at 470 mV in Fc2 with a peak visible at a similar potential to the lowest potential peak **Figure 5.9 (shown by arrow)** but there is a very weak indication of one reduction signal at around 415mV, this may be due to irreversible oxidation of alanine which is a part of CQ-ala compound, or could be presented from the highest potential signal.

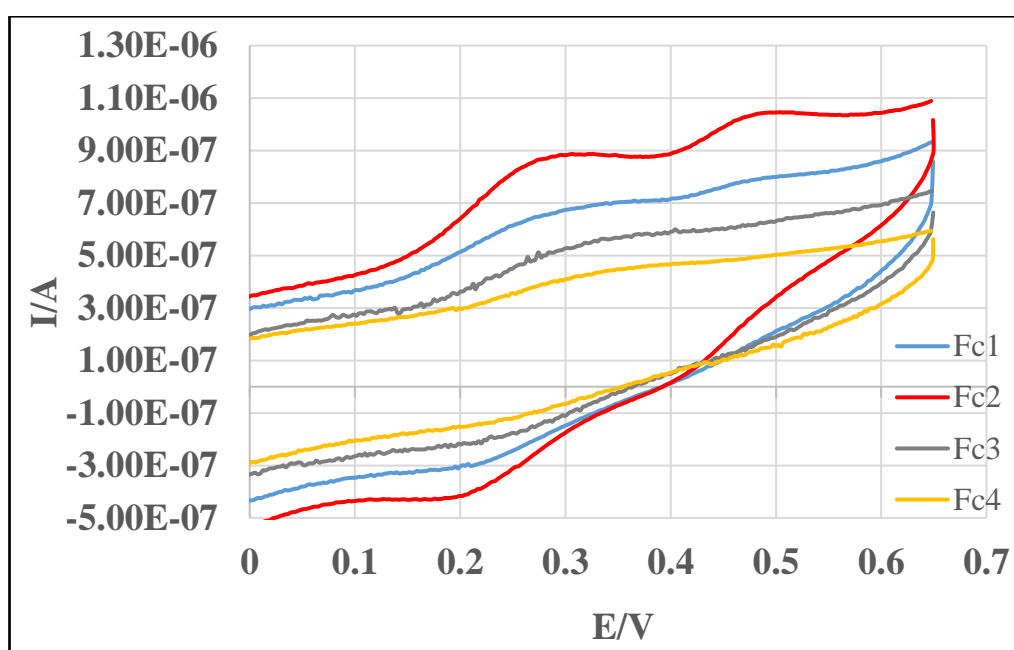


**Figure 5.8** Cyclic voltammogram of ferrocene modified CPMV particles at 15mV. (Fc1), CPMV- Fc. (Fc2), CPMV-CQ-ala-Fc. (Fc3), CPMV-CQp-Fc and (Fc4), CPMV-CQ-val-Fc.

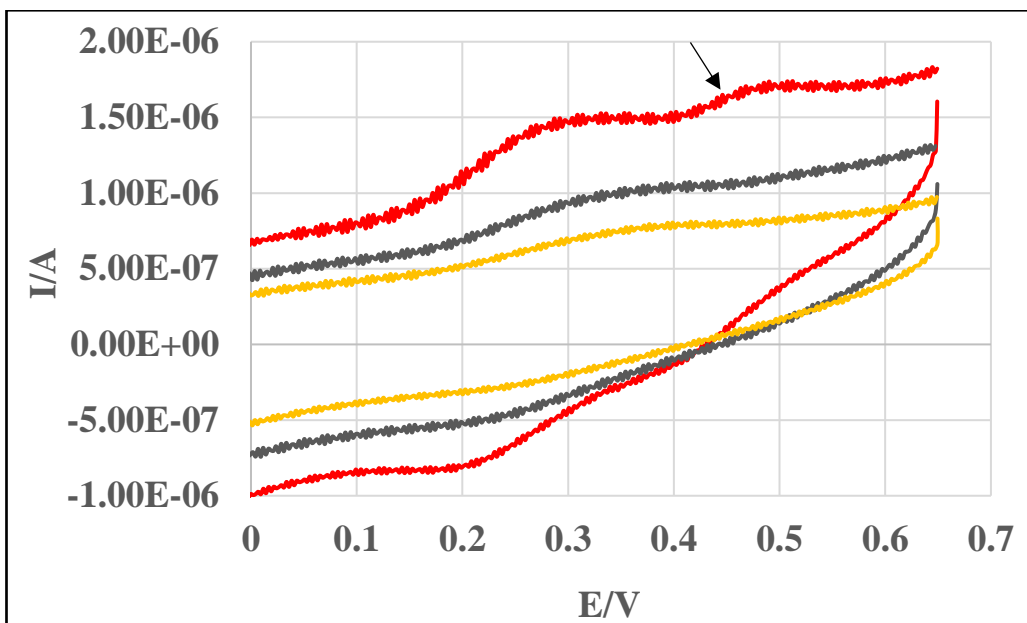


**Figure 5.9** Cyclic voltammogram for some of ferrocene modified CPMV-CQ particles at 30mV. Red line is Fc2, grey line is Fc3 and yellow line is Fc4. Very weak reduction signal has been observed (shown by black arrow) may be due to irreversible oxidation of alanine or could be presented from the highest potential signal.

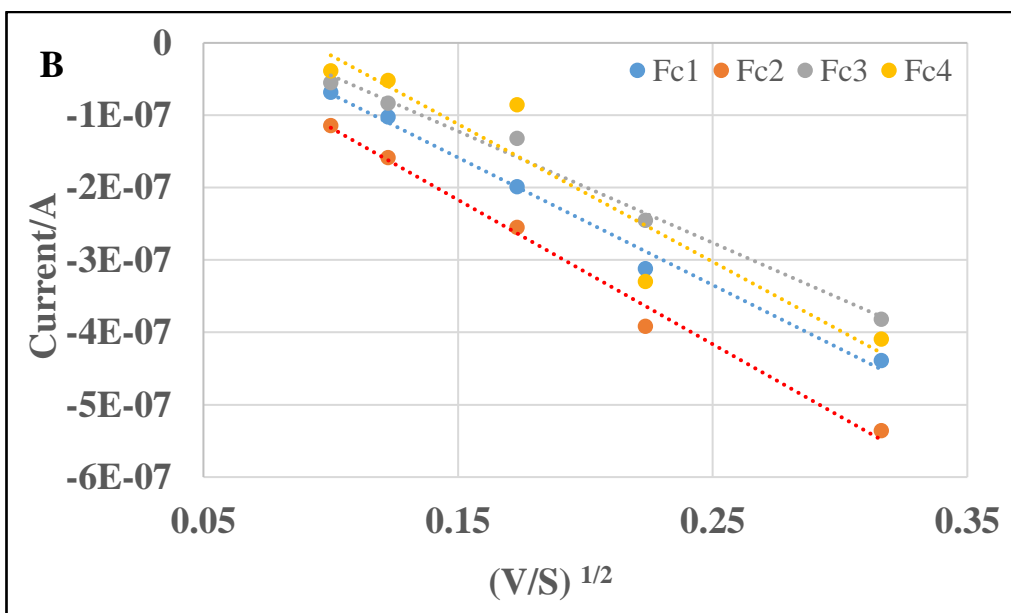
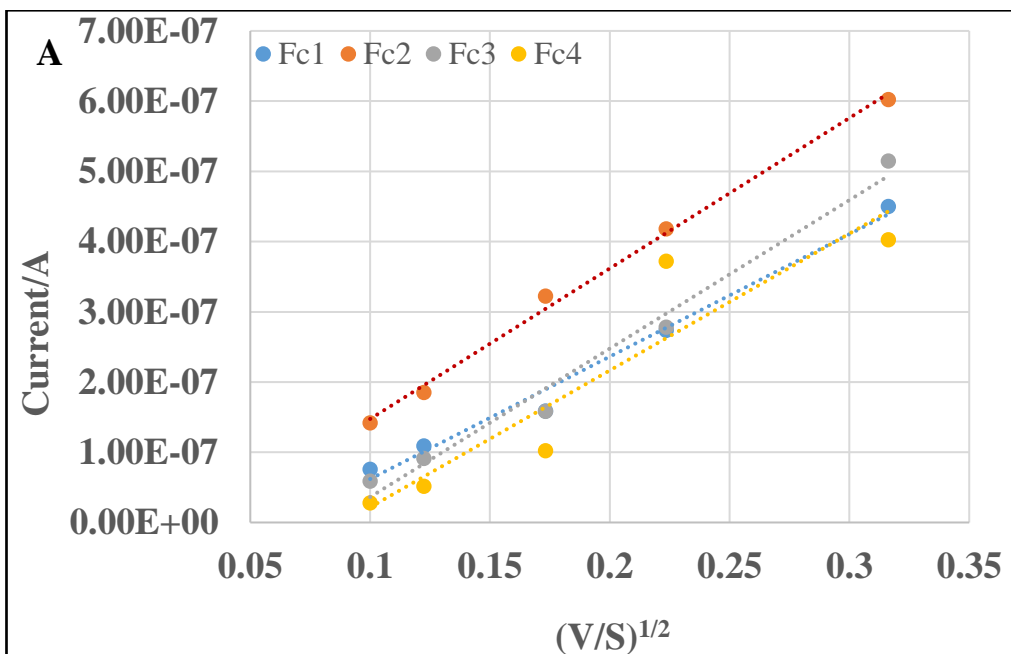


**Figure 5.10** Variation of peak current with the square root of the scan rate of; A. anodic current and B. cathode current.

The ratio of the peak currents to the square root of the scan rate, showing that oxidation and reduction distribution were controlled are shown in **Table 5.4**.

**Table 5.4 The ratio of the peak currents to the square root of the scan rate.**

<b>Fc modified CPMV particle</b>	<b>Ratio of anodic peak current to the square root of the scan rate (<math>I_{pa} R^2</math>)</b>	<b>Ratio of cathodic peak current to the square root of the scan rate(<math>I_{pc} R^2</math>)</b>
Fc1	0.9854	0.9916
Fc2	0.9958	0.9915
Fc3	0.9818	0.9878
Fc4	0.8649	0.9013

For comparison Inductivity Coupled Plasma Optical Emission Spectrometry Principle (ICP-OES) was also used to determine the number of modified Fc with CPMV particles as shown in **Table 5.5**. The results confirmed that the maximum number of Fc labelling on each modified CPMV surface was close to the number determined by electrochemical measurements **Table5.1, 5.2 and 5.3**.

**Table 5.5 The average number of attached ferrocene per CPMV particle using ICP-OES and electrochemical measurements.**

<b>Fc modified CPMV particle</b>		<b>Number of Fc on viral surface by ICP-OES</b>	<b>Number of Fc on viral surface from electrochemistry</b>
CPMV-Fc	Fc1	173	174
CPMV-CQ <sub>P</sub> -Fc	Fc3	87	82
CPMV-CQ-ala-Fc	Fc2	140	134
CPMV-CQ-val-Fc	Fc4	114	117

## ***5.4 Conclusions***

The chemical modification of single and double modified viral nanoparticles with ferrocene generated redox-active conjugates through covalent modification.

The carboxylate groups on the external surface of CPMV and CPMV-CQ-derivatives can be decorated with ferrocene using EDC/NHS conjugation strategy. The number of ferrocenes has been determined electrochemically and analytically. In addition, two different strategies have been adopted to generate successful conjugation of ferrocene with CPMV-CQ-derivatives: first CPMV was modified with Fc to form CPMV-Fc which was then reacted with each CQ-derivative, second CPMV was modified with each CQ-derivative to form CPMV-CQ-derivatives to which ferrocene is then conjugated. It was found that the number of ferrocene per virus particle decreased when CPMV was modified first with CQ derivatives. In addition, cyclic voltammetry was used to both verify and quantify the active functionalities of immobilised ferrocene onto the virus capsid. The number of ferrocenes coupled to each virus ranged from approximately 82–174 dependent on the priority of conjugation to the CPMV particle.

## ***6 Malaria and chloroquinoline derivatives (CQ-derivatives) as inhibitor of haemozoin or beta-haematin formation in vitro***

*In vitro* tests have been developed to select candidate antimalarial drugs based on their capacity to inhibit beta-haematin (BH) formation.

Intravascular mechanisms for chloroquinoline compounds are advantageous as antimalarial drugs because of the ability of these compounds to accumulate in the food vacuole of the parasite. Recently, many workers have suggested that quinolone antimalarial drugs inhibit formation of BH or haemozoin. There are three different theories:

- Slater and Cerami initially suggested that these drugs have the ability to inhibit haem polymerase enzyme.<sup>202</sup>
- Fitch and Chou have extended this hypothesis by suggesting that these drugs are possible regulators of the putative haem polymerase enzyme.<sup>203</sup>
- Egan and co-workers have shown that chloroquine and its derivatives can directly inhibit formation of synthetic BH and suggested that activity of these drugs *in vivo* involves inhibition of haemozoin formation by direct interaction with iron (III) protoporphyrin IX (Fe(III) PPIX).<sup>204</sup> This hypothesis has also been supported by Dorn and co-workers<sup>205</sup> and further support for this type of mechanism has been presented by several other laboratories.<sup>153, 206, 207</sup>

In studies presented here, three different chloroquinoline derivatives (CQ-derivatives) were used as BH inhibitors. In this chapter two different methods were used to determine the growth rate of BH with and without CQ-derivatives: spectrophotometry using a colorimetric change and a purification method. The difference in growth rate of (BH)

before and after treatment with CQp, CQ-ala and CQ-val was studied, the results were supported by FT-IR spectroscopy, XRD and SEM. Moreover, the effect of iron oxide on BH formation was studied by spectrophotometric analysis, FT-IR and SEM.

## **6.1 Malaria**

Malaria is a disease that is endemic in many tropical countries and is caused by a single-celled microorganism called *Plasmodium*, which lives in the red blood cells. These malarial pathogens are mostly found in the underprivileged zones of the world, where the treatments cost too much and may take a large amount of a family's earnings. Malaria disease must be cured. It is most severe in pregnant women, babies, young children and the elderly, if it is not diagnosed and treated promptly, it can be fatal.<sup>208, 209</sup>

It is carried from person to person or host to host by the female anopheles mosquito. This mosquito is described as a vector, or carrier, of the microorganism.<sup>208</sup> Usually the female mosquito injects her saliva into the healthy person before she starts to suck the blood needed for her development. The saliva contains a chemical to stop the blood from clotting. If the mosquito has previously taken blood from a person infected with malaria, it may also contain the parasite *Plasmodium*.<sup>210</sup> The parasite is transferred from the blood of one host, where it lives and develops, to the blood of the second host, the malarial parasite attacks the liver cells and the red blood cells (RBCs) and reproduces in them asexually. The *Plasmodium* sporozoites are injected into the blood of a person through the bite of an infected female anopheles mosquito.<sup>211</sup> These sporozoites then continue to the next stage, where they mature into hepatic schizonts and afterwards into merozoite which are released into the bloodstream starting the intraerythrocytic stage, during this stage of infection the infected RBCs are destroyed and parasitic septic waste products are released, which then causes fever in the host, usually accompanied by chills, shivering and ending in profuse sweating. Eventually the merozoite develops into a circle-shaped

trophozoite. This causes complete disintegration of RBCs releasing around 20 new merozoites into the blood stream allowing the disease to continue.<sup>212</sup>

## 6.2 Haemozoin or beta-haematin formation

*B-Haematin* (BH) is a dimer of haematin in which an iron-oxygen bond links the central iron of one haematin to the oxygen of one of the carboxylates of the neighbouring haematin as shown below **Figure 6.1**

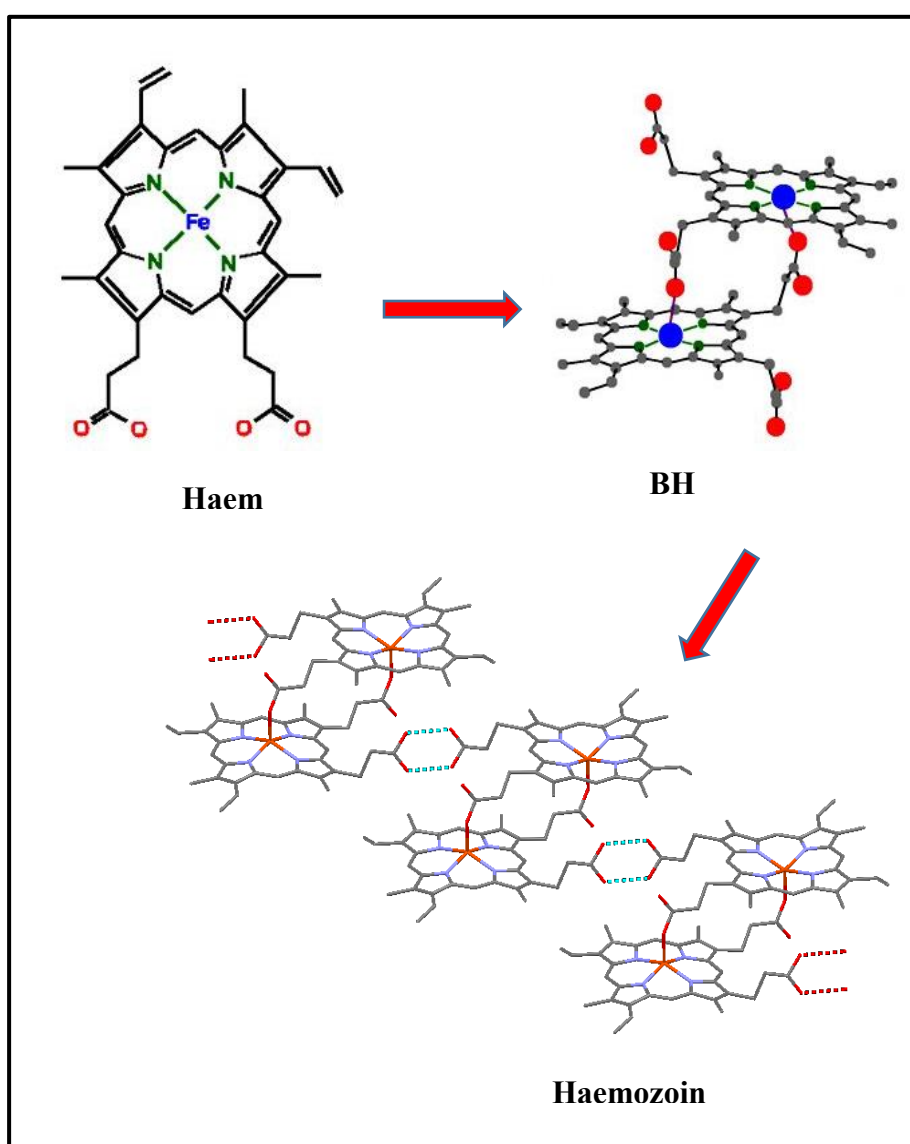


**Figure 6.1** Chemical structure of haem, BH, and haemozoin. The structure of haemozoin, showing hydrogen bonds between BH units as dotted lines, and coordinate bonds between iron atoms and carboxylate side chains as red lines.<sup>213</sup>

Insoluble haemozoin is a malarial pigment, a waste product made by the ingestion of blood by the blood feeding parasites, it is a polymer of BH and it is an insoluble solid form of haem. The blood contains haemoglobin, which is a protein digested by malaria parasites to release excessive amounts of haem.<sup>213</sup> The digestion of hemoglobin releases monomeric  $\alpha$ -haematin (ferriprotoporphyrin IX). This compound is toxic, as it is a pro-oxidant and catalyzes the production of reactive oxygen species causing oxidative stress which is believed to be generated during the conversion of haem (ferroprotoporphyrin) to haematin (ferriprotoporphyrin). Free haematin can also bind to and interrupt cell membranes, damaging cell structures and causing the lysis of the host erythrocyte.<sup>214</sup> The malaria parasite, therefore, detoxifies the haematin by biocrystallization converting it into BH dimer which polymerises to insoluble and chemically inert haemozoin.<sup>215-217</sup>

In addition, when the haemoglobin is digested by the parasite small peptides are formed that change their location and move to the parasite cytosol where they are digested to amino acids by cytosolic exopeptidases, these amino acids are then used by the parasites for their development. During all these processes, about 75% of the host's haemoglobin is consumed by the parasite by the process of pinocytosis via cytostomes, leading to a reduction in the protein content in the host's blood stream and illness.<sup>218-220</sup>

Due to this breakdown of haemoglobin a very massive volume of toxic waste product (haem) is released. However, the toxic haem is harmful also for the parasites and may cause their death, there are several metabolic reactions occurring in the body of the parasite for detoxification of the haem by mechanisms that include peroxidative degradation within the parasite food vacuoles and glutathione-mediated degradation in the parasite cytosol.<sup>221, 222</sup> **Figure 6.2.**

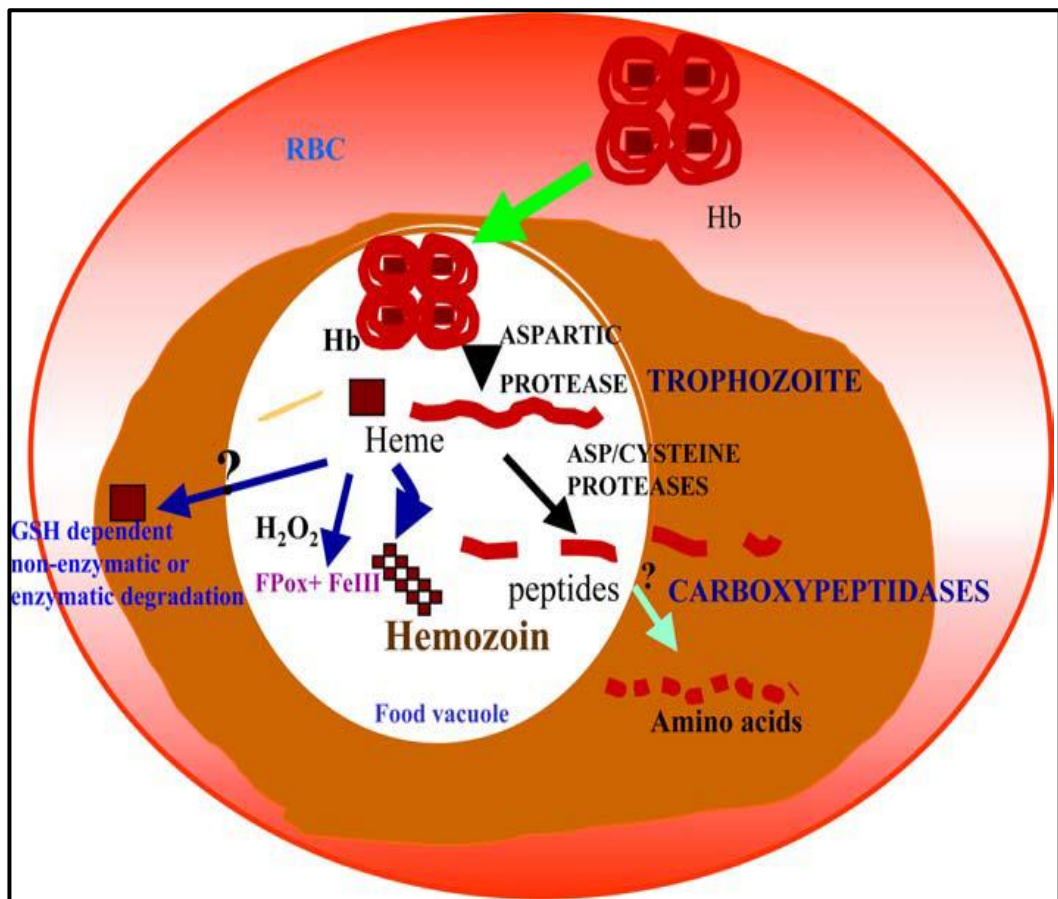


Figure 6.2 Process of haemoglobin degradation and haem detoxification by intraerythrocytic malaria parasite.<sup>223</sup>

### 6.3 Antimalarial drugs as beta-haematin or haemozoin inhibitors

As parasitic diseases are increasing so there is a more demanding need for drugs that help to fight against them. The most effective antimalarial drugs are chloroquine or 4-aminochloroquinoline derivatives, they are weak bases that disperse steadily in the cytoplasm of the cell.<sup>224</sup> They accumulate within the acidic digestive vacuole through an ion trapping mechanism. When chloroquine or 4-aminochloroquinoline derivatives enter the acidic environment, they are protonated and cannot pass through the vacuole membrane resulting in an increase in concentration to reach millimolar compared with nanomolar in the plasma. This is advantageous as it allows for low doses of chloroquine

to be given to malaria victims, as it is subsequently concentrated in the location of biological activity.<sup>206</sup>

*In vitro* studies of the formation of BH is very important for the development of antimalarial drugs, as it is essential for the parasites life. It has been reported that quinolone and its derivatives have the ability to decrease the rate of BH formation.<sup>225</sup>

Drug resistance against chloroquine has been a big issue in malaria elimination plans, even though chloroquine and some other 4-aminoquinolines, **Figure 6.3**, have played major roles in the past years. Therefore, the search for novel, cheap, and structurally varied drugs has become an urgent need.

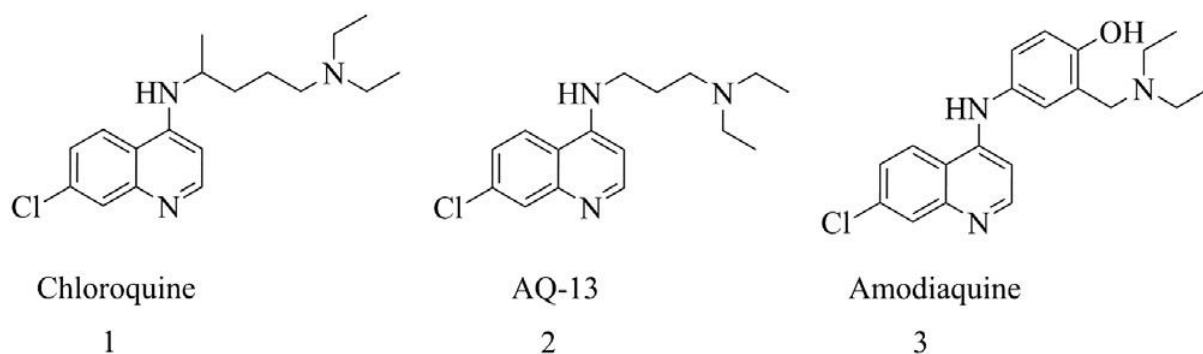


**Figure 6.3 Structures of CQ and related 4-aminoquinolines having antimalarial activity.**

Due to gene mutation of the *Plasmodium falciparum*, CQ-resistance transporter (PfCRT) results in rapid efflux of CQ from the intracellular loci and a study by Ridley et al. has established that drug resistance is compound specific. Thus, moving research activity towards changing the CQ side chain to obtain molecules active against CQ-resistant parasite.<sup>226</sup>

Currently, several antimalarial drugs have been used, such as chloroquine and mefloquine to develop antimalarial drugs with the ability to inhibit the biocrystallization

mechanism of haemozoin *in vivo* or to inhibit its dimer (BH) formation *in vitro*. Additionally, much research has been to transform the CQ side chain to overcome drug resistance.<sup>227</sup>

Recently, high-throughput screening for BH inhibition of new antimalarial compounds has been suggested as a beneficial tool in the discovery of new antimalarial compounds. Several methods have been described for the measurement of BH crystallization by antimalarial drugs.<sup>228</sup> Some of these methods included:

- Colorimetric method - a technique used to determine the concentration of coloured compounds in solution.<sup>229</sup> The concentration of a solution is determined by measuring its absorbance at a specific wavelength of light. The colorimetric method has several advantages over more complicated methods:
  - (1) It does not use pyridine that is mutagenic and carcinogenic,
  - (2) there is no purification or preparation of BH,
  - (3) it is a simple technique using equipment freely available in most laboratories,
  - (4) crystal growth rate can be followed without adding any additional reagents.<sup>174</sup>
- Purification method - which uses ferriprotoporphyrin IX at acid pH in the presence of acetic acid or acetate buffer at different concentrations and degrees of ionization, higher temperatures and long reaction times.<sup>230</sup>

## ***6.4 The relationship between malaria and iron oxide treatment***

Redox-active metals such as iron, copper and chromium, undergo redox cycling that may cause an increase of reactive oxygen species (ROS) production, such as superoxide radical ( $O_2^{\cdot-}$ ), hydroxyl radical ( $HO^{\cdot}$ ), or hydrogen peroxide ( $H_2O_2$ ). Increased ROS can damage antioxidant defences and produce oxidative stress. Cells under oxidative stress show unlikely disfunctions because of lesions which are caused by ROS to lipids, proteins and DNA. Consequently, it has been suggested that metal induced oxidative stress in cells can be partially responsible for the toxic effects of heavy metals.<sup>231</sup> Some workers have invoked a correlation between increased capacity to oxidative stress and erythrocyte haemolysis.<sup>232, 233</sup> Other work has suggested a sequence of events including increased membrane bound denatured haemoglobin species, membrane damage, and loss of cellular deformability and decreased erythrocyte survival, since the parasite uses this molecule as a source of amino acids for its own nutrition during the erythrocytic stage of the disease.<sup>234</sup>

It was reported that large amounts of ROS can be caused by an imbalance between the production of oxidizing species and the activity of antioxidants. This imbalance is a crucial mechanism of human hosts' infections and in the case of malaria, can cause the death of the parasites. Thus proving the ability of oxidative stress to help kill malaria parasites *in vitro* studies.<sup>235</sup>

## **6.5 Methods**

### **6.5.1 Determination of beta-haematin crystal growth using colorimetric method**

BH with and without treatment with each CQ-derivative was determined as described (section 2.8).<sup>174</sup>

### **6.5.2 Purification method to measure beta-haematin crystal growth**

Synthetic BH was obtained by the method described by Slater et al. (1991),<sup>175</sup> as described (section 2.9).

### **6.5.3 Beta-haematin production for FT-IR and SEM measurements synthetic**

BH with and without treatment with each CQ-derivative was determined using acetic acid instead of acetate buffer to get a good BH pellets for FT-IR and SEM measurements as described (section 2.10).<sup>175</sup>

### **6.5.4 The reaction of iron oxide with beta-haematin (BH) in vitro**

A mixture of solutions of ferric and ferrous sulfate in a molar ratio of 2:1 (1.5 ml, 10mM: 5 mM) was used as BH inhibitors as described (section 2.11).<sup>175</sup>

## 6.6 Results and discussion

Saroj *et al* 2016 reported that the main reason for BH inhibition after treatment with CQ compounds is the interaction of CQ with BH due to a polar interaction of nitrogen with the iron of ferriprotoporphyrin. Moreover, a hydrogen bond can be formed between the NH of CQ and the carboxyl group of one of the propionic acid side chains of haem causing delay of BH formation.<sup>236</sup>

To confirm whether or not synthesised CQ-derivatives from this thesis can work in the same way that Saroj *et al* suggested, these CQ-derivatives were tested by using colorimetric and purification methods *in vitro* test against BH formation.

The colorimetric method provides information on the growth rate of BH crystals and identifies the differences between BH formation with and without CQ-derivatives. The results showed significant inhibition of BH formation after treatment with each CQ-derivative. It appears that CQp, CQ-ala and CQ-val act as an antinucleator and as an inhibitor of crystal growth. This could be due to the capacity of CQ to complex with haem and to interact and block the active growth site of BH.<sup>225</sup>

The absorbance at two different wavelengths (400 and 650 nm) was recorded and the fraction (*f*) of haem converted to BH was calculated as described (section 6.6.1).

The results represent data from three independent experiments as shown in **Figures 6.4-6.6**.

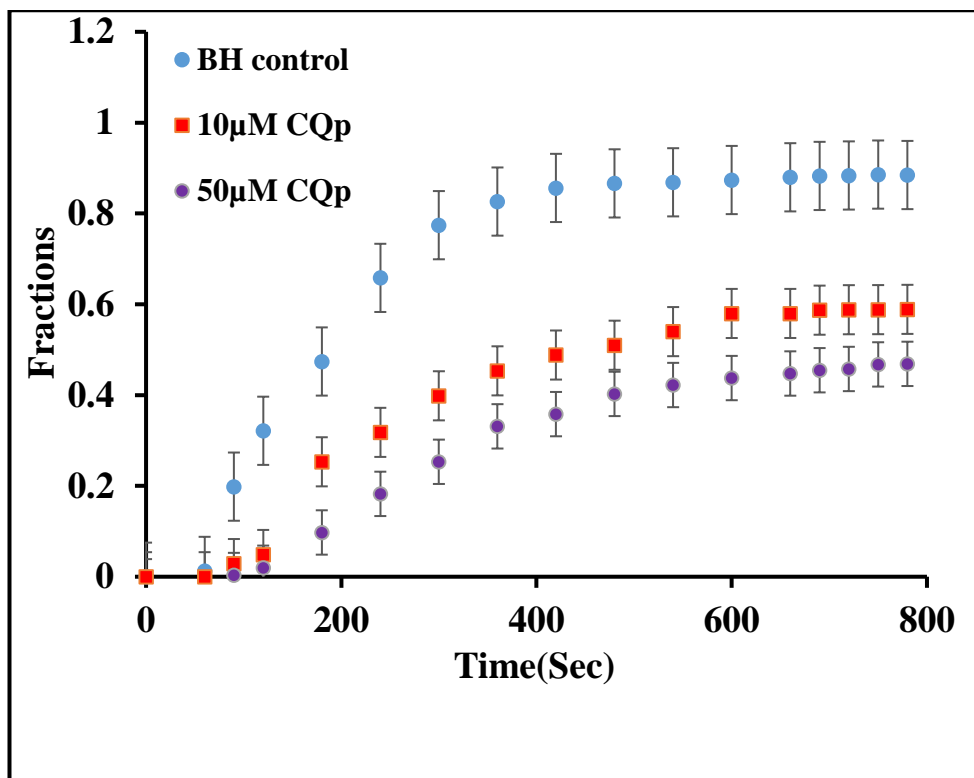


Figure 6.4 Time courses of BH crystal growth in acetate buffer in the presence of 10  $\mu\text{M}$  and 50  $\mu\text{M}$  CQp.

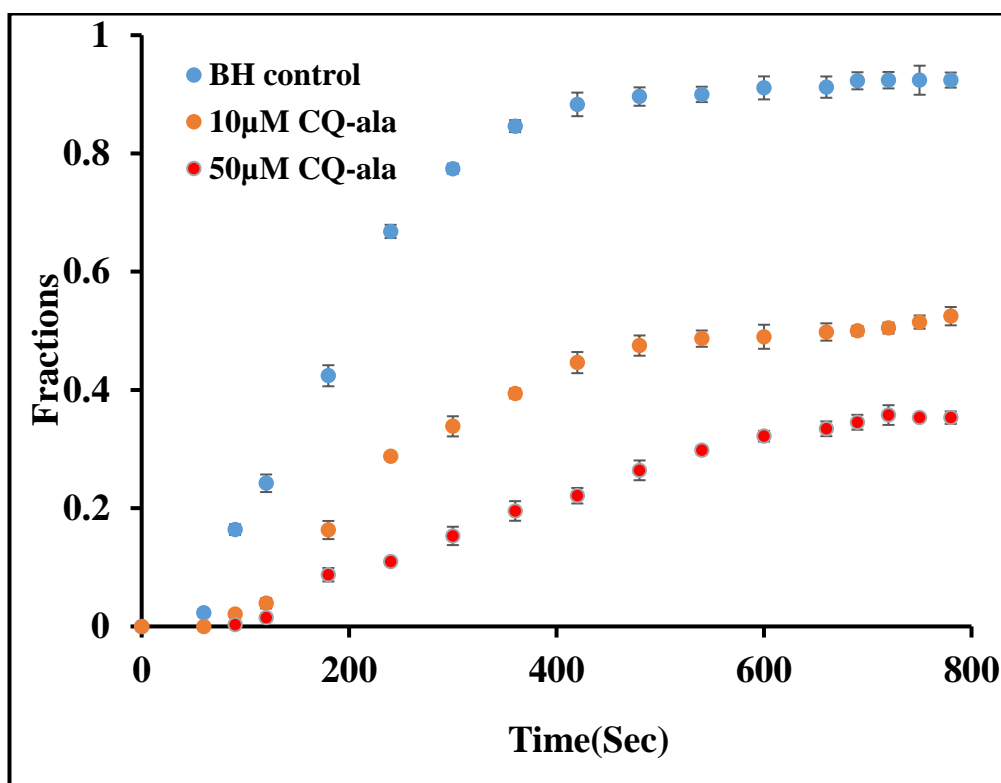


Figure 6.5 Time courses of BH crystal growth in acetate buffer in the presence of 10  $\mu\text{M}$  and 50  $\mu\text{M}$  of CQ-ala.

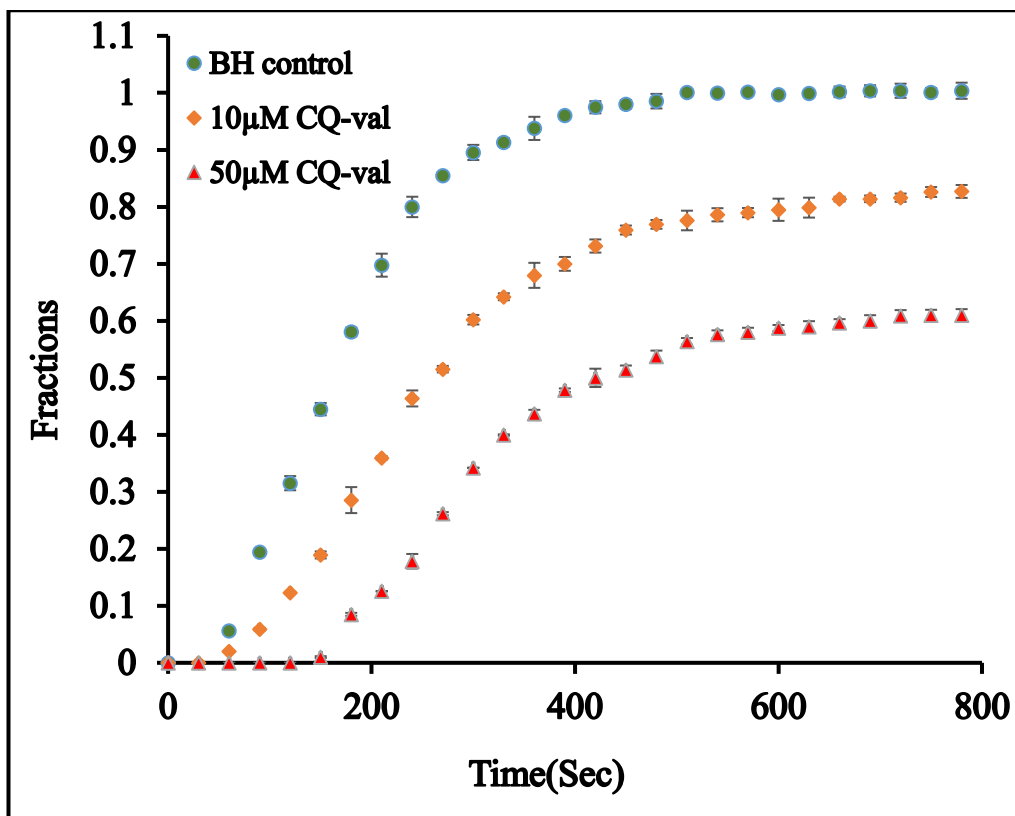


Figure 6.6 Time courses of BH crystal growth in acetate buffer in the presence of 10 µM and 50 µM CQ-val.

A large difference was observed between the growth rate of BH in the presence of CQ-derivatives compared to untreated BH, which provides evidence to the role of CQ derivatives as a BH inhibitor especially with the CQ-ala treatment as shown in **Table 6.1** and **Figures 6.4-6.6**.

**Table 6.1 The effect of CQ-derivatives on BH formation after 800 sec.**

<b>CQ-derivatives</b>	<b>CQ- derivatives dose</b>	<b>Amount of BH formation %</b>	<b>BH inhibition %</b>
CQp	10 $\mu$ M	66	34
	50 $\mu$ M	53	47
CQ-ala	10 $\mu$ M	56	44
	50 $\mu$ M	38	62
CQ-val	10 $\mu$ M	82	18
	50 $\mu$ M	61	39

Moreover, there was a delay in the growth rate of BH after treatment compared to untreated and that delay increased when the dose of each CQ-derivative was increased from 10  $\mu$ M to 50  $\mu$ M. This supports the suggestion that CQ-derivatives are better BH inhibitors.

To find out the difference between the activity of commercial CQ and the synthetic CQ-derivatives as BH inhibitors, 10 $\mu$ M of each CQ-derivative with the same quantity of commercial 4-aminochloroquinoline were added separately to the haemin chloride and the rate growth of BH was determined by spectrophotometry, the overall results showed an enhanced inhibition of BH formation after adding CQ-derivatives compared with commercial CQ **Figure 6.7**.

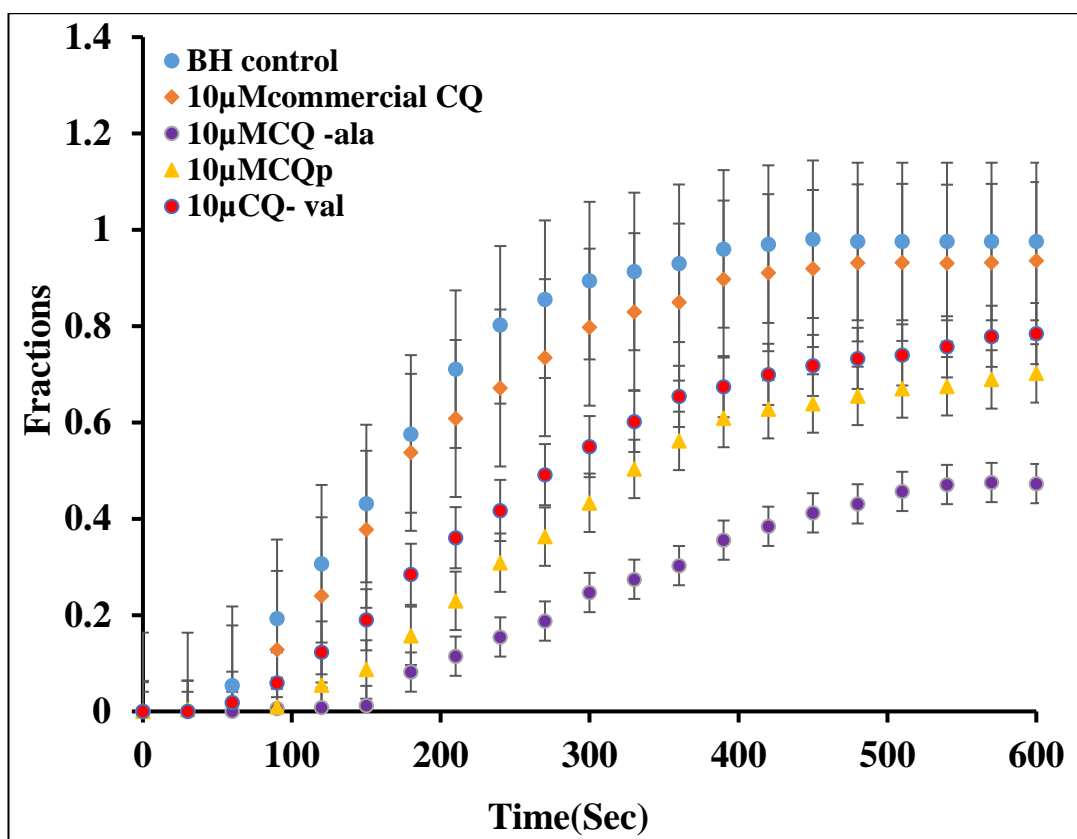


**Figure 6.7** Time courses of BH crystal growth in acetate buffer in presence of 10  $\mu\text{M}$  CQ- derivatives and commercial CQ.

For more confirmation, the purification method was used to determine BH formation with and without CQ-derivatives as described (sections 6.6.2 and 6.6.3).

All CQ-derivatives displayed significant inhibition to BH formation but the most effective derivative was CQ-ala **Figures 6.8 and 6.11**.

It was found that a high dosage of each CQ-derivative reduced the growth of BH significantly as presented in **Table 6.2**.

**Table 6.2 The effect of CQ-derivatives on BH formation after 20 h reaction using purification method.**

<b>CQ-derivatives</b>	<b>Dosage</b>	<b>Amount of BH formation %</b>	<b>BH inhibition %</b>
CQp	10 $\mu$ M	83	17
	20 $\mu$ M	72	28
	30 $\mu$ M	60	40
	40 $\mu$ M	51	49
	50 $\mu$ M	43	57
CQ-ala	10 $\mu$ M	65	35
	20 $\mu$ M	59	41
	30 $\mu$ M	51	49
	40 $\mu$ M	40	60
	50 $\mu$ M	30	70
CQ-val	10 $\mu$ M	88	12
	20 $\mu$ M	79	21
	30 $\mu$ M	68	32
	40 $\mu$ M	62	38
	50 $\mu$ M	55	45

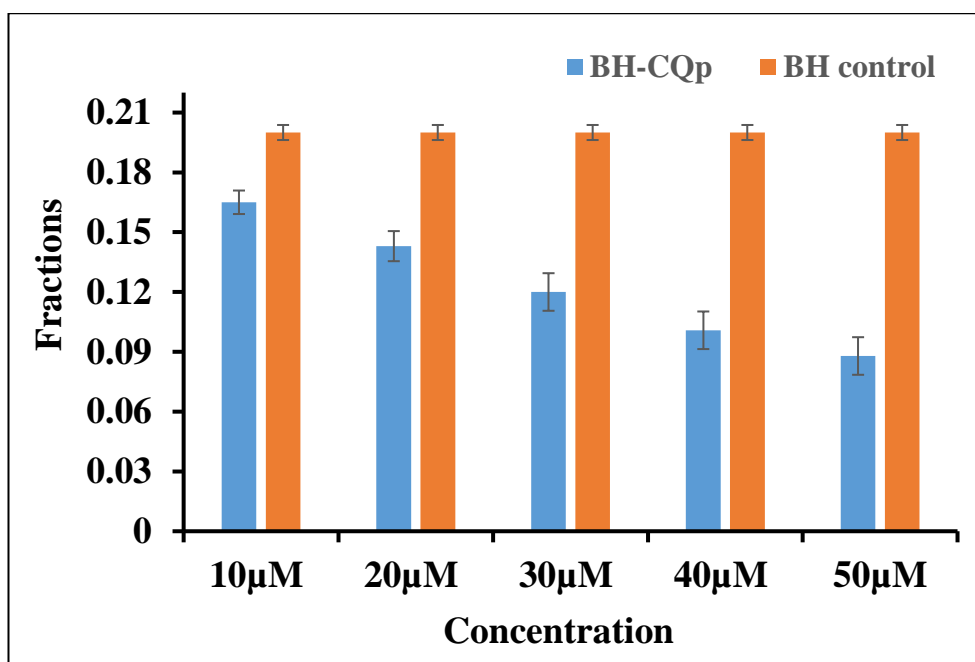


Figure 6.8 Inhibition of BH growth after treatment with 10 - 50 μM CQp. The fraction of haem converted to BH was calculated from the absorbance at two different wavelengths (400 and 650 nm) for treated and untreated BH.

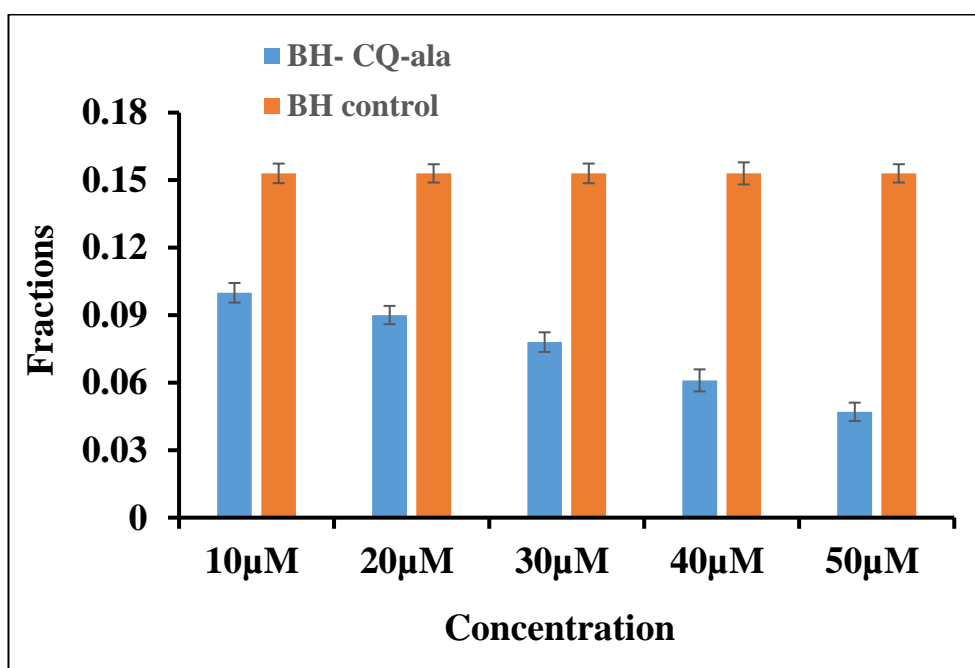
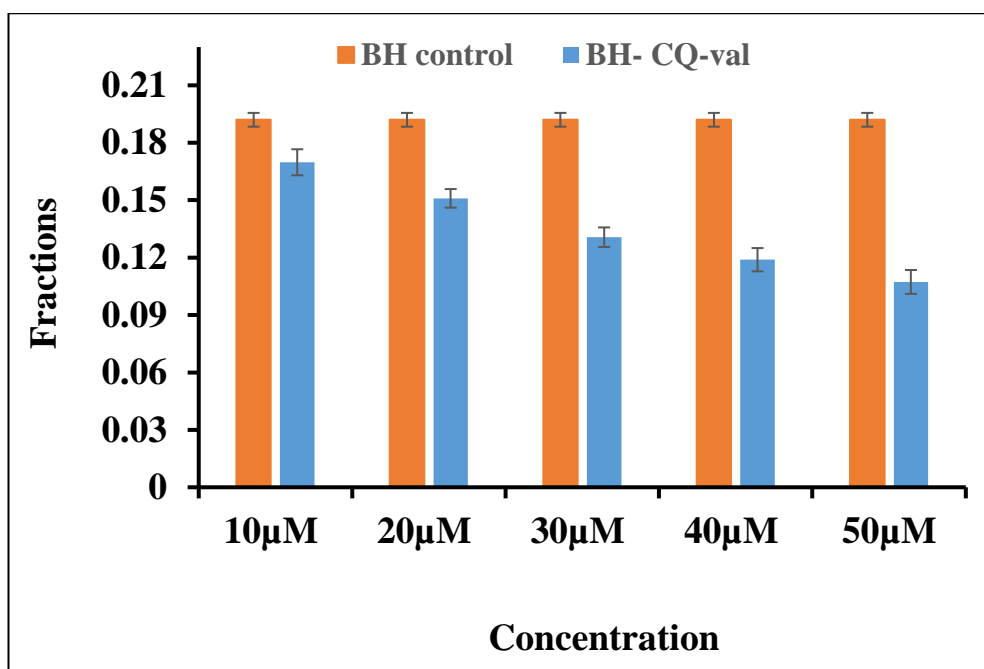


Figure 6.9 Inhibition of BH growth after treatment with 10 - 50 μM CQ-ala. The fraction of haem converted to BH was calculated from the absorbance at two different wavelengths (400 and 650 nm) for treated and untreated BH.



**Figure 6.10** Inhibition of BH growth after treatment with 10 - 50  $\mu\text{M}$  CQ-val. The fraction of haem converted to BH was calculated from the absorbance at two different wavelengths (400 and 650 nm) for treated and untreated BH.

A similar procedure was used using glacial acetic acid instead of acetate buffer, this method showed the same results with very good pellets for FT-IR and SEM measurements.

For comparison between the activity of synthetic CQ-derivatives and the activity of commercial CQ, CQ-ala and commercial CQ were added separately to haemin chloride under acidic environment and reacted overnight at 80 °C. After purification the growth of BH for each sample was determined by spectrophotometry **Figure 6.11**.

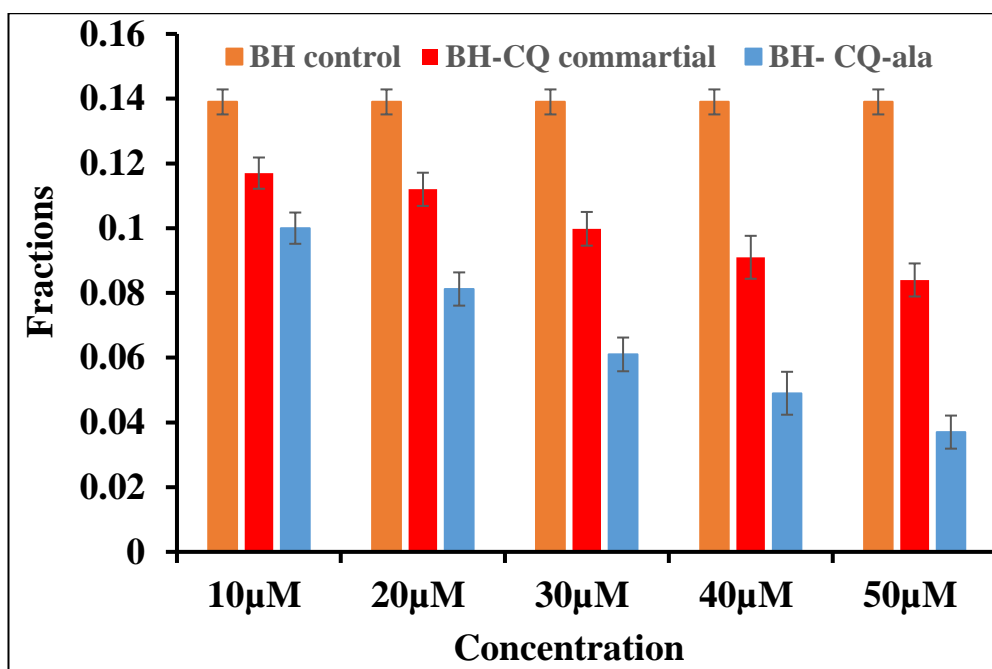


**Figure 6.11** Inhibition of BH growth using 10 - 50  $\mu\text{M}$  of CQ-alanine and commercial CQ as BH inhibitors.

CQ-ala showed higher inhibition of BH growth than commercial CQ, due to the short side chain. That means it may show an interesting result against *P. falciparum* sensitive strain and CQ-resistance strain.

For more confirmation FT-IR for BH formation with and without treatment was studied. The two most notable absorbance peaks of the BH compound are at  $1666\text{ cm}^{-1}$  and  $1211\text{ cm}^{-1}$ , which are relatively close to the peaks at  $1663$  and  $1210\text{ cm}^{-1}$  in the spectrum of purified haemozoin published by Egan *et al.* who inferred that the two peaks resulted from a vibrational band of the propionate C=O and C-O stretching, respectively (as shown in red arrows) attached to the iron centre,<sup>237</sup> **Figure 6.12**. All these peaks are still visible after treatment with each CQ-derivative with a slight shift.

There was no significant change observed from the FT-IR spectrum of BH after treatment with each CQ-derivative compared to untreated BH, the extra peak at  $1710.3\text{ cm}^{-1}$

confirms conversion of haemin to BH and is close to the reported value.<sup>238</sup> All FT-IR spectra are shown in appendix 2.

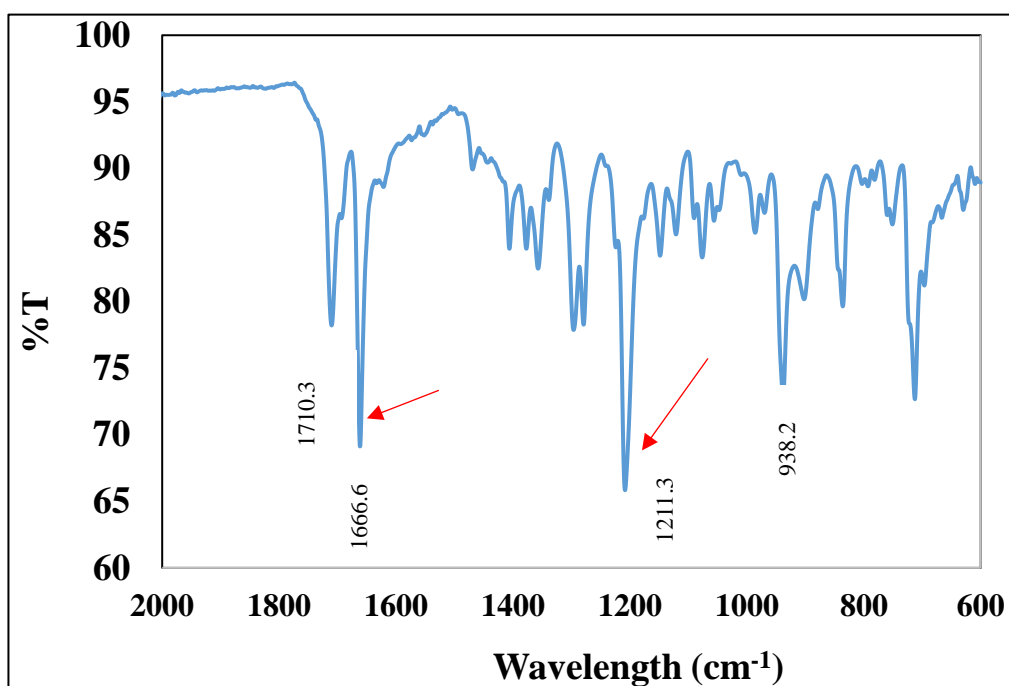


**Figure 6.12** FT-IR spectrum of BH formation without treatment with CQ-derivatives. The two most main absorbance peaks of the BH shown by red arrows.

Scanning electron microscopy of BH products from preparations with and without CQ-derivatives exhibit a change in morphology **Figure 6.13**

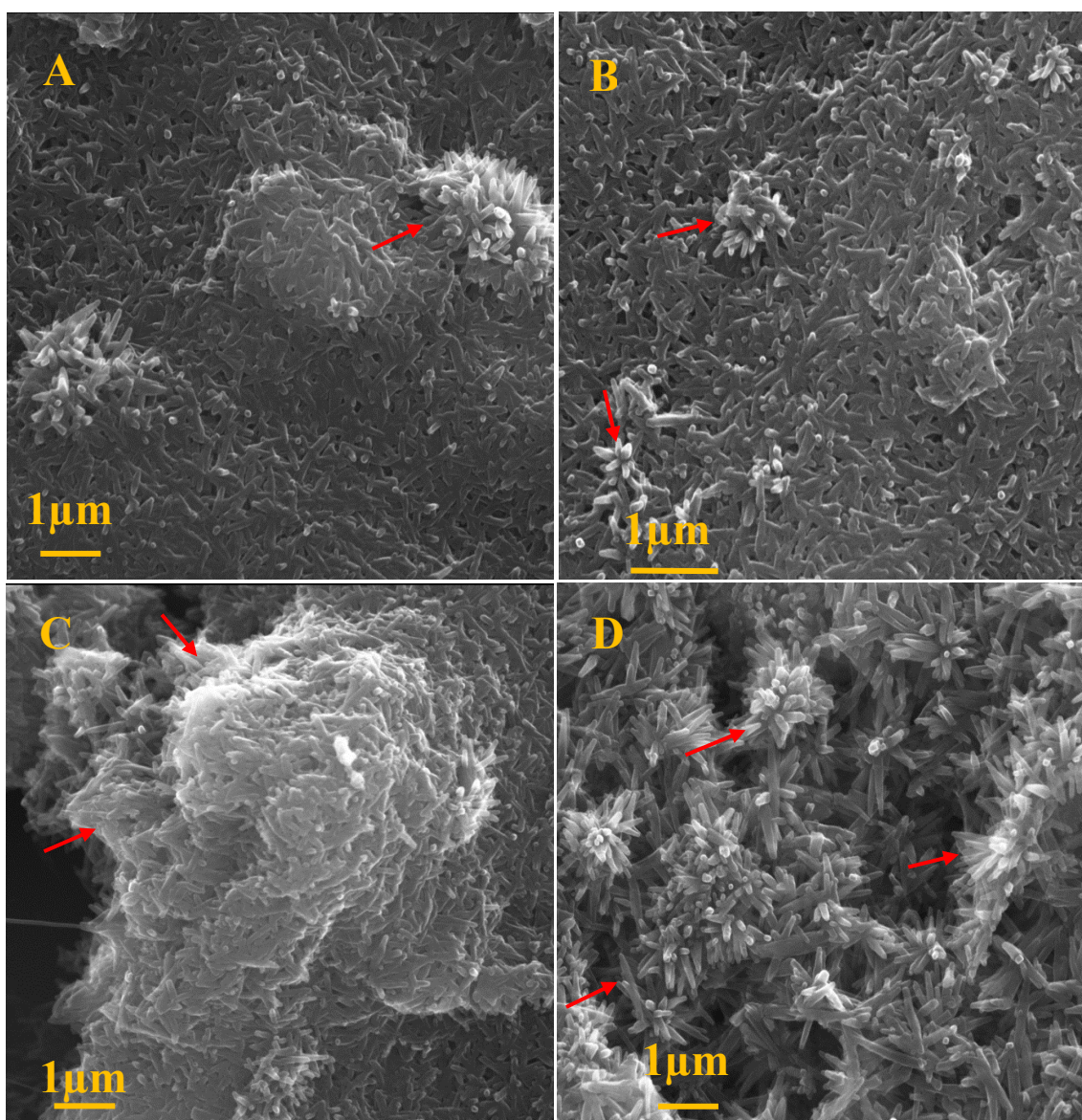


**Figure 6.13** Scanning electron micrographs (SEM) of (A) BH formation without treatment, (B) BH formation with 10  $\mu\text{M}$  CQp, (C) BH formation with 10  $\mu\text{M}$  CQ-ala, (D) BH formation with 10  $\mu\text{M}$  CQ-val (red arrows shown the differences of BH crystal structures).

The BH crystal without treatment appeared as long thin tapered crystals of varying size with smooth surfaces, similar to those in a previous report.<sup>239</sup> After treatment with CQp the crystal becomes slightly thicker, **Figure, 6.13 B** compared to untreated BH crystal, the arrangement of BH crystals was changed to fine needle-like crystals when CQ-ala was used as BH inhibitor **Figure 6.13C**. While, the crystal showed a

different arrangement after using CQ-val to inhibit BH formation; it appears to be arranged around a central point in some places like petals of a flower, **Figure 6.13D**.

From SEM it was observed that increasing the concentration of each CQ-derivative made the crystals bigger and broader, the BH crystal after treatment with 50  $\mu\text{M}$  of each CQ-derivative showed a different arrangement to that of a 10  $\mu\text{M}$  treatment, **Figure 6.14**.

When CQ-val was used as an inhibitor, the crystals of BH changed significantly, they appeared more organized, forming a globular structure arranged around a central point, **Figure 6.14G**.

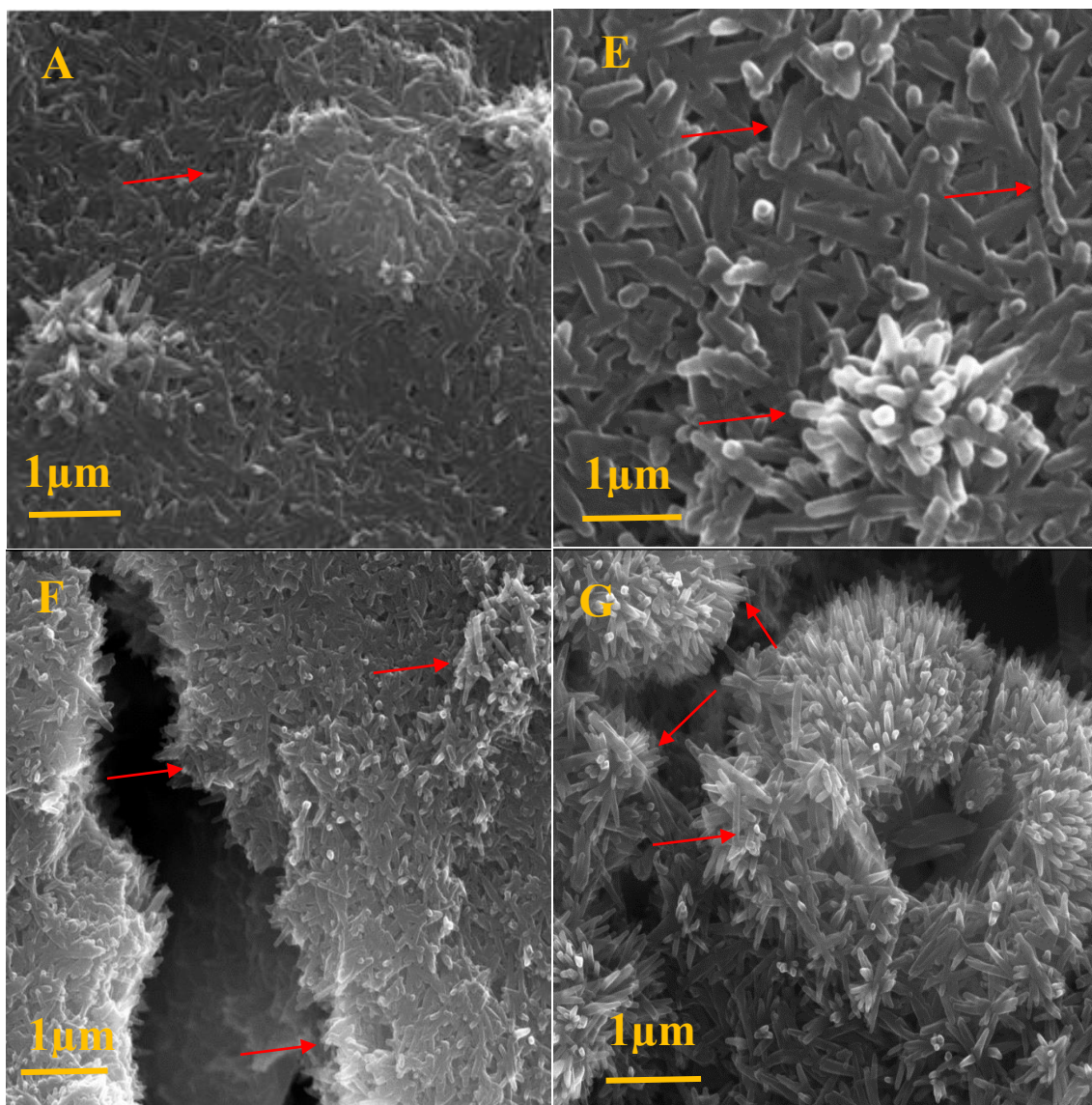


**Figure 6.14** Comparative Analysis of Different Synthetic BH. Scanning electron micrographs of (A) BH formation without treatment, (E) BH formation with 50  $\mu\text{M}$  CQp, (F) BH formation with 50  $\mu\text{M}$  CQ-ala, and (G) BH formation with 50  $\mu\text{M}$  CQ-val (red arrows shown the differences of BH crystal structures).

BH formed with and without treatment with CQ-derivatives has also been investigated by using X-ray powder diffraction (XRD) which is mostly used to characterize and identify phases at  $2\theta$  range  $0\text{--}30^\circ$  with Cu radiation ( $\lambda=1.5418 \text{ \AA}$ ). The pattern is shown in **Figure 6.15** and **Figure 6.16**, respectively.

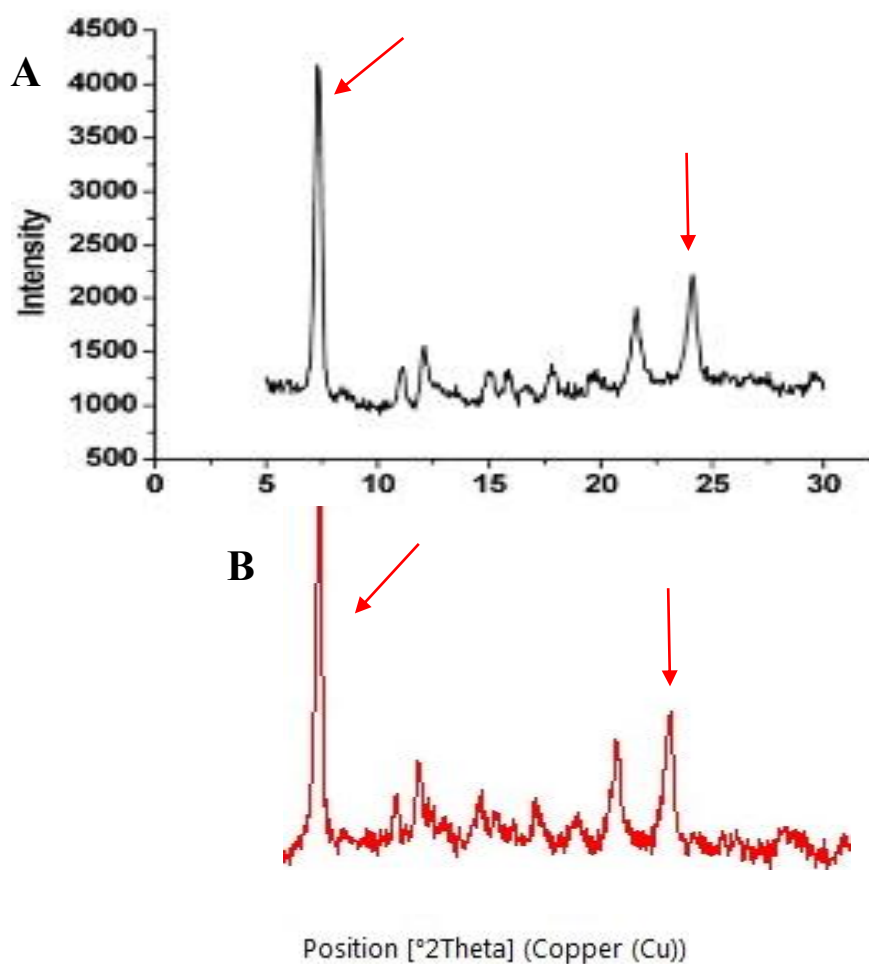


**Figure 6.15** X-ray powder diffraction patterns (Cu) of A. published BH-crystal, B. synthesised BH without treatment. The pattern of synthetic BH from this work is identical to that previously reported as shown in red arrows.

As expected the pattern of synthetic BH from this work is identical to that reported as previously prepared in acidic medium,<sup>240</sup> **Figure 6.15**; both have the same crystalline structure.

When CQ-derivatives are used as BH inhibitors, none of the BH pattern after treatment with each CQ-derivative appears to be mixed with the synthesised untreated BH pattern. Specific peaks are completely changed in the powder diffraction patterns of BH and a few not identical peaks were also observed after treatment (as shown in black arrows). This may be due to the addition of each CQ-derivative, **Figure 6.19**.

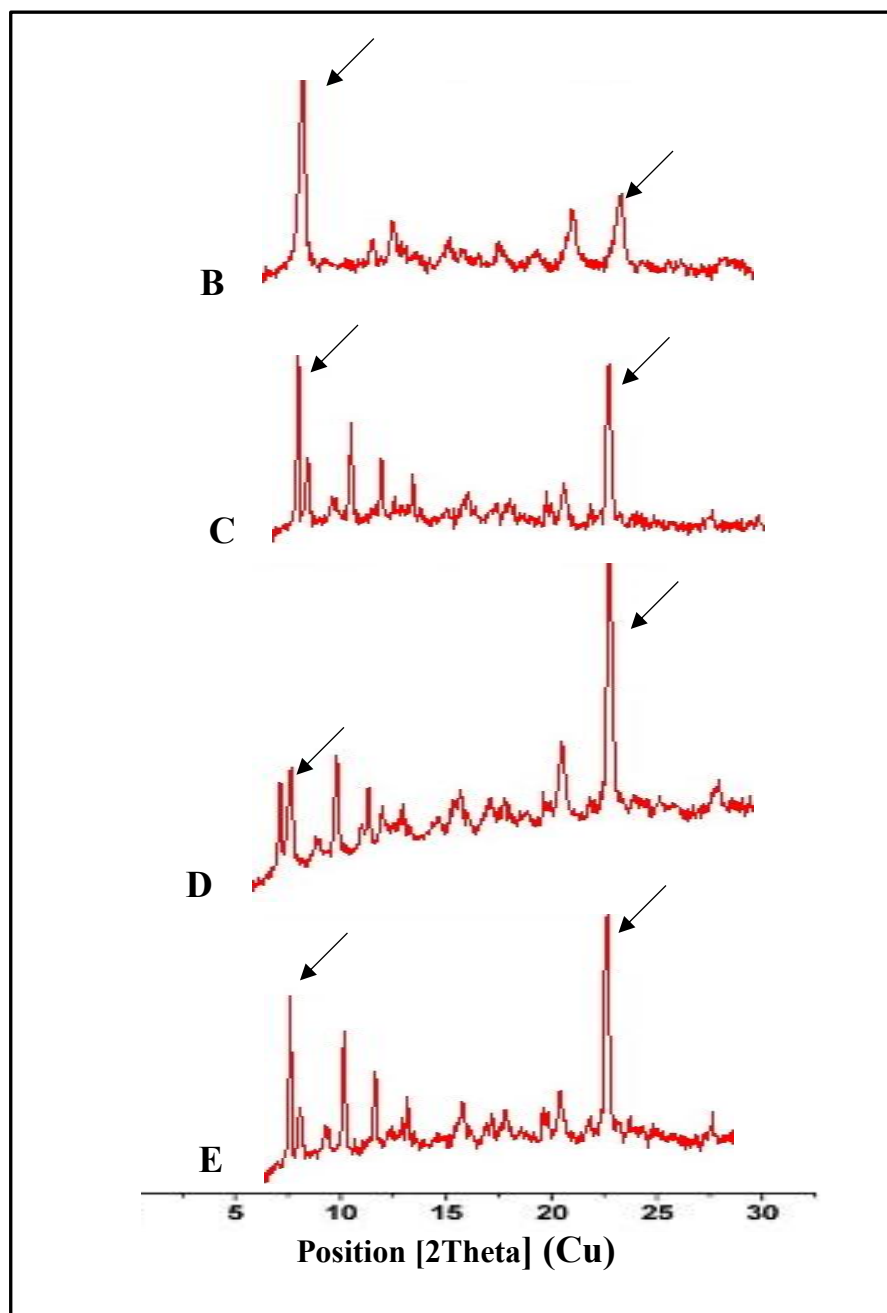


**Figure 6.16 X-ray powder diffraction patterns (Cu) of B. synthesised BH without treatment, C. BH-CQp treated, D. BH-CQ-val treated and E. BH-CQ-ala treated.**

### 6.6.1 The effect of iron oxide on BH formation

Iron is crucial for many biochemical reactions involved in the growth and reproduction of the malaria parasite. Iron as redox-active metal has ability to reduce cells' major antioxidants, especially thiol-containing antioxidants and enzymes generating reactive oxygen species (ROS).<sup>231</sup> It has been reported that iron-catalysed radical formation is significantly involved in the antimalarial BH inhibition, when the production of peroxide and superoxide can exhibit a number of biological effects, they are damaging at physiological concentrations.<sup>241</sup> This inhibition of BH or haemozoin formation may develop oxidative stress in *P. falciparum* due to the accumulation of free haem as evident from the decreased level of glutathione and increased formation of lipid peroxide, H<sub>2</sub>O<sub>2</sub>, and hydroxyl radical (OH<sup>•</sup>).<sup>242</sup>

The most important reaction of hydrogen peroxide with free iron (II) is the Fenton reaction, leading to the very reactive and damaging hydroxyl radical (OH<sup>•</sup>) which is one of the most reactive and stable free radical species known in aerobic cells as shown in Eq2 and Eq7 below:



Additionally, superoxide can also react with ferric iron in the centre of haematin by the Haber Weiss reaction to reproduce Fe (II) causing release of toxic free haem which can damage the cell membrane.<sup>243</sup>



As a chelator iron may interact with the carboxyl group of one of the propionic acid side chains of haem. This kind of interaction may subsequently delay BH formation from free

haem and may lead to inhibition of parasite growth.<sup>244, 245</sup> The effect of iron oxide and  $\text{Fe}^{2+}/\text{Fe}^{3+}$  mixture on BH formation was studied by FT-IR and SEM.

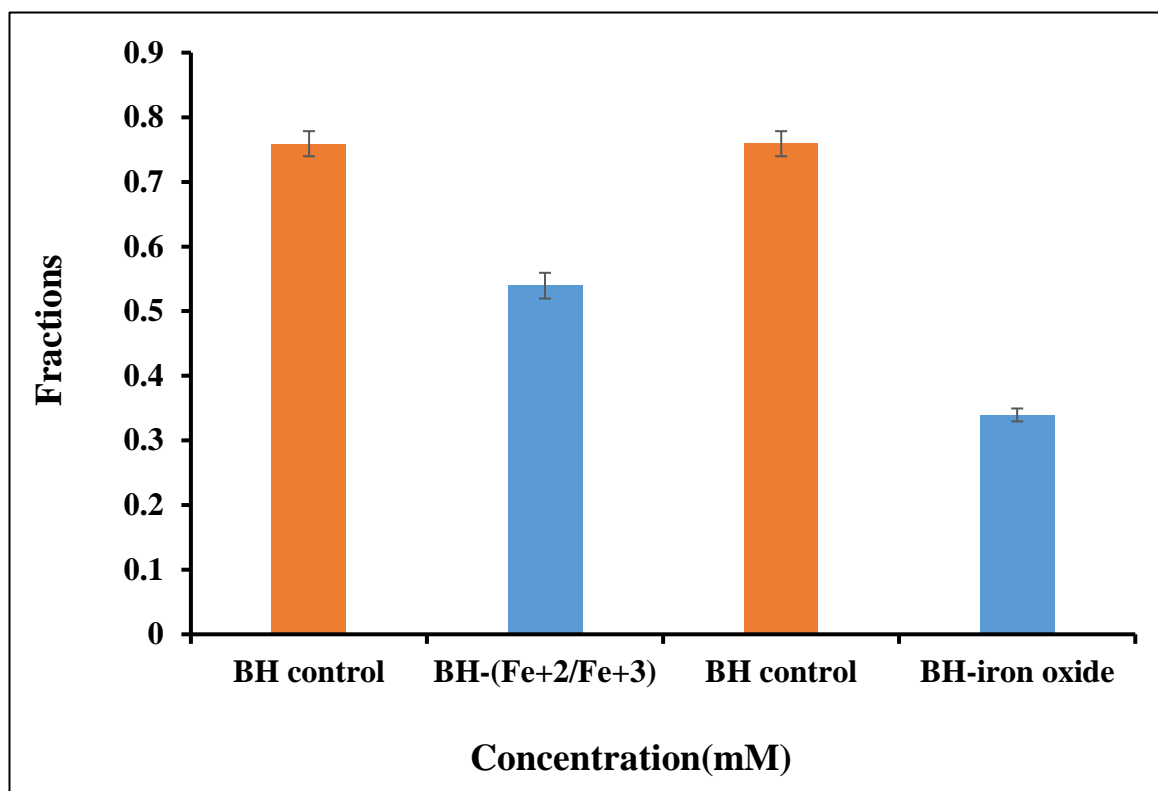


**Figure 6.17** BH formation with and without 10 mM of both iron oxide and ( $\text{Fe}^{2+}/\text{Fe}^{3+}$ ) mixture.

Due to the ability of haem to change membrane permeability by intercalating into the cell membrane, oxidative stress may arise and cause parasite death.<sup>245</sup> Therefore, iron oxide or  $\text{Fe}^{2+}/\text{Fe}^{3+}$  mixtures have been used here as an oxidative stress producer to inhibit BH formation. In this experiment both iron samples (suspended iron oxide and iron ions mixture) were added in 2:1 volume ratio separately to haemin chloride and the reaction was left to proceed overnight at 80°C. After purification the concentration of each BH sample was evaluated by spectrophotometry. The results showed that both samples (suspended iron oxide and iron ions mixture) inhibited the growth rate of BH to 66% and 39% respectively, **Figure 6.17**.

FT-IR spectrophotometry showed that most IR peaks for untreated BH totally disappeared after adding iron oxide to haemin chloride. The position of the BH peak at  $1666.6\text{ cm}^{-1}$  was shifted for BH after treatment with iron oxide compounds to  $1638.4\text{ cm}^{-1}$  and  $1632.88\text{ cm}^{-1}$ , **Figure 6.18**.

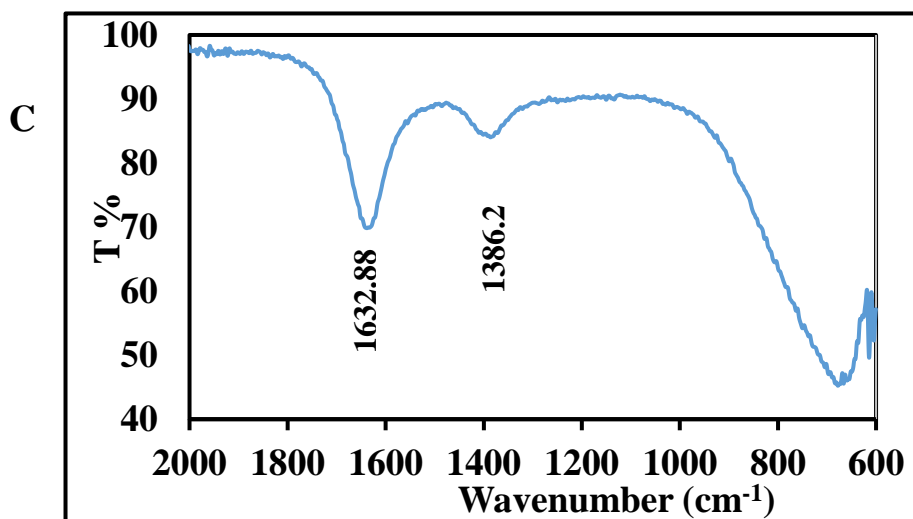
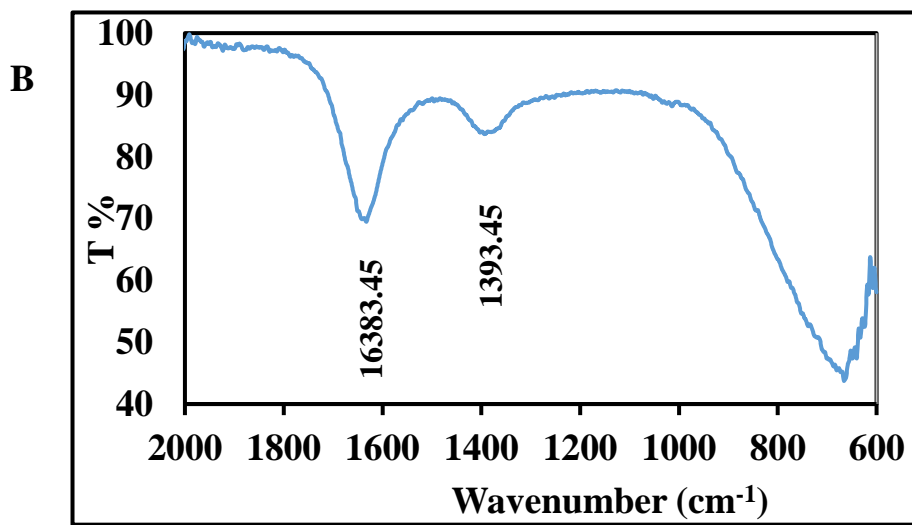
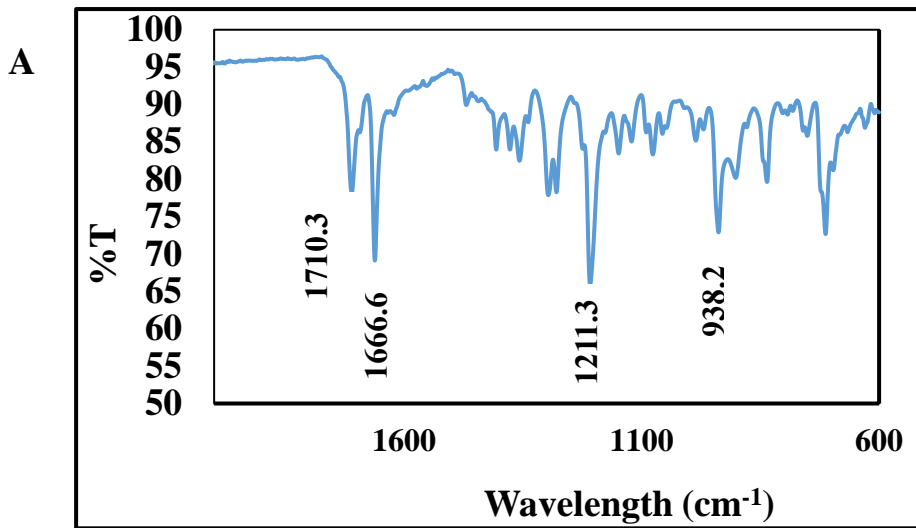


**Figure 6.18 FT-IR spectra of BH after different treatments. A. BH formation without treatment. B. BH formation after Fe<sup>2+</sup>/Fe<sup>3+</sup> treatment, C. BH formation after iron oxide treatment.**

To confirm whether or not these peaks arise from the binding of propionate C=O in one haem molecule to the central Fe in the neighbouring haem molecule, necessary to produce BH, the FT-IR of iron oxide without any haem was recorded. A band around 1632 cm<sup>-1</sup> appearing in the sample is attributed to the characteristic vibration of iron hydroxide and the band at 680 cm<sup>-1</sup> is due to Fe–O stretching vibration, **Figure 6.19**. The FT-IR spectrum of (Fe<sub>3</sub>O<sub>4</sub>) was shown the linkage between BH which is treated with iron oxide or (Fe<sup>2+</sup>/Fe<sup>3+</sup>) and Fe<sub>3</sub>O<sub>4</sub> alone by peaks at 680 and 1632 cm<sup>-1</sup> confirmed BH-functionalized Fe<sub>3</sub>O<sub>4</sub> **Figure 6.19**.

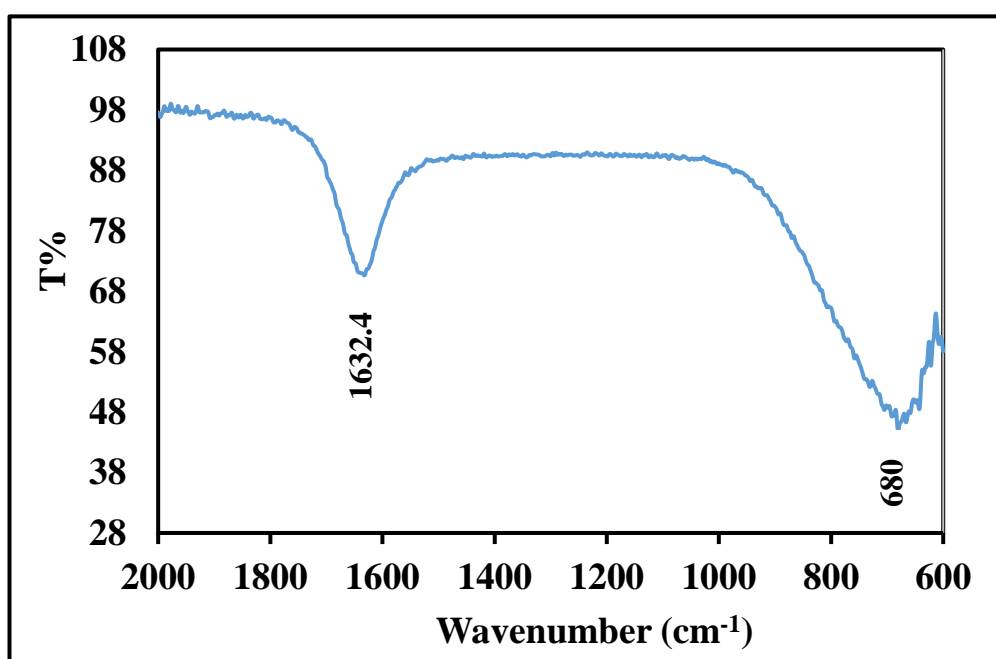


**Figure 6.19 FTIR spectra for iron oxide (Fe<sub>3</sub>O<sub>4</sub>).**

SEM images of BH after treatment with iron oxide and iron ions mixture suggested that the resultant crystals may have higher crystallinity and bigger size compared to BH crystals without treatment. Two different types of crystal morphology interweaving

together like branches of a tree are observed, one of these two different crystal is closed to the reported SEM image of iron oxide ( $\text{Fe}_3\text{O}_4$ )<sup>246</sup> as shown in **Figure 6.20 B**.

This morphological change to the BH structure after treatment with ( $\text{Fe}^{2+}/\text{Fe}^{3+}$ ) mixture and iron oxide could occur due to infusion of each metal oxide on to the external surface of BH and this change was highlighted by red arrows in **Figure 6.20**.

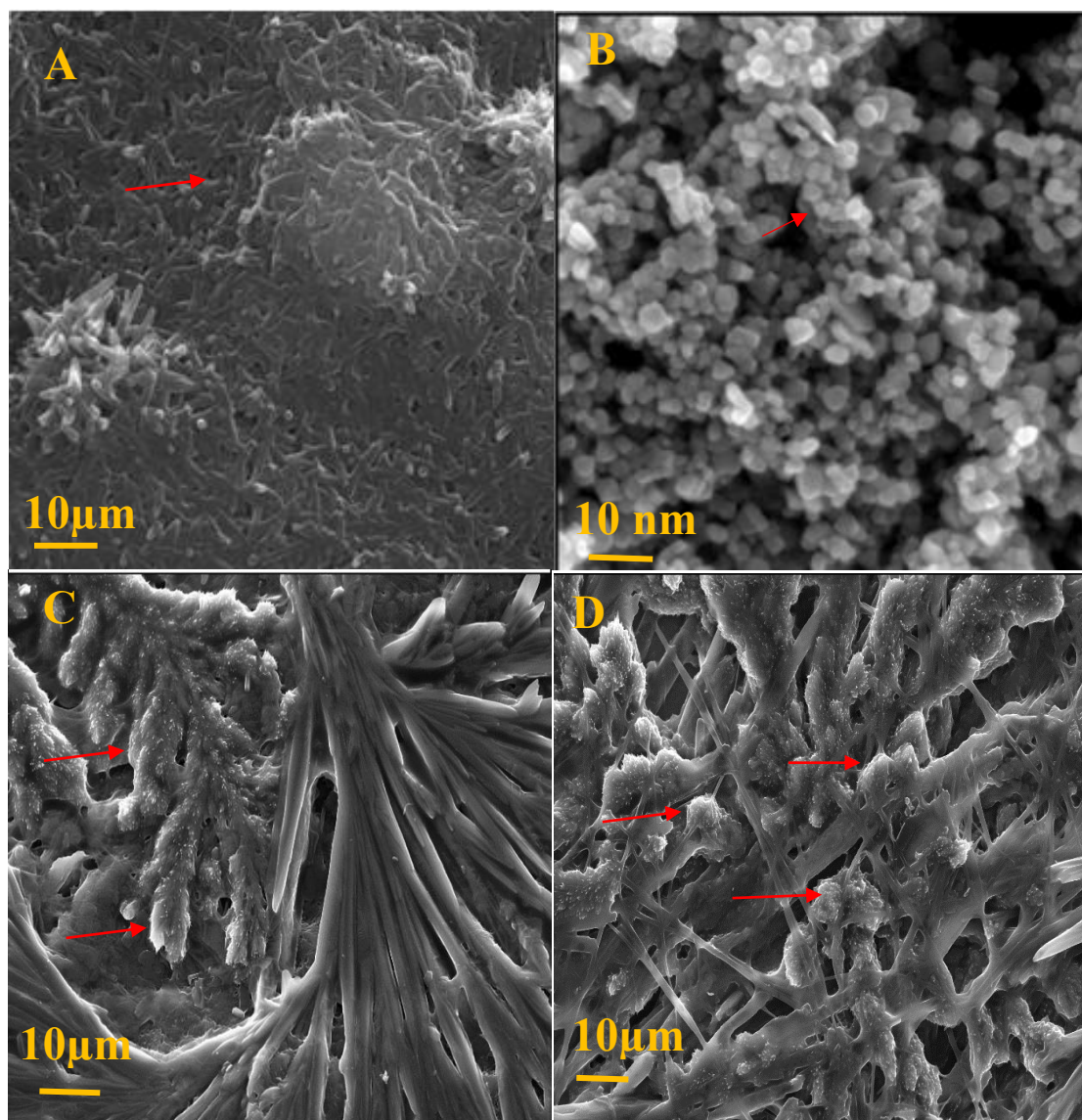


**Figure 6.20** Scanning electron micrographs of different synthetic BH. (A) BH formation without treatment, (B) iron oxide nanoparticles ( $\text{Fe}_3\text{O}_4$ )<sup>237</sup>, (C) BH formation with  $\text{Fe}^{2+}/\text{Fe}^{3+}$ , (D) BH formation with iron oxide. The change in the crystal shapes was highlighted by red arrows.

## **6.7 Conclusions:**

Upon addition of CQ-derivatives (CQp, CQ-ala and CQ-val) to haemin chloride the amount of BH generated compared to commercial CQ. The CQ-derivatives have an inhibitory effect on the growth stages of BH. The collected results from two different methods were used to determine the formation of BH with and without CQ- derivatives. CQ-ala has the largest effect on BH formation compared to the other CQ-derivatives. Further, two different iron oxide samples improved the activity of CQ-derivatives as BH inhibitors. The effectivity of CQ-ala, with and without conjugation to CPMV as a BH inhibitor *in vivo* is described in the next chapter.

## ***7 Chloroquinoline as haemozoin or beta-haematin inhibitor***

### ***7.1 Chloroquine-Resistant Malaria***

The spread of malaria is caused by unicellular eukaryotes that are obligate parasites of various insects. The nature of this species is that it cannot complete its life cycle without occupying a host.<sup>247</sup> There has been an increased resistance to traditional antimalarial drugs in recent years. The ineffectiveness has been specifically observed for the current dangerous malaria parasite *P. falciparum*.<sup>248</sup> The majority of recent medical reports have been based upon both the *vivo* and *vitro* ineffectiveness of chloroquine against the malaria parasites.<sup>249</sup>

In this work, two different studies have been investigated. The first follows the formation of beta-haematin (BH) or haemozoin which are necessary for a parasite's life. It was shown in the previous chapter how the growth rate and synthesis of BH can be affected by the presence of CQ-derivatives. The second study, described in this chapter, investigated the formation of BH or haemozoin in the presence of biological material in the form of a trophozoite membrane extract.<sup>204</sup> Drugs such as chloroquine have the ability to inhibit haemozoin formation in the food vacuole parasite. This feature has been the keystone for many of the current developments in screening methods and drug discovery.<sup>225</sup> Although heavy use of chloroquine has led to an increased resistance against the malaria parasites *P.falciparum* and *P. vivax*, it is still used as an antimalarial due to its mild effectiveness which is key to the overall control of malaria. Chloroquine's effectiveness is believed to lie in its ability to interrupt haematin detoxification in the red blood cells of the host parasites.<sup>250, 251</sup>

Haematin is normally detoxified by polymerization into harmless haemozoin crystals and possibly by a glutathione mediated process of destruction. Chloroquine (CQ) binds with

the  $\mu$ -oxo dimer haematin to form a CQ-haematin  $\mu$ -oxo dimer complex, this can delay detoxification and destroy the parasite.<sup>206, 216, 251</sup> The three different CQ- derivatives, reported in this thesis, before and after conjugation to CPMV, have been tested *in vitro* against a *P. falciparum* strain (3D7).

## **7.2 Materials and methods**

### **7.2.1 Drugs**

The three different synthesised CQ-derivatives (CQp, CQ-ala and CQ-val) were prepared as described earlier, either free or conjugated to CPMV. The *P. falciparum* strain (3D7) and its culture media were provided from the Department of Immunology & Infection, Faculty of Infectious & Tropical Diseases, London School of Hygiene & Tropical Medicine. Where all the *in vitro* tests were carried out by Dr. Don van Schalkwyk.

### **7.2.2 Growth inhibition assays**

Two different methods were investigated in the *in vitro* study to show the effectivity of each CQ-derivative. This included non-isotopic methods, namely the fluorometric SYBR Green I assay and the colorimetric lactate dehydrogenase (LDH) assay.<sup>252</sup>

The following stock solution for each CQ derivative were prepared and described below, all CQ solutions were formulated and stored in a refrigerator at a constant 4 °C:

- 1- CQp (0.001 g, 0.79 mM) in DMSO (5 ml)
- 2- CQ-ala (0.1 g, 36 mM) in DMSO (11 ml)
- 3- CQ-ala (0.1 g, 0.036 mM) in 50% aqueous DMSO (1 ml)

- 4- CQ-val (0.022g, 40 mM) in 5/95 volume ratio of DMSO/ sodium phosphate buffer (2 ml)
- 5- CPMV-CQp, CPMV-CQ-ala and CPMV-CQ-val were prepared as described (section 2.5.1) and the concentration of each CQ-derivative was calculated to be 2.40, 2.23 and 3.00 nM respectively.

The experiment was run for one complete *P. falciparum* parasite life cycle (48 h) at a starting parasitaemia concentration of 1% (asynchronous) and the haematocrit also set to 1%. All serial dilutions were 2-fold (10 µl) from each CQ-derivative used against *P. falciparum* strain (3D7) and control CQ was run for comparison. The parasite suspensions were added to 96-well plates pre-dosed with anti-malarial drugs and incubated for 48 h at 23.8 °C.

### ***7.3 Results and discussion***

*In vitro* studies measuring the ability of the CQ-derivatives, before and after conjugation to CPMV, as a *P. falciparum* killer, has been investigated using the two methods mentioned previously.

#### ***7.3.1 The fluorometric SYBR Green I assay***

Two different dosages of each CQ-derivative were used. The first range started from 10 µM for each CQ-derivative followed by a 3-fold serial dilution, the second range began at 50 µM followed by a 2-fold dilution. No 'kill' effect was observed for each of the CQ-derivative except for CQ-ala at the highest concentration (50%) as compared to the control CQ (4- aminochloroquinoline). There was not enough data to generate a full curve to determine an accurate IC<sub>50</sub> value.

The same experiment was repeated using CQp in two-fold serial dilutions carried out across the (1) 1:50 dilution, (2) 1:100 dilution, (3) 1:200 dilution, (4) 1:400 and (5) 1:500 range. CQp remains show poor toxicity against the malaria parasites. CQp had also not eliminated all the parasites even when operating at a high concentration (100  $\mu$ M) as compared with the control CQ which was very potent at 10 nM. This data is illustrated in **Figure 7.1**.

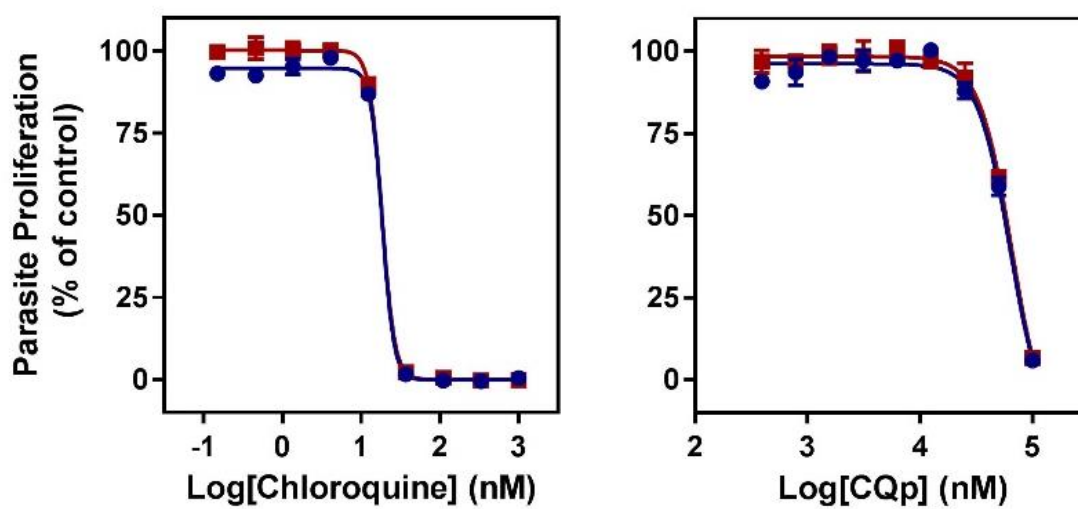


**Figure 7.1** Antimalarial activity of CQp and control CQ against *Plasmodium falciparum* (strain 3D7).

In this assay after one cycle life with *P. falciparum* there was variation in  $IC_{50}$  values for CQ-ala 48 h exposure. CQ-ala was shown to be more effective against *P. falciparum* (strain 3D7) than the other CQ-derivatives. With the CQ-ala suspended in DMSO the experiment started with a 1:20 dilution, this was always going to be toxic because of the high DMSO content. Pure DMSO was run as a control in parallel with the CQ-ala, this provided the ability to detect where the solvent toxicity ended and the compound activity became evident. The  $IC_{50}$  value was calculated from the data as described below:

The stock concentration was generated at 0.036 mM, this means that the first concentration was  $0.036/20 = 1.8$  mM or 1800  $\mu$ M.

Two-fold dilutions from 1:20 means a dilution of 1:40, IC<sub>50</sub> values were found to be 44 $\mu$ M as compared to control CQ (8.9 nM), shown in **Figure 7.2**.

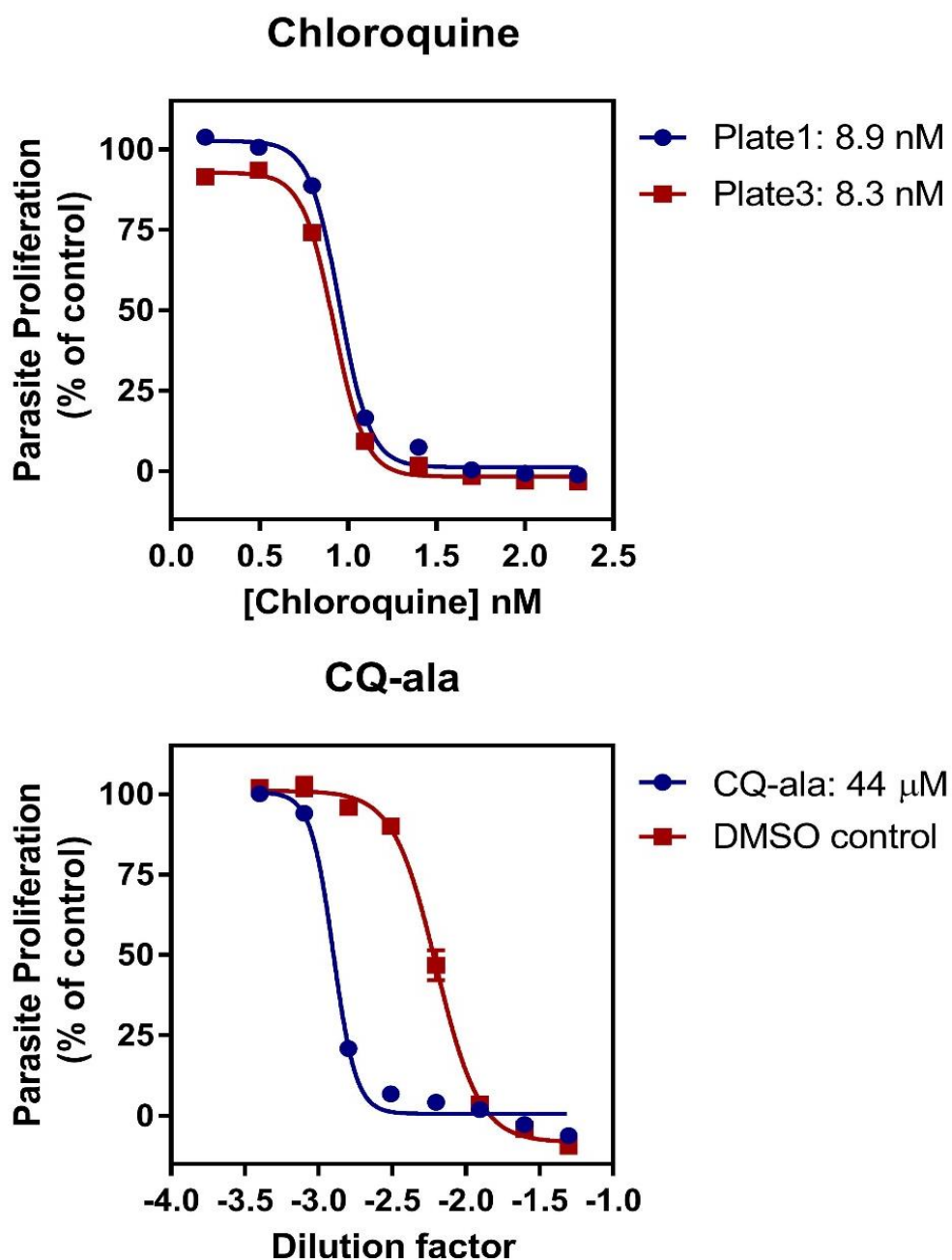


**Figure 7.2** Antimalarial activity of CQ-ala against *Plasmodium falciparum* (strain 3D7).

This experiment was repeated to prove reproducibility before moving to modified CPMV. Two CQ-derivatives before and after conjugation with CPMV were tested against the *P. falciparum* (strain 3D7) using the fluorometric SYBR Green I assay. The CQ-val derivative was diluted (1:10) from the stock CQ-val and tested against the parasite. This was found to be marginally effective at the highest concentrations; however this 'kill' effect could be due to the DMSO content. CQ-ala stocks were diluted, the highest concentration used was a 1:500. The data proved that at this concentration the parasite was eliminated. The concentration of CQ-ala in 100% DMSO was 0.036 M (36 mM) where as for the 50% DMSO stock the concentration was 0.036 mM (36  $\mu$ M), this is a 1000-fold difference. It was found that the CQ-ala sample in 50% DMSO was more effective as a parasite killer than the same sample in 100% DMSO. The IC<sub>50</sub> value for each sample before conjugation with CPMV was found to be 72  $\mu$ M and 0.072  $\mu$ M respectively, **Figure 7.3**.

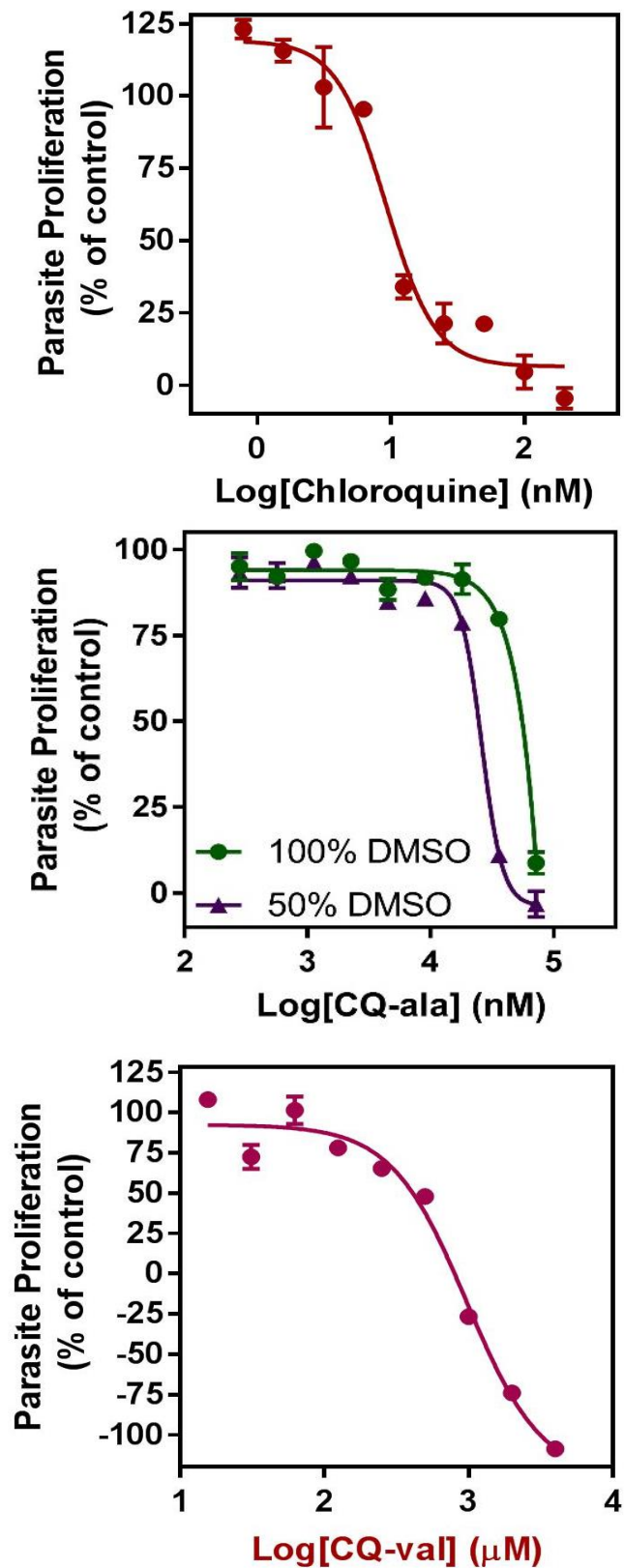
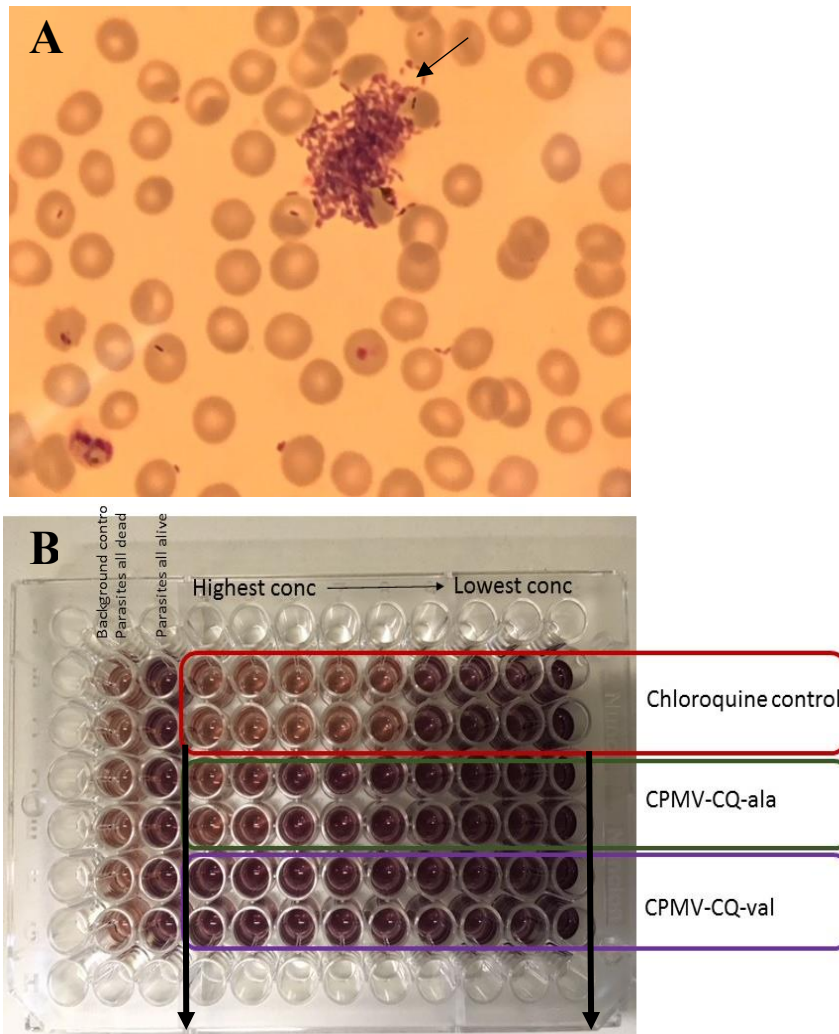


Figure 7.3 Antimalarial activity of CQ-derivatives analogues against *P. falciparum* (strain 3D7).

Overall the results showed that CQ-ala is the most effective malaria killer compared with other CQ-derivatives. This being said, it proved to be less active than the control CQ. In an attempt to enhance activity, CPMV particle was used as a carrier with 145 CQ-ala per particle. The  $IC_{50}$  value reduced from 72nM to 0.25 nM demonstrating significant enhanced activity when CPMV is used as a carrier.

To confirm this result, the experiment was repeated many times using the same modification of CPMV with CQ-ala and CQ-val but, unfortunately both samples showed no activity against the malaria parasites even at the highest concentration tested. This is due to contamination; **Figures 7.4 and 7.5.**



**Figure 7.4** A: Microscopic image shown the contamination due to pollution by bacteria in CPMV-CQ-ala and CPMV-CQ-val solutions, B: Example of a 96-well plate were screened for their ability to inhibit BH formation. The dark colour observed from CPMV samples in each plate identical the contamination (between black arrows) compared with the light colour of control CQ.

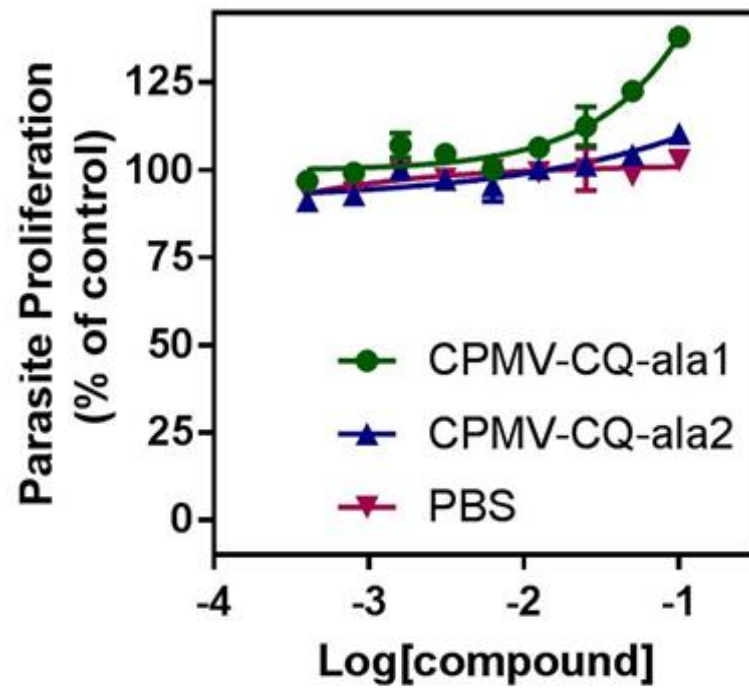
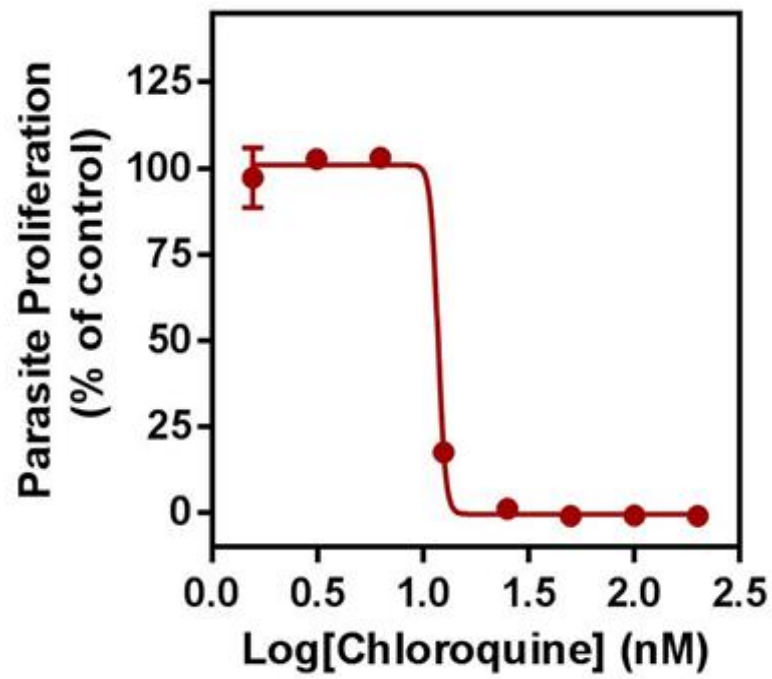


Figure 7.5 Antimalarial activity of CPMV-CQ-ala analogues against *P. falciparum* (strain 3D7).

### 7.3.2 *The colorimetric lactate dehydrogenase (LDH) assay*

Modified CPMV with CQ-ala and CQ-val were used against *P. falciparum* (strain 3D7). The highest starting concentration being at 10-fold dilution from each stock solution (6.6 nM for CPMV-CQ-ala and 3 nM for CPMV-CQ-val) a 10mM sodium phosphate buffer solution (PBS) (pH7) was run as a control using the same dilution series as the modified CPMV.

In the fluorescence assay after one life cycle (48 h) with *P. falciparum*, the control solutions (CQ and PBS) both worked as expected with no effect on the parasite growth. Meanwhile, the same phenomenon for each CPMV-CQ derivative has been observed to have over 100% viability relative to the control because of a bacteria or fungus contaminant in the well that takes up the fluorophore into its DNA. The process increases its signal over that of the parasites growing. Whereas, when the method of (LDH) assay was used, the results for CPMV-CQ-ala were significantly changed **Figure 7.6**.

The control CQ (green curve) delivers  $IC_{50}$  values that are identical when tested using an LDH assay method. The initial life cycle stage had a negligible effect on the  $IC_{50}$  value (from 7.8 to 7.2).

For CPMV-CQ-val, (purple curve) it remains inactive across the concentration range tested (>100% viability), these results are summarized in **Table 7.2**. Nevertheless, the CPMV-CQ-ala (green curve) shows a kill effect at the two highest concentrations (1:10 and 1:20 dilution of the stock solution which was 6.6 nM). The  $IC_{50}$  value is estimated to be at 1:24 dilution of the stock sample. This means that the  $IC_{50}$  value is 0.275 nM, this value is a significantly less than the  $IC_{50}$  value from the control CQ. Therefore the conjugated CQ-ala is more potent than the standard control CQ. This information is illustrated in **Figure 7.6**.

The yield of LDH assay method was good with a Z factor of 0.52. The Z factor of treated *P. falciparum* with CPMV-CQ-ala was calculated by using assay plates containing six negative control wells and six positive control wells as described previously.<sup>252</sup>

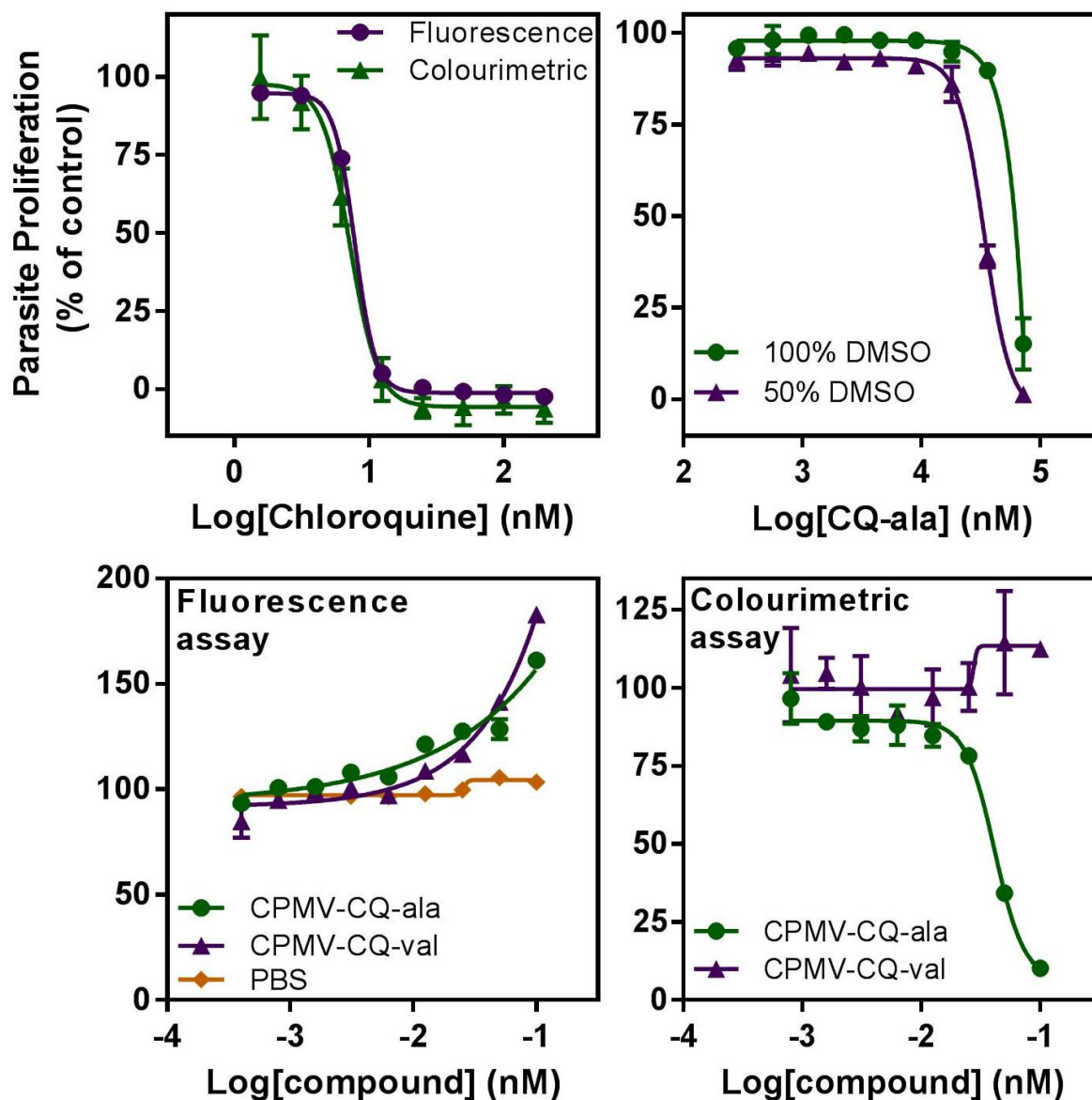


**Figure 7.6** Antimalarial activity of CPMV-CQ-derivatives analogues against *P. falciparum* (strain 3D7). Two different CQ-ala samples have been tested one was dissolved completely in DMSO and another one was dissolved in 50% volume ratio DMSO/ PBS buffer.

**Table 7.1 Proliferation of *P. falciparum* for CPMV-CQ-ala inhibitor assessed using the (LDH) assay.**

<b>Fold of dilution of stock CPMV-CQ-ala</b>	<b>CPMV-CQ-ala concentrations (nM)</b>	<b>CPMV-CQ-ala Log (nM)</b>	<b>%viability</b>
1 in 10	0.66	-0.180	<b>10.19</b>
1 in 20	0.33	-0.481	<b>34.21</b>
1 in 40	0.165	-0.783	78.22
1 in 80	0.0825	-1.084	84.74
1 in 160	0.04125	-1.385	88.02
1 in 320	0.020625	-1.686	86.89
1 in 640	0.0103125	-1.987	89.12
1 in 1280	0.00515625	-2.288	96.53

**Table 7.2 Proliferation of *P. falciparum* for CPMV-CQ-val inhibitor assessed using the (LDH) assay.**

Fold of dilution of stock CPMV-CQ-val	CPMV-CQ-ala concentrations (nM)	CPMV-CQ-ala Log (nM)	%viability
1 in 10	0.3	-0.523	112.45
1 in 20	0.15	-0.824	114.47
1 in 40	0.075	-1.125	100.25
1 in 80	0.0375	-1.426	<b>96.97</b>
1 in 160	0.01875	-1.727	<b>91.74</b>
1 in 320	0.009375	-2.028	100.35
1 in 640	0.0046875	-2.329	104.70
1 in 1280	0.00234375	-2.630	104.10

**Table7.1** shows that the CPMV-CQ-ala sample has a significant reduction in the viability of the parasite after a 10-fold dilution as compared with the abundance of the parasite without treatment, this would be interesting to test against CQ-resistance strain. In contrast, CPMV-CQ-val showed no kill effect against the same parasite. This means the parasite has the capability to survive **Table7.2**. This may be due to short accumulation of the CQ-val inside the digestive vacuole.<sup>253</sup> Resulting in an increase in haem polymerization which is necessary for parasite life. Malaria parasites have ability to solve the chloroquine's toxicity problem by preventing drug-haem interactions or to control the damage from these complexes.<sup>150</sup> This is only when the drug has no ability to accumulate for long time inside the food vacuole parasite due to long side chain and low basicity,

therefore, CQ-ala has been shown a significant effect as parasite killer compared to other CQ-derivatives because its short side chain and high basicity.

The same experiment was run for another CPMV modification using control CQ and CPMV-Fc modified particle against *P. falciparum* (strain 3D7) **Figure 7.7**. The control CQ (purple curve) delivers IC<sub>50</sub> values that are identical using an LDH assay method. The initial life cycle stage had a negligible effect on the IC<sub>50</sub> value (from 7.8 to 8.2).

For CPMV-Fc (black curve) it shows good activity with an IC<sub>50</sub> value of 0.309 nM, compared to control CQ. The results are summarized in **Table 7.3**.

**Table 7.3 Proliferation of *P. falciparum* for CPMV-Fc inhibitor assessed using the (LDH) assay.**

Fold of dilution of stock CPMV-Fc	CPMV-Fc concentrations (nM)	CPMV-Fc Log (nM)	%viability
1 in 10	0.3370	-0.472	47.05
1 in 20	0.1685	-0.773	72.24
1 in 40	0.0843	-1.074	86.17
1 in 80	0.0421	-1.376	89.01
1 in 160	0.0211	-1.676	94.48
1 in 320	0.0105	-1.979	94.65
1 in 640	0.0053	-2.275	100.85
1 in 1280	0.0026	-2.585	102.18

CPMV-Fc (black curve) shows around 50% inhibition of the parasite proliferation at the highest concentrations (1:10 dilution of the stock solution which was 3.37 nM). The IC<sub>50</sub> value is estimated to be between 1:10 and 1:20 dilution of the stock sample. This

means that the  $IC_{50}$  value is 0.309 nM, this value is a significantly less than the  $IC_{50}$  value from the control CQ as shown in **Figure 7.7**.

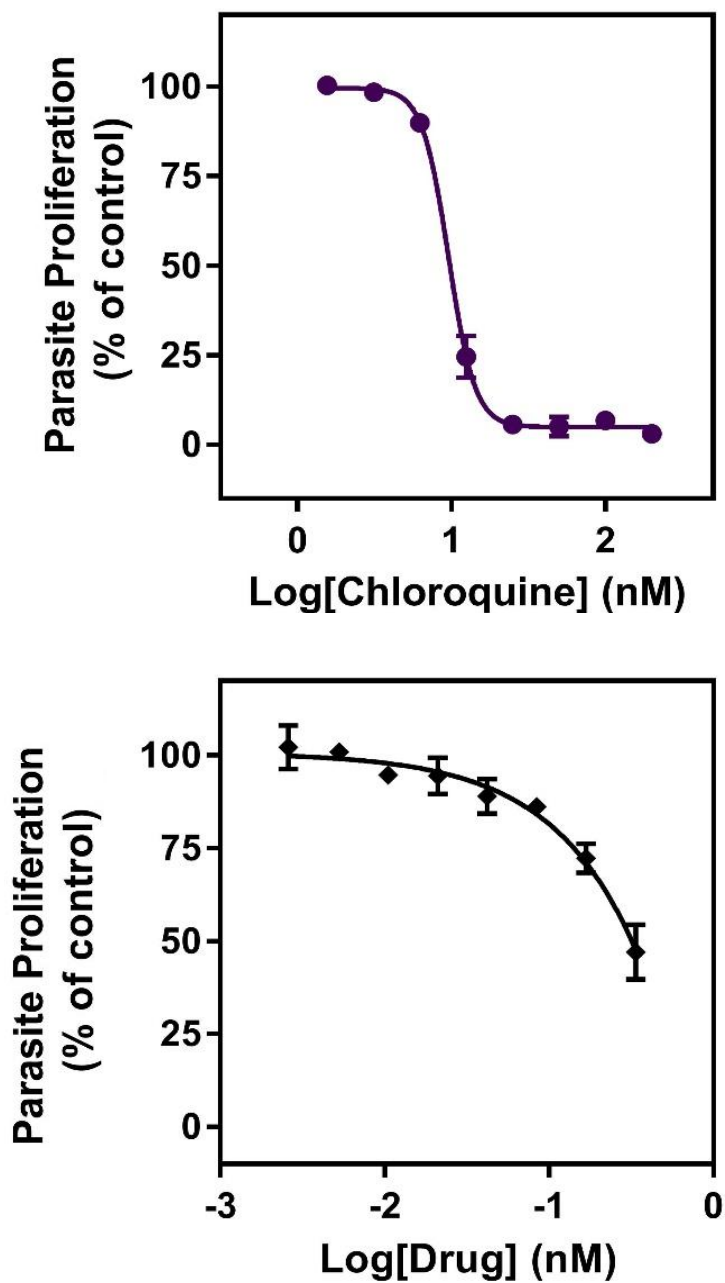


**Figure 7.7** Antimalarial activity of CPMV-Fc analogues against *P. falciparum* (strain 3D7).

In the above experiment Fc was conjugated to CPMV giving 174 Fc per virus particle. Thus increasing the effectiveness of Fc as a killer for malaria parasite. The yield of LDH assay method was good with a Z factor of 0.76.

Conjugation of Fc to CPMV can improve the activity of Fc when it is enclosed on the external surface of CPMV due to its redox properties ferrocene ( $\text{Fe}^{2+}$ )/ferrocenium ( $\text{Fe}^{3+}$ ) system, iron from ferrocene alone can completely release within the liver while iron from conjugated ferrocene is assumed to be accessible to the cells. Thus suggesting generating oxidative stress, creating a reactive oxygen species through a Fenton-like reaction in the FV of the parasite causing parasite's death.<sup>254, 255</sup> This could be the reason behind the remarkable result above. Moreover, the acidic nature of the FV leads to protonate the amines groups as a part of 174 of aminoferrocene which are conjugated to CPMV converted Fc from unprotonated membrane permeable compound to protonated and membrane impermeable then accumulates as a charged form  $\text{Fc}^+$  that can interfere with the polymerization of toxic haem causing parasite's death.<sup>59</sup>

This preliminary observation is remarkable and unprecedented. It has been reported that ferrocene by itself did not have antimalarial activity but it can enhance the effectiveness of the chloroquine when it is bound covalently to the chloroquine to produce (FQ).<sup>255</sup>

Alternatively, when CPMV was modified with both CQ-derivatives and Fc in a double modification, there was no kill effect observed, **Figure 7.8**. There are two reasons to explain this: first the low concentration of CQ-derivatives and ferrocene used in this modification (1.4 nM), second, CPMV aggregation.

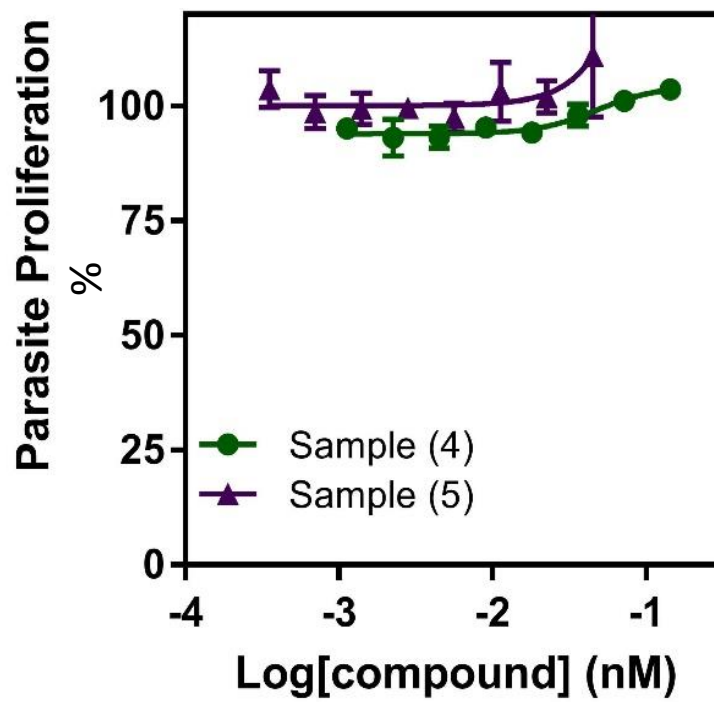
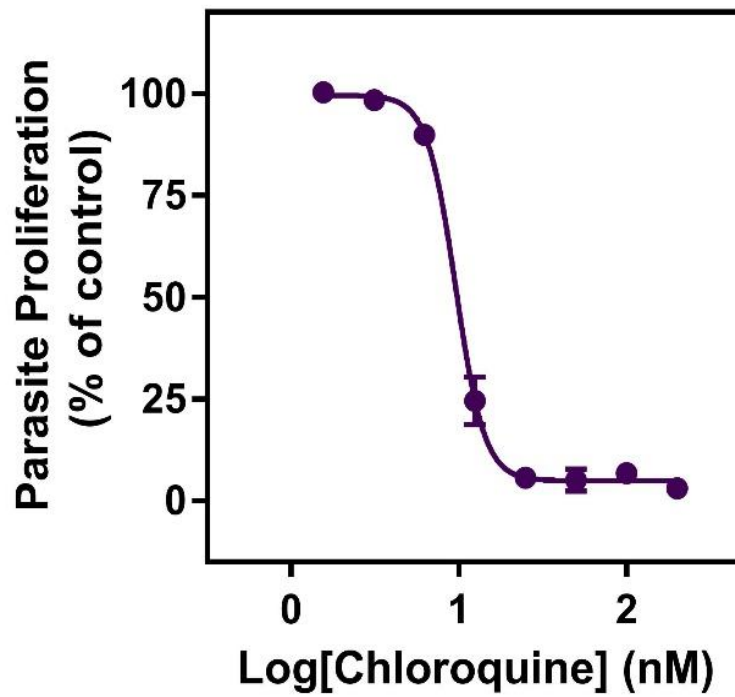


Figure 7.8 Antimalarial activity of CPMV-CQ-derivatives-Fc analogues against *P. falciparum* (strain 3D7). Sample 4 is CPMV-CQp-Fc and sample 5 is CPMV-CQ-ala-Fc.

**Table 7.4 IC<sub>50</sub> value against *P. falciparum* 3D7 for some of known antimalarial drugs.<sup>256</sup>**

<b>Antimalarial drugs</b>	<b>SYBR I assay IC<sub>50</sub></b>	<b>LDH assay IC<sub>50</sub></b>	<b>Treated time in hours</b>
Chloroquine	7.69 ± 2.2 nM	9.55± 3.1 nM	72
Artemisinin	7.88 ±1.3 nM	12.47± 2.3 nM	72
Pyrimethamine	13.89±1.3 nM	12.27± 4.2 nM	72
CPMV-CQ-ala	0.25± 0.02 nM	0.275± 0.01 nM	48
CPMV-Fc	-----	0.309± 0.012 nM	48

For comparison the IC<sub>50</sub> value of some known antimalarial drugs and the IC<sub>50</sub> value of the conjugated CQ-ala and Fc are shown in **Table 7.4**.

The results have shown that CPMV as a carrier vehicle played an important role in increasing the activity of CQ-ala and, apparently, Fc as an antimalarial, compared to many other known antimalarial drugs.

## 7.4 Conclusions

The development of chloroquine (CQ) as an antimalarial drug and the consequent growth of the drug resistant *Plasmodium* strains has had a major effect on global public health in the 20th century.

The major point to be taken from this chapter is that a CQ derivative (CQ-ala) can be used as an effective treatment for *P. falciparum* with an IC<sub>50</sub> range from (44-0.072 μM). A significantly improved kill effect was observed when CPMV was used as a carrier of CQ-ala. This resulted in a drop of the IC<sub>50</sub> value to 0.275nM. Evidencing the importance of the drug delivery system for antimalarial treatment. In addition, and surprisingly, CPMV coupled Fc provided high effectivity as an antimalarial agent although ferrocene alone has no antimalarial activity.

## 8 *Conclusions and future work*

The main purpose of this thesis was to develop non-resistance antimalarial drugs based on the external surface of CPMV which was used as a nanocarrier. The work in this thesis started by synthesis of three different chloroquinoline derivatives with a short side-chain. After that each CQ-derivative was conjugated to the external surface amines of CPMV and the number of each CQ binding to the surface was calculated. Additionally, the thesis explores the stability of CPMV after double modification (CPMV-CQ-derivatives-G.A). Glucuronic acid (G.A) was used here as it has the potential to target relevant tissue. The addressability of carboxylates on the external surface of CPMV was utilised for binding aminoferrocene. Two different strategies were used for the modification of CPMV with ferrocene; first CPMV was modified with each CQ-derivative in a single modification and then modified with ferrocene. The second strategy involved the modification of CPMV with ferrocene first then with each CQ-derivative. It was found that fewer ferrocene bound if the CPMV was modified first with CQ-derivatives.

The chemical modification of CPMV particles to carry multivalent functionalities has driven researchers to develop CPMV as a drug carrier and delivery agent. Here I have demonstrated that CPMV could be functionalised with antimalarial drugs, such as chloroquinoline derivatives. The activity of each CQ-derivative as a beta-haematin inhibitor was investigated compared with control CQ using two different methods. These methods proved to be a good indicator on the activity of the synthesised CQ-derivatives and opened the door for another investigation for these compounds. This included the formation of BH or haemozoin in the presence of biological material in an *in vitro* test against a *P. falciparum* strain (3D7) before and after conjugation to CPMV particles. CQ-ala has the largest effect on BH formation compared to the other CQ-derivatives. The effectivity of CQ-ala with and without conjugation with CPMV as BH inhibitor was

confirmed and a significantly improved kill effect was shown on treatment with CQ-ala after conjugation to CPMV, reducing in the  $IC_{50}$  value to be 0.275nM. This demonstrated that using CPMV as a nano carrier enhanced the activity of CQ-ala as an antimalarial drug.

In addition, the modification of CPMV with ferrocene (Fc) showed surprisingly, high effectivity for Fc as antimalarial compound as ferrocene alone did not have antimalarial activity.

In conclusion, CPMV has been found to be a good carrier vehicle for antimalarial drugs.

For future work, it is important to confirm all antimalarial activity, especially for CPMV-ferrocene, and to assess the CPMV-derivatives for activity against drug resistant malarial strains. Synthesis of more chloroquinoline derivatives with longer side chains (more than 10 carbons atoms long) should help to maintain full activity against resistant strains, and perhaps their activity enhanced when conjugated to the external surface of CPMV. There is a possibility to synthesis ferroquine (FQ) compounds from the synthesised CQ-derivatives described in this study to increase their activity as antimalarial drugs both before and after binding to CPMV. Alternatively, CPMV could be developed as a drug carrier for targeted malarial therapy by modifying the internal surface of CPMV particles with CQ-derivatives.

## 9 References

1. M.C. Daniel and D. Astruc, *Chemical Reviews*, 2004, **104**, 293-346.
2. www.nano.gov, 12/10/2016.
3. H. S. Mansur, *Wiley Interdisciplinary Reviews: Nanomedicine and Nanobiotechnology*, 2010, **2**, 113-129.
4. S. Horikoshi and N. Serpone, *Microwaves in Nanoparticle Synthesis: Fundamentals and Applications*, John Wiley and Sons, 2013.
5. S. Laurent, D. Forge, M. Port, A. Roch, C. Robic, L. Vander Elst and R. N. Muller, *Chemical Reviews*, 2008, **108**, 2064-2110.
6. E. C. Dreaden, A. M. Alkilany, X. Huang, C. J. Murphy and M. A. El-Sayed, *Chemical Society Reviews*, 2012, **41**, 2740-2779.
7. W. K. Shin, J. Cho, A. G. Kannan, Y.-S. Lee and D.-W. Kim, *Scientific Reports*, 2016, **6**, 26332.
8. I. Khan, K. Saeed and I. Khan, *Arabian Journal of Chemistry*, 2017. In Press, <https://doi.org/10.1016/j.arabjc.2017.05.011>
9. www.jnanobiotechnology.com, 08/10/2016.
10. S. K. Murthy, *International Journal of Nanomedicine*, 2007, **2**, 129-141.
11. P. Kumar, P. Kulkarni and A. Srivastava, *Journal of Chemical and Pharmaceutical Research*, 2015, **7**, 703-712.
12. E. Baran and V. Hasirci, *Journal of Materials Science: Materials in Medicine*, 2002, **13**, 1113-1121.
13. R. Duncan, *Nature reviews Drug Discovery*, 2003, **2**, 347-360.

14. M. G. Cascone, L. Lazzeri, C. Carmignani and Z. Zhu, *Journal of Materials Science: Materials in Medicine*, 2002, **13**, 523-526.
15. W. H. De Jong and P. J. Borm, *International Journal of Nanomedicine*, 2008, **3**, 133-149.
16. N. F. Steinmetz, S. N. Shah, J. E. Barclay, G. Rallapalli, G. P. Lomonosoff and D. J. Evans, *Small*, 2009, **5**, 813-816.
17. S. N. Shah, N. F. Steinmetz, A. A. Aljabali, G. P. Lomonosoff and D. J. Evans, *Dalton Transactions*, 2009, 8479-8480.
18. S. Brumfield, D. Willits, L. Tang, J. E. Johnson, T. Douglas and M. Young, *Journal of General Virology*, 2004, **85**, 1049-1053.
19. R. Goldbach, G. Rezelman and A. van Kammen, *Nature*, 1980, **286**, 297-300.
20. R. Langer and N. A. Peppas, *American Institute of Chemical Engineers Journal*, 2003, **49**, 2990-3006.
21. T. Douglas and M. Young, *Science (New York, N.Y.)*, 2006, **312**, 873-875.
22. M. Manchester and P. Singh, *Advanced Drug Delivery Reviews*, 2006, **58**, 1505-1522.
23. T. Stylianopoulos, M.-Z. Poh, N. Insin, M. G. Bawendi, D. Fukumura, L. L. Munn and R. K. Jain, *Biophysical Journal*, 2010, **99**, 1342-1349.
24. N. Steinmetz, *PhD Thesis*, East Anglia, 2006.
25. Z. Wu, K. Chen, I. Yildiz, A. Dirksen, R. Fischer, P. E. Dawson and N. F. Steinmetz, *Nanoscale*, 2012, **4**, 3567-3576.
26. N. F. Steinmetz and D. J. Evans, *Organic and Biomolecular Chemistry*, 2007, **5**, 2891-2902.

27. K. E. Sapsford, W. R. Algar, L. Berti, K. B. Gemmill, B. J. Casey, E. Oh, M. H. Stewart and I. L. Medintz, *Chemical Reviews*, 2013, **113**, 1904-2074.
28. K. B. Narayanan and S. S. Han, *Advances in Colloid and Interface Science*, 2017, **248**, 1-19.
29. M. J. Roossinck, *Philosophical Transactions of the Royal Society B: Biological Sciences*, 2010, **365**, 1899-1905.
30. S. M. Gray and N. Banerjee, *Microbiology and Molecular Biology Reviews*, 1999, **63**, 128-148.
31. L. P. Villarreal, V. R. Defilippis and K. A. Gottlieb, *Virology*, 2000, **272**, 1-6.
32. R. Timian, *Phytopathology*, 1974, **64**, 342-345.
33. J. R. Edwardson and R. G. Christie, *CRC handbook of Viruses Infecting Legumes*, CRC Press, 1991.
34. K. Richert-Poeggeler, C. Staginnus, G. Harper, T. Schwarzacher, C. H. Teo, P. Teycheney, I. C. ML and R. Hull, 2008.
35. J. Handelsman, *Microbiology and Molecular Biology Reviews*, 2004, **68**, 669-685.
36. Q. Wu, Y. Luo, R. Lu, N. Lau, E. C. Lai, W. X. Li and S.-W. Ding, *Proceedings of The National Academy of Sciences*, 2010, **107**, 1606-1611.
37. R. Hull, *Comparative Plant Virology*, Academic Press, 2009.
38. T. Lin, Z. Chen, R. Usha, C. V. Stauffacher, J. B. Dai, T. Schmidt and J. E. Johnson, *Virology*, 1999, **265**, 20-34.
39. G. Lomonosoff and J. Johnson, *Progress in Biophysics and Molecular Biology*, 1991, **55**, 107-137.
40. N. Sanvicens and M. P. Marco, *Trends in Biotechnology*, 2008, **26**, 425-433.

41. Q. Wang, E. Kaltgrad, T. Lin, J. E. Johnson and M. Finn, *Chemistry and Biology*, 2002, **9**, 805-811.
42. G. Lomonossoff and M. Shanks, *The EMBO Journal*, 1983, **2**, 2253-2258.
43. M. Fischer and F. Vögtle, *Angewandte Chemie International Edition*, 1999, **38**, 884-905.
44. V. P. Torchilin, *Advanced Drug Delivery Reviews*, 2012, **64**, 302-315.
45. E. M. Plummer, D. Thomas, G. Destito, L. P. Shriver and M. Manchester, *Nanomedicine*, 2012, **7**, 877-888.
46. C. E. Green, T. Liu, V. Montel, G. Hsiao, R. D. Lester, S. Subramaniam, S. L. Gonias and R. L. Klemke, *PloS one*, 2009, **4**, e6713.
47. H. S. Leong, N. F. Steinmetz, A. Ablack, G. Destito, A. Zijlstra, H. Stuhlmann, M. Manchester and J. D. Lewis, *Nature Protocols*, 2010, **5**, 1406-1417.
48. C. S. Rae, W. Khor, Q. Wang, G. Destito, M. J. Gonzalez, P. Singh, D. M. Thomas, M. N. Estrada, E. Powell and M. Finn, *Virology*, 2005, **343**, 224-235.
49. K. Dalsgaard, Å. Uttenthal, T. D. Jones, F. Xu, A. Merryweather, W. D. Hamilton, J. P. Langeveld, R. S. Boshuizen, S. Kamstrup and G. P. Lomonossoff, *Nature Biotechnology*, 1997, **15**, 248.
50. N. F. Steinmetz, D. J. Evans and G. P. Lomonossoff, *ChemBioChem*, 2007, **8**, 1131-1136.
51. G. Destito, R. Yeh, C. S. Rae, M. Finn and M. Manchester, *Chemistry and Biology*, 2007, **14**, 1152-1162.
52. J. D. Lewis, G. Destito, A. Zijlstra, M. J. Gonzalez, J. P. Quigley, M. Manchester and H. Stuhlmann, *Nature Medicine*, 2006, **12**, 354-360.

53. C.F. Cho, A. Ablack, H.-S. Leong, A. Zijlstra and J. Lewis, *Journal of Visualized Experiments: JoVE*, 2011.
54. E. Strable and M. Finn, in *Viruses and Nanotechnology*, Springer, 2009, pp. 1-21.
55. M. Mammen, S.-K. Choi and G. M. Whitesides, *Angewandte Chemie International Edition*, 1998, **37**, 2754-2794.
56. B. Olenyuk, M. D. Levin, J. A. Whiteford, J. E. Shield and P. J. Stang, *Journal of The American Chemical Society*, 1999, **121**, 10434-10435.
57. K. Saunders and G. P. Lomonossoff, *New Phytologist*, 2013, **200**, 16-26.
58. N. F. Steinmetz, G. P. Lomonossoff and D. J. Evans, *Langmuir*, 2006, **22**, 3488-3490.
59. A. Chatterji, W. F. Ochoa, M. Paine, B. Ratna, J. E. Johnson and T. Lin, *Chemistry and Biology*, 2004, **11**, 855-863.
60. N. F. Steinmetz, T. Lin, G. Lomonossoff and J. Johnson, in *Viruses and Nanotechnology*, Springer, 2009, pp. 23-58.
61. A. A. Aljabali, J. E. Barclay, G. P. Lomonossoff and D. J. Evans, *Nanoscale*, 2010, **2**, 2596-2600.
62. S. K. Dixit, N. L. Goicochea, M.-C. Daniel, A. Murali, L. Bronstein, M. De, B. Stein, V. M. Rotello, C. C. Kao and B. Dragnea, *Nano Letters*, 2006, **6**, 1993-1999.
63. D. E. Prasuhn Jr, R. M. Yeh, A. Obenaus, M. Manchester and M. Finn, *Chemical Communications*, 2007, 1269-1271.
64. A. J. Love, V. Makarov, I. Yaminsky, N. O. Kalinina and M. E. Taliany, *Virology*, 2014, **449**, 133-139.

65. A. A. Aljabali, S. Shukla, G. P. Lomonossoff, N. F. Steinmetz and D. J. Evans, *Molecular Pharmaceutics*, 2012, **10**, 3-10.
66. J. Shi, Z. Xiao, N. Kamaly and O. C. Farokhzad, *Accounts of Chemical Research*, 2011, **44**, 1123-1134.
67. I. Yildiz, S. Shukla and N. F. Steinmetz, *Current Opinion in Biotechnology*, 2011, **22**, 901-908.
68. G. P. Lomonossoff and D. J. Evans, in *Plant Viral Vectors*, Springer, 2011, pp. 61-87.
69. T. Lin and J. E. Johnson, *Advances in Virus Research*, 2003, **62**, 167-239.
70. P. Pescador, I. Katakis, J. L. Toca-Herrera and E. Donath, *Langmuir*, 2008, **24**, 14108-14114.
71. J. E. Besong-Ndika, *PhD Thesis*, University of Helsinki, 2016.
72. P. Yanez-Sedeno and J. Pingarron, *Analytical and Bioanalytical Chemistry*, 2005, **382**, 884-886.
73. F. Caruso and C. Schüller, *Langmuir*, 2000, **16**, 9595-9603.
74. Q. Wang, T. Lin, L. Tang, J. E. Johnson and M. G. Finn, *Angewandte Chemie Int. Ed.*, 2002, **114**, 477-480.
75. T. Lin, Z. Chen, R. Usha, C. V. Stauffacher, J. B. Dai, T. Schmidt and J. E. Johnson, *Virology*, 1999, **265**, 20-34.
76. A. M. Wen, S. Shukla, P. Saxena, A. A. Aljabali, I. Yildiz, S. Dey, J. E. Mealy, A. C. Yang, D. J. Evans and G. P. Lomonossoff, *Biomacromolecules*, 2012, **13**, 3990-4001.

77. Q. Wang, K. S. Raja, K. D. Janda, T. Lin and M. G. Finn, *Bioconjugates Chemistry*, 2003, **14**, 38-43.
78. N. F. Steinmetz, *Journal Pharmaceutics*, 2013, **10 (1)**, 1–2.
79. E. Alemzadeh, A. Dehshahri, K. Izadpanah and F. Ahmadi, *Colloids and Surfaces B: Biointerfaces*, 2018, **167**, 20-27.
80. S. M. Moghimi, A. C. Hunter and J. C. Murray, *The FASEB Journal*, 2005, **19**, 311-330.
81. L. Costa, M. A. F. Faustino, M. G. P. Neves, Â. Cunha and A. Almeida, *Viruses*, 2012, **4**, 1034-1074.
82. I. Yildiz, I. Tsvetkova, A. M. Wen, S. Shukla, M. H. Masarapu, B. Dragnea and N. F. Steinmetz, *RSC Advances*, 2012, **2**, 3670-3677.
83. D. Vandenheuvél, A. Singh, K. Vandersteegen, J. Klumpp, R. Lavigne and G. Van den Mooter, *European Journal of Pharmaceutics and Biopharmaceutics*, 2013, **84**, 578-582.
84. J. K. Pokorski and N. F. Steinmetz, *Molecular Pharmaceutics*, 2010, **8**, 29-43.
85. K. J. Koudelka and M. Manchester, *Current Opinion in Chemical Biology*, 2010, **14**, 810-817.
86. C. Wells, M. Maddaus, S. Erlandsen and R. Simmons, *Infection and Immunity*, 1988, **56**, 278-282.
87. I. Yildiz, K. L. Lee, K. Chen, S. Shukla and N. F. Steinmetz, *Journal of Controlled Release*, 2013, **172**, 568-578.
88. World Health Organization, *World Malaria Report 2015*, World Health Organization, 2016.

89. M. L. Mabaso, B. Sharp and C. Lengeler, *Tropical Medicine and International Health*, 2004, **9**, 846-856.
90. B. L. Sharp, I. Kleinschmidt, E. Streat, R. Maharaj, K. I. Barnes, D. N. Durrheim, F. C. Ridl, N. Morris, I. Seocharan and S. Kunene, *The American Journal of Tropical Medicine and Hygiene*, 2007, **76**, 42-47.
91. J. M. Cohen, D. L. Smith, C. Cotter, A. Ward, G. Yamey, O. J. Sabot and B. Moonen, *Malaria Journal*, 2012, **11**, 122.
92. C. Naing, M. A. Whittaker, V. N. Wai and J. W. Mak, *PLoS Neglected Tropical Diseases*, 2014, **8**, e3071.
93. M. Ahmed and J. Cox - Singh, *ISBT science series*, 2015, **10**, 134-140.
94. A. F. Cowman, J. Healer, D. Marapana and K. Marsh, *Cell*, 2016, **167**, 610-624.
95. L. M. Coronado, C. T. Nadovich and C. Spadafora, *Biochimica et Biophysica Acta (BBA)-General Subjects*, 2014, **1840**, 2032-2041.
96. WWW.embibe.com, 2018.
97. D. R. Bell, P. Jorgensen, E. M. Christophel and K. L. Palmer, *Nature*, 2005, **437**, E3.
98. H. Reyburn, H. Mbakilwa, R. Mwangi, O. Mwerinde, R. Olomi, C. Drakeley and C. J. Whitty, *Bmj*, 2007, **334**, 403-410.
99. C. Wongsrichanalai, M. J. Barcus, S. Muth, A. Sutamihardja and W. H. Wernsdorfer, *The American Journal of Tropical Medicine and Hygiene*, 2007, **77**, 119-127.
100. WHO, Weekly Epidemiol. Rep. 3.(1996) **17**, 913 - 936.
101. WHO, Weekly Epidemiol. Rep. 4 (1996) **25**, 624 - 638.

102. WHO, *Weekly Epidemiol. Rep.* 5 (1996) **37**, 324 - 340.
103. N. White, F. Nosten, S. Looareesuwan, W. Watkins, K. Marsh, R. Snow, G. Kokwaro, J. Ouma, T. Hien and M. Molyneux, *The Lancet*, 1999, **353**, 1965-1967.
104. D. J. Krogstad, *Epidemiologic Reviews*, 1996, **18**, 77-89.
105. N. J. White, *The Journal of Clinical Investigation*, 2004, **113**, 1084-1092.
106. I. Petersen, R. Eastman and M. Lanzer, *FEBS letters*, 2011, **585**, 1551-1562.
107. T. J. Egan, *Mini Reviews in Medicinal Chemistry*, 2001, **1**, 113-123.
108. D. De, F. M. Krogstad, F. B. Cogswell and D. J. Krogstad, *The American Journal of Tropical Medicine and Hygiene*, 1996, **55**, 579-583.
109. J. Wiesner, R. Ortmann, H. Jomaa and M. Schlitzer, *Angewandte Chemie International Edition*, 2003, **42**, 5274-5293.
110. P. M. O'Neill, D. J. Willock, S. R. Hawley, P. G. Bray, R. C. Storr, S. A. Ward and B. K. Park, *Journal of Medicinal Chemistry*, 1997, **40**, 437-448.
111. D. A. Fidock, T. Nomura, A. K. Talley, R. A. Cooper, S. M. Dzekunov, M. T. Ferdig, L. M. Ursos, B. Naudé, K. W. Deitsch and X. Z. Su, *Molecular Cell*, 2000, **6**, 861-871.
112. J. Burckhalter, F. Tendick, E. M. Jones, P. A. Jones, W. Holcomb and A. Rawlins, *Journal of the American Chemical Society*, 1948, **70**, 1363-1373.
113. B. Rouveix, L. Coulombel, J. Aymard, F. Chau and L. Abel, *British Journal of Haematology*, 1989, **71**, 7-11.
114. E. Păunescu, S. Susplugas, E. Boll, R. Varga, E. Mouray, I. Grosu, P. Grellier and P. Melnyk, *ChemMedChem*, 2009, **4**, 549-561.

115. A. P. Gorka, *Investigating the cytostatic and cytotoxic mechanisms of quinoline drug resistance in Plasmodium falciparum*, Georgetown University, 2013.
116. I. Solomonov, M. Osipova, Y. Feldman, C. Baetz, K. Kjaer, I. K. Robinson, G. T. Webster, D. McNaughton, B. R. Wood and I. Weissbuch, *Journal of the American Chemical Society*, 2007, **129**, 2615-2627.
117. S. R. Hawley, P. G. Bray, P. M. O'Neill, B. K. Park and S. A. Ward, *Biochemical Pharmacology*, 1996, **52**, 723-733.
118. N. Juge, S. Moriyama, T. Miyaji, M. Kawakami, H. Iwai, T. Fukui, N. Nelson, H. Omote and Y. Moriyama, *Proceedings of the National Academy of Sciences*, 2015, **112**, 3356-3361.
119. A. R. Parhizgar and A. Tahghighi, *Iranian Journal of Medical Sciences*, 2017, **42**, 115-128.
120. R. H. Fish and G. Jaouen, *Organometallics*, 2003, **22**, 2166-2177.
121. K. E. Dombrowski, W. Baldwin and J. E. Sheats, *Journal of Organometallic Chemistry*, 1986, **302**, 281-306.
122. P. Meunier, I. Ouattara, B. Gautheron, J. Tirouflet, D. Camboli and J. Besancon, *European Journal of Medicinal Chemistry*, 1991, **26**, 351-362.
123. S. Top, J. Tang, A. Vessières, D. Carrez, C. Provot and G. Jaouen, *Chemical Communications*, 1996, 955-956.
124. A. Štimac, J. Lapić, V. Blasina, M. Lukinac, S. Djaković, I. Crnolatac, L. Frkanec and R. Frkanec, *Applied Organometallic Chemistry*, 2017, **32**, 4042-4056.
125. P. Kopf-Maier and H. Kopf, *Drugs of the Future*, 1986, **11**, 297-307.

126. C. Biot, N. François, L. Maciejewski, J. Brocard and D. Poulain, *Bioorganic and Medicinal Chemistry Letters*, 2000, **10**, 839-841.
127. T. Itoh, S. Shirakami, N. Ishida, Y. Yamashita, T. Yoshida, H.-S. Kim and Y. Wataya, *Bioorganic and Medicinal Chemistry Letters*, 2000, **10**, 1657-1659.
128. C. Baldoli, S. Maiorana, E. Licandro, G. Zinzalla and D. Perdicchia, *Organic Letters*, 2002, **4**, 4341-4344.
129. C. S. Allardyce, A. Dorcier, C. Scolaro and P. J. Dyson, *Applied Organometallic Chemistry*, 2005, **19**, 1-10.
130. C. Biot, G. Glorian, L. A. Maciejewski, J. S. Brocard, O. Domarle, G. Blampain, P. Millet, A. J. Georges, H. Abessolo and D. Dive, *Journal of Medicinal Chemistry*, 1997, **40**, 3715-3718.
131. C. Biot, W. Daher, C. M. Ndiaye, P. Melnyk, B. Pradines, N. Chavain, A. Pellet, L. Fraisse, L. Pelinski and C. Jarry, *Journal of Medicinal Chemistry*, 2006, **49**, 4707-4714.
132. C. Biot, L. Delhaes, C. N'Diaye, L. Maciejewski, D. Camus, D. Dive and J. Brocard, *Bioorganic and Medicinal Chemistry*, 1999, **7**, 2843-2847.
133. C. Biot, D. Taramelli, I. Forfar-Bares, L. A. Maciejewski, M. Boyce, G. Nowogrocki, J. S. Brocard, N. Basilico, P. Olliaro and T. J. Egan, *Molecular Pharmaceutics*, 2005, **2**, 185-193.
134. R. L. Prior, *The American Journal of Clinical Nutrition*, 2003, **78**, 570S-578S.
135. A. R. Manolescu, K. Witkowska, A. Kinnaird, T. Cessford and C. Cheeseman, *Physiology*, 2007, **22**, 234-240.
136. S. A. Desai, D. J. Krogstad and E. W. McCleskey, *Nature*, 1993, **362**, 643-646.

137. S. A. Desai and R. L. Rosenberg, *Proceedings of the National Academy of Sciences*, 1997, **94**, 2045-2049.
138. K. Kirk, H. A. Horner and J. Kirk, *Molecular and Biochemical Parasitology*, 1996, **82**, 195-205.
139. C. J. Woodrow, J. I. Penny and S. Krishna, *Journal of Biological Chemistry*, 1999, **274**, 7272-7277.
140. A. P. Patel, H. M. Staines and S. Krishna, *Travel Medicine and Infectious Disease*, 2008, **6**, 58-66.
141. I. D. Goodyer, D. J. Hayes and R. Eiseenthal, *Molecular and Biochemical Parasitology*, 1997, **84**, 229-239.
142. J. I. Penny, S. T. Hall, C. J. Woodrow, G. M. Cowan, A. M. Gero and S. Krishna, *Molecular and Biochemical Parasitology*, 1998, **93**, 81-89.
143. J.M. Liu, *Reprinted from Acta Chimica Sinica.*, 1979, **37**, 129-143.
144. S. R. Meshnick, A. Thomas, A. Ranz, C. M. Xu and H. Z. Pan, *Molecular and Biochemical Parasitology*, 1991, **49**, 181-189.
145. C. C. R. Group, *Journal of Traditional Chinese Medicine*, 1982, **2**, 1-16.
146. A. J. Lin, L. Q. Li, S. L. Andersen and D. L. Klayman, *Journal of Medicinal Chemistry*, 1992, **35**, 1639-1642.
147. A. Olliaro and T. Wells, *Clinical Pharmacology and Therapeutics*, 2009, **85**, 584-595.
148. T. N. Wells, P. L. Alonso and W. E. Gutteridge, *Nature Reviews Drug Discovery*, 2009, **8**, 879-891.

149. T. J. Egan, J. Y. Chen, K. A. de Villiers, T. E. Mabotha, K. J. Naidoo, K. K. Ncokazi, S. J. Langford, D. McNaughton, S. Pandiancherri and B. R. Wood, *FEBS letters*, 2006, **580**, 5105-5110.
150. M. J. Gardner, N. Hall, E. Fung, O. White, M. Berriman, R. W. Hyman, J. M. Carlton, A. Pain, K. E. Nelson and S. Bowman, *Nature*, 2002, **419**, 498-511.
151. J. N. Domínguez, J. E. Charris, G. Lobo, N. G. de Domínguez, M. A. M. Moreno, F. Riggione, E. Sanchez, J. Olson and P. J. Rosenthal, *European Journal of Medicinal Chemistry*, 2001, **36**, 555-560.
152. V. P. Sharma, *Malaria Journal*, 2007, **6**, 105-110.
153. P. M. O'Neill, P. G. Bray, S. R. Hawley, S. A. Ward and B. K. Park, *Pharmacology and Therapeutics*, 1998, **77**, 29-58.
154. S. Tripathy, S. Das, S. P. Chakraborty, S. K. Sahu, P. Pramanik and S. Roy, *International Journal of Pharmaceutics*, 2012, **434**, 292-305.
155. Y. Kato, H. Onishi and Y. Machida, *Current Pharmaceutical Biotechnology*, 2003, **4**, 303-309.
156. D. Bhadra, S. Bhadra and N. Jain, *Pharmaceutical Research*, 2006, **23**, 623-633.
157. C. Biot, W. Castro, C. Y. Botté and M. Navarro, *Dalton Transactions*, 2012, **41**, 6335-6349.
158. M. F. Fouda, M. M. Abd-Elzaher, R. A. Abdelsamaia and A. A. Labib, *Applied Organometallic Chemistry*, 2007, **21**, 613-625.
159. P. Beagley, M. A. Blackie, K. Chibale, C. Clarkson, J. R. Moss and P. J. Smith, *Journal of the Chemical Society, Dalton Transactions*, 2002, 4426-4433.
160. C. Biot, J. Dessolin, I. Ricard and D. Dive, *Journal of Organometallic Chemistry*, 2004, **689**, 4678-4682.
161. P. F. Salas, C. Herrmann and C. Orvig, *Chemical Reviews*, 2013, **113**, 3450-3492.

162. C. L. Ferreira, C. B. Ewart, C. A. Barta, S. Little, V. Yardley, C. Martins, E. Polishchuk, P. J. Smith, J. R. Moss and M. Merkel, *Inorganic Chemistry*, 2006, **45**, 8414-8422.
163. K. Saunders, F. Sainsbury and G. P. Lomonossoff, *Virology*, 2009, **393**, 329-337.
164. A. A. Aljabali, *PhD thesis*, University of East Anglia, 2011.
165. T. Sakai and J. Gross, *Biochemistry*, 1967, **6**, 518-528.
166. S. J. Burgess, A. Selzer, J. X. Kelly, M. J. Smilkstein, M. K. Riscoe and D. H. Peyton, *Journal of Medicinal Chemistry*, 2006, **49**, 5623-5625.
167. S. Delarue-Cochin, P. Grellier, L. Maes, E. Mouray, C. Sergheraert and P. Melnyk, *European Journal of Medicinal Chemistry*, 2008, **43**, 2045-2055.
168. C. Ruß, F. Ilgen, C. Reil, C. Luff, A. H. Begli and B. König, *Green Chemistry*, 2011, **13**, 156-161.
169. J. Das, S. N. Patil, R. Awasthi, C. P. Narasimhulu and S. Trehan, *Synthesis*, 2005, **2005**, 1801-1806.
170. N. F. Steinmetz, G. P. Lomonossoff and D. Evans, *Small*, 2006, **2**, 530-533.
171. A. M. Wen, K. L. Lee, P. Cao, K. Pangilinan, B. L. Carpenter, P. Lam, F. A. Veliz, R. A. Ghiladi, R. C. Advincula and N. F. Steinmetz, *Bioconjugate Chemistry*, 2016, **27**, 1227-1235.
172. C.F. Cho, S. Shukla, E. J. Simpson, N. F. Steinmetz, L. G. Luyt and J. D. Lewis, *Virus Hybrids as Nanomaterials: Methods and Protocols*, 2014, 211-230.
173. A. A. Aljabali, J. E. Barclay, J. N. Butt, G. P. Lomonossoff and D. J. Evans, *Dalton Transactions*, 2010, **39**, 7569-7574.
174. N. T. Huy, D. T. Uyen, M. Sasai, T. Shiono, S. Harada and K. Kamei, *Analytical Biochemistry*, 2006, **354**, 305-307.
175. A. F. Slater, W. J. Swiggard, B. R. Orton, W. D. Flitter, D. E. Goldberg, A. Cerami and G. B. Henderson, *Proceedings of the National Academy of Sciences of the United States of America*, 1991, **88**, 325-329.
176. R. M. Silverstein, G. C. Bassler and T. C. Morrill, *Spectroscopic Identification of Organic Compounds*, John Wiley and Sons, New York, 1981.

177. S. Tabassum, T. S. Kumara, J. P. Jasinski, S. P. Millikan, H. Yathirajan, P. S. Ganapathy, H. Sowmya, S. S. More, G. Nagendrappa and M. Kaur, *Journal of Molecular Structure*, 2014, **1070**, 10-20.
178. J. Ursing, P.-E. Kofoed, A. Rodrigues, L. Rombo and J. P. Gil, *The American Journal of Tropical Medicine and Hygiene*, 2007, **76**, 844-848.
179. S. Kondaparla, P. Agarwal, K. Srivastava, S. K. Puri and S. B. Katti, *Chemical Biology and Drug Design*, 2017, **89**, 901-906.
180. G. Tojo and M. Fernández, *Oxidation of Alcohols to Aldehydes and Ketones: A Guide to Current Common Practice*, Springer, 2006, pp.1-5.
181. J. Wellink, *In Plant Virology Protocols*, Springer, 1998, pp. 205-209.
182. J. M. Berg, J. L. Tymoczko and L. Stryer, *Biochemistry (5th ed.)*. New York: WH Freeman, 2002, 851-854.
183. D. S. Kryndushkin, I. M. Alexandrov, M. D. Ter-Avanesyan and V. V. Kushnirov, *Journal of Biological Chemistry*, 2003, **278**, 49636-49643.
184. D. L. Smisek and D. A. Hoagland, *Macromolecules*, 1989, **22**, 2270-2277.
185. H. Schägger, *Nature Protocols*, 2006, **1**, 16-22.
186. R. R. Sinden, *DNA Structure and Function*, Elsevier, 2012.
187. R. E. Feeney, R. B. Yamasaki and K. F. Geoghegan, *Chemical Modification of Proteins: An Overview*, American Chemical Society, 1982, pp. 3–55.
188. J. E. Kinsella and K.J. Shetty, *Chemical Modification for Improving Functional Properties of Plant and Yeast Proteins*, American Chemical Society, 1979, PP. 37–63.
189. A. Agrawal and M. Manchester, *Biomacromolecules*, 2012, **13**, 3320-3326.
190. A. M. Lehane, R. Hayward, K. J. Saliba and K. Kirk, *Journal of Cell Science*, 2008, **121**, 1624-1632.
191. P. Sudre, J. G. Breman, D. McFarland and J. Koplan, *International Journal of Epidemiology*, 1992, **21**, 146-154.
192. D. P. Iwaniuk, E. D. Whetmore, N. Rosa, K. Ekoue-Kovi, J. Alumasa, A. C. de Dios, P. D. Roepe and C. Wolf, *Bioorganic and Medicinal Chemistry*, 2009, **17**, 6560-6566.

193. E. W. Abel, N. J. Long, K. G. Orrell, A. G. Osborne and V. Šik, *Journal of Organometallic Chemistry*, 1991, **403**, 195-208.
194. C. A. Nijhuis, B. J. Ravoo, J. Huskens and D. N. Reinhoudt, *Coordination Chemistry Reviews*, 2007, **251**, 1761-1780.
195. C. E. Housecroft, *Inorganic chemistry*, Prentice Hall, Harlow: 4th ed. edn., 2012.
196. N. G. Connelly and W. E. Geiger, *Chemical Reviews*, 1996, **96**, 877-910.
197. M. Malischewski, M. Adelhardt, J. Sutter, K. Meyer and K. Seppelt, *Science (New York, N.Y.)*, 2016, **353**, 678-682.
198. D. Conroy, A. Moisala, S. Cardoso, A. Windle and J. Davidson, *Chemical Engineering Science*, 2010, **65**, 2965-2977.
199. D. R. Van Staveren and N. Metzler-Nolte, *Chemical Reviews*, 2004, **104**, 5931-5986.
200. K. M. Taylor, V. E. Spall, P. Jonathan, G. Butler and G. P. Lomonosoff, *Virology*, 1999, **255**, 129-137.
201. R. N. Adams, *Electrochemistry at Solid Electrodes*, Marcel Dekker, Inc., New York, 1969.
202. A. Slater and A. Cerami, *Nature*, 1992, **355**, 167-169.
203. C. D. Fitch and A. C. Chou, *Molecular and Biochemical Parasitology*, 1996, **82**, 261-264.
204. T. J. Egan, D. C. Ross and P. A. Adams, *FEBS letters*, 1994, **352**, 54-57.
205. A. Dorn, R. Stoffel, H. Matile, A. Bubendorf and R. G. Ridley, *Nature*, 1995, **374**, 269.
206. D. J. Sullivan, I. Y. Gluzman, D. G. Russell and D. E. Goldberg, *Proceedings of the National Academy of Sciences*, 1996, **93**, 11865-11870.
207. N. Basilico, D. Monti, P. Oliaro and D. Taramelli, *Febs Letters*, 1997, **409**, 297-299.
208. D. Gollin and C. Zimmermann, *Malaria: Disease Impacts and Long-Run Income Differences*, Discussion Paper No. 2997 August 2007.

209. Teklehaimanot and A. Paola Mejia, *Annals of the New York Academy of Sciences*, 2008, **1136**, 32-37.
210. K. Matuschewski, A. C. Nunes, V. Nussenzweig and R. Ménard, *The EMBO Journal*, 2002, **21**, 1597-1606.
211. M. Prudêncio, A. Rodriguez and M. M. Mota, *Nature Reviews Microbiology*, 2006, **4**, 849-856.
212. L. Tilley, M. W. Dixon and K. Kirk, *The International Journal of Biochemistry and Cell Biology*, 2011, **43**, 839-842.
213. R. Lemberg and J. Legge, *Hematin Compounds and Bile Pigments; Their Constitution, Metabolism, and Function*, New York, 1949.
214. C. D. Fitch, R. Chevli, P. Kanjananggulpan, P. Dutta, K. Chevli and A. C. Chou, *Blood*, 1983, **62**, 1165-1168.
215. C. D. Fitch and P. Kanjananggulpan, *Journal of Biological Chemistry*, 1987, **262**, 15552-15555.
216. S. Pagola, P. W. Stephens, D. S. Bohle, A. D. Kosar and S. K. Madsen, *Nature*, 2000, **404**, 307-310.
217. E. Hempelmann, *Parasitology Research*, 2007, **100**, 671-676.
218. S. E. Francis, D. J. Sullivan Jr, Goldberg and D. E, *Annual Reviews in Microbiology*, 1997, **51**, 97-123.
219. I. Y. Gluzman, S. E. Francis, A. Oksman, C. E. Smith, K. L. Duffin and D. E. Goldberg, *The Journal of Clinical Investigation*, 1994, **93**, 1602-1608.
220. D. Goldberg and A. Slater, *Parasitology Today*, 1992, **8**, 280-283.
221. P. Loria, S. Miller, M. Foley and L. Tilley, *Biochemical Journal*, 1999, **339**, 363-370.
222. H. Ginsburg, O. Famin, J. Zhang and M. Krugliak, *Biochemical Pharmacology*, 1998, **56**, 1305-1313.
223. A. K. Tripathi, S. I. Khan, L. A. Walker and B. L. Tekwani, *Analytical Biochemistry*, 2004, **325**, 85-91.
224. C. Wongsrichanalai, A. L. Pickard, W. H. Wernsdorfer and S. R. Meshnick, *The Lancet Infectious Diseases*, 2002, **2**, 209-218.

225. T. J. Egan, *Journal of Inorganic Biochemistry*, 2002, **91**, 19-26.
226. R. G. Ridley, W. Hofheinz, H. Matile, C. Jaquet, A. Dorn, R. Masciadri, S. Jolidon, W. F. Richter, A. Guenzi and M.-A. Girometta, *Antimicrobial Agents and Chemotherapy*, 1996, **40**, 1846-1854.
227. Y. Kurosawa, A. Dorn, M. Kitsuji-Shirane, H. Shimada, T. Satoh, H. Matile, W. Hofheinz, R. Masciadri, M. Kansy and R. G. Ridley, *Antimicrobial Agents and Chemotherapy*, 2000, **44**, 2638-2644.
228. A. Dorn, S. R. Vippagunta, H. Matile, A. Bubendorf, J. L. Vennerstrom and R. G. Ridley, *Biochemical Pharmacology*, 1998, **55**, 737-747.
229. T. B. Ozcelik, B. Yilmaz, I. Ozcan and C. Kircelli, *Journal of Prosthetic Dentistry*, 2008, **99**, 193-202.
230. T. J. Egan, *Journal of Inorganic Biochemistry*, 2008, **102**, 1288-1299.
231. N. Ercal, H. Gurer-Orhan and N. Aykin-Burns, *Current Topics in Medicinal Chemistry*, 2001, **1**, 529-539.
232. M. K. Roders, E. A. Glende and R. O. Recknagel, *Science (New York, N.Y.)*, 1977, **196**, 1221-1222.
233. A. Benedetti, A. F. Casini, M. Ferrali and M. Comporti, *Biochemical Journal*, 1979, **180**, 303-312.
234. J. Peisach, W. Blumberg and E. Rachmilewitz, *Biochimica et Biophysica Acta (BBA)-Protein Structure*, 1975, **393**, 404-418.
235. S. Kumar and U. Bandyopadhyay, *Toxicology Letters*, 2005, **157**, 175-188.
236. S. Verma, S. Pandey, P. Agarwal, P. Verma, S. Deshpande, J. K. Saxena, K. Srivastava, P. M. Chauhan and Y. S. Prabhakar, *RSC Advances*, 2016, **6**, 25584-25593.
237. T. J. Egan, W. W. Mavuso and K. K. Ncokazi, *Biochemistry*, 2001, **40**, 204-213.
238. M. Jaramillo, M. J. Bellemare, C. Martel, M. T. Shio, A. P. Contreras, M. Godbout, M. Roger, E. Gaudreault, J. Gosselin and D. S. Bohle, *PloS one*, 2009, **4**, e6957.
239. Y. Gossuin, P. O. Ndjolo, Q. L. Vuong and P. Duez, *Scientific Reports*, 2017, **7**, 14557-14564.

240. M. Olivier, K. Van Den Ham, M. T. Shio, F. A. Kassa and S. Fougeray, *Frontiers in Immunology*, 2014, **5**, 25-33.
241. B. Halliwell and J. M. Gutteridge, in *Methods in Enzymology*, Elsevier, 1990, vol. 186, pp. 1-85.
242. S. Kumar, S. K. Das, S. Dey, P. Maity, M. Guha, V. Choubey, G. Panda and U. Bandyopadhyay, *Antimicrobial Agents and Chemotherapy*, 2008, **52**, 705-715.
243. P. Aravind and M. Prasad, *Plant Science*, 2004, **166**, 1321-1327.
244. C. Yuen and Q. Liu, *Journal of Biomedical Optics*, 2012, **17**, 017005.
245. S. Sarkar, A. A. Siddiqui, S. J. Saha, R. De, S. Mazumder, C. Banerjee, M. S. Iqbal, S. Nag, S. Adhikari and U. Bandyopadhyay, *Antimicrobial Agents and Chemotherapy*, 2016, **60**, 4217-4228.
246. F. Hosseini, M. Seyedsadjadi and N. Farhadyar, *Oriental Journal of Chemistry*, 2014, **30**, 1609-1618.
247. L. H. Miller, H. C. Ackerman, X.-z. Su and T. E. Wellems, *Nature Medicine*, 2013, **19**, 156-167.
248. W. H. Organization, *Antimicrobial Resistance: Global Report on Surveillance*, World Health Organization, 2014.
249. Y. F. Chehuan, M. R. Costa, J. S. Costa, M. G. Alecrim, F. Nogueira, H. Silveira, L. W. Brasil, G. C. Melo, W. M. Monteiro and M. V. Lacerda, *Malaria Journal*, 2013, **12**, 226-231.
250. A. C. Chou, R. Chevli and C. D. Fitch, *Biochemistry*, 1980, **19**, 1543-1549.
251. A. Dorn, S. R. Vippagunta, H. Matile, C. Jaquet, J. L. Vennerstrom and R. G. Ridley, *Biochemical Pharmacology*, 1998, **55**, 727-736.
252. D. A. van Schalkwyk, R. W. Moon, B. Blasco and C. J. Sutherland, *Journal of Antimicrobial Chemotherapy*, 2017, **72**, 3051-3058.
253. S. R. Hawley, P. G. Bray, M. Mungthin, J. D. Atkinson, P. M. O'Neill and S. A. Ward, *Antimicrobial Agents and Chemotherapy*, 1998, **42**, 682-686.
254. A. Singh, J. Gut, P. J. Rosenthal and V. Kumar, *European Journal of Medicinal Chemistry*, 2017, **125**, 269-277.

255. O. Domarle, G. Blampain, H. Agnanié, T. Nzadiyabi, J. Lebibi, J. Brocard, L. Maciejewski, C. Biot, A. Georges and P. Millet, *Antimicrobial Agents and Chemotherapy*, 1998, **42**, 540-544.
256. S. Moon, S. Lee, H. Kim, L. H. Freitas-Junior, M. Kang, L. Ayong and M. A. Hansen, *PloS one*, 2013, **8**, e61812.

## *Publications*

- 1- The 6<sup>th</sup> PhD experience conference (attendance), university of Hull 2015.
- 2- The 7<sup>th</sup> PhD experience conference (poster), university of Hull 2016.
- 3- Mercia 3<sup>th</sup> Annual Meeting (poster), university of Keel 2017.
- 4-Taming Plant Virus-Fundamental Biology to Bionanotechnology (poster), Scotland 2016.
- 5-PG colloquia, (presentation) university of Hull 2018.

## Appendix 1

FT-IR spectrum for BH formed with and without treatment by CQ-derivatives.

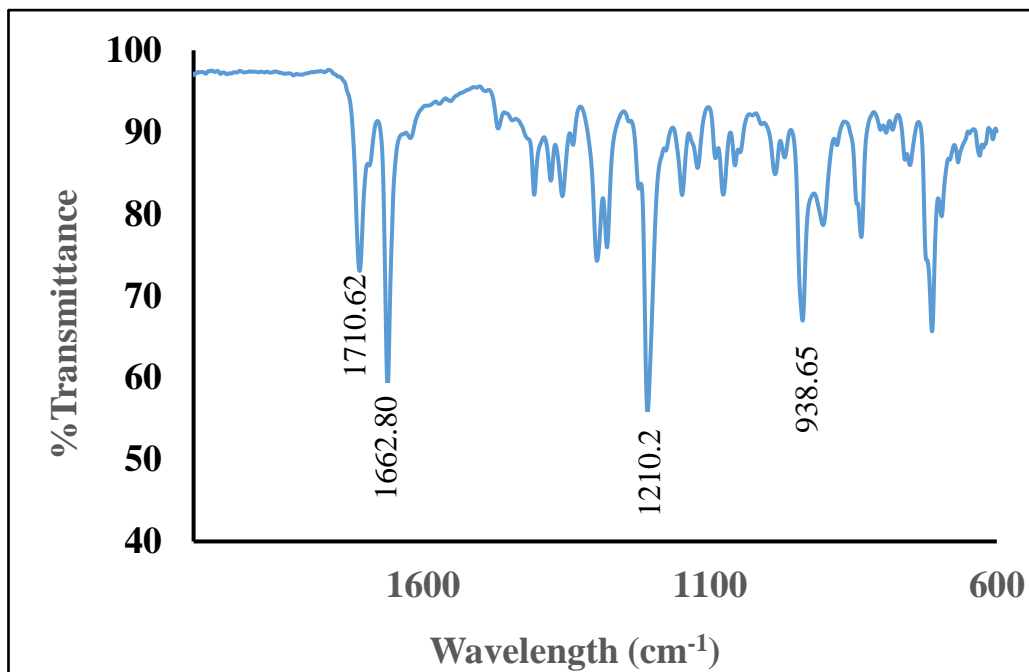


**Figure1** FT-IR spectra of BH formation after 10  $\mu$ M CQp treatment.

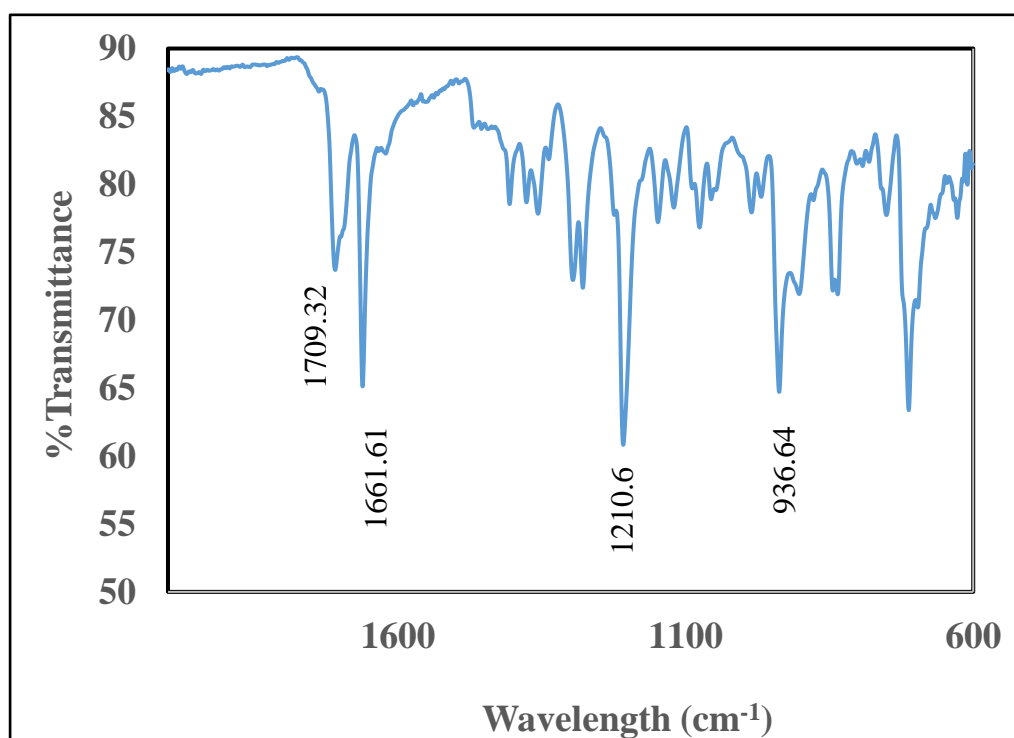


**Figure2** FT-IR spectra of BH formation after 10  $\mu$ M CQ-ala treatment.

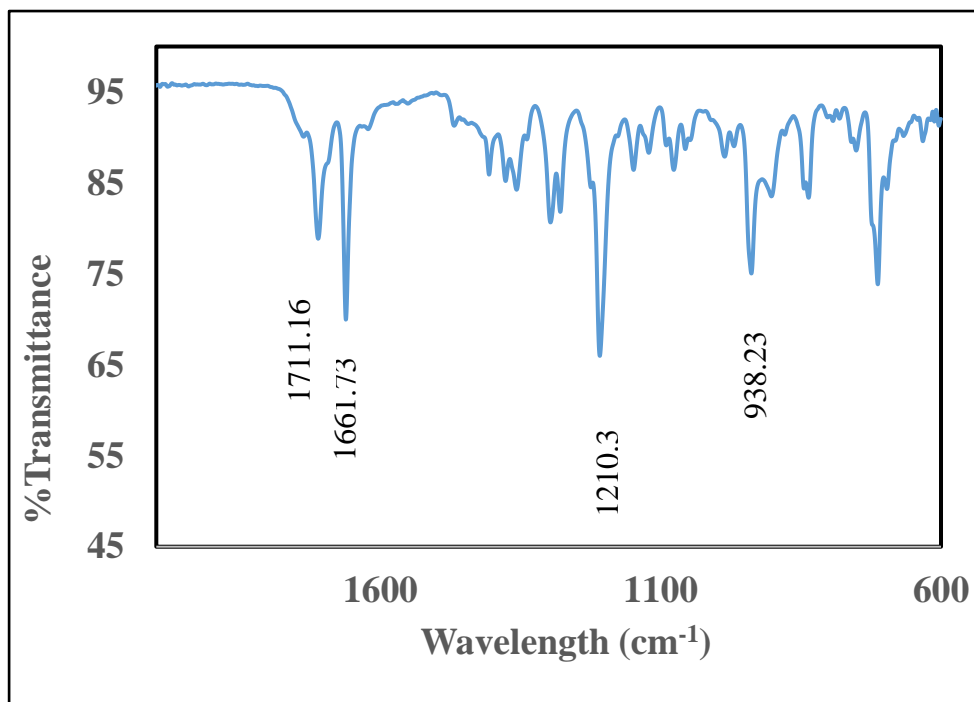


**Figure3** FT-IR spectra of BH formation after 10  $\mu$ M CQ-val treatment.

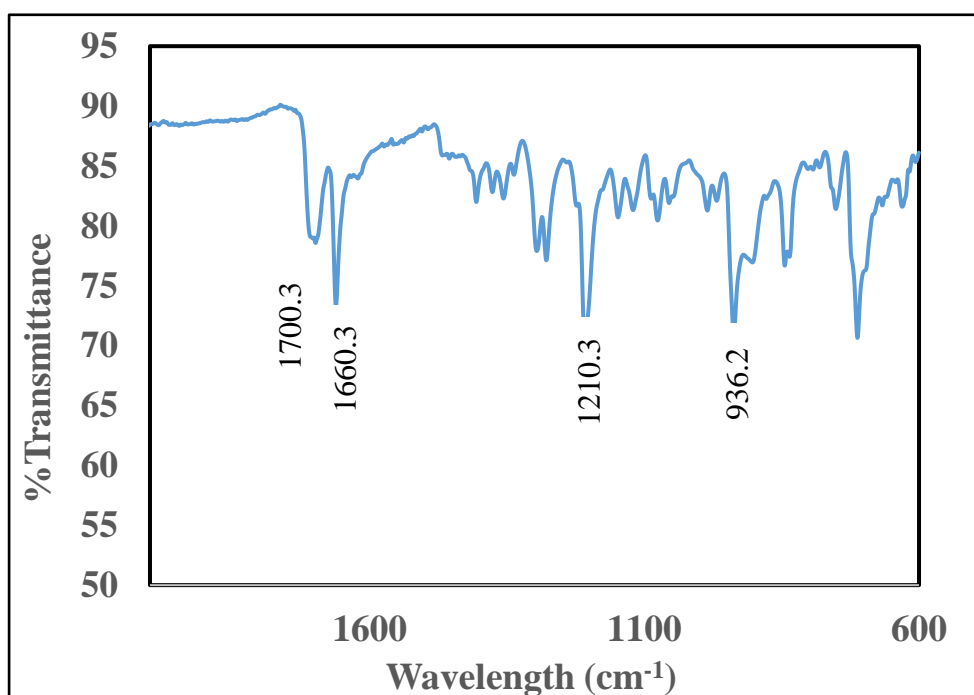


**Figure4** FT-IR spectra of BH formation after 50  $\mu$ M CQp treatment.

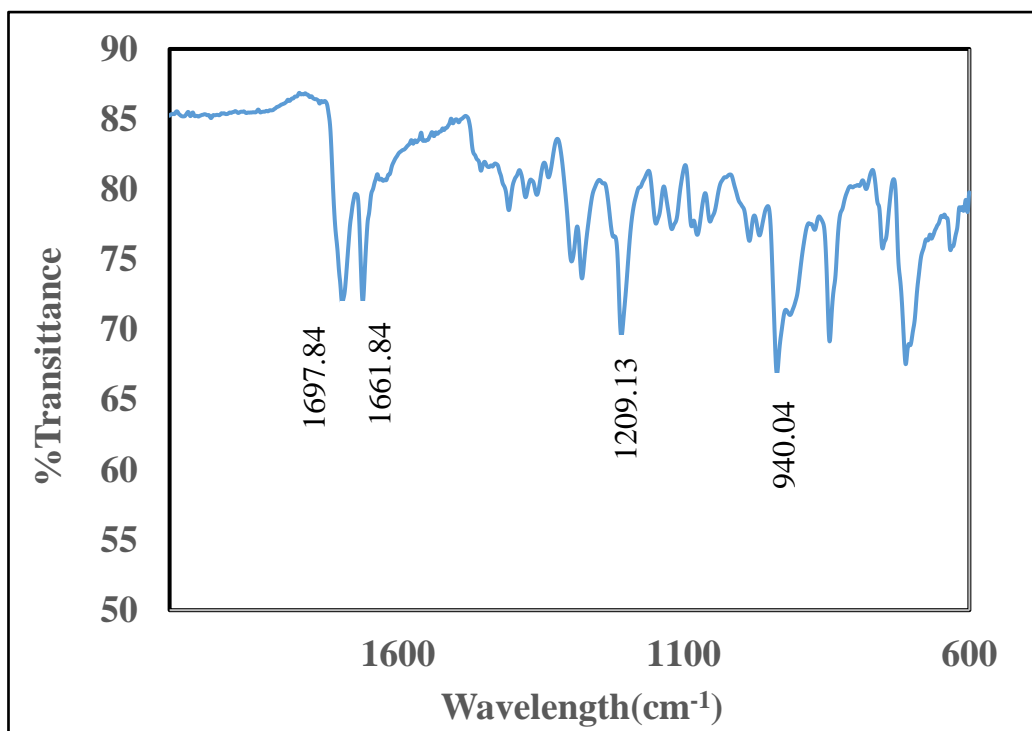


**Figure 5** FT-IR spectra of BH formation after 50  $\mu$ M CQ-ala treatment.

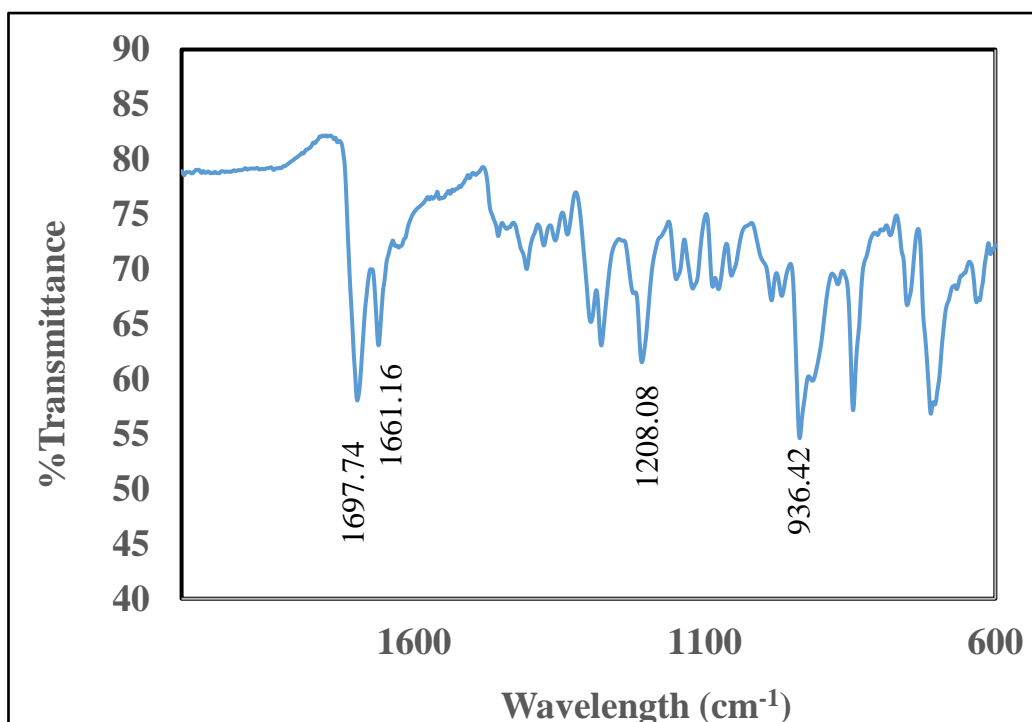


**Figure 6** FT-IR spectra of BH formation after 50  $\mu$ M CQ-val treatment.

## Appendix 2

### Crystal structure details for 3-(7-chloroquinolin-4-ylamino) propan-1-ol

The crystal structure confirms the expected composition. The asymmetric unit contains a single chlorquinoline molecule ( $C_{12}H_{13}Cl_1N_2O_1$ ). There is no solvent and no disorder in the structure. The compound crystallises in the centrosymmetric space group  $P2_1/n$  with a single molecule in the asymmetric unit as shown below.

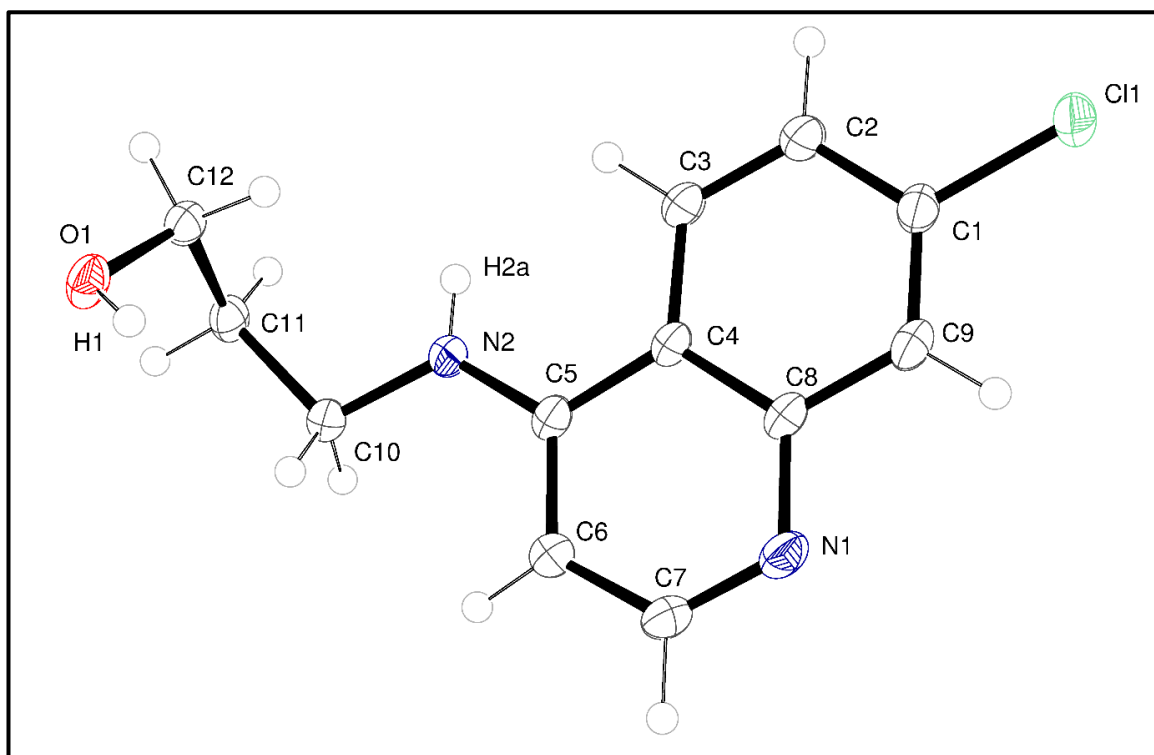


**Figure 1** Asymmetric unit of 3-(7-chloroquinolin-4-ylamino) propan-1-ol with atoms drawn as 50% probability ellipsoids. (Selected hydrogen atoms are labelled)

There is extensive hydrogen bonding present within the crystal. Chloroquinine molecules assemble into dimers by hydrogen bonding through the alcohol group. (see below)

D-H	d(D-H)	d(H..A)	$\angle$ DHA	d(D..A)	A
O1-H1	0.789	2.051	175.79	2.838	N1 [ -x+1, -y+1, -z ]

These dimers are then held together into sheets by hydrogen bonding. These hydrogen-bonded sheets run perpendicular to the  $xz$ -plane, parallel with the  $[101]$  direction.

D-H            d(D-H)   d(H..A)    $\angle$ DHA   d(D..A)   A

N2-H2A        0.812    2.327   167.21   3.124   O1 [  $-x+1/2, y+1/2, -z+1/2$  ]

Between the sheets there are further C–H $\cdots$ Cl interactions, notably the centrosymmetric  $R^2_2(8)$  embrace shown below.

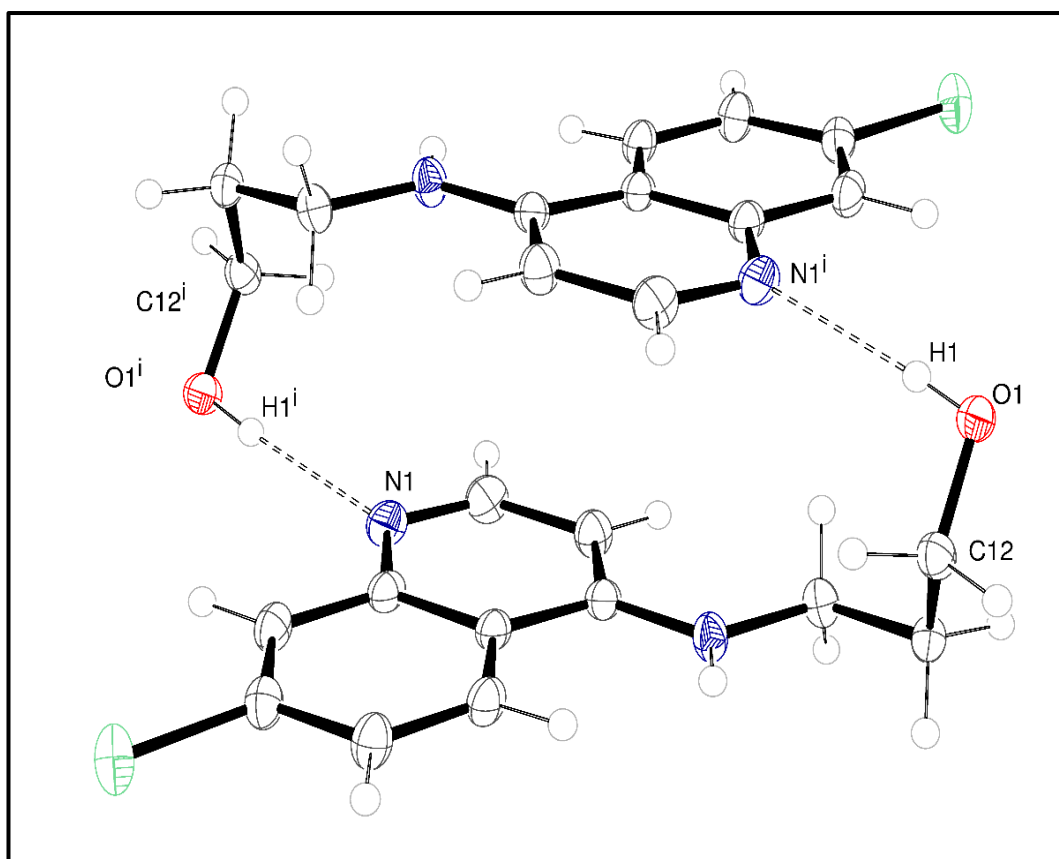


**Figure 2** Centrosymmetric embrace formed by two 3-(7-chloroquinolin-4-ylamino)propan-1-ol molecules with atoms drawn as 50% probability ellipsoids. Dashed lines represent hydrogen bonds. Symmetry operations used to generate equivalent atoms:  $i = 1-x, 1-y, -z$

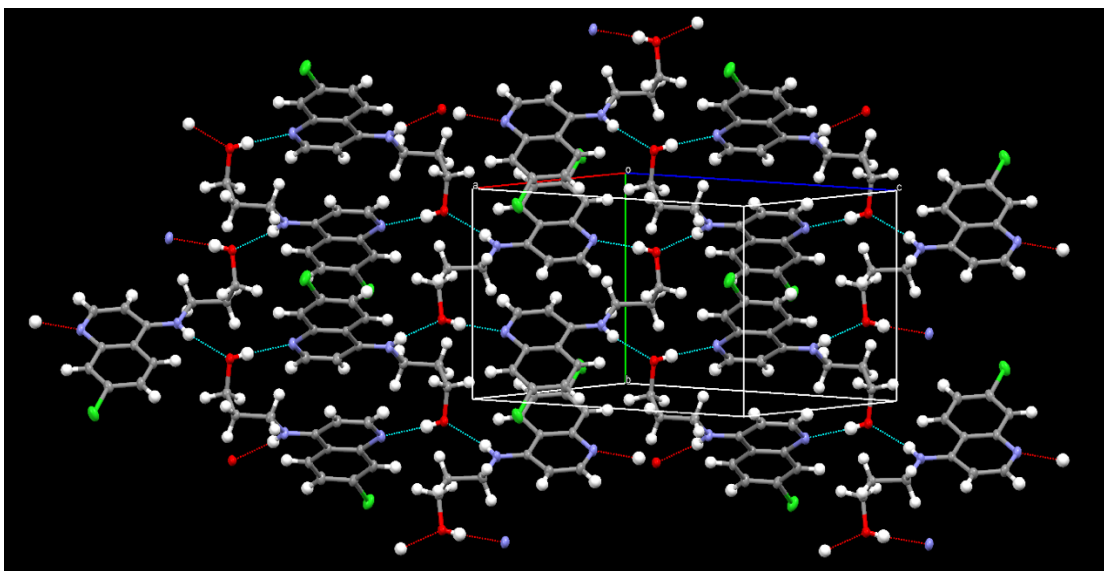


**Figure 3** Hydrogen bonded sheet running along the [101] direction. Dashed blue lines represent hydrogen bonds.

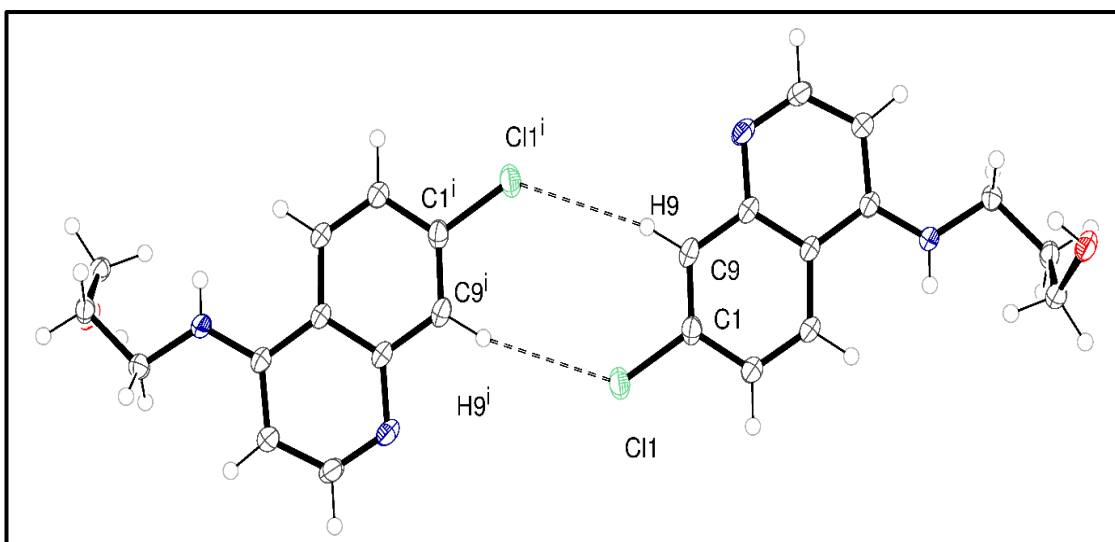


**Figure 4** Centrosymmetric embrace formed by two 3-(7-chloroquinolin-4-ylamino)propan-1-ol molecules with atoms drawn as 50% probability ellipsoids. The C–H $\cdots$ Cl interaction is one of several that hold the hydrogen-bonded sheets together. Dashed lines represent hydrogen bonds. Symmetry operations used to generate equivalent atoms:  $i = 2-x, 2-y, -z$

The bond length and angles are shown in **Table 1**.

**Table 1 Bond lengths [Å] and angles [°] for compound (1).**

C(1)-C(9)	1.3695(15)
C(1)-C(2)	1.4078(14)
C(1)-Cl(1)	1.7423(12)
C(2)-C(3)	1.3668(16)
C(2)-H(2)	0.993(12)
C(3)-C(4)	1.4160(14)
C(3)-H(3)	0.958(12)
C(4)-C(8)	1.4217(13)
C(4)-C(5)	1.4375(15)
C(5)-N(2)	1.3540(12)
C(5)-C(6)	1.3944(14)
C(6)-C(7)	1.3981(15)
C(6)-H(6)	0.942(13)
C(7)-N(1)	1.3227(16)
C(7)-H(7)	0.985(12)
C(8)-N(1)	1.3752(13)
C(8)-C(9)	1.4156(16)
C(9)-H(9)	0.966(12)
C(10)-N(2)	1.4531(14)
C(10)-C(11)	1.5250(14)
C(10)-H(10A)	0.988(9)
C(10)-H(10B)	0.988(9)
C(11)-C(12)	1.5192(15)
C(11)-H(11A)	0.964(9)
C(11)-H(11B)	0.964(9)
C(12)-O(1)	1.4310(13)
C(12)-H(12A)	0.976(9)
C(12)-H(12B)	0.976(8)
N(2)-H(2A)	0.812(15)
O(1)-H(1)	0.789(16)
C(9)-C(1)-C(2)	121.73(10)
C(9)-C(1)-Cl(1)	120.49(8)
C(2)-C(1)-Cl(1)	117.78(9)

C(3)-C(2)-C(1)	118.97(10)
C(3)-C(2)-H(2)	120.5
C(1)-C(2)-H(2)	120.5
C(2)-C(3)-C(4)	121.63(9)
C(2)-C(3)-H(3)	119.2
C(4)-C(3)-H(3)	119.2
C(3)-C(4)-C(8)	118.46(10)
C(3)-C(4)-C(5)	123.05(9)
C(8)-C(4)-C(5)	118.49(9)
N(2)-C(5)-C(6)	122.28(10)
N(2)-C(5)-C(4)	120.80(9)
C(6)-C(5)-C(4)	116.92(9)
C(5)-C(6)-C(7)	119.42(10)
C(5)-C(6)-H(6)	120.3
C(7)-C(6)-H(6)	120.3
N(1)-C(7)-C(6)	125.93(10)
N(1)-C(7)-H(7)	117
C(6)-C(7)-H(7)	117
N(1)-C(8)-C(9)	117.54(9)
N(1)-C(8)-C(4)	123.17(10)
C(9)-C(8)-C(4)	119.30(9)
C(1)-C(9)-C(8)	119.76(9)
C(1)-C(9)-H(9)	120.1
C(8)-C(9)-H(9)	120.1
N(2)-C(10)-C(11)	109.16(8)
N(2)-C(10)-H(10A)	109.8
C(11)-C(10)-H(10A)	109.8
N(2)-C(10)-H(10B)	109.8
C(11)-C(10)-H(10B)	109.8
H(10A)-C(10)-H(10B)	108.3
C(12)-C(11)-C(10)	112.75(9)
C(12)-C(11)-H(11A)	109
C(10)-C(11)-H(11A)	109
C(12)-C(11)-H(11B)	109

C(10)-C(11)-H(11B)	109
H(11A)-C(11)-H(11B)	107.8
O(1)-C(12)-C(11)	112.53(9)
O(1)-C(12)-H(12A)	109.1
C(11)-C(12)-H(12A)	109.1
O(1)-C(12)-H(12B)	109.1
C(11)-C(12)-H(12B)	109.1
H(12A)-C(12)-H(12B)	107.8
C(7)-N(1)-C(8)	115.97(9)
C(5)-N(2)-C(10)	123.95(9)
C(5)-N(2)-H(2A)	117.8(10)
C(10)-N(2)-H(2A)	118.2(10)
C(12)-O(1)-H(1)	108.2(12)